KINETIC AND FRICTION HEAD LOSS IMPACTS ON HORIZONTAL WATER SUPPLY AND AQUIFER STORAGE AND RECOVERY WELLS

A Thesis

by

BENJAMIN JOSEPH BLUMENTHAL

Submitted to the Office of Graduate and Professional Studies of
Texas A&M University
in partial fulfillment of the requirements for the degree of

MASTER OF SCIENCE

Chair of Committee,	Hongbin Zhan
Committee Members,	Peter Knappett
	Sungyon Lee
Head of Department,	John R. Giardino

December 2014

Major Subject: Geology

ABSTRACT

Groundwater wells can have extreme pressure buildup when injecting and extreme pressure drawdown when extracting. Greater wellbore contact with the aquifer minimizes pressure buildup and pressure drawdown. Aquifers are usually much more laterally extensive than vertically thick. Therefore, horizontal wells can be longer than vertical wells thus increasing aquifer contact and minimizing pressure issues. The length and therefore the effectiveness of horizontal wells are limited by two factors, either well construction or intra-wellbore head loss.

Currently no analytical groundwater model rigorously accounts for intra-wellbore kinetic and friction head loss. We have developed a semi-analytical, intra-wellbore head loss model dynamically linked to an aquifer. This model is the first of its kind in the groundwater literature. We also derived several new boundary condition solutions that are rapidly convergent at all times. These new aquifer solutions do not require approximation or pressure pulse tracking.

We verified our intra-wellbore head loss model against MODFLOW-CFP and found matches of three significant figures. We then completed 360 simulations to investigate intra-wellbore head loss. We found that only when aquifer drawdown was small will intra-wellbore head loss be relatively important. We found intra-wellbore head loss is relatively important only in extreme scenarios. We also found that kinetic head loss was greater than friction head loss if the well was less than 10m – 100m long.

To investigate well construction limitations, we developed an equation for the optimal slant rig entry angle, a drilling forces model, and a well construction cost model. We then collected well cost data and combined these models to make 60 well cost estimates. We found the relative cost of a horizontal well, compared to a vertical well, decreases with depth.

We then used our aquifer model to investigate the benefits of horizontal wells. We found several parameters that increase the number of vertical wells replaced by a horizontal well. These parameters include less time since pumping began, nearby recharge boundaries, vertical fractures, lower permeability, higher specific storativity, and thinner aquifers. Comparing horizontal well benefit with cost, we found that horizontal wells may or may not be economically advantageous depending on site specific conditions.

DEDICATION

I would like to dedicate this thesis to my wonderful, beautiful wife, Kristen Blumenthal. She has been a treasured companion throughout our time together at Texas A&M. Her love has been a sustaining force though all of my studies and work. I love her a bushel.

ACKNOWLEDGEMENTS

I would like to give a special thanks to the Texas Water Resources Institute, the United States Geological Survey, and the Mills Endowment for funding my graduate work including this thesis. The funding from these sources made this work possible, and for that I am grateful. I would also like to thank Texas Water Resources Institute management for supporting this thesis proposal, especially Kevin Wagner and Lucas Gregory.

I am very thankful for the support of my committee chair, Dr. Hongbin Zhan. He was great to work with, supportive of my ideas, and very knowledgeable. I learned much under his guidance. I would also like to thank my committee members for their input on the thesis, Dr. Peter Knappett and Dr. Sungyon Lee.

The drilling portions of this thesis would not have been possible without the tireless support of Mr. Fred Dupriest. Mr. Dupriest was not obligated take time out of his busy schedule to help me, yet he did. Mr. Dupriest did not only help me understand a question here or there, but he went great lengths to explain concepts and calculations to me. He spent countless hours corresponding with me and reviewing the drilling sections of this thesis. Without his help, a major portion of this thesis would not have been possible.

I would also like to thank all of the industry professionals who helped me throughout this thesis. I would especially like to thank Ms. Theresa Jehn-Dellaport and Mr. Vern Rash for their perspective on horizontal water supply wells that they worked

on. I would like to thank Mr. James Dwyer for his insights on current issues facing groundwater professionals investigating horizontal wells and Mr. David Pyne for his thoughts on horizontal well ASR. I also would like to thank Mr. Marvin Glotfelty for all his data; without his extensive collection of groundwater well cost data, the cost analysis section of my thesis would have been much less rigorous. Special thanks also goes out to the two service companies that collect industry data and were gracious enough to share it with me for free; RigData.com and Susan Murphy with The OCTG Situation Report®. There were many other professionals who helped me along the way from advice, to cost data collection, to helpful literature references; without these people this thesis would not have been possible.

Finally I would like to thank my parents, Brent and Julie, and my brother Sam, for all the work and love they have invested in me. I would not be the person I am today without them. They have always encouraged me to push my limits and to work hard. Their support and love is something that I hold very dear. I am forever grateful for all that they have done.

TABLE OF CONTENTS

Page

ABSTRACT ii

DEDICATION iv

ACKNOWLEDGEMENTS v

TABLE OF CONTENTS vii

LIST OF FIGURES xi

LIST OF TABLES xvii

CHAPTER I INTRODUCTION AND LITERATURE REVIEW 1

- Motivation 1
- Literature Review of Aquifer Storage and Recovery 2
  - Types of Injection Well ASR 4
    - Reason for ASR Storage and ASR Source Water 4
    - Method of Storage 6
      - Physically Bound ASR 6
      - Chemically Bound ASR 7
      - Blended ASR 8
  - ASR Modeling 9
    - Reactive Geochemical & Bio-Geochemical 10
    - Flow and Transport 10
  - Texas ASR 16
  - Horizontal Well ASR 17
- Literature Review of Horizontal Wells 19
  - Drilling Rig and Well Terminology 22
    - Borehole Completion Type 24
    - Borehole Measures 25
  - Historical Perspective 28
  - Directional Groundwater Well Case Studies 42
    - Directional Wells for Water Supply Production 42
      - Des Moines, Iowa (1998) 42
      - Antelope Hills, Bennett, Colorado (2002-03) 45
      - Castle Pines North Metro District, Colorado (2004) 49
    - Directional Environmental Wells 53
      - Savannah River Site, Aiken, South Carolina (1988-1991) 53
      - Williams Air Force Base, Chandler, Arizona (1992) 53

Page

Well Construction 54
Drilling 54
Subsurface Entry Angle 54
Directional Control 55
Wellbore Measurements 57
Mud Control 58
Well Limitations 59
Well Completion 62
Well Development 63
Horizontal Well Modeling 64
Finite Difference / Finite Element Models 65
Analytical Models 66
Early Groundwater Derivations 68
Petroleum Derivations 69
Petroleum Derivations with Intra-Wellbore Head Loss 71
Recent Groundwater Derivations 73
Summary of Literature Review 76
Research Needs from Literature Review 80
Thesis Objectives 82

CHAPTER II KINETIC AND FRICTION INTRA-WELLBORE HEAD LOSS 84

Introduction 84
Model Development 87
New Aquifer Discharge-Drawdown Solutions 87
Intra-Wellbore Friction and Kinetic Head Loss 90
Model Verification 91
Model Results 102
Uniform Flux Assumption 102
Intra-Wellbore Head Loss 113
Conclusions 119

CHAPTER III DERIVATION OF A UNIFORM FLUX WELL 122

Derivation of a Point Sink / Source 122
No Flux Boundaries on Each Side 124
Other Boundary Conditions 131
Series Convergence 131
Poisson Re-Summation 132
Catalog of Solutions Rapidly Convergent at All Times 135
Summation Method Switch 139
Iterations Required for Convergence 141

Page

Early Time Three Term Convergence 143
Analytical Integration 146
All Poisson Re-Sum 151
Only Time Integration 151
Space and Time Integration 153
Two Series Require Poisson Re-Summation 156
One Series Requires Poisson Re-Summation 158
No Series Require Poisson Re-Summation 161
Analytical Integrations Used in Model 166

CHAPTER IV DEVELOPMENT OF A NON-UNIFORM FLUX WELL 173

Steady State Numerical Solution 173
Transient Numerical Solution 177
Head Loss 180
Kinetic (Acceleration / Velocity) 181
Friction 182
Wellbore Skin Effects 183
Aquifer Loss 185
MATLAB Implementation 186
Steady State 189
Transient 190
Intra-Wellbore Head Loss 192
MATLAB Tips and Tricks 193

CHAPTER V SIMPLE DRILLING MODELS 195

Introduction 195
Well Construction Force Model 196
Lateral Section Forces 198
Buildup Section Forces 200
Running-In Forces 201
Pulling Out Forces 202
Neutral Forces 204
Torque 204
Upper Section Forces 205
Bending Force 206
Drill Rig Selection 206
Casing and Drill Pipe Selection 208
Optimal Slant Rig Entry Angle Derivation 210
Results and Discussion of Model Output 213

Page

CHAPTER VI HORIZONTAL WELL COST – BENEFIT ANALYSIS 223

Introduction 223
Well Cost Components 223
Drilling & Well Completion 224
Pumps 226
Connections and Structures 226
Operations and Maintenance 227
Well Cost Model Considerations 227
Well Cost Model 229
Well Cost Data Collection 231
Results & Discussion 231
Drilling Cost 231
Utility HDD 232
Slant Petroleum 232
Directional Equipment and Services 233
Vertical Daily Rig Rate 236
Length Dependent Costs 246
Casing Costs 246
Other Costs 249
Cost – Benefit Results 250
Cost Model Input 250
Cost Model Output 257
Aquifer (Benefit) Model Input 260
Aquifer (Benefit) Model Output 261
Conclusions 271

CHAPTER VII CONCLUSIONS 274

Literature Review 274
Research Completed 275
Future Work 280

REFERENCES 282

LIST OF FIGURES

FIGURE		Page
1	Conceptual representation of an ASR system	4
2	Conceptual model of ASR storage methods	9
3	Effect of permeability on recovery efficiency in a saline aquifer	13
4	Effect of aquifer thickness on recover efficiency in a saline aquifer	13
5	Hypothesized non-uniform flux along wellbore	19
6	Horizontal wells can facilitate greater contact with the aquifer than vertical wells	21
7	Rig and well types	23
8	Slant rig entry angles	24
9	Cross section of a slant rig HDD well	26
10	Cross section of a qanat	28
11	Plan view of a Ranney Well	30
12	Killing the Conroe well, an early form of directional drilling	31
13	Mud motor with bent-sub operating in a sliding and a rotating mode	33
14	North American petroleum rig count from 1991 to 2013 categorized by well type	36
15	North American petroleum rig count percentages from 1991 to 2013 categorized by well type	36
16	Worldwide Extended Reach Drilling Database, all wells	37
17	Worldwide Extended Reach Drilling Database, all land wells	38
18	Worldwide Extended Reach Drilling Database, all shallow land wells	39
19	Horizontal environmental wells through 2000	40

FIGURE Page

20 Horizontal wells for various environmental purposes 41

21 Nose plot of horizontal environmental wells 41

22 Horizontal groundwater well along the Raccoon River, Des Moines, Iowa 43

23 Submersible pump used for a horizontal well along the Raccoon River, Des Moines Iowa 44

24 Directional groundwater well in Antelope Hills, Bennett, Colorado 46

25 Antelope Hills pre-packed screen 47

26 Antelope Hills directional groundwater well rig 48

27 Directional groundwater well in Castle Pines North Metro District, Colorado 50

28 Castle Pines North Municipal District directional groundwater well rig 52

29 Castle Pines North Municipal District directional well rig in snow 52

30 Discretization of a function using three points 65

31 Infinite train of boxes from *x* equals one to four, generated from (2) 67

32 Aquifer conceptual model with source / sink and sample point 88

33 Steady state drawdown verification against MODFLOW-MNW2 95

34 Steady state discharge verification against MODFLOW-MNW2 95

35 Model Muse MODFLOW-CFP discretization 97

36 Steady state drawdown distribution verification between our model and MODFLOW-CFP 97

37 Steady state discharge distribution verification between our model and MODFLOW-CFP 98

38 Transient drawdown verification between our model and MODFLOW-CFP at first time step (20s) 99

FIGURE Page

39 Transient discharge verification between our model and MODFLOW-CFP at first time step (20s) 99

40 Transient drawdown verification between our model and MODFLOW-CFP at last time step (one hour) 100

41 Transient discharge verification between our model and MODFLOW-CFP at last time step (one hour) 100

42 Transient discharge verification of the constant head segment between our model and MODFLOW-CFP 101

43 Transient discharge verification of the segment furthest from the constant head segment between our model and MODFLOW-CFP 101

44 Transient drawdown verification of the segment furthest from the constant head segment between our model and MODFLOW-CFP 102

45 Discharge per unit length using model input data from Table 8 104

46 Drawdown for a given number of segments using model input data from Table 8 104

47 Discharge per unit length using model input data from Table 9 106

48 Drawdown for a given number of segments using model input data from Table 9 107

49 Discharge per unit length using model input data from Table 10 108

50 Drawdown for a given number of segments using model input data from Table 10 109

51 Discharge per unit length using model input data from Table 11 110

52 Total discharge for a given number of segments using model input data from Table 11 110

53 Penetration ratio impact on discrepancy between uniform flux and uniform head assumptions 112

54 Wellbore length to radius ratio impact on discrepancy between uniform flux and uniform head assumptions 112

FIGURE Page

55 Absolute head losses and importance of kinetic effects 114

56 Head loss impact on drawdown distribution in a low hydraulic conductivity aquifer 116

57 Head loss impact on flux distribution in a low conductivity aquifer 116

58 Head loss impact on drawdown distribution in a high hydraulic conductivity aquifer 117

59 Head loss impact on flux distribution in a high conductivity aquifer 117

60 Relative head loss in a low hydraulic conductivity aquifer 118

61 Relative head loss in a high hydraulic conductivity aquifer 119

62 Aquifer conceptual model with source / sink and sample point 122

63 Comparison of series iterations until convergence between the Poisson Re-Summed series and the unaltered series 140

64 Graphical depiction of integration approximation for the upper error bound . 143

65 Representation of function only requiring three series iterations 145

66 Integration of the point sink and sample point along the centerline of the wellbore and the circumference of the wellbore 148

67 Wellbore subdivided into four segments 174

68 Storage of results from the aquifer response function *F* 174

69 Flow components within a wellbore used to determine kinetic head loss 181

70 Function map of model MATLAB code 187

71 Numerical implementation of head loss between segments 192

72 Implementation of the try-catch framework during numeric tiled integration 193

73 Angle convention 196

74 Sections of a directional well 198

FIGURE Page

75 Angles used during optimal slant rig entry angle calculation 211

76 Optimal entry angle, lateral angle at zero degrees 213

77 Optimal entry angle, lateral angle at 45° 214

78 MD vs. TVDr and lateral length, full range of entry angle 215

79 MD vs. TVDr and lateral length, entry angle 7°-23° 216

80 MD vs. TVDr and lateral length, entry angle 45°-90° 216

81 Rig pullback from data in Table 12 217

82 Rig thrust from data in Table 12 218

83 Rig torque from data in Table 12 218

84 Casing tensile strength from data in Table 12 219

85 Casing compressive strength from data in Table 12 219

86 Vertical and horizontal well cost flow chart 230

87 Utility rig cost per foot to drill & ream versus rig pullback 234

88 Mobilization/demobilization costs 239

89 Site preparation costs 239

90 Cost per foot to drill and ream 240

91 Geophysical logging costs 240

92 Well development and testing costs 241

93 Unavoidable delay with crew, cost per hour 241

94 Daily rig rates from Rig Data (2014) and *Unavoidable Delay with Crew* 243

95 Rated depth to rig pullback relationship 245

96 Daily rig rate using a regression of rated depth to pullback capacity 246

97 OCTG cost per cubic foot 248

FIGURE Page

98 Casing cost per cubic foot versus yield strength.....249

99 North American petroleum rig count percentages from 1991 to 2013 categorized by drilling type 273

LIST OF TABLES

TABLE		Page
1	Reasons to implement an ASR system	5
2	ASR injection water types	6
3	Summary of directional well technology	27
4	Model verification against the Theim equation	92
5	Model verification against the Theis equation	93
6	Model verification against MODFLOW-MNW2	94
7	Model parameters used for MODFLOW-CFP verification	96
8	First model input for investigation of uniform flux assumptions	103
9	Second model input for investigation of uniform flux assumptions	106
10	Third model input for investigation of uniform flux assumptions	108
11	Fourth model input for investigation of uniform flux assumptions	109
12	Sample input for well construction force model	217
13	Drilling cost for HDD utility rigs from three companies	234
14	Slant petroleum daily rig rates	235
15	Day rates for down hole directional equipment and services	235
16	Cost for traditional vertical water well rigs	237
17	Timetable for nine Texas, municipal, vertical water wells constructed in 2012	238
18	Hourly to day rig rates calculated from post bids: *Unavoidable Delay with Crew* and Williams (2008)	242
19	Cost of casing per cubic foot	248
20	Cost data from Petrey and Bennett (2006) adjusted for inflation using CCI	250

TABLE Page

21 Cement and filter pack costs from post bid data 250

22 Rig overpull determination 252

23 Model input / output setup with constant parameters 256

24 Cost model output assuming ROP is 50 ft/day 258

25 Cost model output assuming ROP is 50 ft/day, normalized to vertical well cost 258

26 Cost model output assuming ROP is 1,000 ft/day 259

27 Cost model output assuming ROP is 1,000 ft/day, normalized to vertical well cost 259

28 Vertical well replacement ratios for first set of model input, gravel aquifer ... 261

29 Vertical well replacement ratios for first set of model input, silt aquifer 262

30 Vertical well replacement ratios for second set of model input, gravel aquifer 263

31 Vertical well replacement ratios for second set of model input, silt aquifer ... 263

32 Vertical well replacement ratios for third set of model input, gravel aquifer .. 264

33 Vertical well replacement ratios for third set of model input, silt aquifer 265

34 Vertical well replacement ratios for fourth set of model input, gravel aquifer 266

35 Vertical well replacement ratios for fourth set of model input, silt aquifer 266

36 Vertical well replacement ratios for sixth set of model input, shale aquifer ... 267

37 Vertical well replacement ratios for seventh set of model input, shale aquifer 268

38 Vertical well replacement ratios for eighth set of model input, sand aquifer .. 270

39 Vertical well replacement ratios for eighth set of model input, silt aquifer 270

CHAPTER I

INTRODUCTION AND LITERATURE REVIEW

MOTIVATION

Access to water supplies is vital to the continued growth and success of any community. The Texas Water Development Board, TWDB (2012) has asserted that, "unreliable water supplies could have overwhelming negative implications for Texas." The population of the state is expected to grow 82% by 2060, with a water demand increase of 22% (TWDB, 2012). In *Water for Texas 2012: State Water Plan*, planning groups identified a water supply need [demand – supply] of 3.6 million acre feet in 2010 and 8.3 million acre feet by 2060 (TWDB, 2012).

While additional surface water reservoirs are in the planning stages, they contain many drawbacks. Annual evaporation of lakes ranges 51 cm to 218 cm in the United States (Viessman et al., 1977). Lake seepage may also be of concern, as in the extreme case of Medina and Diversion reservoirs near San Antonio, which lose between 209-326 cm each year (Lambert et al., 2000). Other challenges to surface water development are the lack of suitable land, the high cost of land acquisition, environmental impacts / permits, disruption of nearby communities, silt deposition and high construction costs (Bouwer, 2002; Malcolm Pirnie Inc et al., 2011). Given these considerations, new water supplies are likely to be derived from groundwater aquifers.

Two new technologies have the potential to increase groundwater supplies. The first is aquifer storage and recovery (ASR). ASR is generally defined as storing water in

aquifers during times of excess for use in times of deficit or drought (Pyne, 1995). The other new technology is directional / horizontal drilling. Directional / horizontal wells facilitate greater contact with the aquifer thereby allowing higher pumping rates per well.

A combination of ASR with directional drilling is the next logical progression. Drilling horizontal wells for ASR could bring the benefits of each technology into one system, thereby significantly increasing groundwater availability. The combination of horizontal well technology with aquifer storage and recovery requires a thorough understanding of each system. Combining these two technologies without a thorough understanding of their components, operating parameters, history, and construction may result in miscalculation of expected cost and benefit.

A rigorous literature review is necessary given the technical complexity of directional wells and ASR. The literature review will determine the origins, failures and success of each technology. It will investigate modern construction and operational performance of each system. Finally, the literature review will investigate modeling methods of each system. Upon completion of the literature review, future research needs will be identified. Thesis objectives will then be defined based on these research needs.

LITERATURE REVIEW OF AQUIFER STORAGE AND RECOVERY

Artificial groundwater recharge is the human alteration of the natural environment so as to promote percolation from the surface to the subsurface. Artificial groundwater recharge and has been implemented in Europe since the 1850's and perhaps much earlier in other parts of the world (Pyne, 1995; Todd, 1959). Managed Aquifer

Recharge (MAR) is a more recent subset of this concept. MAR is any process by which water is placed in aquifers via human design with a thought for use at a later date (Dillon et al., 2009). MAR projects have included injection wells, and infiltration basins (leaky ponds). A subset of MAR is Aquifer Storage and Recovery. ASR occurs when water is placed into an aquifer via an injection well, stored, and then subsequently pumped from the same well (Pyne, 1995). This thesis focuses on well based ASR as previously defined and does not investigate infiltration basins.

While various rudimentary forms of ASR began in the late 19th century, the first successful ASR test was not completed until 1946 in Virginia (Cederstrom, 1947; Cederstrom, 1957; Maliva and Missimer, 2010). The first long term operating ASR system began in 1967 at Wildwood, New Jersey (Lacombe, 1996; Maliva and Missimer, 2010; Pyne, 1995). ASR is a cost competitive technique to store vast quantities of water when compared to new surface water reservoirs. Through time, its use and acceptance has increased. The number of ASR wells in the United States has more than quadrupled since 1999. There are currently 542 wells in operation across 90 sites (Frederick et al., 2010). Las Vegas has the largest system with a recharge capacity of 103 million gallons per day (MGD) and extraction of 157 MGD (Frederick et al., 2010).

Conceptually, injection well ASR systems may be thought of as an expanding "bubble" or "bottle-brush" (Vacher et al., 2006). This bubble / bottle-brush of injected water is surrounded by native groundwater. As water is injected, the bubble expands. As water is extracted, the bubble retracts. The interface between the injected water and the native groundwater is termed the buffer zone or mixing zone (Figure 1).

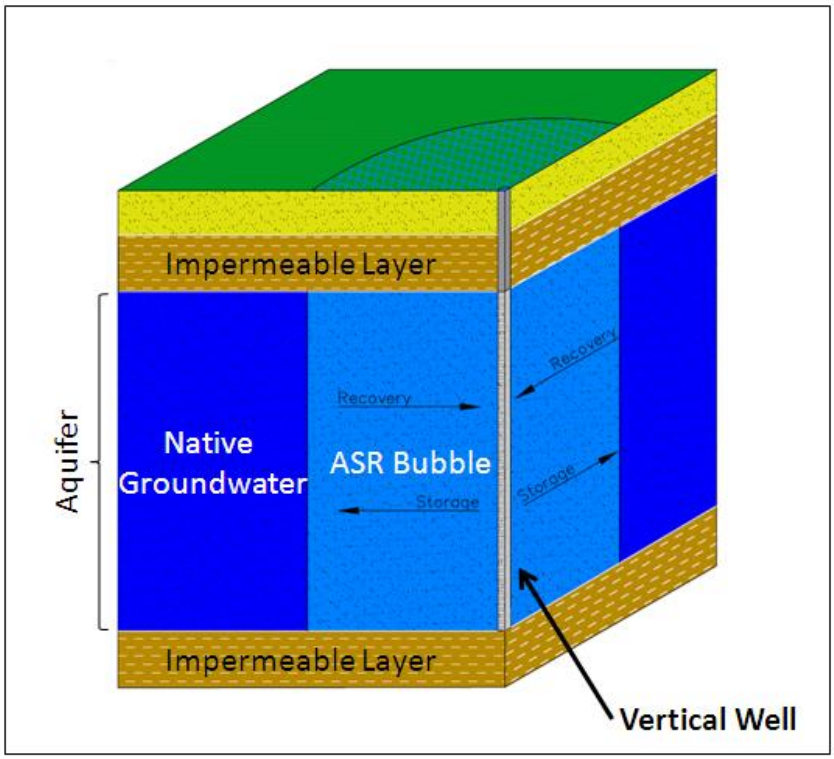

Figure 1. Conceptual representation of an ASR system.

Types of Injection Well ASR

Types of ASR systems may be based upon operating principles. ASR may be subdivided first by the reason for storage, then the source water type, and finally the method of storage. While all of these parameters are inherently interrelated, it is outside the scope of this report to document preferred combinations.

Reason for ASR Storage and ASR Source Water

The source waters and reasons for ASR are fragmented, yet in many cases closely related. Given these considerations, Table 1 & Table 2 summarize various presentations, conversations and literature detailing reasons for ASR and ASR source

waters (Maliva and Missimer, 2010; National Research Council, 2008; Pyne, 1995; Pyne, 2005).

Table 1. Reasons to implement an ASR system.

REASONS FOR ASR	
INCREASE USEABLE WATER SUPPLY	
Length of Storage	
1. Seasonal Storage	Water is stored and used on a sub-yearly basis.
2. Long-term Drought Management	Water is stored for periods of greater than a year for use during droughts of record.
Regulations	
1. Regulatory Storage	The permitted water rights are used to the fullest. This method ensures a full use of water rights, which is advantageous in a 'use it or lose it' scenario.
System Optimization	
1. Water Treatment Optimization	Operating a water treatment plant (desalinization, direct reuse, etc.) at maximum efficiency will minimize costs. ASR allows for storage at low demand times for use at high demand times.
Improve or Maintain Water Quality	
1. Soil-Aquifer Treatment (SAT)	Treatment of injected waters for disinfection byproducts and pharmaceutically active compounds. More widely used during infiltration basin MAR.
2. Salinity Barrier	Salt water intrusion barriers.
ENVIRONMENTAL DISTURBANCE MITIGATION	
1. Environmental Stream Flow Maintenance	Maintenance of flows for at risk species.
ENERGY STORAGE	
1. Aquifer Thermal Energy Storage (ATES)	Storage of energy via water (hot or cold) for use at a later date to minimize energy consumption.

Table 2. ASR injection water types.

ASR SOURCE WATER
1. Surface Water
2. Groundwater
3. Direct Reuse Water (Reclaimed Wastewater)
4. Stormwater
5. Desalinated Water

Method of Storage

Although source waters and the reasons for ASR are varied, the interactions of injected water and native groundwater are more readily defined. Maliva and Missimer (2010) have divided ASR storage methods into three categories. Typically ASR injection water quality is good, but the native groundwater quality may vary. If the native groundwater quality is good, then the constraints on the ASR system are only physical-hydraulic; these systems are referred to as **physically bound ASR**. Physically bound ASR systems only constraint is the typical physical-hydraulic limitations of any injection or extraction well. If the native groundwater quality is poor, then the constraints on the ASR system are both physical and chemical; these systems are referred to as **chemically bound ASR**. While there are many methods to define a chemically bound ASR system, the usual groundwater quality impairment is total dissolved solids (TDS), salts. ASR systems with groundwater quality between good and poor are referred to as **blended ASR**.

Physically Bound ASR

Mixing of native and injected water is non-detrimental in physically bound ASR. The only boundary is hydraulic. The human secondary drinking water standard for TDS

is 500 mg/L (U.S. EPA, 2013). This standard suggests that native groundwater quality of physically bound ASR systems should have a TDS of less than 500 mg/L.

The hydraulic boundary for physically bound ASR may vary from a fault (no flux boundary) to a river (constant pressure boundary). The key to determining the appropriate aquifer physical boundary depends on control. Most regulatory storage ASR will not require injected water to be controlled; therefore other entities' may extract injected water. In other cases, entire basins have been regulated by a single authority. This is the case for the Las Vegas Valley Water District & Southern Nevada Water Authority (Maliva and Missimer, 2010).

Recovery efficiency is the ability to recapture injected water or pump usable (potable) groundwater. Recovery efficiency for physically bound systems is greater than or equal to 100%. The recovery efficiency may exceed 100% because the native groundwater can be pumped as a water source in addition to the injected water. However, if this is regulatory storage ASR with a 'tax' scheme, then only a fraction of injected water is allowed to be extracted. With taxed ASR, less than 100% recovery efficiency is enforced by government regulation.

Chemically Bound ASR

Mixing of source water and native groundwater is detrimental to system performance in chemically bound ASR. These systems inherently have physical bounds, but the chemical constraints are more important. Generally, the native groundwater quality of chemically bound ASR systems is of brackish to sea water quality. Total

dissolved solids of native groundwater in chemically bound ASR systems are typically greater than 1,000 mg/L.

Differences in water density become important in chemically bound ASR systems because the less dense injected water rises vertically and then spreads out laterally across the aquifer's upper layer. While the exact density difference at which buoyancy stratification depends on several factors (Ward et al., 2007); generally, density effects may become important at native groundwater TDS of 10,000-20,000 mg/L (Brown, 2005; Missimer et al., 2002). Recovery efficiency of less than 60% may be expected with values less than 10% possible, all depending on site specific hydrogeology.

Blended ASR

Blended ASR systems benefit from the mixing of injected waters with native groundwater. Mixing is encouraged because marginal native water quality is mixed with higher quality injected water with an end result of greater total usable water, albeit of lesser quality. These systems rely on both physical and chemical bounds. Generally native groundwater TDS ranging between 500-5,000 mg/L may be considered blended systems. Recovery efficiencies are likely between 80-100%, but may be lower depending on native water quality and other aquifer parameters. Figure 2 presents a conceptual model of ASR storage methods based on these literature findings.

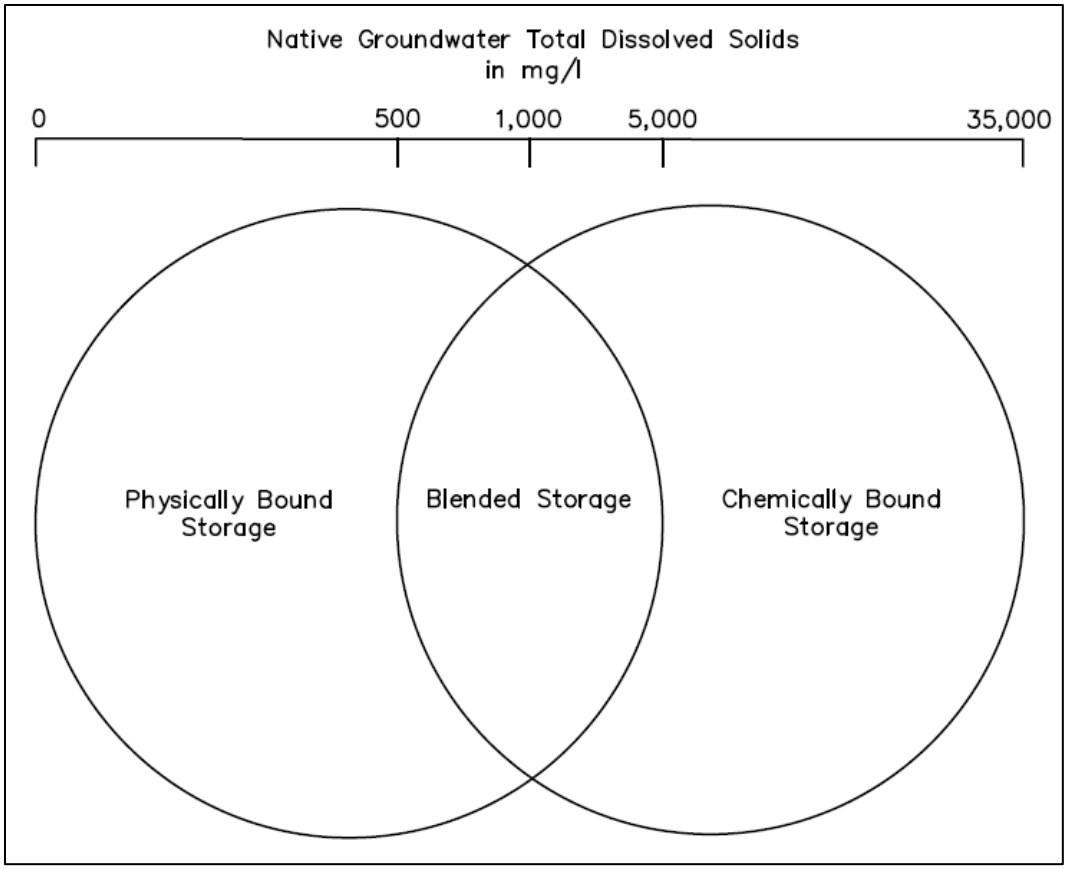

Figure 2. Conceptual model of ASR storage methods. Possible groundwater quality cutoffs between ASR system types derived from literature (Brown, 2005; Missimer et al., 2002; U.S. EPA, 2013; Ward et al., 2007).

ASR Modeling

The most important factor controlling ASR success is recovery efficiency. Models are implemented to predict not only site specific recovery efficiency, but also to make generalizations of efficiencies based on certain hydrogeologic factors. There are two main types of models used to describe ASR systems: geochemical / bio-geochemical models and flow / transport models.

Reactive Geochemical & Bio-Geochemical

Geochemical / bio-geochemical reactions are any process that alters the water quality in a reactive way, i.e. processes other than mixing. Loss of injection capacity via biological clogging in the well and nearby formation is a recognized problem (Oberdorfer and Peterson, 1985; Rinck-Pfeiffer et al., 2000). Growth of bacteria between injection and extraction cycles has also been encountered (Rebhun, 1968; Vecchioli, 1970). As oxic, dissimilar pH waters are injected into groundwater aquifers, geochemical reactions may also occur to diminish water quality, especially oxidation of pyrite leading to arsenic contamination (Jones and Pichler, 2007; Price and Pichler, 2006).

Most bio-geochemical problems are avoided through injection of anoxic, low suspended solid, pH matched, abiotic waters. By injecting these 'clean' waters, the potential for bio/geo-chemical reactions is reduced. Conversely, aquifer hydraulics is a less remediable problem. As this thesis is focused on aquifer hydraulics in relation to horizontal and vertical wells, geo-chemical / bio-geochemical reactions will not be investigated further. In spite of the focus of this thesis, it should be noted that without an understanding of possible chemical reactions, an ASR system can easily fail.

Flow and Transport

Flow and transport aquifer processes incorporate the movement of groundwater and the substances that said flow transports. No reactions are considered, only mixing and movement of mass. While technically a flow and transport process, clogging of the formation by suspended solids will not be discussed in this thesis. As with the

geochemical reactions, clogging can be easily avoided through the injection of clean water. Those interested in physical clogging should consult Crawford and Johnson (1967) and Rinck-Pfeiffer et al. (2000).

Processes characterized in flow and transport models may be described by three parameters: advection, diffusion, and dispersion. Advection describes the physical movement of solute due to hydraulic gradients. Diffusion describes the spreading of solute due to concentration gradients. Dispersion describes the random spreading of solute due to processes such as turbulent flow, and differences in pore velocities. Several modeling studies have been completed on flow and transport in ASR systems.

Esmail and Kimbler (1967) developed a computer model for freshwater injection into saline aquifers accounting for diffusion-dispersion (mixing). First, a physical model was constructed for the purpose of verifying equations and determining coefficients. Once the coefficients were determined, computer simulation was completed for various ASR parameters.

Esmail and Kimbler (1967) made several important conclusions. First, injected freshwater and native saline water mixing impedes gravity segregation. Second, gravity segregation is more detrimental to ASR than mixing. Third, freshwater storage in saline aquifers is possible when conditions are favorable: low permeability (10 Darcies or less), and large volumes of injected water. Processes and parameters limiting density stratification improve freshwater storage in saline aquifers

Kimbler (1970) used results from laboratory flow models combined with computer modeling to examine ASR processes. He then tested these results against a

three-dimensional laboratory model. Kimbler (1970) found that recovery efficiency improved with each injection and extraction cycle. Recovery efficiencies of less than 75% may be expected for the first cycle. He also found that parameters improving recovery efficiency include: minimal density differences between injected and native groundwater, lower permeability aquifers, thin aquifers, and large dispersion coefficients.

Kumar and Kimbler (1970) improved upon the initial work of Esmail and Kimbler (1967) leading to a major revision of the original computational procedure. Kumar and Kimbler (1970) added other components to the computational procedure which allowed for new parameters to be investigated. Kumar and Kimbler (1970) made similar conclusions as the previous two studies. ASR is feasible when aquifer salinity is low (minimization of density stratification), aquifer permeability is low (Figure 3), and the aquifer is thin (Figure 4). Recovery efficiency increases with each injection and extraction cycle. Porosity in and of itself (i.e. not influencing other parameters such as permeability etc.) does not greatly influence recovery efficiency. Kumar and Kimbler (1970) concluded that processes minimizing density stratification are beneficial to ASR in saline aquifers (chemically bound ASR).

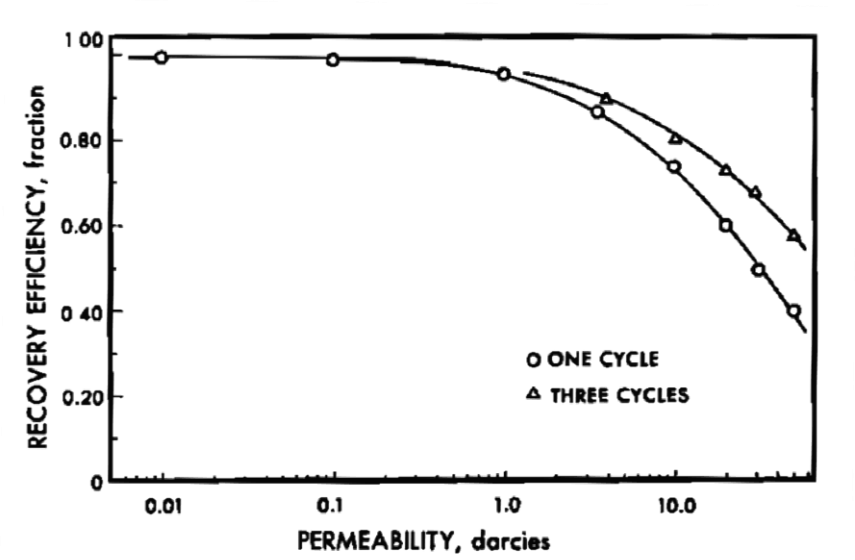

Figure 3. Effect of permeability on recovery efficiency in a saline aquifer (Kumar and Kimbler, 1970). Reprinted by permission. Copyright © 1970, John Wiley and Sons.

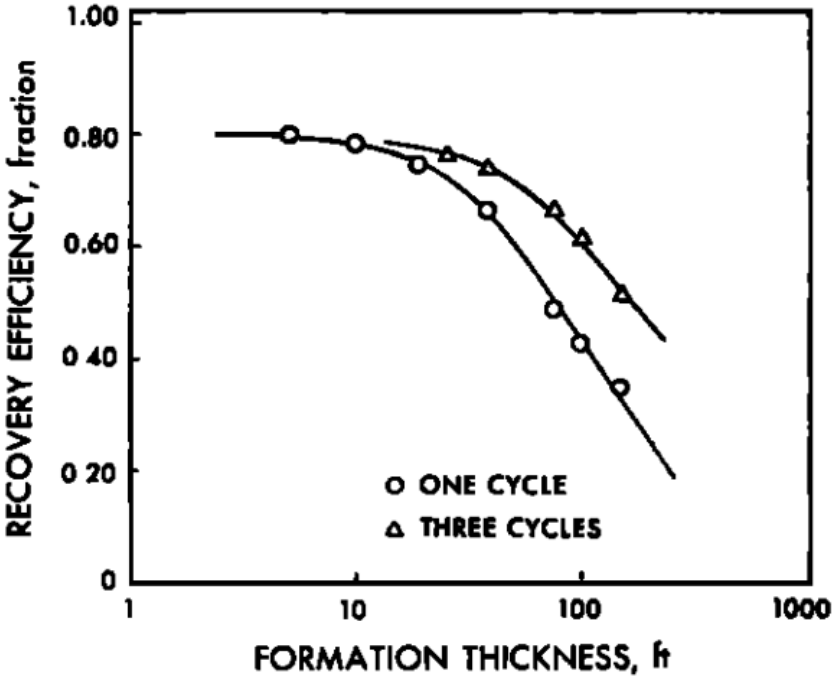

Figure 4. Effect of aquifer thickness on recover efficiency in a saline aquifer (Kumar and Kimbler, 1970). Reprinted by permission. Copyright © 1970, John Wiley and Sons.

Merritt (1986) modeled ASR using a three-dimensional numerical finite-difference model, INTERA Deep Well Waste Disposal Model. This model accounted for diffusion-dispersion processes and used hydraulic solvers to model density stratification. Merritt (1986) found that greater recovery efficiencies occurred with: lower permeability aquifers, lower hydrodynamic dispersion, similar water densities, minimized regional hydraulic gradient, large injection volume, and multiple cycles (more than three cycles). Formation thickness, porosity, and multi-well layout had only minor effects on recovery efficiency, on the order of five percent.

Merritt (1986) found that factors contributing to greater ASR recovery efficiencies minimize: mixing, movement of the fresh water bubble, and non-symmetric injection and extraction flow patterns. Most importantly, low volumes of injection can dramatically reduce recovery efficiencies. This occurs as dispersion dominates so as to rapidly contaminate the small amount of injected water essentially mixing out all potable water instantly. Given these findings, aquifers that minimize movement of the freshwater bubble will benefit ASR. These aquifers will have a combination of low hydraulic conductivities, low density differences, and/or low regional hydraulic gradients.

Lowry and Anderson (2006) used MODFLOW, the United States Geological Survey's finite-difference groundwater model by Harbaugh (2005), to evaluate ASR. MODPATH was used to track particles and MT3DMS was used to simulate solute mixing (Pollock, 1994; Zheng and Wang, 1999). The inclusion of MODPATH (no mixing) and MT3DMS (mixing) was used to compare advection (non-mixing

component) versus dispersion-diffusion (mixing component) when calculating recovery efficiencies.

Lowry and Anderson (2006) found that higher recovery efficiencies occurred at an optimum hydraulic conductivity (not low or high), short storage times, high injection and extraction volumes and low dispersion. Detrimental scenarios readily return recovery efficiencies of less than 40%. Because buoyancy effects were not modeled, lower permeability aquifers and/or thin aquifers were not necessarily preferred for greater recovery efficiency.

In Lowry and Anderson (2006), mixing was an important consideration for ASR performance. When compared to dispersion modeling techniques, particle tracking schemes significantly over predict recovery efficiencies by perhaps 30%. Although dispersion-diffusion is an important process, it remains a difficult parameter to quantify and is typically unknown.

Ward et al. (2007) rigorously investigated the density stratification effect on ASR recovery efficiency using the numerical finite-element model FEFLOW. Ward et al. (2007) found that density differences between injected and native groundwater were not sufficient in determining the importance of density stratification. Other parameters influencing density stratification such as permeability, pumping rate, storage length, and dispersion must be considered in addition to density differences.

While the modeling studies in this section have found higher recovery efficiencies in thin, low permeability aquifers, such aquifers also increase pressure buildup and drawdown during injection and extraction respectively. This increase in

pressure buildup and drawdown translates to more vertical wells needed to reach a given ASR storage capacity. There is a tradeoff between the ability to recapture injected water and the ability to inject and extract the water.

Texas ASR

There are currently three ASR systems in Texas: El Paso, Kerrville and San Antonio (Malcolm Pirnie Inc et al., 2011; Sheng, 2005). ASR systems have been identified in the Texas 2012 state water plan as a water management strategy to provide 81,000 acre feet per year by 2060 (TWDB, 2012b). San Antonio Water System's (SAWS) ASR is the largest. As of October 2012, SAWS ASR had 91,000 acre feet in storage, with a maximum capacity of 120,000 acre feet (SAWS, 2012). The SAWS ASR system may be classified as a groundwater source, regulatory, physically bound system.

While only three ASR systems are currently operational, several other ASR projects have been proposed across the state. The feasibility report on a proposed Laredo ASR system cited both thin aquifers and low permeability formations as the chief obstacle to development (Anglea, 1999). The optimal ten million gallon per day Laredo ASR could not be built because of a thin aquifer with low hydraulic conductivity (excessive pressure buildup and drawdown). Therefore a five million gallon per day facility was proposed at a cost of $6.3 million for twenty-eight wells and associated hardware.

Anglea (1998) considered directional drilling for the SAWS ASR as it would intersect vertical fractures in the formation and thus increase production. In the report, Halliburton Drilling Systems estimated an additional cost of $75,000 for 2,000 linear

feet of directional drilling. Despite this option being available, traditional vertical wells were used instead.

Horizontal Well ASR

Results and conclusions from previous workers in the *Flow and Transport Modeling* section suggest that horizontal ASR systems may be very useful for certain hydrogeologic conditions. ASR in saline aquifers (chemically bound ASR) is sensitive to buoyancy stratification; for this reason, it has been shown that low hydraulic conductivity, thin aquifers would yield greater recovery efficiencies for these systems (Esmail and Kimbler, 1967; Kimbler, 1970; Kumar and Kimbler, 1970; Merritt, 1986).

However, lower conductivities and thin aquifers limit injection and extraction rates because of excess pressure buildup and drawdown. To achieve a high enough short term storage capacity in low permeability, thin aquifers, many additional vertical wells will have to be constructed. Furthermore, not all physically bound ASR locations have high enough hydraulic conductivities or thick enough aquifers to promote rapid injection and extraction as is the case for Laredo. Horizontal wells are useful in that they have greater aquifer contact, thus reducing pressure buildup and drawdown. Therefore, horizontal wells may be advantageous for chemically bound ASR attempting to maximize recovery efficiency by targeting low permeability, thin aquifers. Additionally, horizontal wells may be advantageous for physically bound ASR that happens to be located in low permeability, thin aquifers.

Three Ranney wells operating in reverse are the only occurrences of municipal horizontal well ASR systems (Pyne, 2013). While these few horizontal well systems are

operating as ASR, such a purpose was not their original design. Pyne and Howard (2004) is the only manuscript on a proposed municipal horizontal well ASR system that this author is aware of.

In terms of proposed horizontal municipal ASR systems, designs and cost estimates have been generated for five locations. "The most recent preliminary design and cost estimate was for a project in Georgia in 2011. In 2010, designs and cost estimates were developed for a proposed horizontal, directionally drilled (HDD) ASR well field in South Carolina. Two other systems were proposed in Florida, in 2005. A system for Corpus Christi, Texas was proposed in 2004 (Pyne and Howard, 2004). The technology exists, and in many places the need exists," (Pyne, 2013).

There is only one known horizontal well constructed strictly for an ASR application. Zuurbier et al. (2013) constructed a small directional well to study freshwater-saltwater mixing during ASR injection and extraction cycles. To facilitate recovery estimates before well construction, a two dimensional finite difference model was created. This is the first directional ASR well used in a brackish aquifer. Results have shown the ASR system to be effective at injecting and storing freshwater in a salty aquifer to be retrieved at a later date (Zuurbier et al., 2013).

Maliva and Missimer (2010) suggest that horizontal well ASR systems have not been implemented because of non-uniform flux (friction losses) along the wellbore. Because a horizontal well is significantly longer than a vertical well, there is an increased energy loss due to friction. Such losses reduce pumping rates thereby diminishing the advantage of horizontal wells compared to vertical wells. In addition,

frictional energy losses may result in a non-uniform flux along the wellbore. The greatest flux is hypothesized to be near the pumped end (Figure 5). This non-uniform flux may allow for native salty water at the well toe to be in contact with intra-wellbore freshwater towards the heel. This direct contact of fresh and salty water in the wellbore would allow for rapid diffusion-dispersion within the wellbore. This dispersion-diffusion will rapidly mix out potable water within the wellbore thus resulting in very low recovery efficiencies. However, no studies on this problem have been completed to date.

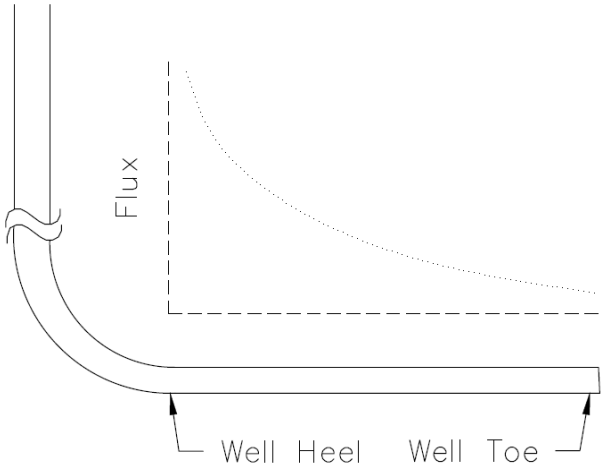

Figure 5. Hypothesized non-uniform flux along wellbore.

LITERATURE REVIEW OF HORIZONTAL WELLS

Horizontal / directional wells have several advantages compared to vertical wells, the most significant of which is less drawdown. Drawdown is defined by several equivalent terms as a decrease in: water level, pressure, hydraulic head, or energy in the wellbore when compared to a time prior to pumping or some point infinitely far away.

Reducing the fluid level / hydraulic head in the well drives fluid flow from the far field towards the well. Drawdown is the cost, production is the benefit. Greater pumping rates lead to greater drawdown. The one dimensional relationship between drawdown and pumping is mathematically represented by Darcy's Law as

$$Q = KA\frac{(h_2 - h_1)}{\lambda}, \quad (1)$$

where Q is the pumping rate [L^3T^{-1}], K is hydraulic conductivity [LT^{-1}], A is the area through which flow occurs [L^2], ($h_2 - h_1$) is the difference in hydraulic head (drawdown) between two points [L], and λ is the distance between these two point [L] (Fetter and Fetter, 2001).

Darcy's Law states that if the flow area and/or hydraulic conductivity are high, then a small drawdown will generate a high flow rate. Conversely, if the pumping rate is high but the hydraulic conductivity and/or surface area is low, then a high drawdown will be generated. It is clear from this simple one dimensional mathematical relationship that longer wells will outperform shorter wells because longer wells have an increased surface area for flow to occur. The maximum length of a vertical well is the thickness of the aquifer. Aquifers are typically much more laterally extensive than vertically thick. Therefore, horizontal wells are typically able to contact more of the aquifer than vertical wells (Figure 6).

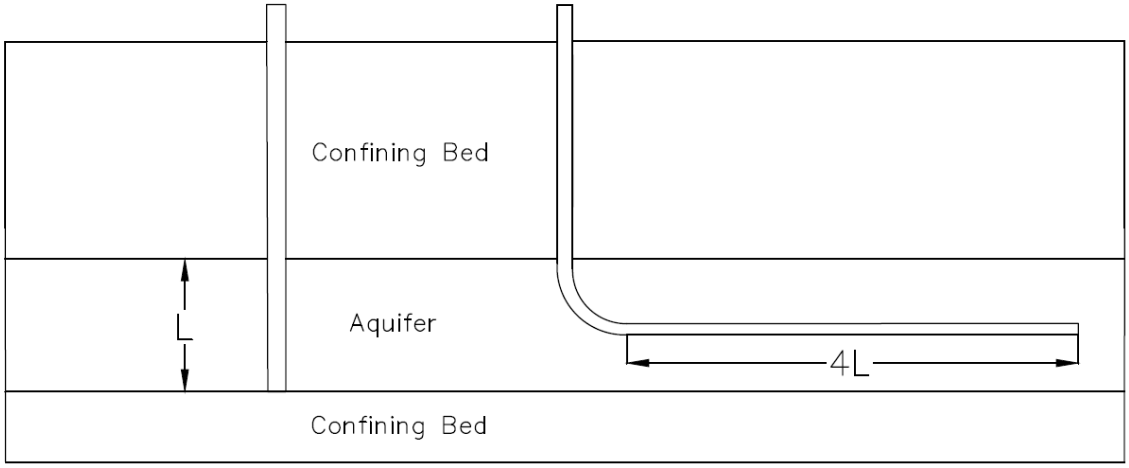

Figure 6. Horizontal wells can facilitate greater contact with the aquifer than vertical wells.

Stated another way, if drawdown is a concern then the length of aquifer exposed to the wellbore is the most important factor to consider when deciding between horizontal and vertical wells. If the vertical well length equals the horizontal well length, then a vertical well should be constructed as there is no horizontal well benefit. Conversely, if the aquifer is thin then the vertical well has only limited contact with the formation. In this case significant drawdown is expected in the vertical well. Aquifers are much more laterally extensive than vertically thick. A horizontal well in a thin aquifer intersects the formation for a greater distance than a vertical well (Figure 6). This additional wellbore length (surface area) in the aquifer increases flow area and thus reduces drawdown compared to the vertical well.

In addition to the drawdown benefits, horizontal / directional wells may be more advantageous than vertical wells for several other reasons. Horizontal / directional wells may be used to access formations that cannot be drilled from above, such as underneath

a city. Horizontal wells may also be used to target removal of gravity segregated fluids (gas, oil, water, brine, etc.).

Drilling Rig and Well Terminology

It will be shown that horizontal wells for water supply production must rely upon technology from the petroleum industry, utility pipe laying industry, and environmental remediation industry. Given this reliance on several different technologies, it is important to understand the terminology of each discipline before any discussion of the technology occurs.

To begin, a horizontal well refers to any borehole completed in a horizontal or nearly horizontal fashion. These may include wells that have been drilled vertically to a specific depth (kickoff point – KOP) and then drilled directionally until the wellbore angle is horizontal. Directional drilling refers to any borehole that has been intentionally drilled at an angle other than vertical. Horizontal directional drilling (HDD) is another term for boreholes that are directionally drilled to a horizontal plane. This terminology, however, has typically been restricted to the utility industry although it could be applicable to any similar boring. The term trenchless technology is also exclusive to the HDD utility industry. This term is used for describing the use of directional boring to install pipelines, rather than surface trenches.

Slant or angle wells are wells drilled at some angle between vertical and horizontal (Figure 7). A slant or angle well may or may not begin vertically at the surface. However at some point, by definition, the well will be at a constant angle between vertical and horizontal for an extended distance. Slant rigs refer to specialized

rigs with drilling structures that are tilted so that the borehole can begin at an angle. Slant rigs allow the borehole to achieve a horizontal trajectory at a much shallower depth (Figure 8).

When conventional vertical rigs are used, the well is drilled vertically beginning at ground surface to a planned depth. Once reaching this planned depth, termed the kickoff point (KOP), directional tools above the bit allow the wellbore inclination to be built to the desired angle. The tools then maintain the fixed desired angle until reaching the desired true vertical depth (TVD).

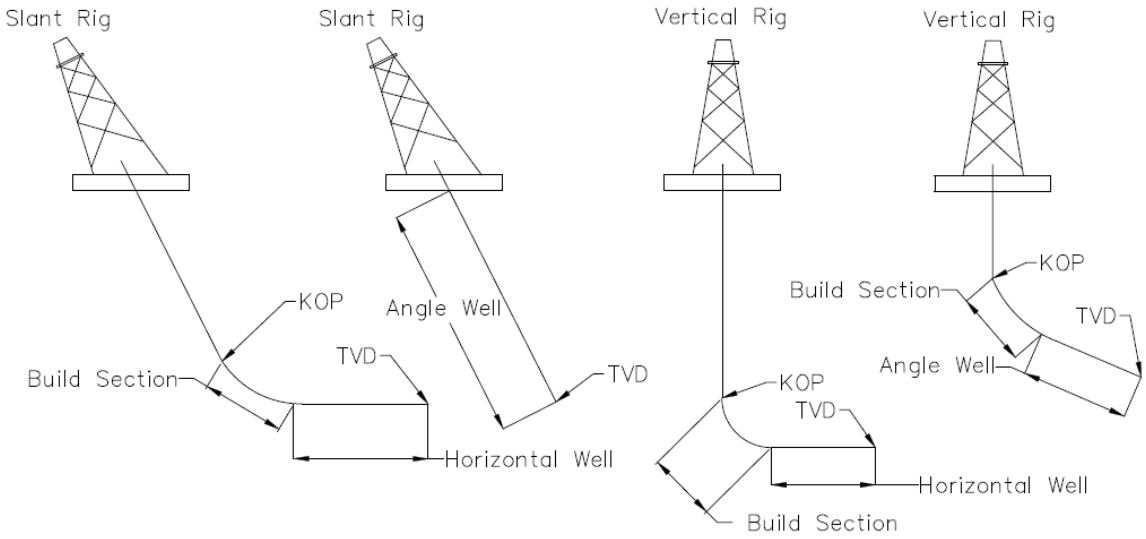

Figure 7. Rig and well types.

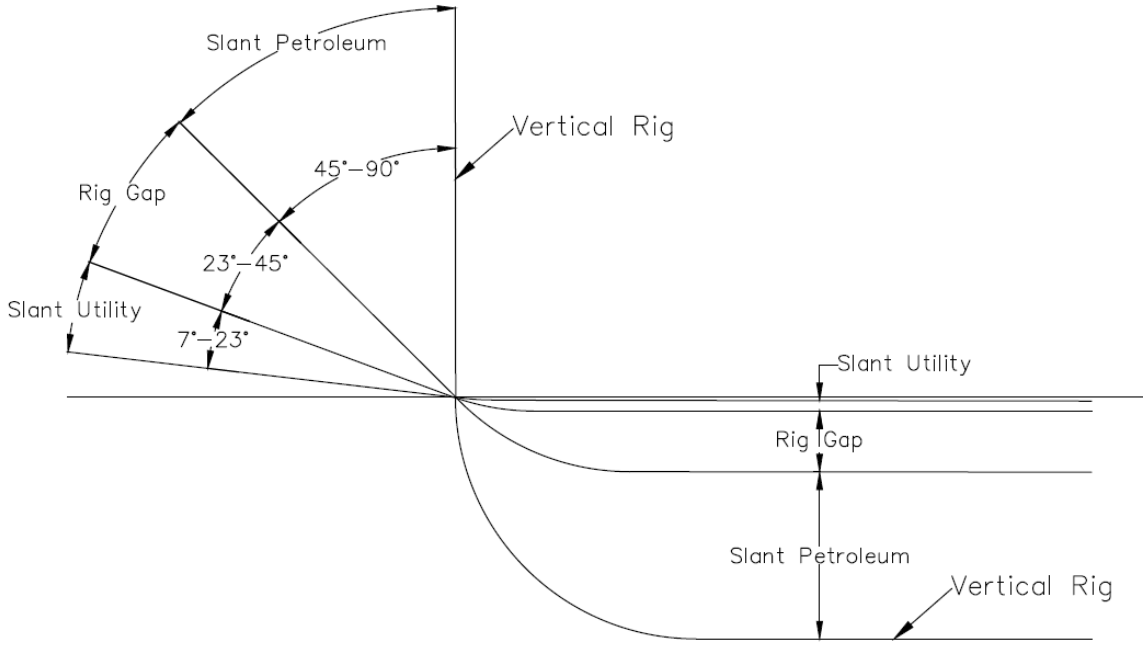

Figure 8. Slant rig entry angles. Note the advantage of slant rigs at reaching the horizontal plane at shallower depths.

Borehole Completion Type

For the placement of utilities, a continuous borehole is drilled. A continuous borehole has an entry and exit point at the land surface separated by some horizontal displacement; similar to a tunnel. Examples of continuous boreholes include river and road crossing in the utility industry. Continuous boreholes have been drilled for many shallow horizontal groundwater wells. Continuous boreholes are restricted to utility rigs. An opposing method is the blind borehole. A blind completion only has one intersection with the land surface. Blind completions are typical of water wells and petroleum wells.

Borehole Measures

Kickoff point (KOP) is the depth at which deviation begins, perhaps as early as the ground surface (Figure 9). Build rate or radius of curvature is used to describe the rate at which the borehole inclination angle is changed (Figure 9). Directional tools allow the wellbore to be steered to increase inclination angle or change direction; both can also be done simultaneously. The rate at which the inclination angle or azimuth can be altered depends upon the drilling technology used and diameter of the hole. This is referred to as the turning radius, or radius of curvature (ROC). The rate at which the angle is changed is limited by the capabilities of the downhole tools for the given borehole size. A general rule of thumb is to allow 100 feet of turning radius per inch of borehole diameter. For example, a 12 inch wellbore requires a 1,200 foot turning radius (radius of curvature). While this is the general rule of thumb, this is a conservative radius, with much tighter radii commonly drilled.

Another prevalent term describing horizontal wells is true vertical depth (TVD) which simply refers to the vertical depth reached by the well. Horizontal displacement, reach, throw, departure, and step-out are complementary terms. These terms refer to the total distance that a wellbore has traveled from the initial surface location to some other point on the surface directly above the borehole.

The term measured depth (MD), or measured length refers to the total length of the borehole. For a vertical borehole, MD would nearly equal TVD. For horizontal wells, MD would be significantly greater than TVD.

An additional term to describe horizontal drilling is step-out ratio which was defined originally as the horizontal departure divided by TVD, but more recently has been defined as MD/TVD (Jerez et al., 2013; Mason and Judzis, 1998). A step out ratio of greater than 1:1 or 2:1 is generally described as an extended reach well (Allen et al., 1997; Jerez et al., 2013). Directional drilling can be separated into categories based upon several factors as found in Table 3.

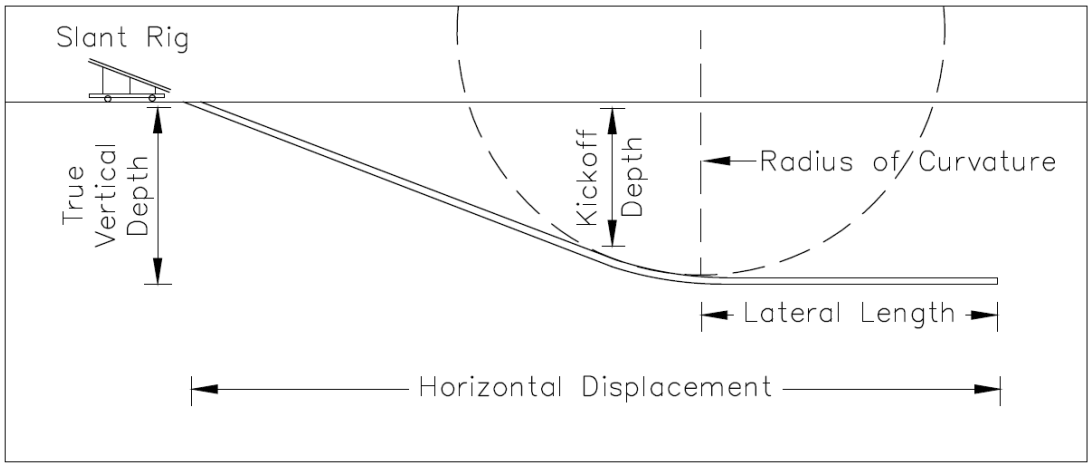

Figure 9. Cross section of a slant rig HDD well.

Table 3. Summary of directional well technology. Note these are generalities and do not constitute limits of all systems available; turning/reach capabilities are dependent several factors where these presented represent perhaps an 8" hole.

Rig Type	Work Type	Entry Angle, Degrees Below Horizon	Feet		Max Diameter in inches	
			TVD	Horizontal Reach	Hole	Casing
Slant	Utility	7-23	< 800	< 8,000	60	40
	Petroleum	45-90	< 4,000	< 4,000	17.5	14
Vertical	Water, Petroleum	90	20,000+	20,000+	17.5	14

Feet	
Radius of Curvature	
Short	2-6
Medium	300-900
Long	1,000-3,000

Historical Perspective

The earliest horizontal wells were qanats (karez, falaj, foggara) which have been in existence for over 2,500 years (Cech, 2009; Lightfoot, 2000; Tamburrino, 2010). The typical qanat is five to ten miles in length and ten to several hundred meters deep (Cressey, 1958). These wells are constructed in sloping terrain where a hand dug passage intersects the ground surface (Wulff, 1968). The horizontal tunnel is usually only large enough for the laborer. Water in the tunnel typically flows six inches to a foot deep, at a rate of a few miles per hour (Cressey, 1958). Vertical shafts intersect the horizontal tunnel every 50 to 100 meters for ventilation and material extraction (English, 1968). Qanats produce water at rates of several thousands of gallons per minute and are still in use today, especially in the Middle East, see Figure 10 (Motiee et al., 2006).

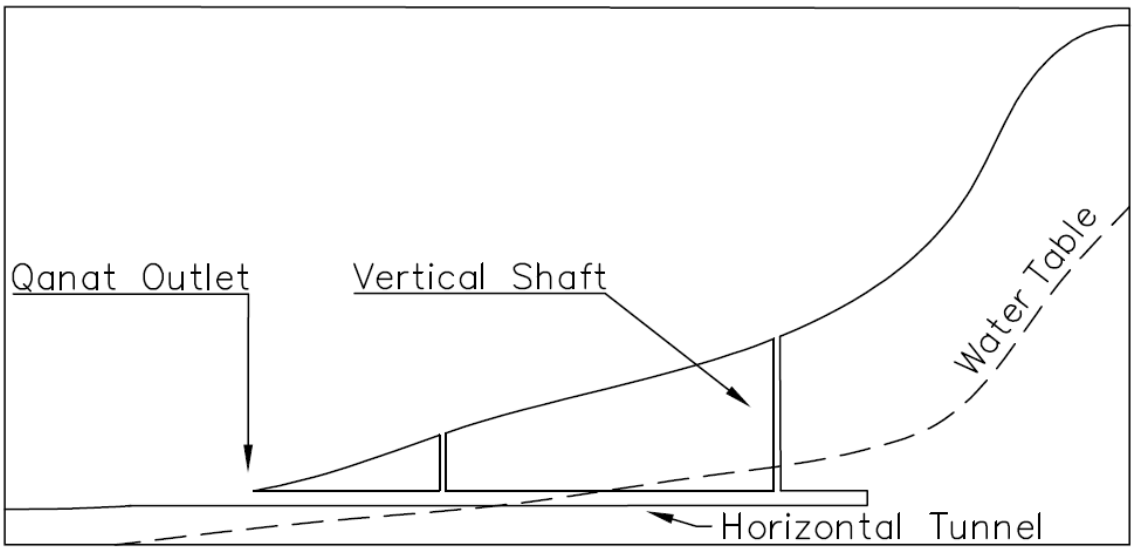

Figure 10. Cross section of a qanat.

Infiltration galleries and adits are similar to qanats. Infiltration galleries and adits were widely used in the 19th century (Hardcastle, 1987). The adit is a horizontal tunnel used to increase well production or dewater mines. Infiltration galleries are constructed along rivers where shallow open trenches (collector wells) are dug and then backfilled with filter material (Williams, 2008). These horizontal collector wells are then intersected by a vertical shaft to extract the water.

The next horizontal well innovation originated in the petroleum industry with Leo Ranney in the 1920s (Hardcastle, 1987; Hunt, 2002; Hunt, 2003). These Ranney wells were constructed with a large diameter (40 feet wide), vertical (70 feet deep), central caisson with various collector wells (16 collectors, 950 feet in length) emanating from the central caisson (Hunt, 2003). It was noted that vertical wells took several years to produce what the Ranney well could produce in only six months (Hunt, 2003). The entire system resembling the spokes of a bicycle wheel (L Espoir, 2003).

Ranney well technology was transferred to water wells upon a deflation of petroleum prices. The first Ranney water well (horizontal collector well) was constructed in London, 1933 (Hardcastle, 1987; Hunt, 2002). Most horizontal collector wells are located near surface waterbodies to induce infiltration into the aquifer and thereby achieve source water treatment (Figure 11). This natural treatment of surface water is referred to as river bank filtration (Spiridonoff, 1964).

Typically, the central caisson is 3-6m in diameter and sunk into the ground less than 46m (Hunt, 2002), although one such caisson has been sunk to 61m depth (Spiridonoff, 1964). Collector wells are jacked into the aquifer from the caisson (Hunt,

2002; Moore, 1995). Two or more collector wells may emanate from each caisson, with each collector roughly 30cm in diameter and 60m in length (Hunt, 2002; Spiridonoff, 1964). As of 2003, there were about 250 horizontal collector wells in the United States producing up to 28,000 gallons per minute (Hunt, 2003; Moore, 1995).

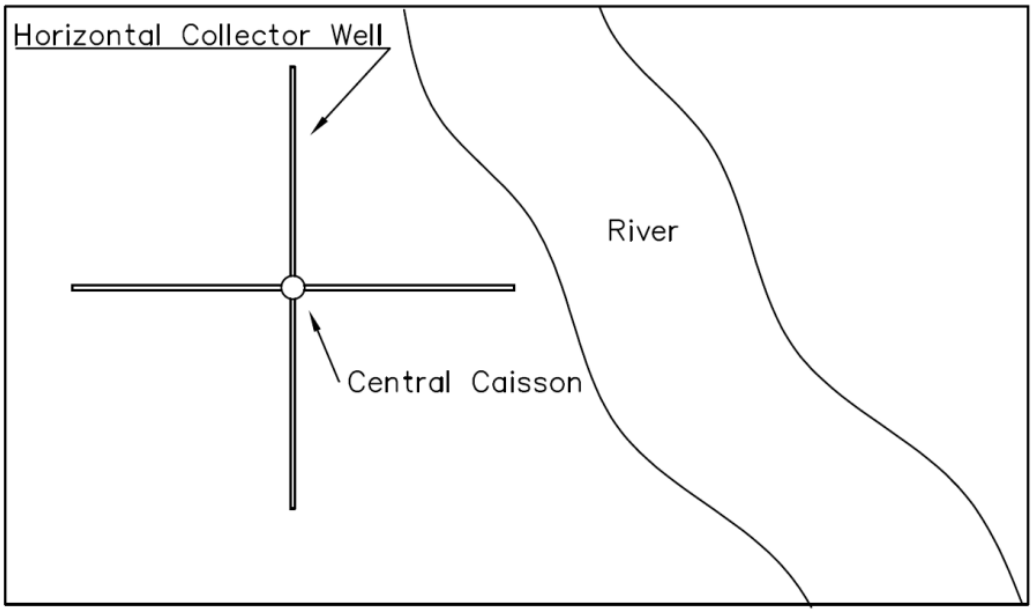

Figure 11. Plan view of a Ranney Well.

The next horizontal well innovation occurred in the petroleum industry with directional drilling. Directional drilling occurs when a drill is maneuvered from a starting angle (vertical or slated) and then steered into another direction. The first directional well was constructed in 1929 (King, 1993; Morgan, 1992). H. John Eastman has received major recognition for his early directional technology work in 1934 to control an ablaze petroleum well near Conroe, Texas (Thompson, 1979; Wells, 2006). A vintage schematic of Eastman's work can be seen in Figure 12.

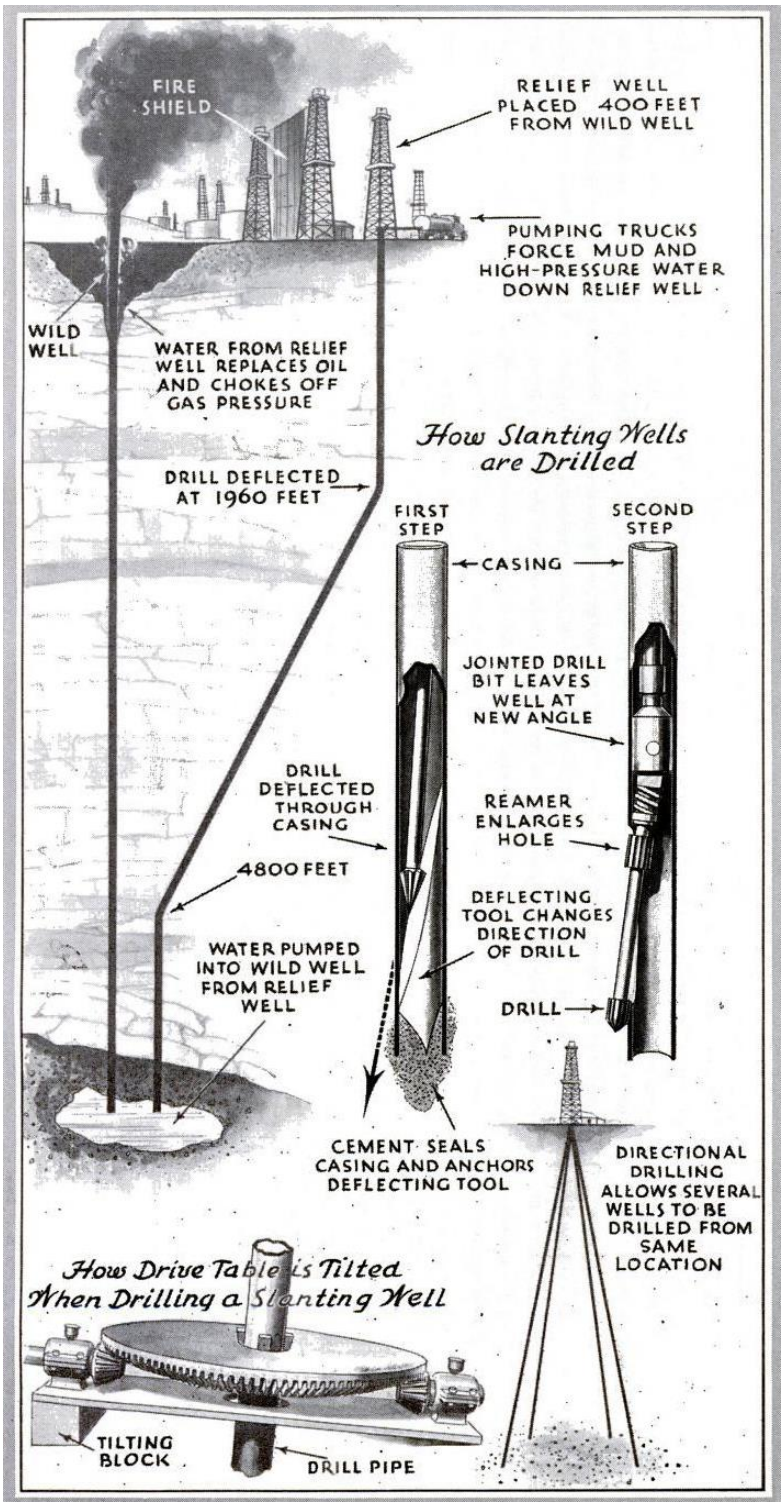

Figure 12. Killing the Conroe well, an early form of directional drilling. Reprinted from Gleason (1934).

Interestingly, mechanical borehole deviation methods were originally developed to ensure vertical boreholes were drilled plumb (Gleason, 1934). Not until the invention of the single shot (borehole tracking technique) was it realized that wells may have accidently traveled several hundred feet horizontally (Gleason, 1934). Early single shots were typically accomplished via acid etching or photographing a compass and split-bubble while down hole (Killeen et al., 1995; Short, 1993).

Directional drilling was transformed again in the mid-1950s through 1970s with the use of bent-sub housing (steerable) downhole motors, measurement while drilling, and slant rigs (Downton et al., 2000; Thompson, 1979; Wells, 1955; Williams, 2008). While mud motors had been originally developed in the 19th century, coupling this technology with a bent sub-housing allowed for directional control (Downton et al., 2000; Warren, 1998; Wells, 1955). Figure 13 depicts a bent-sub downhole mud motor operating in two modes, sliding and rotating.

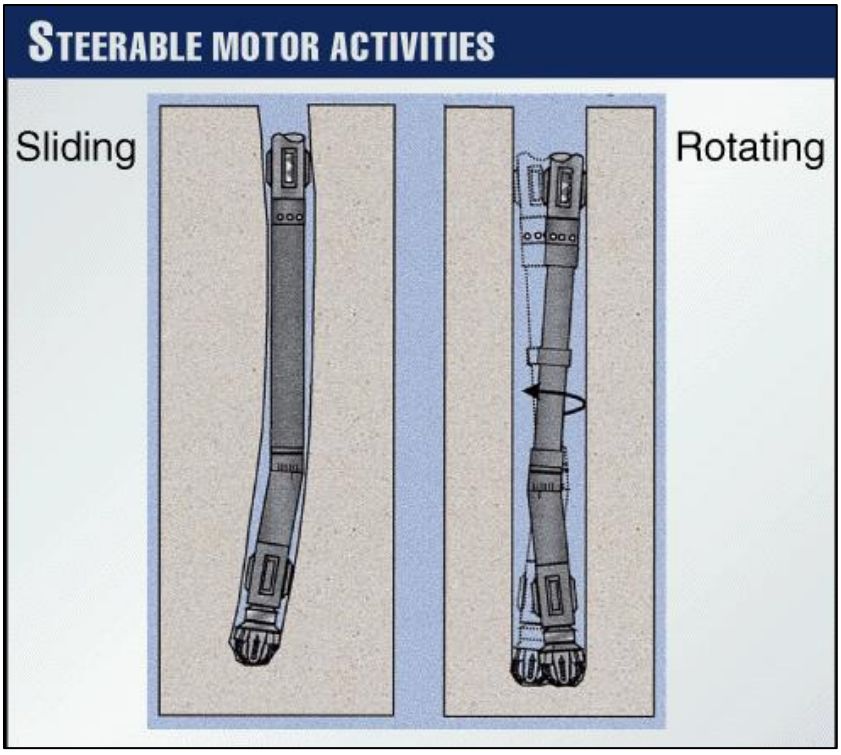

Figure 13. Mud motor with bent-sub operating in a sliding and a rotating mode (Warren, 1998). Reprinted by permission.

Martin Cherrington is credited with developing slant rig innovations which led to the extensive use of directional drilling for utility boring (Hashash et al., 2011). The first major use of Cherrington's shallow directional drilling technology came in 1971 to cross underneath a California river (Allouche et al., 2000; Williams, 2008). Shallow petroleum applications (500-800m TVD) used slant rigs and directional equipment beginning in the late 1970s to extract gas and heavy oil in Alberta, Canada (Hart and Jankowski, 1984; Rushford, 1993). Modern petroleum slant rigs typically operate at depths of 600 ft TVD or greater (Dean, 2001).

Modern horizontal drilling was used for petroleum production beginning with research and development by Elf Aquitaine in conjunction with the Institut Francais du Petrole in the late 1970s and early 1980s (Giger et al., 1984). General commercial viability of petroleum horizontal drilling was proven in the early to mid-1980s (King, 1993). Major improvements in directional drilling occurred during the 1980s with better steering and downhole monitoring equipment (Allouche et al., 2000).

Coiled tubing was originally developed for petroleum well maintenance in the 1960s (King, 1993). In the early 1990s, coiled tubing drilling began as a new method to drill both vertical and directional holes (Leising and Newman, 1993). Coiled tubing methods rely on rope-like, flexible drill pipe stored on a roll (King, 1993). Coiled tubing drilling has been used extensively in Prudhoe Bay and other places where underbalanced drilling is necessary to avoid formation damage (Dupriest, 2013). However, it is limited to fairly soft formations because higher weight on bit buckles the coiled tube. Currently, coiled tubing drilling is expensive and has limited application for new borehole creation, but remains useful in well servicing and reentry.

The latest development in directional drilling has again come from the petroleum industry with the advent of rotary steerable systems (RSS) in the mid to late 1990s (Stuart et al., 2000; Warren, 1997). This system allows the drill string to continue rotating while the bit is directionally controlled (Allouche et al., 1998; Downton et al., 2000; Warren, 1997; Warren, 1998). This is an advantage over previous mud motors (Figure 13) which are in either a sliding or rotating mode (Downton et al., 2000; Warren, 1997; Warren, 1998). To change direction with a traditional mud motor, drill string

rotation is stopped and the bend in the motor is oriented in the direction one wants to steer. When the drill pipe is not rotating, sliding friction is high and the drill rates are much lower. The ability of the RSS to be steered while rotating reduces wellbore friction on the drill string, thereby increasing the rate of penetration. More importantly, the reduced friction allows wells to be drilled to greater distance and with more directional control (Andreassen et al., 1998; Warren, 1997; Warren, 1998).

The use of horizontal drilling has increased substantially in the petroleum industry over the last twenty years (Figure 14 & Figure 15). Most petroleum rigs were drilling vertical wells until 2009. Since 2009, horizontal drilling has been most common. Currently over half of all active petroleum rigs are drilling horizontal wells (Baker Hughes, 2014; Rig Data, 2014).

It is important to understand the current limitations of horizontal wells. Plots depicting true vertical depth versus horizontal reach for petroleum wells in the *Worldwide Extend Reach Drilling Database* are provided courtesy of K&M Technology Group (Figure 16 - Figure 18). In the petroleum industry, these plots are referred to as dog-nose plots or nose plots. These plots are useful for understanding the relationship between TVD and horizontal reach. Step out ratios (TVD : horizontal reach) may be used to characterize the reach type of horizontal wells (low – medium – extended – very extended). However, as seen in these plots the characterization of reach type may also be derived from the number of wells drilled in a certain TVD to horizontal reach zone.

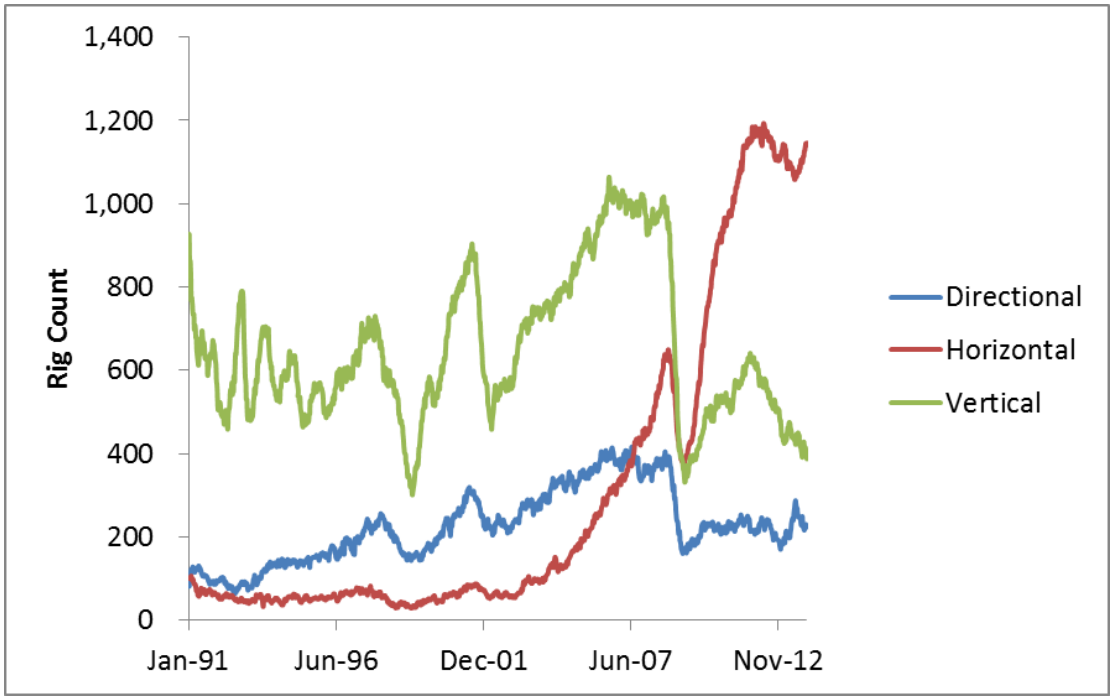

Figure 14. North American petroleum rig count from 1991 to 2013 categorized by well type. Data from Baker Hughes (2014).

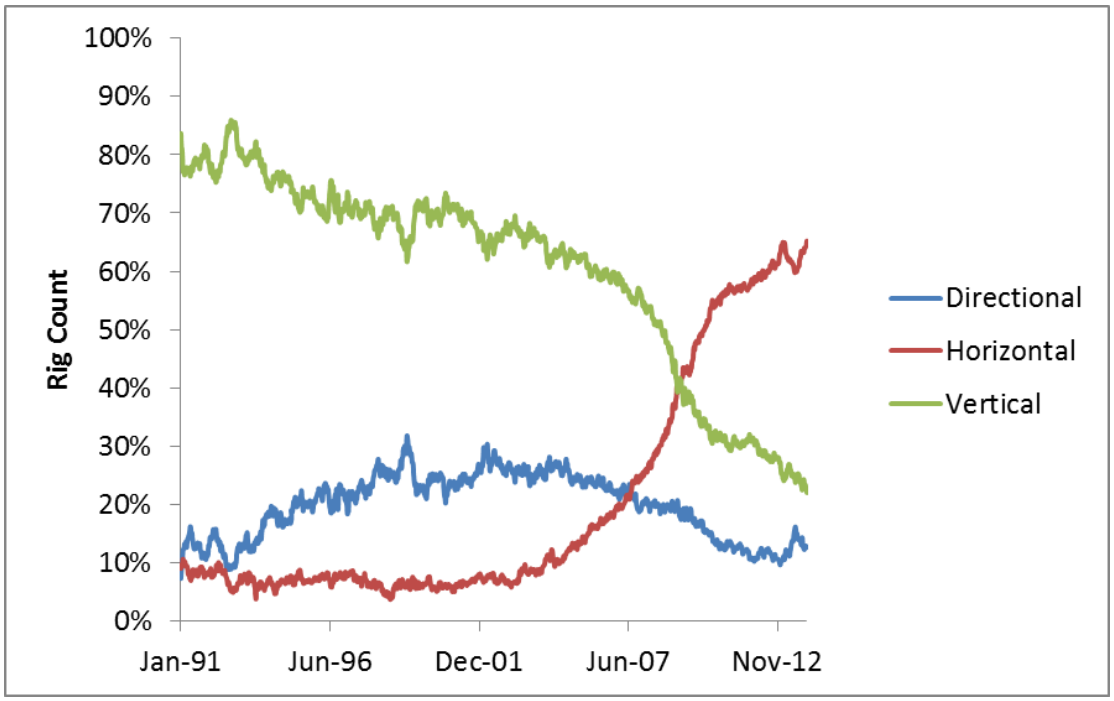

Figure 15. North American petroleum rig count percentages from 1991 to 2013 categorized by well type. Data from Baker Hughes (2014).

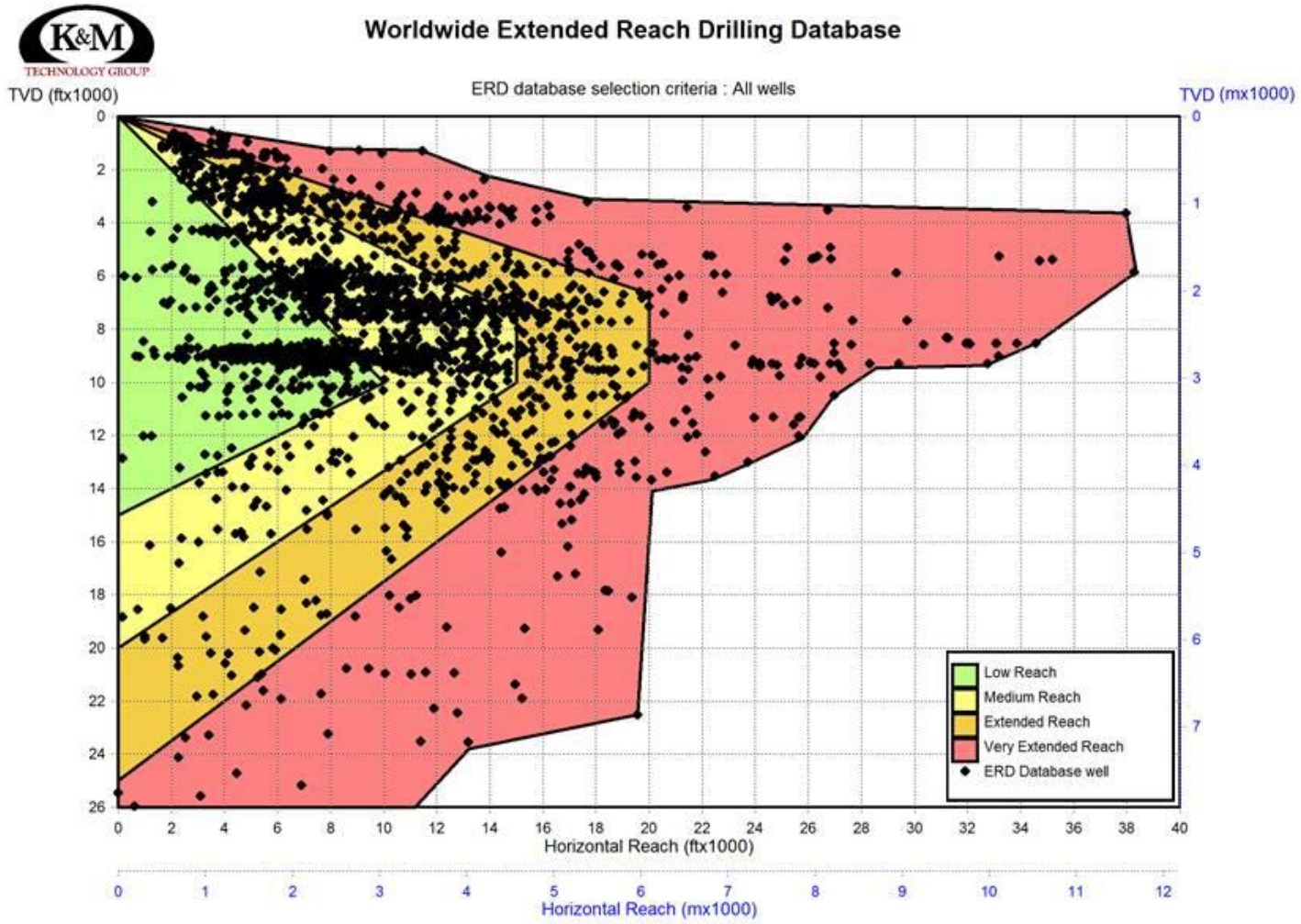

Figure 16. Worldwide Extended Reach Drilling Database, all wells.
Reprinted courtesy of K&M Technology Group (K&M Technology Group, 2013).

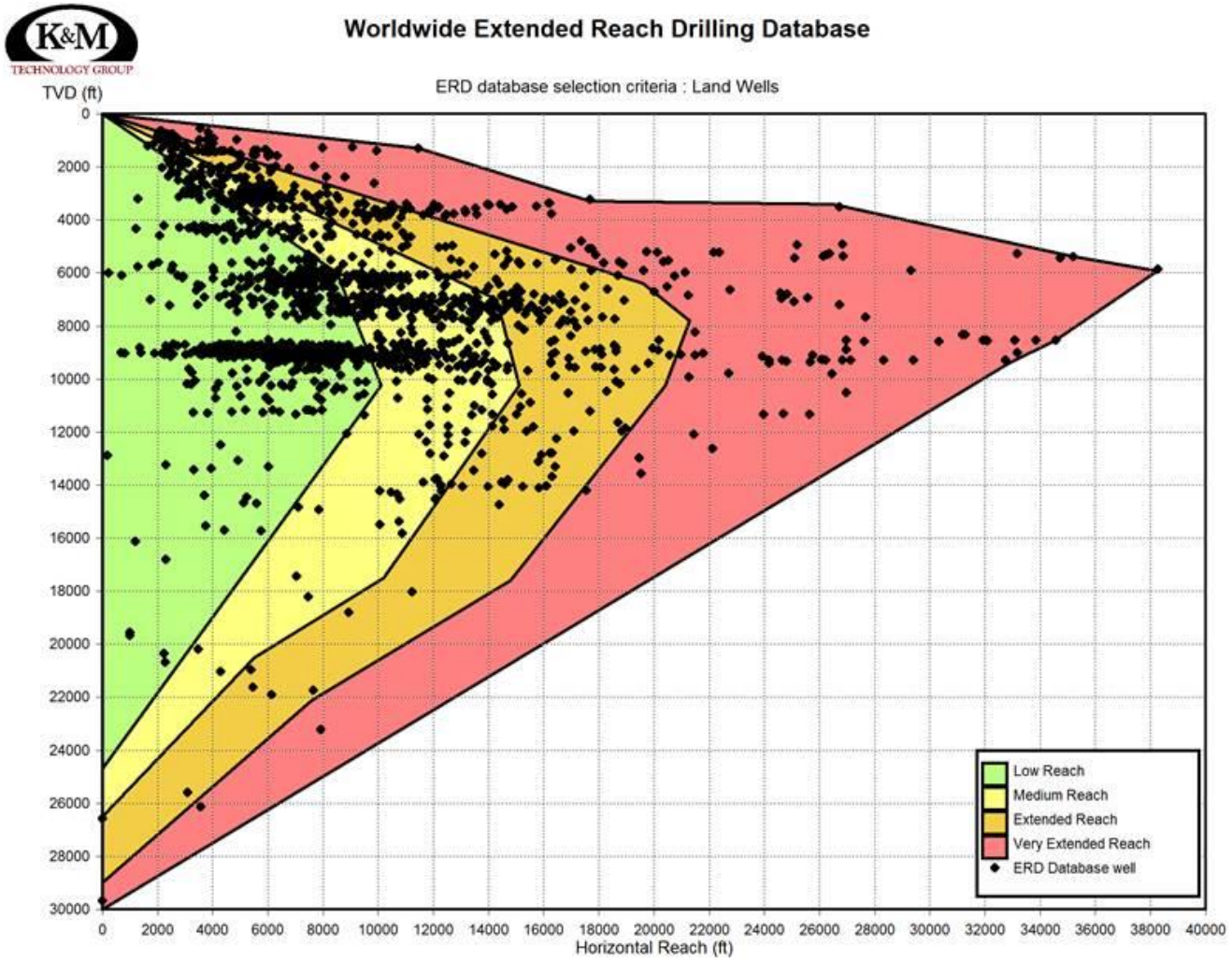

Figure 17. Worldwide Extended Reach Drilling Database, all land wells.
Reprinted courtesy of K&M Technology Group (K&M Technology Group, 2013).

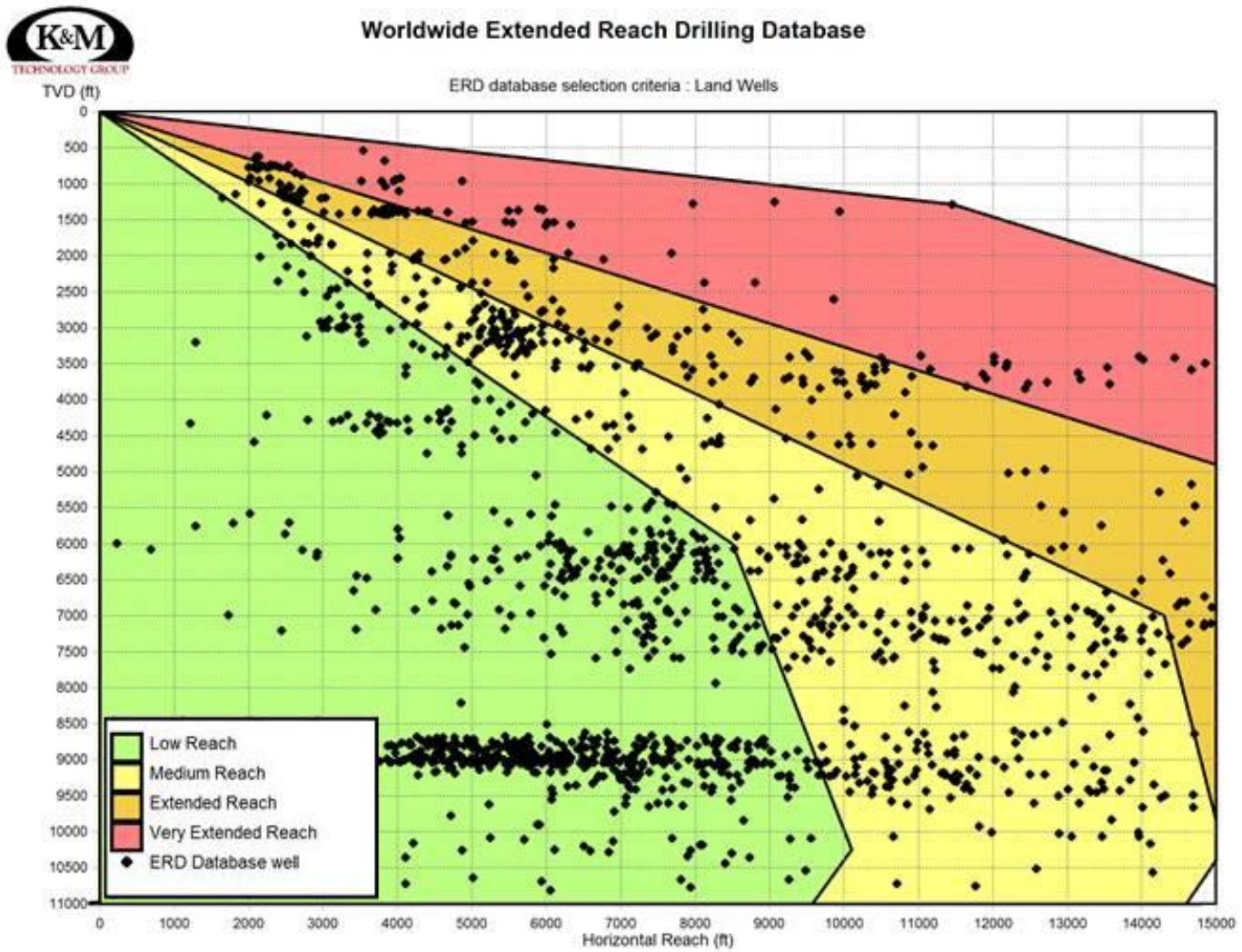

Figure 18. Worldwide Extended Reach Drilling Database, all shallow land wells. Reprinted courtesy of K&M Technology Group (K&M Technology Group, 2013).

Refocusing on groundwater wells, the first directionally drilled environmental remediation well was constructed in 1988 at the U.S. Department of Energy, Savannah River Site to remediate volatile-organic contaminants (Denham and Lombard, 1995; Wilson et al., 1993). Directional wells became popular for groundwater remediation as they allowed greater access to contaminants at a competitive cost benefit compared to vertical wells (Karlsson, 1993; Parmentier and Klemovich, 1996). Kaback (2002) is the last publication of the horizontal environmental well catalog series, which had been updated since Wilson et al. (1993). Graphical summaries of data from Kaback (2002) can be found in Figure 19 - Figure 21.

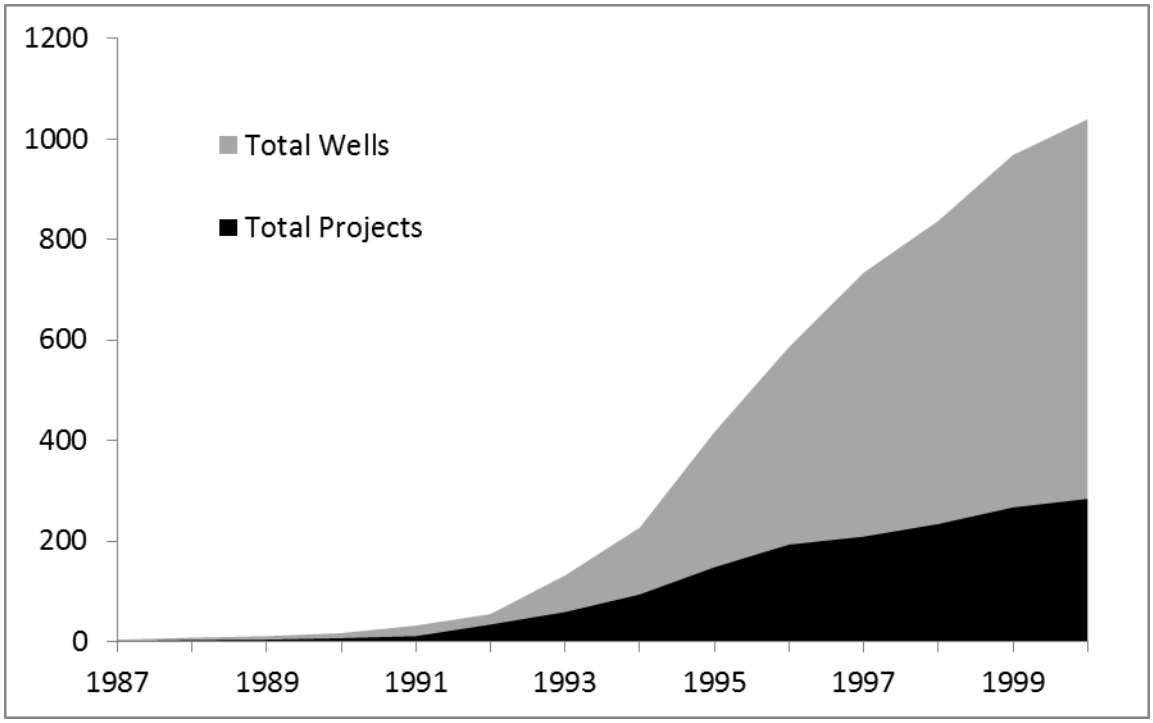

Figure 19. Horizontal environmental wells through 2000. Data from Kaback (2002).

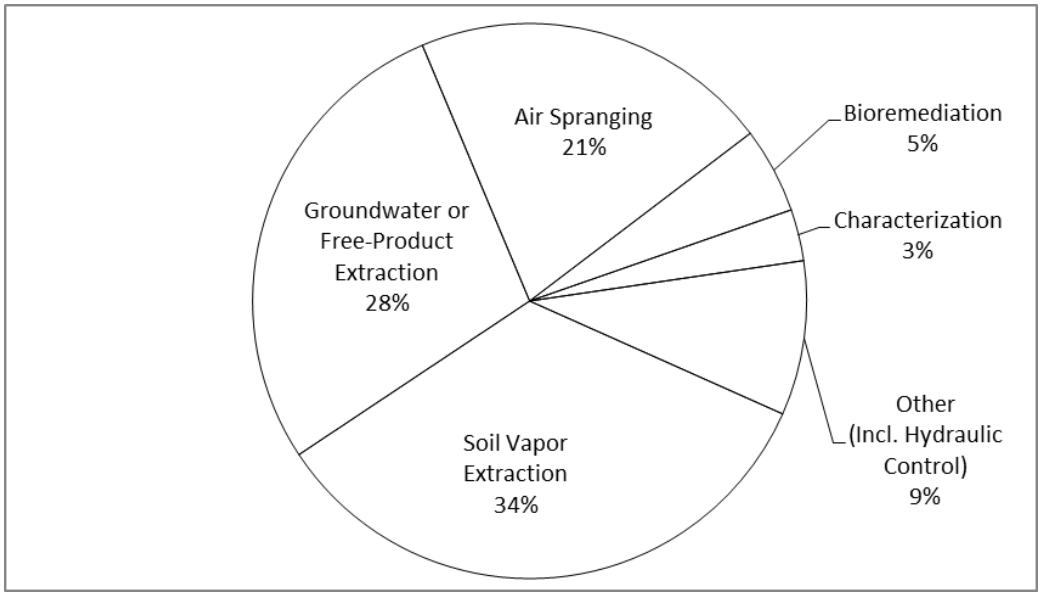

Figure 20. Horizontal wells for various environmental purposes. Data from Kaback (2002).

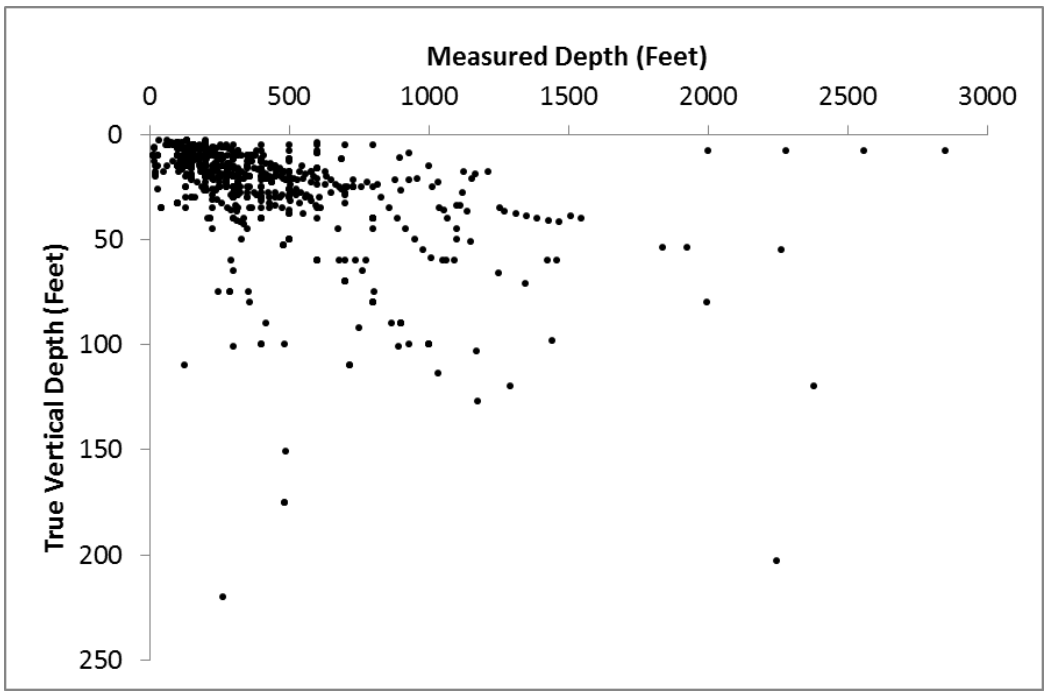

Figure 21. Nose plot of horizontal environmental wells. Data from Kaback (2002); reprinted from Moore (2013). Note total well length is on the *x*-axis, not horizontal displacement. Some data screening for quality control has occurred.

The latest use of directional drilling technology has been for water supply production. The first directional groundwater well dedicated to water supply production was constructed in 1998 for Des Moines, Iowa (Bardsley, 2001; Rash, 2001). Since 1998 there have been several additional HDD water supply wells. Two wells in the Denver area and several in California (Jehn-Dellaport, 2004; Williams, 2008).

Directional Groundwater Well Case Studies

Not counting Ranney wells, the use of horizontal water supply production wells has been very limited. The directional case studies below outline major projects found in the literature. However, it is possible for some undocumented cases to remain so. As previously mentioned, the use of horizontal wells in the environmental sector include pump and treat operations which closely resemble water supply production wells. A few examples of these environmental wells are incorporated here to give more information regarding directional groundwater wells.

Directional Wells for Water Supply Production

Des Moines, Iowa (1998)

Des Moines, Iowa is the site of the first horizontal, dedicated water supply well (Bardsley, 2001). The well was a pilot project, completed as a continuous borehole along the Raccoon River to function as a river bank filtration system (Bardsley, 2001). Drilling was completed by A&L Underground, with Des Moines Water Works designing the well (Rash, 2013). The well was constructed at 30 feet TVD with a screened section of 1,220 feet, Figure 22 (Bardsley, 2001; Rash, 2001). Baroid drilling mud was used (Subsurface Technologies Inc., 2013).

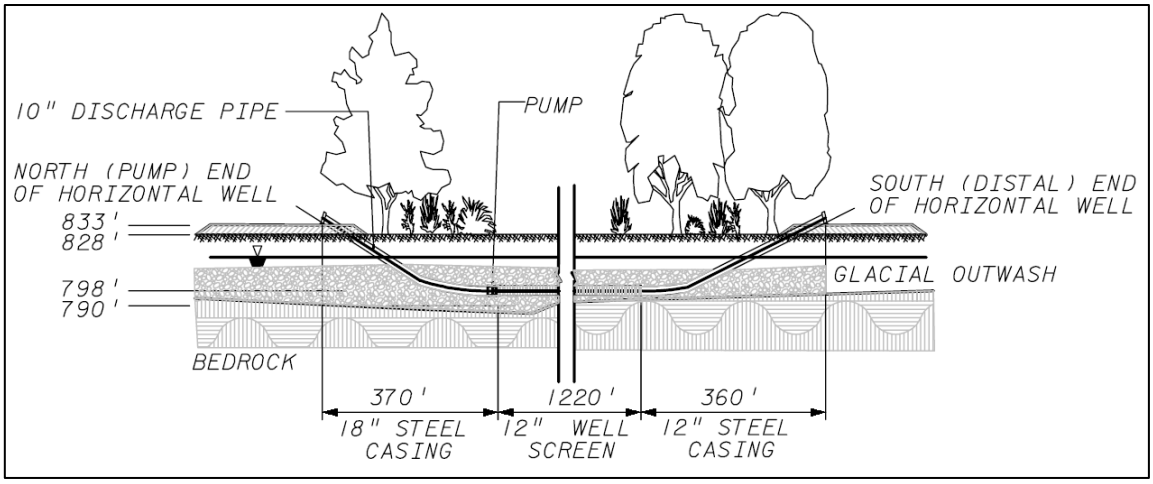

Figure 22. Horizontal groundwater well along the Raccoon River, Des Moines, Iowa; from Rash (2001). Reprinted by permission. Copyright © 2011 the American Water Works Association.

Initially the well was developed using sodium acid pyro phosphate, gas injection, and pumping, yet the production rate of 800 gallons per minute (GPM) persisted which was 1,200 GPM below expectations (Rash, 2013). It was not until Aqua Freed ® used 60 tons of carbon dioxide to develop the well that the production rate increased to 1,800 GPM (Subsurface Technologies Inc., 2013). Development was the most difficult task of the entire well construction process and is the chief limiting factor to further construction of directional wells (Rash, 2013).

To calculate expected yields, Rash (2001) used an equation by Beljin and Losonsky (1992) which was altered from Joshi (1988). This equation was developed for confined aquifers; this well was in an unconfined aquifer. Rash (2001) used justification from Driscoll (1986) that if unconfined drawdown was small compared to aquifer thickness, then reasonable applicability between unconfined equations and confined equations existed. Rash (2001) calculated that at four feet of drawdown, the 1,220 foot

well would produce 2,000 GPM. Upon well completion, it was determined that required drawdown was greater than that calculated, but not significantly (Rash, 2001).

More recently the well has produced on average 917 GPM (Hubbs, 2006). Such a decrease in yield was expected as the well ages (Rash, 2013). The well has not been redeveloped. There have been no problems with the horizontally placed pump or motor, although it should be noted that centering chocks were used (Figure 23). The submersible pump used is a two stage Ingersoll-Dresser Model 12HH220 with a Pleuger/Ingersoll-Dresser 50 horsepower Model M10 electric motor (Rash, 2001).

Figure 23. Submersible pump used for a horizontal well along the Raccoon River, Des Moines Iowa. Reprinted from Rash (2013).

The Des Moines Water Works also operates eight Ranney wells (Rash, 2013). Interestingly, a Ranney well utilizing the same aquifer as the directional well has

comparable yields. The Des Moines Water Works recently constructed two Ranney wells with a one mile transmission main at a cost of $5.2 million (Rash, 2013). The cost of the HDD well is not presented because of extensive R&D costs in addition to a low bids secure the contract (Rash, 2013).

Antelope Hills, Bennett, Colorado (2002-03)

Bennett, Colorado is the site of the first deep directional groundwater well. The well was completed as a blind borehole at a TVD of 1,000 feet and horizontal reach of 2,100 feet, Figure 24 (Jehn-Dellaport, 2004). Water Drilling Inc. of Denver was the drilling contractor, and Schlumberger was the directional service company providing technology, equipment, and technicians to complete the directional components (Jehn-Dellaport, 2013). Ms. Jehn-Dellaport was the consultant for this project.

The saturated screen length for vertical wells in this formation is 265 feet, whereas this directional well achieved 680 feet of saturated screen length (Jehn-Dellaport, 2004). The well utilized a 4.5" X 6" dual pre-packed screen, and has been successfully tested at 83 GPM (Jehn-Dellaport, 2004). A bentonite polymer mud was used, the only type allowed for water well drilling in Colorado (Jehn-Dellaport, 2013). The well was drilled using traditional mud rotary techniques.

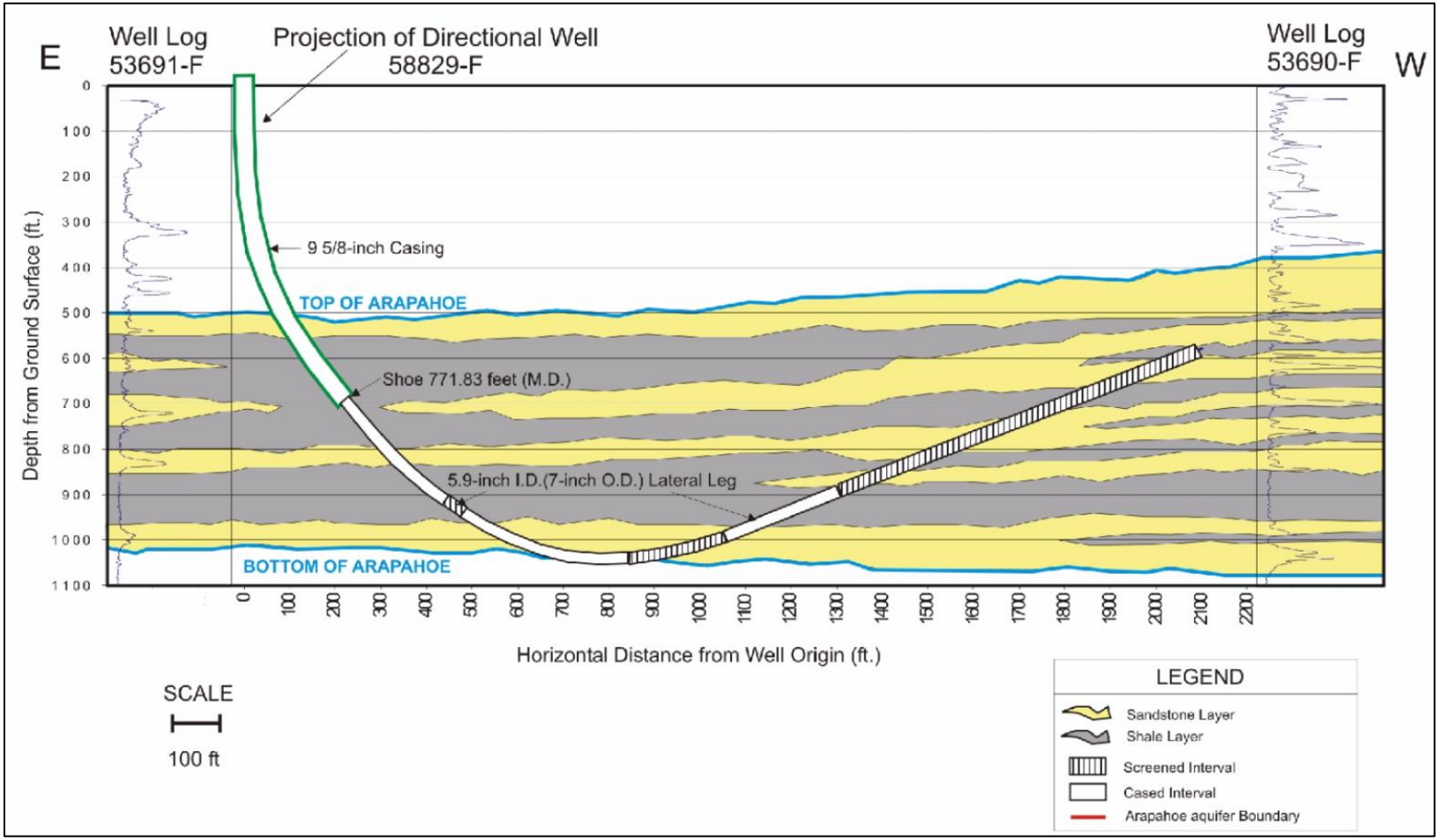

Figure 24. Directional groundwater well in Antelope Hills, Bennett, Colorado.
Reprinted from Jehn-Dellaport (2013).

The rig used for this project was an old oil rig with 300,000 lbs of pullback (Jehn-Dellaport, 2013). The mud pump capacity was large; however the exact specifications have been lost. Given the fact that this was an old oil rig with such a large pullback capacity, max rated MD on the rig was likely over 10,000 feet. While the rig was large enough for the job, it had numerous breakdowns which significantly increased drilling time (Jehn-Dellaport, 2013). This well took over a month to drill and a couple of days to complete. Pictures of the pre-packed screen and rig may be seen in Figure 25 & Figure 26 respectively.

Figure 25. Antelope Hills pre-packed screen.
Reprinted from Jehn-Dellaport (2013).

Figure 26. Antelope Hills directional groundwater well rig.
Reprinted from Jehn-Dellaport (2013).

The most difficult problem during construction of this well was development (Jehn-Dellaport, 2013). This was because no one had completed a well like this before in addition to developing through the pre-packed screen. The development time was significantly greater for this directional well than nearby vertical wells and included jetting, airlifting, and chemical additives (Jehn-Dellaport, 2004). Unfortunately, none of the development methods worked very well (Jehn-Dellaport, 2013). In 2010 there was a

proposal to redevelop the well with a new tool provided by Halliburton, but work never commenced (Jehn-Dellaport, 2013).

A directional well design was chosen because the aquifer was thin and therefore traditional vertical wells would not be cost effective (Jehn-Dellaport, 2004). Costs for drilling directional wells are suggested to be 1.5-3 times more expensive than vertical wells (Jehn-Dellaport, 2004). The final cost for the well was $509,000 which did not include the pump (Jehn-Dellaport, 2013). To this day the well has remained abandoned.

Castle Pines North Metro District, Colorado (2004)

Castle Pines, Colorado is the site of the second deep directional water supply well. This directional well was completed to a TVD of 2,100 feet and a horizontal reach of 1,800 feet (Figure 27). This directional well intersected a vertical well to maximize production. It was determined that the production rate for this well would require a greater than 350 hp for the pump / motor (Jehn-Dellaport, 2013). Ms. Jehn-Dallaport found that such large pump / motor units set in horizontal wells were being replaced every six months in the petroleum industry because the pumps orientation was non-vertical (Jehn-Dellaport, 2013). It was estimated that this well would require a 750 hp unit at an estimated cost of $250,000. Therefore continual pump replacement would be uneconomical and therefore vertical pump orientation was required (Jehn-Dellaport, 2013).

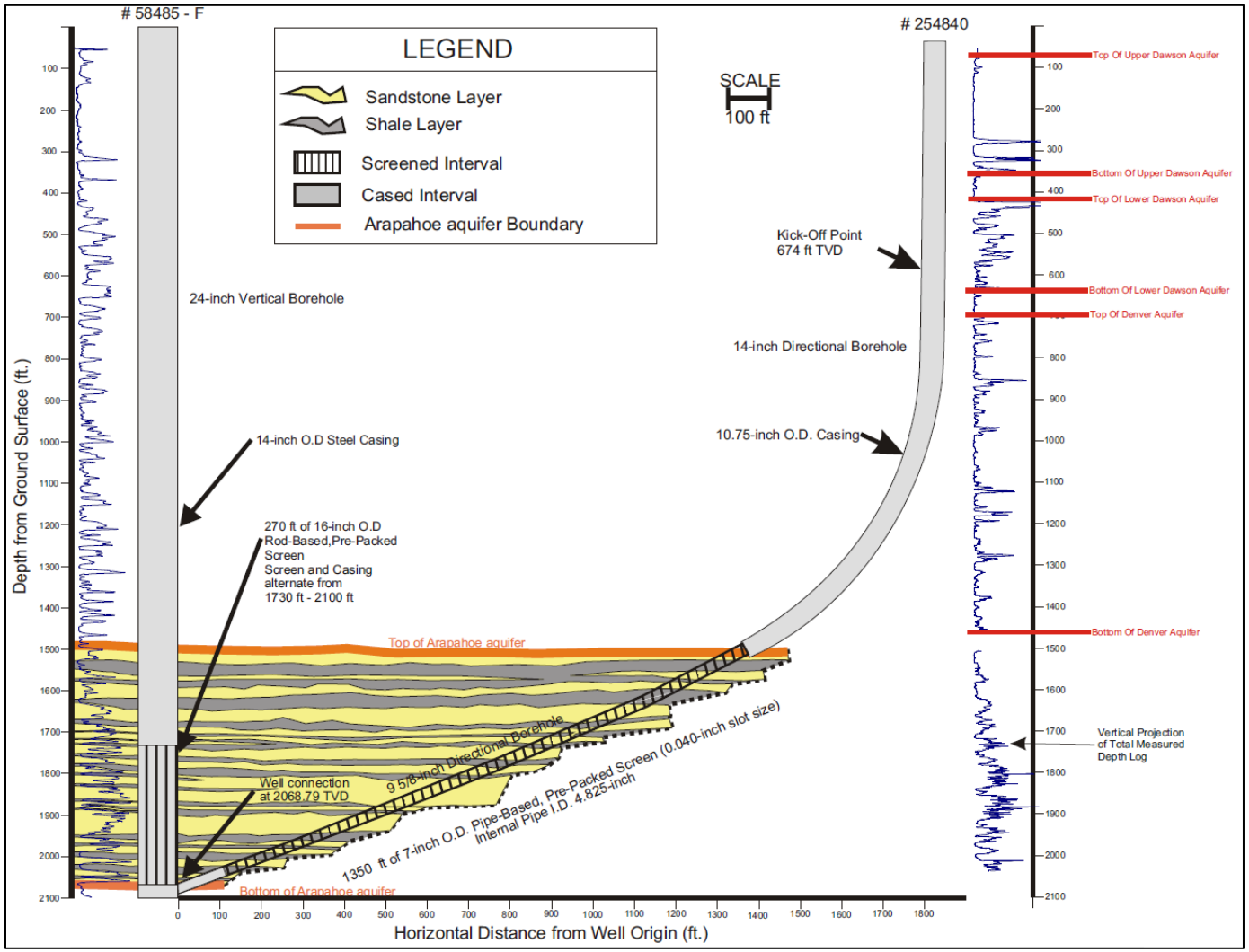

Figure 27. Directional groundwater well in Castle Pines North Metro District, Colorado. Reprinted from Jehn-Dellaport (2013).

This directional well was drilled by Beylik Drilling Company using a 280 Challenger rig (at a day rate of $14,400) with Ms. Jehn-Dallaport consulting (Williams, 2008). Halliburton's Sperry Drilling Services provided mud motors and steering technology (Williams, 2008). Schlumberger completed borehole logging and Layne Christensen developed the well (Williams, 2008). The expected production rate was 2,000-3,000 GPM at total cost at $2 million (Jehn-Dellaport, 2013). Two vertical wells constructed in the same aquifer produced at a combined rate of 950 GPM and at a combined cost of $1.5 million (Jehn-Dellaport, 2013). This cost comparison reveals the potential advantages of directional wells for water supply production.

The greatest challenges for this project were borehole stability and well development (Jehn-Dellaport, 2013). For future projects, a larger drill rig (200,000 lb. pullback instead of 110,000 lbs.), and triplex mud pumps instead of duplex pumps were suggested (Williams, 2008). The rig used was so undersized that many extra services had to be called in such as cranes and casing installers (Jehn-Dellaport, 2013). Total drill time was six weeks with a couple of days for completion. Pictures of the rig may be found in Figure 28 & Figure 29.

Figure 28. Castle Pines North Municipal District directional groundwater well rig. Reprinted from Jehn-Dellaport (2013).

Figure 29. Castle Pines North Municipal District directional well rig in snow. Reprinted from Jehn-Dellaport (2013).

Currently, the well has a connection issue between the vertical well and intersected directional well that requires additional work (Jehn-Dellaport, 2013). The well has remained abandoned. When asked about major hurdles to directional wells for water supply wells, Ms. Jehn-Dallaport cited high costs and unproven increases in production capacity (Jehn-Dellaport, 2013).

Directional Environmental Wells

Savannah River Site, Aiken, South Carolina (1988-1991)

Savannah, South Carolina is the site of the first directionally drilled environmental wells. Seven wells were drilled to investigate the use of directional drilling technology for groundwater contamination treatment (Denham and Lombard, 1995). The technology investigated included short radius petroleum, modified petroleum, and utility river crossing rigs (Denham and Lombard, 1995).

Williams Air Force Base, Chandler, Arizona (1992)

Chandler, Arizona is the site of the deepest HDD environmental well at 235 feet TVD (Bardsley, 2001). The well was a pilot study investigating horizontal versus vertical well treatment of a liquid fuels groundwater plume (Oakley et al., 1994). A three-dimensional finite element model (DYNFLOW) was used to evaluate the horizontal well (Oakley et al., 1994). The horizontal well was installed using a utility HDD river crossing rig. Two boreholes had to be abandoned due to difficulties. The borehole was drilled with a nine inch bit and then reamed to 18 inches. A 10.75 inch outside diameter, six inch inside diameter pre-packed screen was installed (Oakley et al., 1994).

Well Construction

Groundwater drinking supplies span from water table aquifers at the earth's surface to deep confined aquifers over a mile deep. Therefore, a combination of directional drilling technologies is necessary to exploit the resource. At shallow depths less than 800 feet, the use of slant utility rigs is necessary (Bardsley, 2001; Kaback, 1998). At greater depths, the use of oilfield drilling technology is necessary (Jehn-Dellaport, 2004; Williams, 2008). Both of these technologies construction techniques are described in tandem as either technology could be used for a directional groundwater well.

Drilling

The process of drilling involves several components that may or may not be used interchangeably. Directional drilling has three major components: subsurface entry angle, directional control, and wellbore measurements. These processes are then taken into consideration with mud control and well limitations.

Subsurface Entry Angle

Vertical entry drilling is most common for traditional oilfield and groundwater applications. Assuming equal radii of curvature, a vertical rig will require more TVD to reach the horizontal plane than a slat rig (Figure 8). The minimum TVD at which a vertical well can build angle to the horizontal plane is equal to the radius of curvature. Given the turning radius typically required (100' per inch of hole), vertical entry is only able to achieve a horizontal wells at target depths perhaps greater than 900 feet (nine inch hole) or 1,200 feet (twelve inch hole).

Slant / angle entry technology is most common for utility and environmental directional drilling applications, but also limited shallow petroleum applications. This method uses a slant rig to penetrate the ground surface at some angle off vertical. Utility rigs have limited entry angles from 7°-23° (90° being defined as vertical). Slant petroleum rigs fill this gap from the 45°-90°. However, slant petroleum rigs are rare and would therefore be very expensive to mobilize.

Directional Control

Drilling directional control equipment can take the form of five major technologies (Denham and Lombard, 1995; Devereux, 1999; Downton et al., 2000; Short, 1993; Willoughby, 2005):

Whipstocking was the first method used to deviate a vertical wellbore (Gleason, 1934). This method operates on the principle of using metal plates to deflect the bit (Short, 1993). A borehole is first drilled using typical rotary methods, then the drill string is pulled out and a whipstock inserted. Once the whipstock is inserted, drilling commences and is deflected upon contact with the whipstock. While this enables the well to be deviate, it does not allow continued control after side tracking. Whipstocking has facilitated the completion of short radius wellbores (Denham and Lombard, 1995).

Jetting is a process whereby a single bit nozzle with a very high velocity flow is oriented in the direction of desired deviation. The drill string enters a sliding mode so the flow erodes the formation in the direction of the nozzle. This method is limited to soft formations. The build rate at which angle can be changed is also limited (Denham and Lombard, 1995; Short, 1993).

Compaction tools create a wellbore by compacting the sediment and deflecting the bit in a desired direction (Denham and Lombard, 1995). This method is restricted to very soft formations and offers limited directional control. This method is typically limited to unconsolidated formations less than 50 feet TVD (Kaback, 2002). Although compaction does occur, it has been shown not to adversely affect injection or extraction of groundwater (Denham and Lombard, 1995). This method is restricted to utility rigs.

Bent sub-housing mud motors for horizontal drilling were used in the early 1960s, although mud motors were originally patented in the early 1870s (Downton et al., 2000). These tools operate in two modes, rotating or sliding (Figure 13). In rotate mode, the string is rotated so the bent motor is not oriented in any one direction. Once a directional component is desired, the rotating drill string is halted. Then the motor is pointed in the desired direction, and then weight on bit is applied to slide the motor forward in the desired direction. The bend in the motor causes the borehole to change direction. In this mode, mud is circulated through the motor with a pressure drop across the motor creating the power required to turn the bit and cut rock. Mud motors commonly have bends ranging from 0.78° - 2.83°. This technology is used to create medium and long radius wellbores.

Developed in the early to mid-1990s, Rotary Steerable Systems (RSS) are one of the newest directional drilling technologies (Downton et al., 2000). A common problem among all horizontal drilling methods is wellbore friction. As the drill string begins to deviate to the horizontal plane, total friction on the drill pipe increases as the drill string comes in contact with the borehole wall. This friction increases with tighter turn radii

and longer horizontal lengths. Unlike the bent mud motors, RSS allows continual rotation of the drill string (elimination of the sliding mode) which reduces wellbore friction. The RSS uses active push pads near the bit to control direction. These pads retreat and advance as the drill string rotates, applying synchronized lateral force to the bit so that it cuts to the side in the preferred direction. Combinations of this technology with optimal mud densities have facilitated wellbores in excess of 38,000 feet.

Wellbore Measurements

Measurement of wellbore progress is a pivotal component to directionally drilling. As explained in the history section, it was not until the revelation that boreholes naturally deviated that directional drilling became desirable (Gleason, 1934). The ability to accurately determine drill bit location and orientation is necessary to steer the borehole in a desired direction. Drilling measurements can take the form of six different technologies (Devereux, 1999; Short, 1993; Willoughby, 2005):

Magnetic Single-Shot / Multi-Shot instruments are simple tools to record borehole orientation. This measurement may occur once or multiple times during well construction. Typically a compass and split-bubble will be photographed. This method may or may not require tripping (pulling out) the drill string out of the borehole.

Gyroscopes determine orientation without magnets and are therefore accurate near metallic drill strings. This device is lowered into the hole and records measurements that are then retrieved upon reeling in the system. Accuracy of better than five inches is expected.

Electronic Beacons transmit a radio signal that can be received by a surface device. This ‘walk over’ technique requires a person walking above the beacon with a receiver to determine drill position and depth. In 1995 the penetration of the beacon was limited to 50 feet (Murdoch, 1995), but a decade later has been increased to 140 feet (Willoughby, 2005). Accuracy of depth measurements decreases to perhaps within four feet at 75 feet TVD (Willoughby, 2005).

Measurement While Drilling (MWD) includes measurements of wellbore progress and formation parameters used to aid in steering the bit. MWD is the minimal level of measurement required to hit target formations at deeper depths. However, if the geology is well known then methods previously mentioned may be used, especially at shallower depths. This system is expensive, but less so than logging while drilling.

Logging While Drilling (LWD) takes measurements of many formation and bit parameters such as porosity, bit strain, resistivity of the host rock. These parameters are then transmitted to the surface. This system provides a wealth of information but is most expensive.

Mud Control

The most tenuous step in constructing directional water wells has been their development and borehole stability, as evidenced by the case study section. This may be attributed to the lack of expertise on drilling and developing directional water wells. However an alternative hypothesis is presented. Instead of considering the inability to remedy the situation, let us examine the cause of it.

It has been noted that directional wells in the petroleum industry have more skin (drilling mud infiltration) problems than their vertical counterparts (Joshi, 1991). This occurs because of increased drill time (due to increased length and difficulty) and therefore greater mud invasion into the reservoir. Shallow sand permeabilities are often multi-Darcy with large pore throat sizes. The filtration control material typically utilized in groundwater wells, such as bentonite or barite. Bentonite and barite fit within these large pore throats and may travel some distance into the formation matrix. To overcome this problem, bridging solids may be considered.

Bridging solids may take the form of calcium carbonate or sodium chloride (Dick et al., 2000). They are larger than the pore throats and therefore cannot enter the formation. Bridging solids provide a base for the smaller mud material to form a filter cake on within the wellbore. Upon well development these bridging solids lift off as flow begins, unlike drilling mud that may invade deep into the formation if a quality cake is not established. Mud infiltration problems are likely greater in permeable / porous formations because the pores are so large that common drilling fluid materials cannot bridge them. Methods to determine optimal bridging solids regimes may be found in Abrams (1977) and Dick et al. (2000).

Well Limitations

The ability of a drilling rig to efficiently drill a directional hole must be considered. A rig that is not capable or only marginally capable will increase costs and promote poor borehole quality. Furthermore, borehole stability is also a factor to consider. It is industry practice for the directional drillers to calculate the following

parameters and thus recommend rig capabilities. There are four main parameters to consider when determining rig capability.

Drag – Torque: The ability to rotate the drill string must be considered for any drilling project. As more drill string is put down hole, greater contact with the formation increases frictional resistance and therefore reduces the ability of the drill string to be rotated. For traditional mud motor systems, the ability to rotate the drill string is vital for steering and drilling. The literature has a wealth of information of torque issues when drilling (Aadnøy and Andersen, 2001; Aarrestad, 1994; Johancsik et al., 1984; Maidla and Haci, 2004; Sheppard et al., 1987; Wu et al., 2011).

Drag – Pullback: The same frictional forces inhibiting pipe rotation also inhibit movement of the drill string when pulling out. Combining drag forces and the weight of the drill string yields a total pullback required to retrieve downhole equipment. If these forces become too great, the drill string will become permanently stuck in the hole thus losing the entire well and associated bottom hole equipment.

The pullback capacity for oil rigs is typically in excess of 300,000 lbs. Water well rig pullback capacity is typically less than 200,000 lbs. and many are significantly less. The rig used for the Antelope Hills directional water well had 300,000 lbs pullback capacity and was large enough despite many breakdowns. The rig used for the Castle Pines directional water well was too small at 110,000 lbs; a rig with 200,000 lbs would have performed better (Williams, 2008).

Drag – Weight on Bit: The ability to keep sufficient weight on bit is necessary to maintain penetration rates. For a vertical well, this is less important as a translation of

forces around a curve section is not required. However directional drilling must maintain sufficient weight on bit despite the fact that the drill string is operating at some angle off vertical.

When using rigs without a pull down (thrust) capacity, the weight on the bit is created by the weight of the drill string. In horizontal wells the pipe in the horizontal section lays on the bottom of the borehole and therefore its weight does not rest on the bit. Pipe in the curve or vertical section must be put into compression, and this force transferred down the horizontal section. If the friction is high, heavy drill pipe may be used in the vertical section to generate sufficient downward force to overcome this resistance. Slant rigs (utility & petroleum) have a pull down (thrust/push) capabilities that grip the pipe at the surface and push it down. These rigs can thus overcome weight on bit problems. As slant rigs operate at non-vertical angles, it is difficult to generate sufficient weight via the drill string.

Mud Pump Capacity: Mud pumps used for directional drilling must be positive displacement. The mud pumps must maintain high pressures to power downhole equipment (MWD/LWD, mud motor). Mud pumps must also be large to maintain borehole cleaning velocities. For the Castle Pines project, the duplex mud pumps were thought to be undersized, triplex pumps would have been preferred (Williams, 2008). Readers interested in mud pump capacity issues may be interested in petroleum literature on the topic (Gavignet and Sobey, 1989; Larsen et al., 1997; Tomren et al., 1986).

Borehole Stability: The stability of the borehole is crucial for borehole completion. When considering borehole stability, there are two main concerns. The

wellbore may become unstable due to low drilling mud pressures or high drilling mud pressures (Aadnøy and Chenevert, 1987). Low pressures will induce borehole collapse (Aadnøy and Chenevert, 1987). High pressures will induce borehole fracture and thus loss of circulation (Aadnøy and Chenevert, 1987; Mody and Hale, 1993).

Well Completion

The completion strategy (casing and cementing) of horizontal wells may be similar to vertical wells, but is generally more limited. Insertion of casing is similar to vertical wells with the caveat of calculating bending forces, axial forces within the buildup section, and collapse strength of materials (Murdoch, 1995). Environmental horizontal well materials have included fiberglass, high density polyethylene (HDPE), polyvinyl chloride (PVC), steel, and stainless steel (Kaback, 2002).

In the production zone, increased planning is necessary to facilitate a quality well. Previously, traditional gravel packing of horizontal wells was difficult due to the horizontal nature of the wellbore (Murdoch, 1995; Penberthy Jr et al., 1997). However, currently most all horizontal wells offshore are packed (Dupriest, 2013). The major technical difficulty of installing gravel along the production zone is getting the annulus fully packed. As the filter pack sand is pumped downhole, if it runs out of carrier fluid due to permeability or if the sand settles, then the annulus will pack off prematurely. This premature pack off will occur when the sand / liquid ratio rises above about 0.5-0.6 (Dupriest, 2013). If the annulus prematurely packs off, then then there is a void space above the casing. If this void space is not well supported, the formation will collapse and result in fine sediment production. Pre-packed screens may solve this problem, but they

are expensive, difficult to bend, and can significantly increase friction when inserting (Jehn-Dellaport, 2004; Murdoch, 1995).

Geotextile socks have been used to minimize fine sediment production, but may be difficult to install and can become clogged (Allouche et al., 1998; Doesburg, 2005; Faure et al., 2006). Nevertheless, Enviroflex is a geotextile bounded on either side by well screen and is commonly used (Doesburg, 2005). Open hole completions have been used in competent formations and are preferable where feasible (Joshi, 1991; Murdoch, 1995).

Casing while drilling (CwD) is a new casing installation method that combines casing and drilling at the same time. This method may use either rotary steerable or mud motor directional control (Warren et al., 2005). CwD facilitates faster completions and less mud infiltration. However, special rigs are required for this completion method (Tessari et al., 1999). Use of casing while drilling is very rare because of the build rates (radii of curvature) required, rotating friction in the curve and the requirement of stiff casing (Dupriest, 2013).

Well Development

The methods used for development of horizontal wells are similar to vertical wells and may include jetting, swabbing, or flushing. The main difference when developing horizontal wells is that airlifts are not recommended (Doesburg, 2005). When considering development, the major consideration should be to ensure that the tool can make the turning radius and will not get stuck when it enters a horizontal position. Regardless of development method, the time required to develop the well will be longer

than vertical wells (Jehn-Dellaport, 2004; Kaback, 2002). This is due to the fact that the well is longer and may have increased skin effects (Joshi, 1991). Because horizontal wells take longer to drill and case, skin effects may be greater due to increased duration of mud pumping operations (Joshi, 1991). This longer drill time can also cause the skin effects to be disproportionally greater near the heel of the well (Joshi, 1991).

Horizontal Well Modeling

Groundwater wells are modeled to determine relationships between pumping rates and drawdown. Drawdown is proportional to pumping. More pumping causes more drawdown. Drawdown is defined as water level drop, head loss, or pressure loss from some original state. Drawdown is a limiting factor to increased pumping rates. Drawdown in a well cannot drop the water level below the pump, otherwise the pump will be exposed to air and therefore unusable. Significant drawdown also means that the pump must lift the water greater elevations to the surface, thus increasing the operations cost of electricity. High drawdown can also lead to formation damage around the well.

Modeling the transient aquifer responses to pumping / drawdown is useful for determining reservoir properties such as permeability and hydraulic boundary locations. Modeling the pumping / drawdown response is also important for planning purposes when designing wells and calculating the cost for a desired well field capacity. There are two methods used to model groundwater wells. One may use finite difference / finite element models, or one may use analytical models.

Finite Difference / Finite Element Models

Finite difference / finite element models require the user to discretize space and time (Figure 30). Then the model implements simple numerical derivative methods between these points to approximate the differential equation. Then the model steps the solution through space and time. Finite difference / element models will only work if time and space are subdivided into small enough units to approximate the system. This can prove especially difficult and time consuming near points of discontinuity such as a well. Furthermore, finite difference / finite element methods only model drawdown gradients and therefore do not specifically track water drops moving through the aquifer. Because only gradients are modeled, mass balance issues can arise where more water leaves the aquifer than comes into the aquifer.

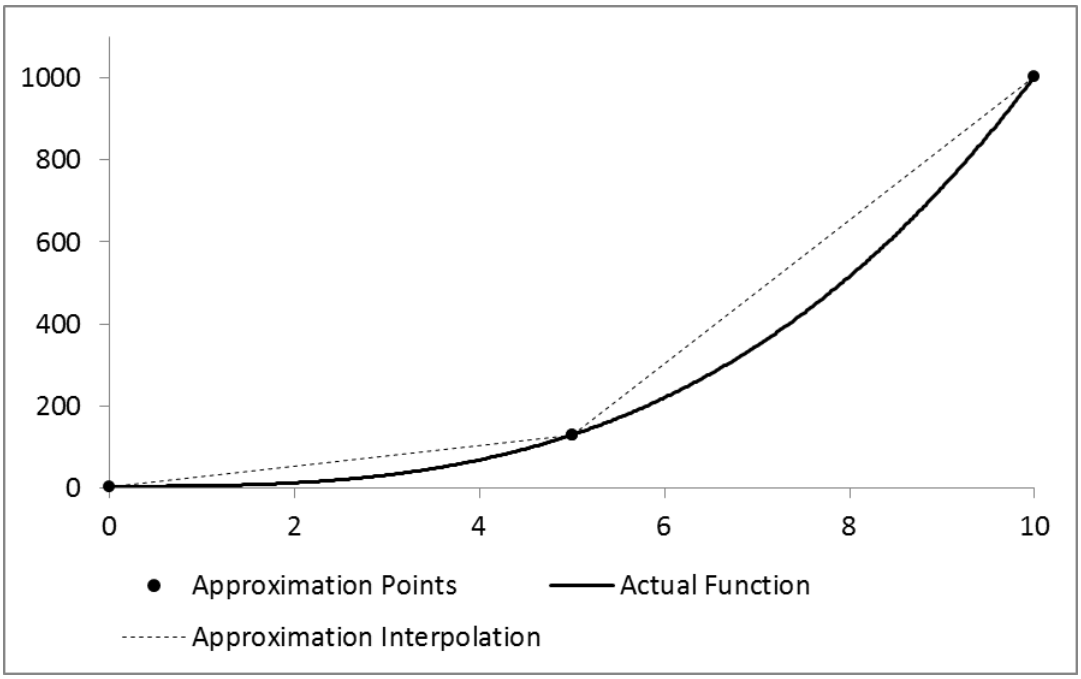

Figure 30. Discretization of a function using three points.

While there are several groundwater finite difference / element models in existence, the United States Geological Survey Modular Ground-Water Flow Model (MODFLOW) is the standard. There are two main packages in MODFLOW that can be used to model horizontal wells. One may use the Multi-Node Well (MNW or MNW2) package which models an infinite conductivity (no friction), non-uniform flux wellbore (Halford and Hanson, 2002). The MNW package can be paired with other packages to model solute transport and variable density effects (Konikow and Hornberger, 2006). The other standard MODFLOW package for horizontal wells is Conduit Flow Processes (CFP) (Shoemaker et al., 2007). MODFLOW-CFP models conduits with frictional head loss. However convergence is difficult to achieve, especially if the wellbore is not sufficiently removed from the aquifer via thick wellbore skin. Outside of these MODFLOW packages there are several other similar models that may also be useful (Arfib and de Marsily, 2004; Reimann et al., 2013; Spiessl et al., 2007).

Analytical Models

Analytical models do not require a temporal or spatial discretization. These models are easy to use and require only limited user input. However, their derivation is more complex. Analytical derivation directly solves the boundary value problem, and therefore does not have mass balance or convergence issues. Analytical derivation can take many different forms. The method we use later in this thesis relies on orthogonal sets. We essentially use the principal that any function can be represented by a series of waves. For example, if one wants an infinite train of boxes one my use the series summation of sine waves

$$\frac{4}{\pi}\sum_{n=1,3,5...}^{\infty}\frac{1}{n}\sin[n\pi x], \tag{2}$$

which yields Figure 31.

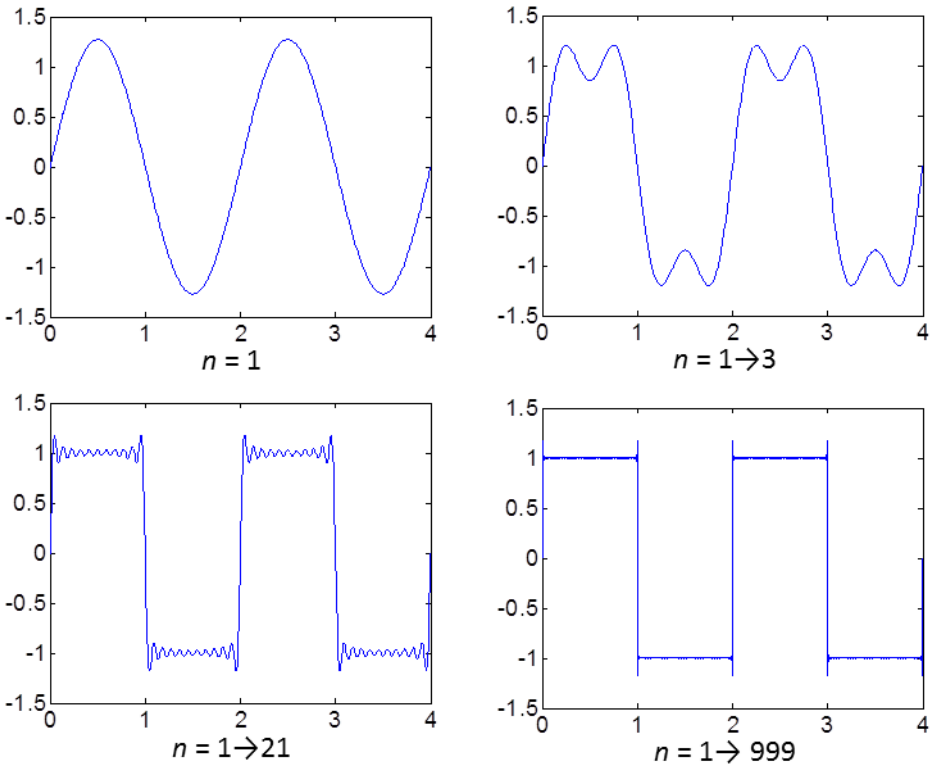

Figure 31. Infinite train of boxes from *x* equals one to four, generated from (2).

Analytical models can be run without boundary conditions which is very useful when the boundary conditions are unknown or very far away. These models are used for pressure transient analysis to determine aquifer hydraulic conductivity and boundary conditions. Analytical models may also be used to forecast expected drawdown. However, analytical models assume homogeneous, anisotropic media which is a

significant drawback. As such, analytical models typically do not account for temporally or spatially complex scenarios as can be modeled with finite difference / element models.

Early Groundwater Derivations

Drawdown calculations for directional wells began with Ranney water supply wells. As cited from Hantush and Papadopulos (1962), these early calculations were completed using the Dupuit-Forchheimer discharge formula assuming a vertical well with radius of perhaps 75% the actual collector well length (Delleur and Simon, 1959; Mikels and Klaer, 1956). The first well documented solutions for horizontal collector wells were developed in Hantush and Papadopulos (1962), and further explained in Hantush (1964).

The methods used in these analytical solutions represent the horizontal well as a uniform strength line sink (Hantush and Papadopulos, 1962). When using the line sink method, uniform flux along the wellbore is usually assumed. Uniform head line sinks may also be derived which are more rigorous but also more mathematically complex (Hantush and Papadopulos, 1962). Well losses were neglected in addition to the radius of the horizontal collectors and the central caisson. Hantush and Papadopulos (1962) developed horizontal collector well steady and transient solutions for a given number of laterals in an infinite horizontal plane, isotropic confined & unconfined aquifers. Using the method of images, stream boundary conditions were also derived.

Petroleum Derivations

Modern horizontal drilling began with research and development by Elf Aquitaine in conjunction with the Institut Francais du Petrole in the late 1970s and early 1980s (Giger et al., 1984). During these research activities, steady state productivity index solutions by Merkulov (1958), Borisov (1964), and Giger (1983) were readily comparable to actual system performance (Giger et al., 1984). Upon general economic acceptance of horizontal wells in the mid-1980s and the subsequent growth of the technology, many solutions were developed for both transient and steady state cases (Joshi, 1987).

Transient horizontal well solutions for pressure drawdown and buildup were developed by Goode (1987). Semi-infinite system bounds in one direction, and uniform wellbore flux were assumed. To reconcile the uniform flux versus uniform head assumptions, Goode (1987) cited the work of Gringarten et al. (1974). Gringarten et al. (1974) found that if pressure is measured at ~0.87 the length of the well/fracture then the uniform flux solution would be corrected to uniform head. When Goode (1987) solutions were compared against those of Hantush (1964), the solutions had only a minor difference at very early time and were identical after one second (Goode, 1987).

Later work by Babu and Odeh (1989b) closed the reservoir boundaries and solved for psuedo-steady state. Psuedo-steady state is the time at which drawdown becomes linear with time in a completely closed system. This solution was well documented and can be implemented with pen and paper (Babu and Odeh, 1989a). Later

work by Odeh and Babu (1990) derived the transient solution for a well in a closed system using several approximations and tracking the pressure pulse.

A translation from petroleum transient equations developed by Goode (1987) and Odeh and Babu (1990) to groundwater transient equations was completed by Kawecki (2000). A useful translation table of common oilfield and groundwater variables was also presented (Kawecki, 2000). In addition, Kawecki (2000) altered the petroleum equations, which were developed for confined flow, to be approximate for unconfined flow.

A less computationally intensive set of steady state well solutions were those developed by Joshi (1988) and expounded on by Joshi (1991). Here, the steady state production of vertical, slant, and horizontal wells were developed in a way to promote comparison. Joshi (1988) divided the three-dimensional problem into two two-dimensional problems. To account for a difference in vertical permeability, the *z*-axis and average permeability were scaled.

Joshi (1988) showed that assuming equal productivity (specific capacity) indexes and equal drainage volumes, one could determine the horizontal to vertical well productivity index ratio. In addition, the replacement ratio (number of vertical wells replaced by a horizontal well) was also further developed by Joshi (1988) from Giger (1983). It was also shown that if the horizontal well location within the reservoir was within +/- 25% of the top or bottom of the reservoir (towards the center), there was less than 10% change in productivity. Work by Joshi (1988) showed only a 7% deviation in his calculated productivities when compared to electric analog studies from the 1950s.

Petroleum Derivations with Intra-Wellbore Head Loss

With the uniform flux (no friction) assumptions used up to this point, a horizontal well will become increasingly efficient at draining a reservoir up to infinite length. Without the practicalities of economics and limitations of drilling, horizontal wells should be infinitely long. These assumptions are no longer valid upon consideration of frictional head loss within the wellbore. At some point, the energy loss will be so great that additional wellbore length does not improve production.

Head loss considerations are especially important once wellbore flow enters the turbulent flow regime. From laminar to turbulent flow, friction loss transitions from proportional to the velocity to proportional to the velocity squared Given the importance of frictional head loss, several analytical models have been developed to account for these effects.

Joshi (1991) proposed that if intra-wellbore head loss is significantly less than reservoir drawdown, then it may be ignored. Possible methods for quick calculation of such criteria require solving two end member scenarios. First, assume all wellbore flow enters from the end of the horizontal well and calculate friction loss, this gives a maximum loss. Then repeat this calculation assuming all flow enters the last foot of the wellbore (closest to pump), this gives a minimum loss. Comparing these values against reservoir drawdown will aid in determining the importance of intra-wellbore head loss.

The first derivation of a turbulent wellbore dynamically linked to the reservoir was developed by Dikken (1990). Dikken (1990) assumed that the flow regime was fully turbulent, showing that the transition from laminar to turbulent flow was insignificant.

He assumed a constant pressure boundary parallel to the wellbore, and an isotropic reservoir. Analytical solutions for infinite and finite well length were presented. This work showed that for many practical petroleum cases, friction loss in the well must be considered.

Novy (1995) used a finite-difference model to solve the boundary value problem of Dikken (1990). His production loss threshold of 10% was used to create various plots denoting well diameter, length of well, and production rate at which losses became significant. Novy (1995) noted that rough wall assumptions by Dikken (1990) tend to overestimate well loss. Novy (1995) calculated losses using rough wall and smooth wall assumptions to present a range of possible head losses.

Landman (1994) improved the model by Dikken (1990) so as to eliminate the need for numerical integration. In addition, specific productivity along the wellbore was allowed to vary so as to evaluate variable perforation patterns or permeabilities along the well. This model allows for determination of optimal perforation density along horizontal wells so as to promote constant drawdown along the wellbore.

Ouyang et al. (1998) and Penmatcha and Aziz (1999) presented a new methodology for analytically modeling horizontal wells with intra-wellbore head loss along the perforated section. These new wellbore models accounted not only for frictional losses but also accelerational / kinetic head loss. These comprehensive models assume a three-dimensional, anisotropic, transient reservoir. These assumptions are significantly more rigorous than previous workers investigating intra-wellbore head loss.

The new models can also compute complex wellbore geometries. In addition, new friction factors were derived to account for pipe inflow and outflow effects.

Recent Groundwater Derivations

In the 1990s, horizontal groundwater wells became increasingly popular for environmental cleanup projects. It was at this time that relationships between horizontal well pumping and drawdown were derived for groundwater systems. While the mathematics of fluid flow are no different between confined groundwater and confined petroleum systems, several valuable additions to the literature were made.

In addition, unconfined flow is an important difference between groundwater and petroleum derivation. Unconfined groundwater flow occurs in shallow water table aquifers. Unconfined flow has a free surface upper bound which makes derivation significantly different from typical petroleum systems. Furthermore as these remediation projects were concerned with capturing contaminants, several studies were completed on the particle capture zones of horizontal wells (Kompani-Zare et al., 2005; Zhan, 1999; Zhan and Cao, 2000).

Tarshish (1992) completed some of the first work on horizontal well modeling during this period of renewed interest. His steady state model was derived for a horizontal well underneath a surface water reservoir. This work was groundbreaking as it discretized the wellbore into variable strength sources thus allowing non-uniform flux. In this way, the model accounted for non-uniform head loss along the well by assuming source strength was proportional to the square of velocity. By assuming head loss proportional to the square of velocity, the Reynolds number must be greater than

100,000 which is high. In spite of this assumption, Tarshish (1992) likely influenced later work which used similar wellbore discretization procedures in petroleum reservoir engineering (Ouyang et al., 1998; Penmatcha and Aziz, 1999).

Zhan et al. (2001) derived solutions for horizontal well pumping tests by a different method than petroleum reservoir engineers. However, upon time integration of the well function and changing out of dimensionless variables, the solutions were found to be equivalent. Zhan et al. (2001) also investigated the uniform flux assumption using MODFLOW. They found that the difference between uniform flux and constant head was only five percent, and thus a uniform flux solution should be used as it was less mathematically complex.

Park and Zhan (2002) investigated the transient hydraulics of a finite diameter horizontal well with confined and semi-confined boundary conditions. Their work integrated the point source into a volume sink. Park and Zhan (2002) derived the relationship between wellbore storage and skin (low permeability zone around wellbore) effects simultaneously and solved in the Laplace domain. Another important contribution was the derived relationship between finite thickness skin and infinitesimally thin skin.

The first transient, three dimensional, horizontal & slanted well derivations for an unconfined aquifer were completed by Zhan and Zlotnik (2002). A significant portion, if not the majority of groundwater wells are constructed in water table (unconfined) aquifers. The derivation of these equations is complex as the water table is a free moving boundary which makes the flow problem non-linear.

More rigorous treatment of friction head loss in a horizontal well was studied by Chen et al. (2003). This study derived equivalent hydraulic conductivities within the wellbore to account for the transition from laminar to fully turbulent flow. Their model is not strictly analytical as it uses a finite element solution procedure. However, the motivation for their model was an investigation of the continued use of uniform head / flux assumptions in analytical derivation; hence it's citation in the analytical models section of the thesis.

It is also noteworthy to mention that the methodology of Chen et al. (2003) predates the MODFLOW-CFP numerical implementation of intra-wellbore head loss. Chen et al. (2003) compared their model against a sandbox aquifer experiment. Good matches between modeled and experimentally derived results were found upon comparison of their numerical model and the experiment.

Previous horizontal well analytical derivations were expanded on by Park and Zhan (2003). This new work found solutions for finite diameter wells in fractured aquifer systems including water table aquifers, and leaky confined aquifers. In addition, these solutions modeled wellbore storage and skin effects. Their model also accounted for storage in the aquitard using a dual porosity system.

Zhan and Park (2003) used the approximation that aquitard flux was perpendicular to the aquitard interface. However, this 'Hantush' assumption was later revisited by Sun and Zhan (2006) by assuming two independent aquifers separated by an aquitard. This later work found that the Hantush approximation was accurate at late times or if the horizontal well was not too close to the aquitard.

Williams (2013) derived the latest horizontal / directional analytical well models. This study vastly simplified drawdown calculation by neglecting partial penetration effects. By neglecting partial penetration effects, Williams (2013) was able to use computationally simple confined aquifer equations such as Jacob and Theis in addition to unconfined aquifer equations by Hantush and Boulton.

Williams (2013) method assumes that a non-vertical well can be vertically projected and then represented by several point sources. This problem is then solved by assuming that the total well pumping rate is distributed across each of the point sources. Uniform flux is not assumed because each segment's drawdown effect on another segment is determined, which thus governs flux. The mathematical model derived by Williams (2013) compared well to that derived by Hantush and Papadopulos (1962), MODFLOW, and field data.

SUMMARY OF LITERATURE REVIEW

From the literature review, we find that in chemically bound ASR systems thinner, lower permeability aquifers favor higher recovery efficiencies (Esmail and Kimbler, 1967). These aquifers favor higher recovery efficiencies for two reasons. First, lower hydraulic conductivity (permeability) impedes advection and mixing of injected waters with native groundwater (Kumar and Kimbler, 1970). Second, lower hydraulic conductivity and/or thin aquifers reduce the effects of density segregation by keeping the injected water from spreading laterally across the upper boundary of the aquifer (Merritt, 1986).

Low permeability and/or thin aquifers have excessive pressure buildup when injecting and excessive pressure drawdown when extracting. So while chemically bound ASR may target low permeability and/or thin aquifers, it will be difficult to inject and extract water from these aquifers at high rates. Traditional groundwater wells and physically bound ASR systems do not target thin, low permeability aquifers. However, if this is the only aquifer available then excessive pressure buildup and drawdown will occur.

Longer wells reduce drawdown and buildup issues because of increased area for flow to occur. Horizontal wells mitigate these pressure buildup and drawdown issues because they have greater contact with the aquifer than vertical wells. The maximum length of a vertical well is the thickness of the aquifer. Aquifers are typically much more laterally extensive than vertically thick. Therefore, horizontal wells are typically able to have greater contact with the aquifer

Despite the promise of horizontal wells for chemically bound ASR, currently there is no method to model all components of such a system. Solute transport and density stratification have been determined as pivotal to predicting recovery efficiency in chemically bound ASR (Lowry and Anderson, 2006; Ward et al., 2007). Intra-wellbore friction head loss has been cited as a possible limitation of horizontal well ASR (Maliva and Missimer, 2010).

The ideal model of a chemically bound ASR system will need to include: solute flow and transport, density effects, and wellbore frictional head loss. While MODFLOW models exist for any two of these components there is no model combining all three of

these components. Chemically bound ASR systems are not as prevalent as physically bound ASR systems due to the possibility of low recovery efficiencies. So although there is no complete model for a chemically bound ASR system, the detrimental impact of such a need has been minimal.

Physically bound ASR systems are the majority of current ASR operations (Pyne, 2013). Physically bound ASR systems are only limited by physical-hydraulic processes. These physical parameters are pressure drawdown when extracting and pressure buildup when pumping. These limitations are no different than traditional injection or extraction wells. Thus, to model a physically bound horizontal / directional ASR system, one may use models derived for a horizontal / directional production well.

While MODFLOW-CFP is the most rigorous finite difference model of aquifer head loss linked to intra-wellbore head loss, it is difficult to use. Use of MODFLOW-CFP requires the user to effectively discretize time and space in a very dynamic system. The dynamic interrelationship between head loss within the wellbore and head loss in the aquifer is difficult to model. MODFLOW-CFP convergence is difficult to attain, especially if the wellbore is not sufficiently removed from the aquifer through higher wellbore skin.

Analytical models have been derived for horizontal wells in both the groundwater and petroleum literature (Odeh and Babu, 1990; Zhan and Zlotnik, 2002). These models are easier to use than finite difference models because there is no discretization of time or space; thus convergence and mass balance issues are avoided. However, these analytical models must track the pressure pulse and make several

assumptions and approximations to achieve rapidly convergent solutions. These analytical models have typically assumed a uniform flux wellbore, thus effectively suggesting that the wellbore should be infinitely long to achieve the best pumping to drawdown ratio (specific capacity).

More recently, a semi-analytical approach has been developed in the petroleum reservoir engineering literature. In this method, the wellbore is sub-divided into segments with each segment's aquifer component being analytically derived (Ouyang and Aziz, 1998; Penmatcha and Aziz, 1999). Head loss between these analytical segments is then defined by energy loss equations. Use of such a methodology has been largely non-existent or unknown in the groundwater literature. While some models have been developed using a similar approach, they lack the completeness of the petroleum methods (Tarshish, 1992; Williams, 2013).

Field examples show that understanding how to model aquifer drawdown relationships is not the only factor impeding the use of horizontal wells for groundwater production (Jehn-Dellaport, 2004; Rash, 2001). Other factors such as drilling, completion, and well development are equally important. Discussion of these factors has been nearly absent in the groundwater literature. Basic drilling forces were discussed in the petroleum literature, although many years ago (Greenip Jr, 1989; Wu and Juvkam-Wold, 1991).

Because longer horizontal wells will have less drawdown, we find two main limitations when attempting to maximize horizontal well length. Either well construction will limit the length that the wellbore can be drilled, or intra-wellbore head loss will

limit the useful length of the wellbore. Stating this second point another way, intra-wellbore head loss may become so great that additional well length only marginally increases production. These two factors limiting horizontal well length reduce the effectiveness of horizontal wells. Understanding these two factors is key when calculating the costs and benefits of horizontal wells.

Research Needs from Literature Review

As water supply aquifers occur at essentially all depths, major work going forward will need to focus on well construction techniques that effectively combine petroleum, utility and environmental remediation methods. As evidenced by the horizontal well field examples, of special concern is the excessive buildup of skin in directional wells. This excessive wellbore skin leads to difficulties when developing the well and may be so severe that the well is not productive. A better understanding of wellbore stability when drilling is also necessary to extend the limits of drilling step out ratios. These wellbore stability and skin issues are inherently related to the drilling mud. From the literature review, we find that the petroleum industry has solutions to these issues through the use of bridging solids. Therefore, additional research is needed in relation to bridging solids used for directional groundwater wells.

More complex finite difference / finite element aquifer models are needed to accurately characterize chemically bound and blended ASR systems. These more complex models will need to account for intra-wellbore head loss, solute transport, and density effects at the same time. While current models exist for any two of these components, there is no model for all three components.

Easy to use horizontal well models are needed to account for intra-wellbore friction and acceleration head loss. While finite difference intra-wellbore head loss models exist, they are difficult and time consuming to use. Easier to use models are needed; analytical models are easier to use. Therefore, analytical models accounting for intra-wellbore head loss are needed. These models have been developed in the petroleum literature. However, these models are unknown to the groundwater community. Furthermore, the petroleum literature explanation regarding numerical implementation has been limited. Also, these petroleum models have not been developed for the various conditions typical of groundwater systems such as unconfined flow (water table aquifers) or constant hydraulic head (river) boundaries.

There has been very limited discussion on the calculation of forces when constructing a horizontal groundwater well. Therefore models of forces during horizontal well drilling and completion are needed. These models would facilitate a quick first estimate of design forces for a specific project. These models would also allow for a better general understanding of forces when constructing a horizontal well.

Most groundwater wells are less than 1,000 feet deep. Horizontal wells at such shallow depths require slant rigs. Currently, there are no equations available to minimize the length of a slant rig well. This optimal slant rig entry angle could reduce the cost of shallow horizontal groundwater wells. An equation is needed to determine the optimal slant rig entry angle.

There has been very limited discussion on the cost of horizontal groundwater wells. Therefore, models and input parameters of horizontal groundwater well cost are

needed. Pairing this cost model with the drilling forces model and optimal entry angle equation would allow for a deterministic estimate of well cost. By pairing the cost model with an aquifer model, a cost – benefit analysis could be performed. Such a cost – benefit analysis is needed as this is likely the most important factor when considering horizontal wells and currently there is no information on the subject.

THESIS OBJECTIVES

New analytical, rapidly convergent aquifer equations will be derived for flow to a directional well. These new equations will be incorporated into a semi-analytical, easy to use aquifer model accounting for intra-wellbore kinetic and frictional head loss. This model will be based on the petroleum reservoir engineering literature (Ouyang and Aziz, 1998; Penmatcha and Aziz, 1999). Important contributions of this thesis will include aspects on numerical implementation and derivation of several new boundary conditions. This model will then be used to investigate the interrelationships and magnitudes of intra-wellbore energy loss on wellbore flux and productivity (specific capacity) assumptions.

A simple, analytical, easy to use model will be developed to calculate directional well geometry, drilling and casing forces. The model will calculate forces on the rig and casing / drill pipe. This model will be based on petroleum drilling literature from the early days of the petroleum horizontal well revolution (Greenip Jr, 1989; Wu and Juvkam-Wold, 1991). This model will give groundwater professionals the ability to make estimates of rig and casing requirements / limitations for a given project. The optimal slant rig entry angle for a directional well will also be derived and added to the

model. The model will then be used to investigate the interrelationships and magnitudes of wellbore construction forces and geometry.

A directional groundwater well cost model will also be created. This simple model will be paired with the well construction model. The combination of these models will facilitate a deterministic cost estimate for directional groundwater wells. Model data parameters will be collected from literature and industry professionals. We will then use the cost model and the cost parameters to generate several well cost estimates. We will then estimate the production benefits of horizontal wells using our aquifer model. Finally, we will combine the output of these two models to make a cost – benefit analysis.

CHAPTER II

KINETIC AND FRICTION INTRA-WELLBORE HEAD LOSS

INTRODUCTION

The ability to calculate intra-wellbore head loss will lead to more accurate determination of aquifer properties during pressure transient analysis. Modeling intra-wellbore head loss will also improve the planning and design of wells for drawdown-discharge relationships in the long term. Without head loss terms, a wellbore should be infinitely long to achieve the best discharge to drawdown ratio (specific capacity). Intra-wellbore head losses are hypothesized to be more important for long wellbores because of the increased length for frictional head losses to occur. Therefore, intra-wellbore head loss terms are more important for horizontal wells as these wells can extend for hundreds of meters.

Kinetic (velocity, acceleration) head losses within a wellbore are typically thought of as insignificant and thus ignored. Frictional head losses are thought of as significant, but typically difficult to rigorously calculate. The frictional well loss component was determined empirically to be proportional to the square of the discharge by Jacob (1947) and later to vary by some power of discharge between one and two by Rorabaugh (1953). In this empirical well loss framework, laminar flows yield a head loss proportional to discharge and fully turbulent flows a head loss proportional to the square of discharge.

Later experimental work by Garg and Lal (1971) and numerical work by Cooley and Cunningham (1979) found that not only was frictional head loss important, but it also creates a non-uniform flux along the wellbore with greatest flux occurring near the pump. Despite the finite element approach taken by Cooley and Cunningham (1979), numerical stability was difficult to attain, especially for hydraulic conductivities greater than 0.283 m/min.

It was not until work by Tarshish (1992) that an easier to compute, more stable solution was found. Tarshish (1992) discretized the wellbore using point sinks and then defined the differences in source strength as proportional discharge squared. His model thus empirically accounted for friction using similar methods to Jacob (1947) although with the ability to model non-uniform flux distributions.

Work in petroleum reservoir engineering has also attempted to accurately characterize intra-wellbore head loss. Early derivations of intra-wellbore friction head loss required unrealistic assumptions or were difficult to use (Dikken, 1990; Landman, 1994; Novy, 1995). Later work in petroleum engineering used more realistic assumptions which allowed for complex wellbore geometries and an inclusion of kinetic head loss (Ouyang and Aziz, 1998; Penmatcha and Aziz, 1999). This later semi-analytical work discretized the wellbore into several uniform flux segments and then linked the segments by defining differences in drawdown between each segment (Ouyang and Aziz, 1998; Penmatcha and Aziz, 1999).

Petroleum engineering work on intra-wellbore friction and acceleration head loss has not been cited in the groundwater literature. Recent work by Williams (2013) does

discretize the wellbore into several segments thus allowing non-uniform flux, however no calculation of intra-wellbore head loss is presented. Except for Tarshish (1992), analytical solutions for horizontal groundwater wells have never accounted for intra-wellbore head loss (Hantush and Papadopulos, 1962; Zhan et al., 2001; Zhan and Zlotnik, 2002), although some work has been completed on wellbore storage and skin effects (Park and Zhan, 2002).

Despite the lack of analytical solutions to wellbore friction head loss, recent finite difference studies have investigated this issue. Chen et al. (2003) derived equivalent hydraulic conductivities within the wellbore to account for the transition from laminar to fully turbulent flow. While such a method is intriguing, it is difficult to implement. The MODFLOW Multi-Node Well Package (MNW & MNW-2) was the first widely available finite difference package to model non-uniform wellbore flux, although with only empirical intra-well loss terms (Halford and Hanson, 2002; Konikow et al., 2009).

The MODFLOW Conduit Flow Process (CFP) package was the first widely available model to rigorously calculate conduit (intra-wellbore) friction head losses (Shoemaker et al., 2007). This model used the Darcy-Weisbach equation to model head loss along a conduit with Colebrook-White turbulent friction factor calculations. While MODFLOW-CFP is rigorous, it requires effort to achieve convergence (especially with low wellbore skin) and relies on the user to determine the correct grid discretization. MODFLOW-CFP also does not account for kinetic head loss.

Given the lack of a rigorous, analytical, easy to use model for intra-wellbore head loss in the groundwater literature, we develop one here. We base our model on that of Ouyang and Aziz (1998) and Penmatcha and Aziz (1999) in petroleum reservoir engineering. To distinguish our work from theirs, we derive several additional boundary conditions not found in their work. The solutions to the boundary conditions are also transformed to be rapidly convergent at all times. This second step has not been used in groundwater derivations and thus may be quite useful to future researchers on this topic.

MODEL DEVELOPMENT

New Aquifer Discharge-Drawdown Solutions

Only a brief outline of our derivation procedure is presented here, for a full derivation and explanation please consult Chapter III. To begin, the mathematical relationship between a well's pumping rate and aquifer drawdown originates with the derivation of a point source / sink. This point source / sink has a pumping rate Q [L^3T^{-1}] that is positive for extraction (sink) and negative for injection (source). The point source / sink may be located anywhere inside a box. The dimensions [L] of the box are a, b, c for the x-axis, y-axis and z-axis respectively. The point source / sink is located at x_0, y_0, z_0 [L]. The point source / sink affects drawdown at some point x, y, z [L]. The point x, y, z is termed the sample point in this thesis (Figure 32).

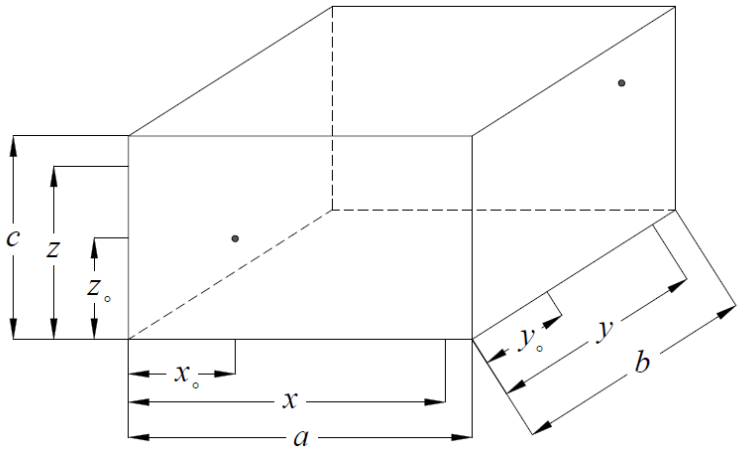

Figure 32. Aquifer conceptual model with source / sink and sample point.

Derivation of our model begins with the partial differential equation governing confined groundwater flow and a point sink represented by Dirac delta functions. The partial differential equation governing groundwater flow is

$$S_s \frac{\partial d}{\partial t} = K_x \frac{\partial^2 d}{\partial x^2} + K_y \frac{\partial^2 d}{\partial y^2} + K_z \frac{\partial^2 d}{\partial z^2} + Q(t)\delta(x - x_0)\delta(y - y_0)\delta(z - z_0), \qquad (3)$$

where S_s is specific storage [L^{-1}], d is drawdown [L], t is time [T], K_x, K_y, K_z are hydraulic conductivities [LT^{-1}], $Q(t)$ [L^3T^{-1}] is the pumping rate (positive for extraction) as a function of time, and δ is the Dirac delta function (Roscoe Moss Company, 1990). We then transform (3) to the Laplace domain to remove time dependence.

With a time independent equation, we then solve the boundary value problem (BVP). The boundary of any one side of the box may be constant head – Neumann or no flux – Dirichlet. The initial conditions are always zero drawdown at time zero. Upon solution of the BVP using the method of undetermined coefficients, we then conduct an

inverse Laplace transform to get back to the real time domain. At this point in the derivation, the solution is described by several infinite series.

Previous researchers have attempted to find approximations for the series summation terms because the series are slowly convergent (Babu and Odeh, 1989b; Goode, 1987; Odeh and Babu, 1990; Zhan et al., 2001). This method requires several assumptions and/or requires tracking of the pressure pulse. One of the major contributions of this thesis is an avoidance of such an approximation approach. Our new approach is more accurate and more elegant than that used by previous workers.

Our methodology is to apply the Poisson Re-Summation formula to these slowly convergent series (Strikwerda, 2004). The Poisson Re-Summation formula transforms slowly convergent series to rapidly convergent series and vice versa (Strikwerda, 2004). The Poisson Re-Summation formula is given by Strikwerda (2004) as

$$\sum_{n=-\infty}^{\infty} \exp\left[-inj\varepsilon\right] \mathrm{u}\left[nj\right] j = \sqrt{2\pi} \sum_{w=-\infty}^{\infty} \mathrm{U}\left[\varepsilon + 2\pi w j^{-1}\right], \tag{4}$$

where the function U is the Fourier Transform of the function u with respect to the summation variable *n* transformed to the frequency variable *w*.

Upon application of the Poisson Re-Summation formula to each BVP solution, we now have solutions that are rapidly convergent at all times and locations. Only eleven iterations are necessary to converge the series upon installation of a switch between the Poisson Re-Summed series and the unaltered series.

We now have a rapidly convergent point source / sink time derivative of the aquifer's response to pumping. To obtain a solution for a wellbore through time, we

need to integrate with respect to time, the length of the wellbore and the circumference of the wellbore. We attempted to find analytical integrations for each of these components. However, upon numerical implementation it was found that only the early time analytical integration was faster than MATLAB numeric integration. For full details, please consult Chapter III.

Intra-Wellbore Friction and Kinetic Head Loss

Only a brief outline of our numerical implementation is presented here, for a full derivation and explanation please consult Chapter IV. To begin, the addition of intra-wellbore friction and kinetic head loss requires that the wellbore be discretized into several uniform flux segments. These uniform flux segments affect themselves and every other segment as defined by the aquifer pumping-drawdown relationships derived in Chapter III.

A matrix of equations is defined for the calculation of drawdown at each segment. We then define the difference in drawdown between each segment through frictional and kinetic head loss equations. The head loss from friction is calculated via the Darcy-Weisbach equation. The head loss coming from acceleration is calculated via

$$h_a = \frac{\left[q_i^2 + 2 q_a q_i \right]}{A^2 g}, \tag{5}$$

where h_a is the head loss (drawdown) caused by acceleration [L], q_a is the axial flow in the wellbore [L^3T^{-1}], q_i is the flow coming in through the wellbore screen [L^3T^{-1}], A is pipe cross-sectional area [L^2], and g is gravity [LT^{-2}] (Penmatcha and Aziz, 1999).

With head losses between each segment defined, the matrix of equations is solved using an iterative method. At each iteration of the method, the drawdown from each segment is updated using the new pumping rate distribution and re-calculation of head loss terms. Upon solution of the matrix of equations, additional segments are added and the procedure repeated until convergence is achieved and thus the spatial discretization solved. If a transient solution is desired, the equations can be marched through time using a superposition approach. For full details, please consult Chapter IV.

MODEL VERIFICATION

Verification our model was conducted to check methodology and code accuracy of both steady state and transient calculations. The model was verified against the Theim equation, Theis equation, MODFLOW-MNW2, and MODFLOW-CFP for accuracy of frictional head loss and aquifer derivation components. We tested all boundary conditions derived: both sides constant head, one side constant head – one side no flux, both sides no flux, and both boundaries infinitely far away.

Model input for the first test, the analytical Theim equation, may be found in Table 4. The Theim equation assumes a steady state, isotropic aquifer with a constant head boundary some distance radially from the well and a no flux boundary at the top and base of the aquifer. The Theim equation assumes a fully penetrating well. This test verifies our derivation of the four sides constant head (*x*,*y*), two sides no flux boundary condition (*z*). Using the Theim equation from Roscoe Moss Company (1990) we find

$$d = \frac{0.001\ \mathrm{m}^3/\mathrm{s}}{2\pi \times 10\ \mathrm{m} \times 1\text{E-}5\ \mathrm{m}/\mathrm{s}} \log\left[\frac{50{,}000\ \mathrm{m}}{0.15\ \mathrm{m}}\right] = 20.239\ \mathrm{m}\,. \tag{6}$$

Our model calculates drawdown to be 20.360 m, which is the same as the Theim equation to two significant figures. The likely cause of the discrepancy is the fact that our model is derived for rectangular boundary conditions, whereas the Theim equation is derived for circular / radial boundary conditions.

Table 4. Model verification against the Theim equation.

Model Parameters					
a	100,000	m	K_x	1E-5	m/s
b	100,000	m	K_y	1E-5	m/s
c	10	m	K_z	1E-5	m/s
x_1	50,000	m	S_s	1E-5	1/m
x_2	50,000	m	Skin	0	
y_1	50,000	m	Density	997	Kg/m^3
y_2	50,000	m	Viscosity	8.9E-4	
z_1	0	m	Gravity	9.8	m/s^2
z_2	10	m	Well Diameter	0.3	m
Bound at $x = 0$	Constant Head		Abs. Pipe Roughness	0.15E-3	m
Bound at $x = a$	Constant Head		Friction	Off	
Bound at $y = 0$	Constant Head		Critical Reynolds	2000	
Bound at $y = b$	Constant Head		Acceleration	Off	
Bound at $z = 0$	No-flux		Num. of Segments	1	
Bound at $z = c$	No-flux		Integral Abs Error	1E-4	
Discharge	0.001	m^3/s	Integral Rel. Error	1E-6	
End Time	Steady State		Chebfun eps	1E-5	

Model input parameters for the second test, the analytical Theis equation, may be found in Table 5. The Theis equation assumes a transient isotropic aquifer with only no-flux boundaries at the top and base of the aquifer and a fully penetrating well. There are no boundaries laterally. This test verified our derivation of the infinite aquifer extents. Using the Theis equation from Roscoe Moss Company (1990)

$$d = \frac{0.01\ \mathrm{m}^3/s}{4\pi \times 10\ \mathrm{m} \times 1\mathrm{E}-4\ \mathrm{m}/s} \int_u^{\infty} \frac{\exp[-X]}{X}\, dX = 22.349518\ \mathrm{m}$$

$$\text{where } u = \frac{(0.15\ \mathrm{m})^2 \times 1\mathrm{E}-5\ \mathrm{m}^{-1} \times 10\ \mathrm{m}}{4 \times 10\ \mathrm{m} \times 1\mathrm{E}-4\ \mathrm{m}/s \times 1.57785\mathrm{E}9\ \mathrm{s}} \quad . \tag{7}$$

Our model calculates drawdown to be 22.349517 m, an accuracy of seven significant figures compared to Theis. Such a high degree of accuracy was expected as the numeric integration relative error used in our model was set to 1E-6.

Table 5. Model verification against the Theis equation.

Model Parameters					
a	Infinity	m	K_x	1E-4	m/s
b	Infinity	m	K_y	1E-4	m/s
c	10	m	K_z	1E-4	m/s
x_1	0	m	S_s	1E-5	1/m
x_2	0	m	Skin	0	
y_1	0	m	Density	997	Kg/m^3
y_2	0	m	Viscosity	8.9E-4	
z_1	0	m	Gravity	9.8	m/s^2
z_2	10	m	Well Diameter	0.3	m
Bound at $x = 0$	N/A		Abs. Pipe Roughness	0.15E-3	m
Bound at $x = a$	N/A		Friction	Off	
Bound at $y = 0$	N/A		Critical Reynolds	2000	
Bound at $y = b$	N/A		Acceleration	Off	
Bound at $z = 0$	No-flux		Num. of Segments	1	
Bound at $z = c$	No-flux		Integral Abs Error	1E-4	
Discharge	0.01	m^3/s	Integral Rel. Error	1E-6	
End Time	50	years	Chebfun eps	1E-5	

Model input parameters for the third test may be found in Table 6. This finite difference, MODLFLOW-MNW2 test verified our calculation of skin effects and the derivation of the one side constant head - one side no flux boundary condition. The

drawdown matches to two significant figures (Figure 33). The discharge per segment between the two models agrees to two significant figures (Figure 34).

Table 6. Model verification against MODFLOW-MNW2.

Model Parameters					
a	500	m	K_x	1E-4	m/s
b	2000	m	K_y	1E-5	m/s
c	100	m	K_z	1E-6	m/s
x_1	250	m	S_s	1E-5	1/m
x_2	250	m	Skin Thickness	0.05	m/s
y_1	1200	m	Skin K	1E-6	
y_2	1200	m	Skin	8.810	
z_1	20	m	Density	997	Kg/m^3
z_2	50	m	Viscosity	8.9E-4	
Bound at $x = 0$	Constant Head		Gravity	9.8	m/s^2
Bound at $x = a$	No Flux		Well Diameter	0.3	m
Bound at $y = 0$	No Flux		Abs. Pipe Roughness	0.15E-3	m
Bound at $y = b$	No Flux		Friction	Off	
Bound at $z = 0$	No-flux		Critical Reynolds	2000	
Bound at $z = c$	No-flux		Acceleration	Off	
Discharge	0.01	m^3/s	Num. of Segments	6	
End Time	Steady State	years	Integral Abs Error	1E-4	
			Integral Rel. Error	1E-6	
			Chebfun eps	1E-5	

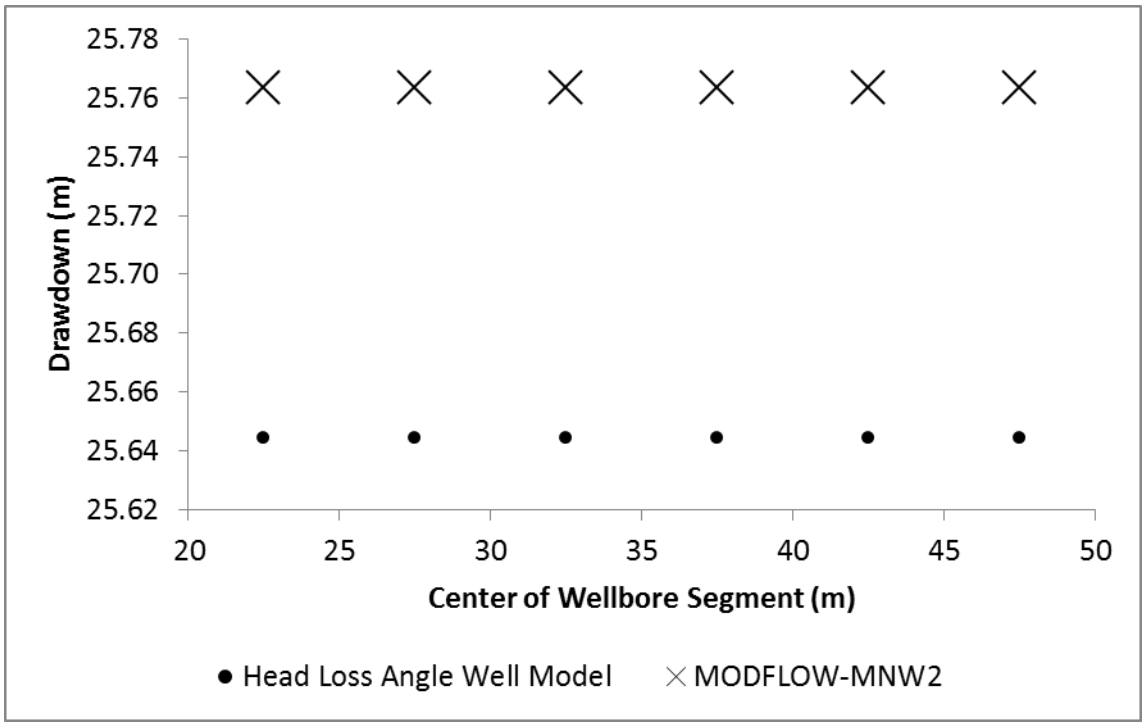

Figure 33. Steady state drawdown verification against MODFLOW-MNW2.

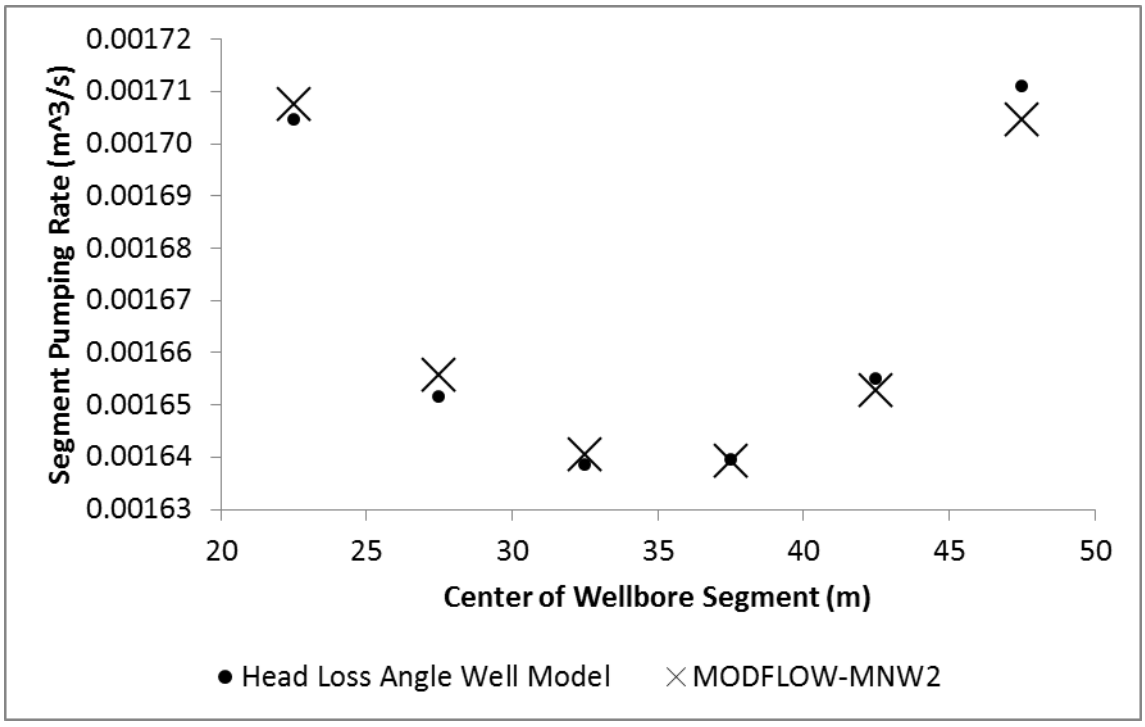

Figure 34. Steady state discharge verification against MODFLOW-MNW2.

Model input parameters for the fourth test, MODFLOW-CFP, may be found in Table 7. We conducted two tests on the input in Table 7, a steady state test and a transient test. In an attempt to achieve the most accurate results, we used a very fine discretization near the wellbore (Figure 35). The steady state model test shows an agreement of three significant figures for drawdown and two significant figures for segment pumping rate (Figure 36 & Figure 37). This test proves the accuracy of our model for intra-wellbore head loss effects at steady state.

Table 7. Model parameters used for MODFLOW-CFP verification.

Model Parameters					
a	1000	m	K_x	0.0001	m/s
b	1000	m	K_y	0.0001	m/s
c	30	m	K_z	0.0001	m/s
x_1	450	m	S_s	1E-5	1/m
x_2	550	m	Skin	13.2	
y_1	500	m	Density	997	Kg/m^3
y_2	500	m	Viscosity	8.9E-4	
z_1	15	m	Gravity	9.8	m/s^2
z_2	15	m	Well Diameter	0.3	m
Bound at $x = 0$	Constant Head		Abs. Pipe Roughness	0.15E-3	m
Bound at $x = a$	Constant Head		Friction	On	
Bound at $y = 0$	Constant Head		Critical Reynolds	2000	
Bound at $y = b$	Constant Head		Acceleration	Off	
Bound at $z = 0$	No-flux		Num. of Segments	10	
Bound at $z = c$	No-flux		Integral Abs Error	1E-4	
Drawdown	50	m	Integral Rel. Error	1E-6	
End Time	Steady & 1 hr		Chebfun eps	1E-5	

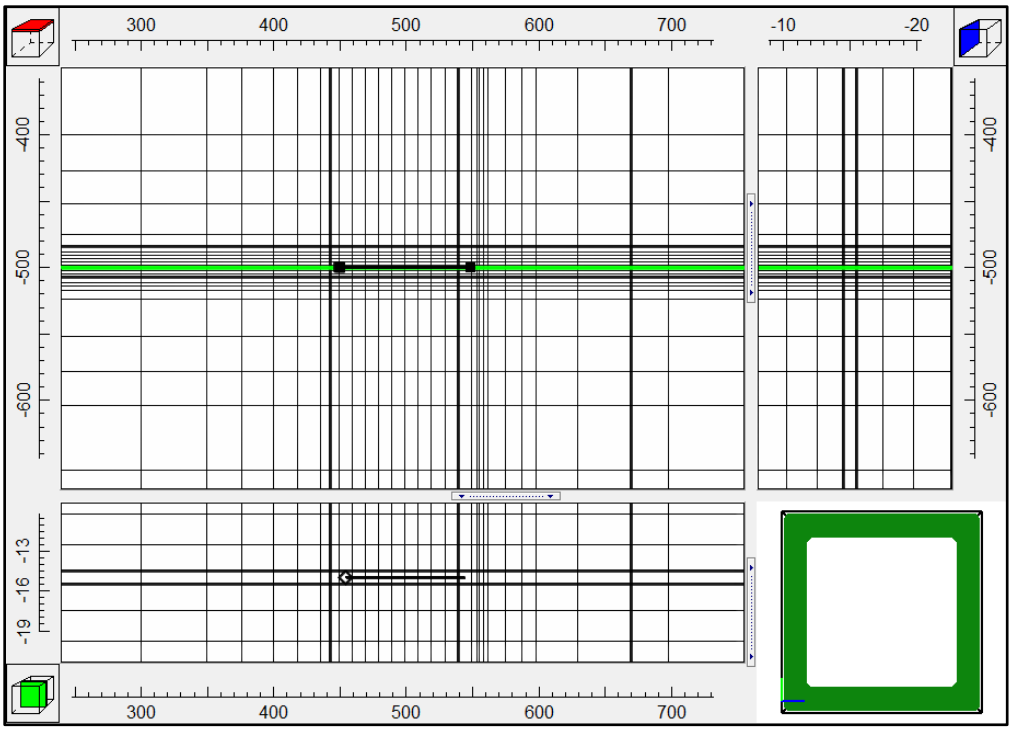

Figure 35. Model Muse MODFLOW-CFP discretization.

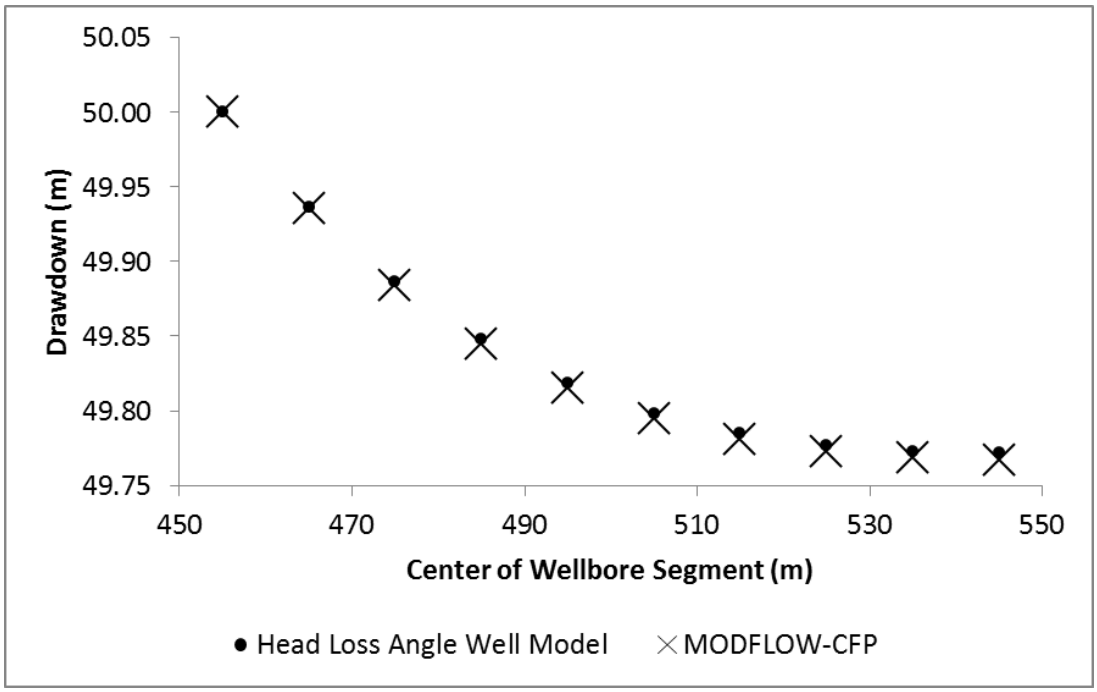

Figure 36. Steady state drawdown distribution verification between our model and MODFLOW-CFP.

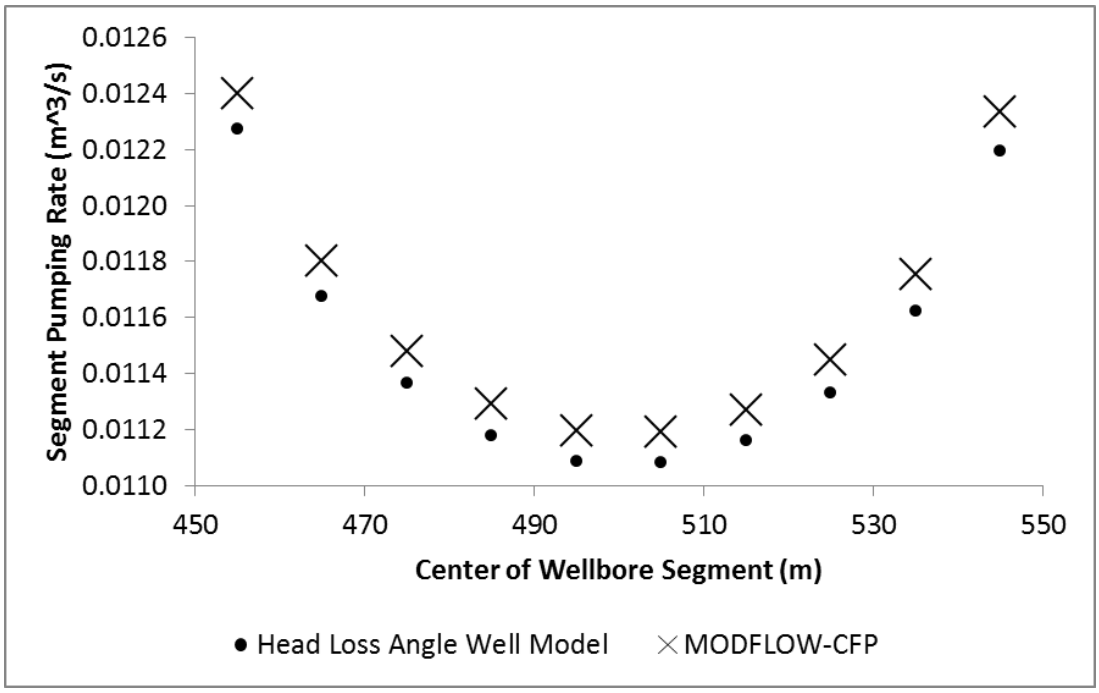

Figure 37. Steady state discharge distribution verification between our model and MODFLOW-CFP.

A transient model for the first hour of pumping using 180 time steps was tested using the same input from Table 7. The transient output agreement between our model and MODFLOW-CFP was very good. The transient model agreement was three significant figures for drawdown distribution at 20s but only one-two significant figures for pumping rate distribution at 20s (Figure 38 & Figure 39). At the end of the hour, agreement between model discharges had improved to two significant figures and remained constant at three significant figures for drawdown (Figure 40 & Figure 41). The constant head (pumping) segment discharge match through time shows very good agreement (Figure 42). The segment furthest form the pump match through time shows very good agreement for both drawdown and discharge (Figure 43 & Figure 44).

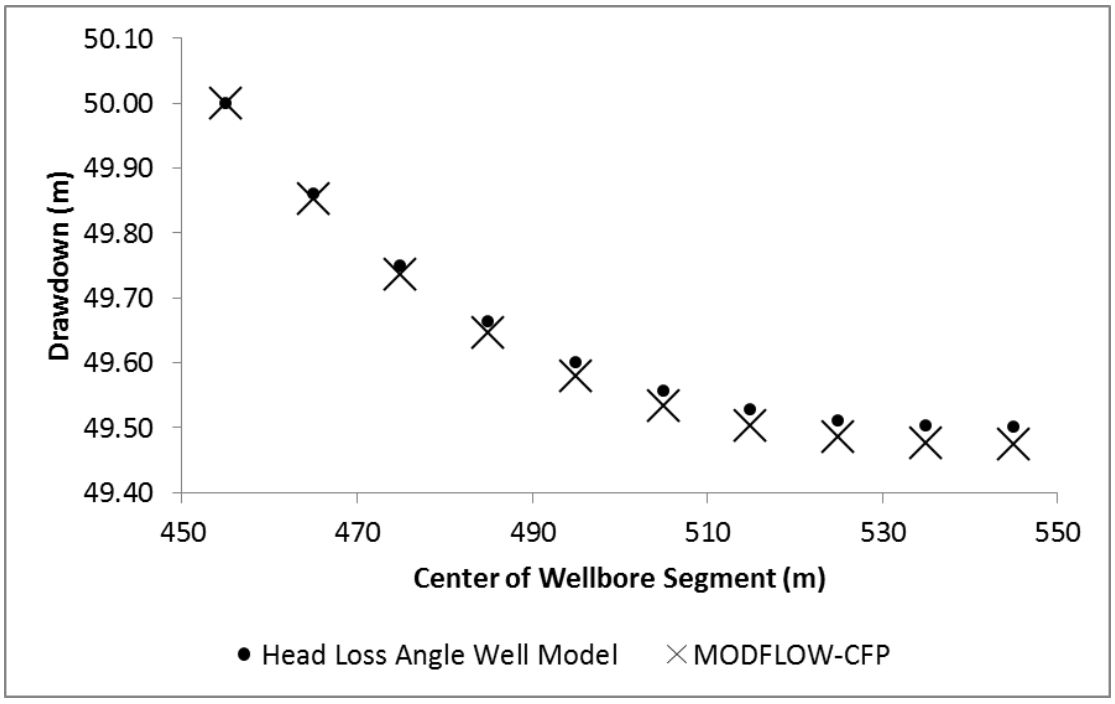

Figure 38. Transient drawdown verification between our model and MODFLOW-CFP at first time step (20s).

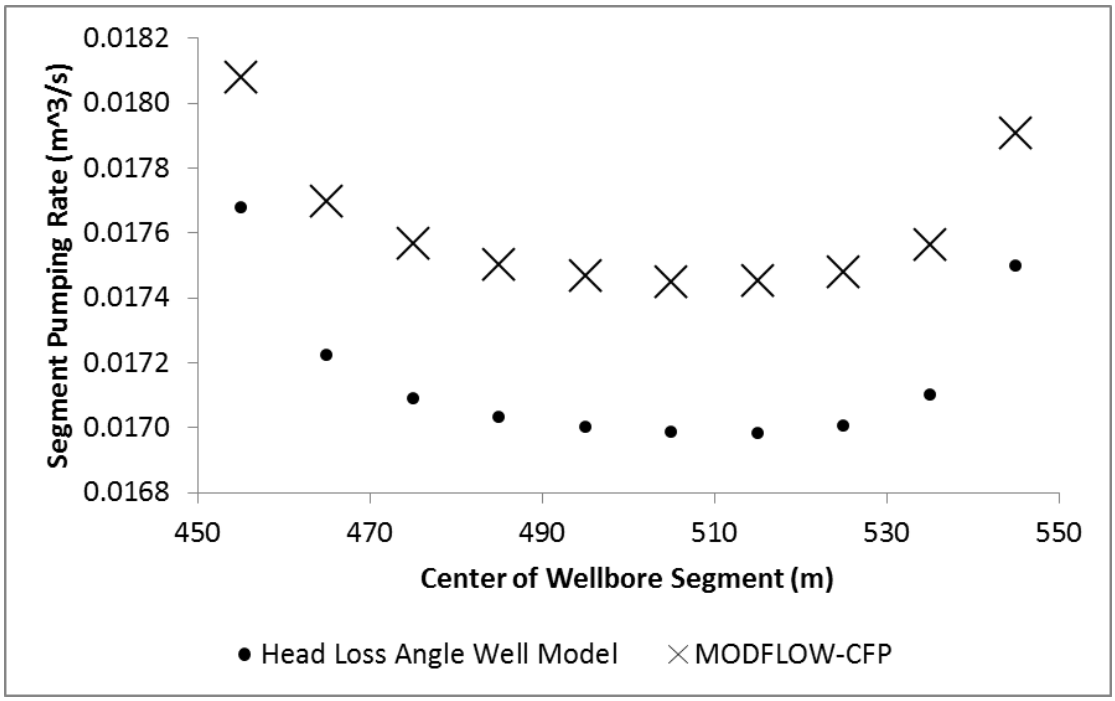

Figure 39. Transient discharge verification between our model and MODFLOW-CFP at first time step (20s).

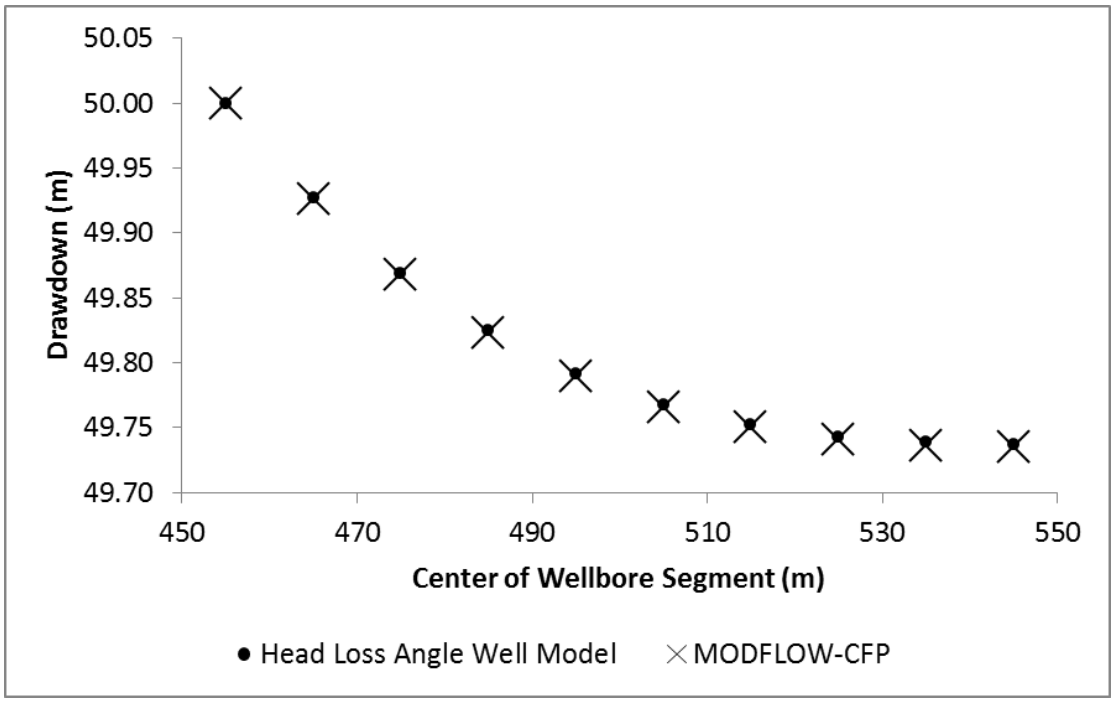

Figure 40. Transient drawdown verification between our model and MODFLOW-CFP at last time step (one hour).

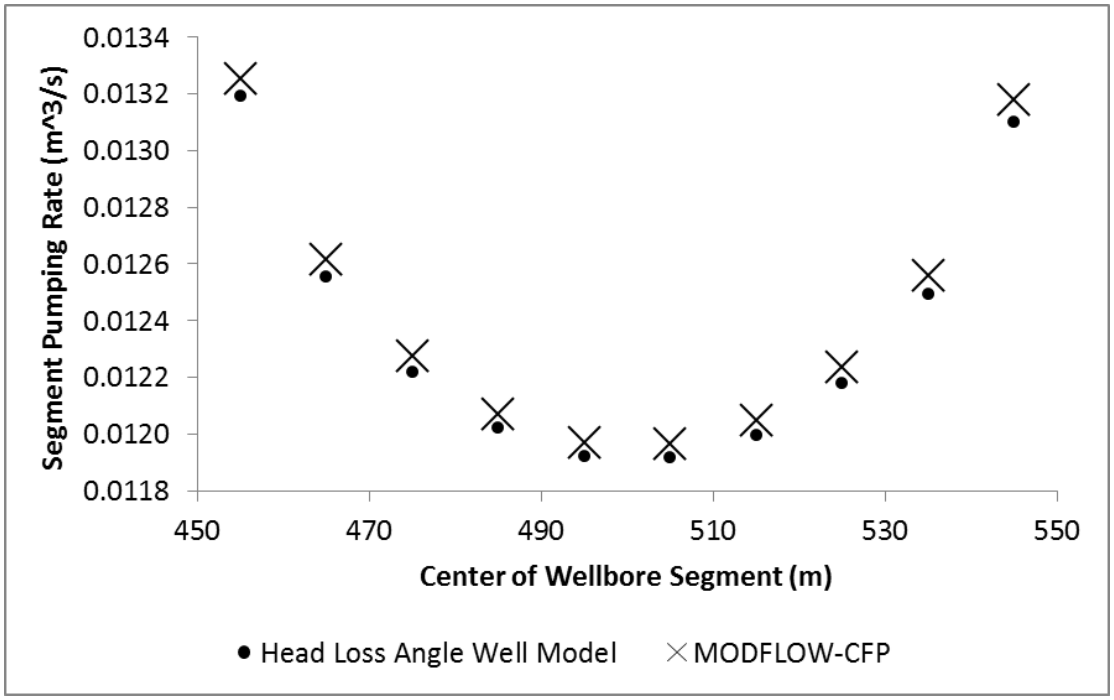

Figure 41. Transient discharge verification between our model and MODFLOW-CFP at last time step (one hour).

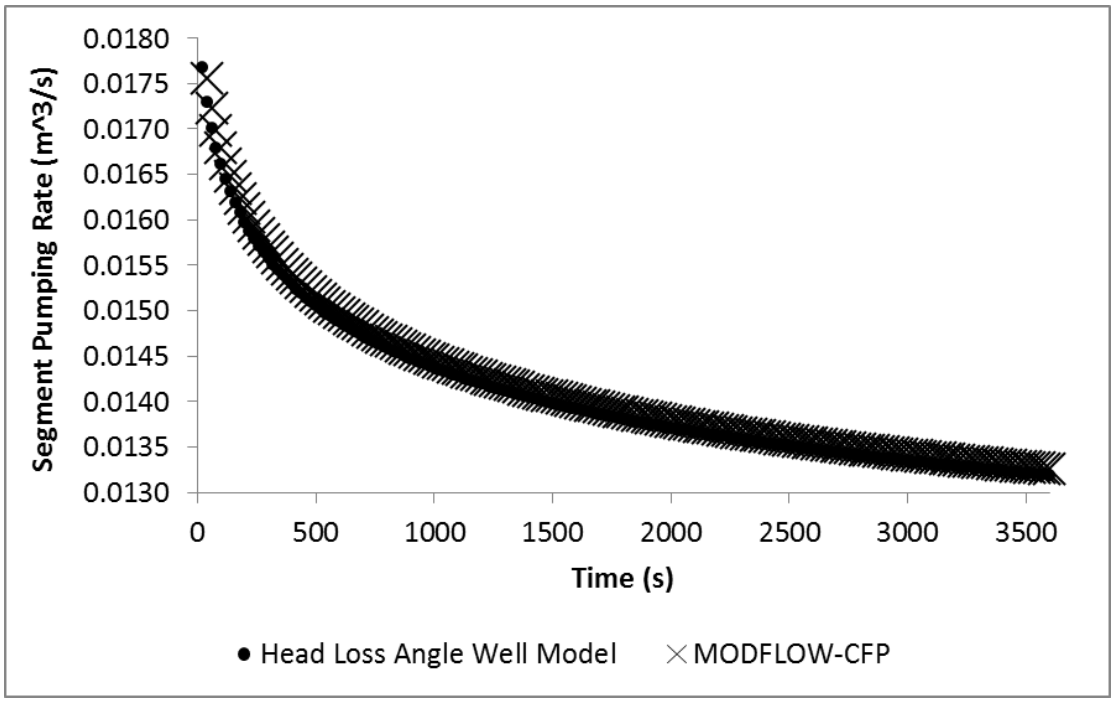

Figure 42. Transient discharge verification of the constant head segment between our model and MODFLOW-CFP.

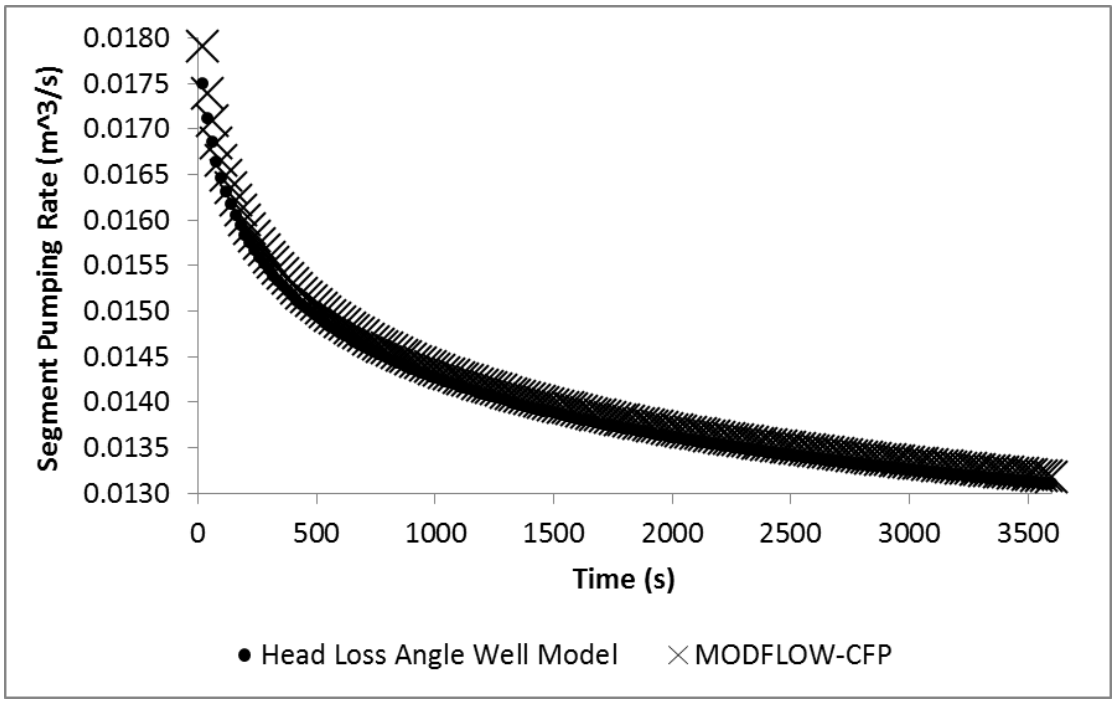

Figure 43. Transient discharge verification of the segment furthest from the constant head segment between our model and MODFLOW-CFP.

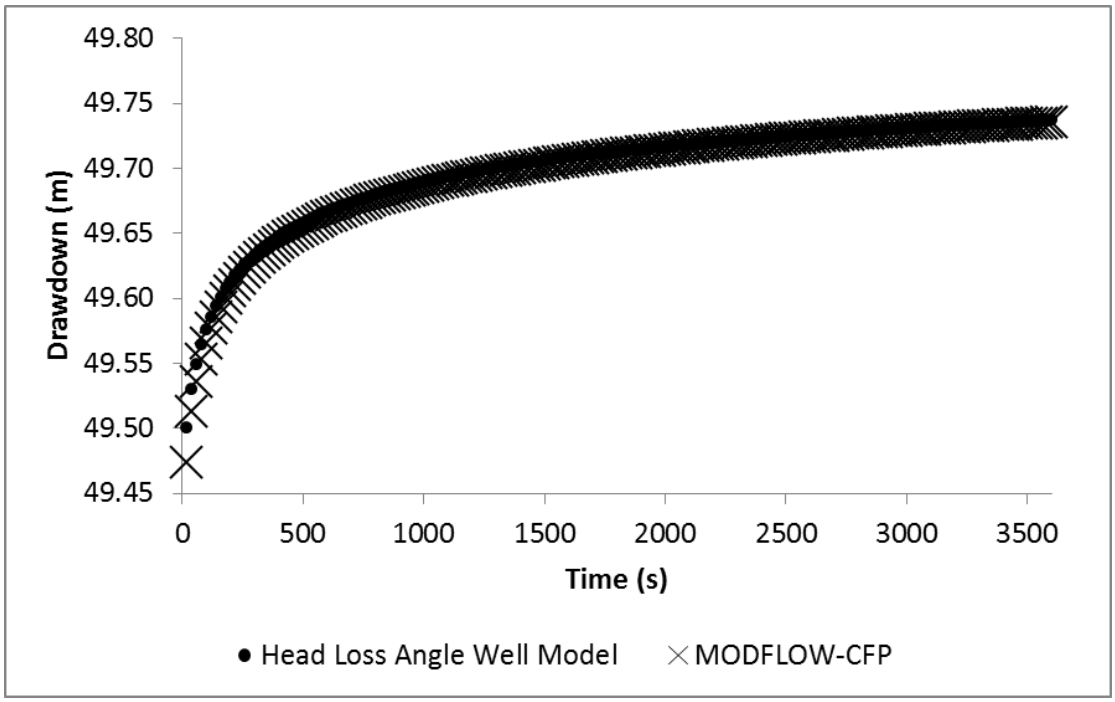

Figure 44. Transient drawdown verification of the segment furthest from the constant head segment between our model and MODFLOW-CFP.

MODEL RESULTS

Uniform Flux Assumption

One of the most debated assumptions of analytical models is whether to use uniform flux or uniform head wellbores (Chen et al., 2003; Debrine, 1970). Most workers use uniform flux as it is easier to implement. Furthermore, it has been found that the uniform flux assumption approximates the uniform head assumption to within about five to ten percent (Zhan et al., 2001; Zhan and Zlotnik, 2002). Work by Ruud and Kabala (1997) found that the well penetration ratio had a strong influence on the uniform flux assumption; short wells in thick aquifers had the most non-uniform flux. However, their work found that such highly non-uniform flux only attributed to roughly a three percent change in head compared to uniform flux calculation. Park and Zhan (2002)

cited Cole and Zlotnik (1994) that if the well length to screen (L/r_w) ratio is greater than 40, then the uniform flux assumption was reasonably close to the uniform head assumption.

These assumptions are investigated with the use of our model by turning friction and acceleration effects off. With the model now operating with a uniform head / infinite conductivity wellbore, we found mixed results. To begin, when the well is fully penetrating we found the uniform flux assumption exactly matches the uniform head assumption (Table 8, Figure 45 & Figure 46). This agreement between uniform flux and uniform head occurs in the fully penetrating case regardless of other model input.

Table 8. First model input for investigation of uniform flux assumptions.

Model Parameters					
a	1000	m	K_x	1E-5	m/s
b	500	m	K_y	1E-5	m/s
c	10	m	K_z	1E-5	m/s
x_1	100	m	S_s	1E-5	1/m
x_2	100	m	Skin	4.60	
y_1	20	m	Density	997	Kg/m^3
y_2	20	m	Viscosity	8.9E-4	
z_1	0	m	Gravity	9.8	m/s^2
z_2	10	m	Well Diameter	0.3	m
Bound at $x = 0$	No Flux		Abs. Pipe Roughness	0.15E-3	m
Bound at $x = a$	No Flux		Friction	Off	
Bound at $y = 0$	No Flux		Critical Reynolds	2000	
Bound at $y = b$	No Flux		Acceleration	Off	
Bound at $z = 0$	No-flux		Integral Abs Error	1E-4	
Bound at $z = c$	No-flux		Integral Rel. Error	1E-6	
One Time Step	Psuedo-Steady State		Discharge Limit	1E-4	m^3/s

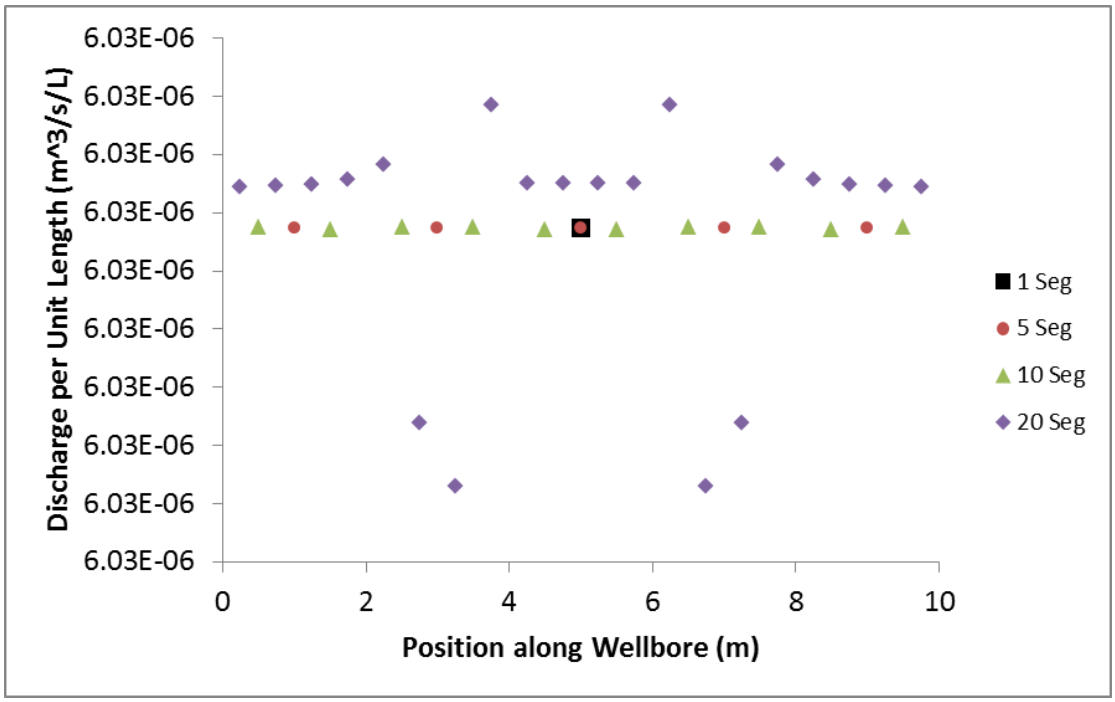

Figure 45. Discharge per unit length using model input data from Table 8.

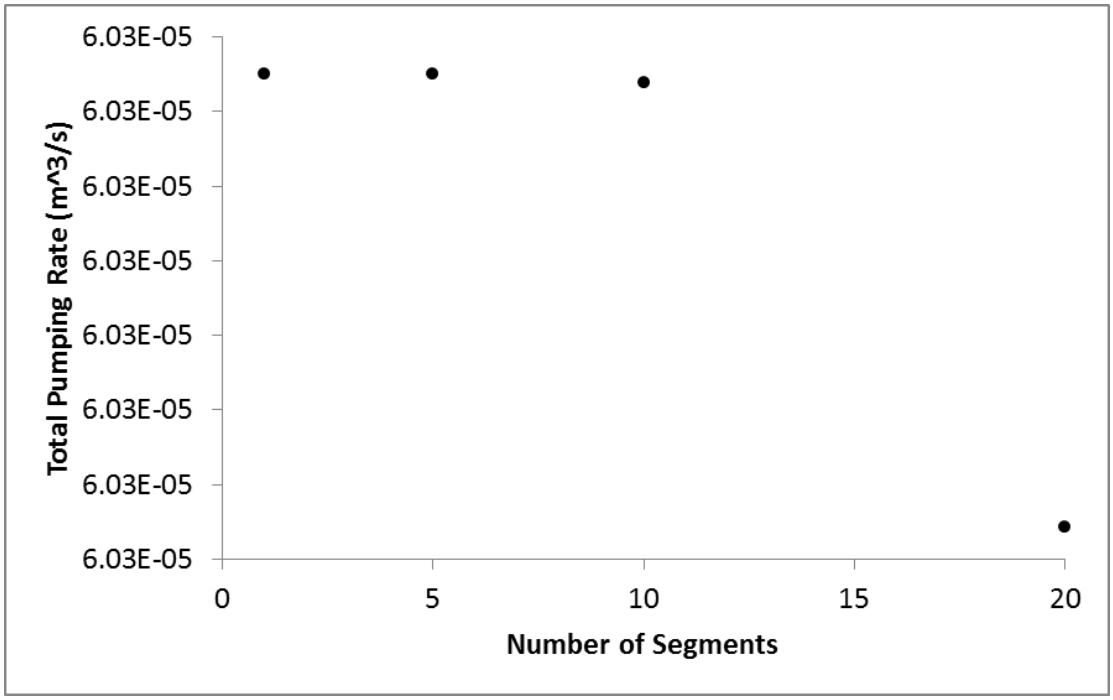

Figure 46. Drawdown for a given number of segments using model input data from Table 8.

When the well is not fully penetrating, two forms of discrepancy occur between the uniform head and the uniform flux assumption. First, there is discrepancy between the distributions of flux along the wellbore. Second, there is discrepancy between the total discharge rates (if a drawdown constraint is used), or drawdown at the pumping segment (if a pumping constraint is used). From the plots generated below, we found that flux per unit length increases dramatically towards the wellbore tips. We do not rigorously quantify the error in wellbore flux distribution but point the reader to the plots and the significant differences therein. However, we do quantify the discrepancy in well total discharge or drawdown at the pumping segment. Error quantified only refers to this second discrepancy; the difference between overall well performance (total drawdown & pumping rate) between the uniform flux / head assumptions.

When we model a well with a penetration ratio of 0.3, we find the difference between uniform flux and uniform head to be 0.31 percent (Table 9, Figure 47 & Figure 48). As a side note, this model run also shows that numerical overshooting is possible with our model as evidenced by the flux per unit length when using 10 and 20 segments. This is caused as the flux per unit length near the well tips increases dramatically. To remedy this issue, the user can select a distribution that adds additional segments to the well tips.

Table 9. Second model input for investigation of uniform flux assumptions.

Model Parameters					
a	1000	m	K_x	1E-4	m/s
b	500	m	K_y	1E-4	m/s
c	10	m	K_z	1E-4	m/s
x_1	100	m	S_s	1E-5	1/m
x_2	100	m	Skin	0	
y_1	20	m	Density	997	Kg/m^3
y_2	20	m	Viscosity	8.9E-4	
z_1	3.5	m	Gravity	9.8	m/s^2
z_2	6.5	m	Well Diameter	0.3	m
Bound at $x = 0$	No Flux		Abs. Pipe Roughness	0.15E-3	m
Bound at $x = a$	No Flux		Friction	Off	
Bound at $y = 0$	No Flux		Critical Reynolds	2000	
Bound at $y = b$	No Flux		Acceleration	Off	
Bound at $z = 0$	No-flux		Integral Abs Error	1E-4	
Bound at $z = c$	No-flux		Integral Rel. Error	1E-6	
One Time Step	Psuedo-Steady State		Discharge Limit	1E-2	m^3/s

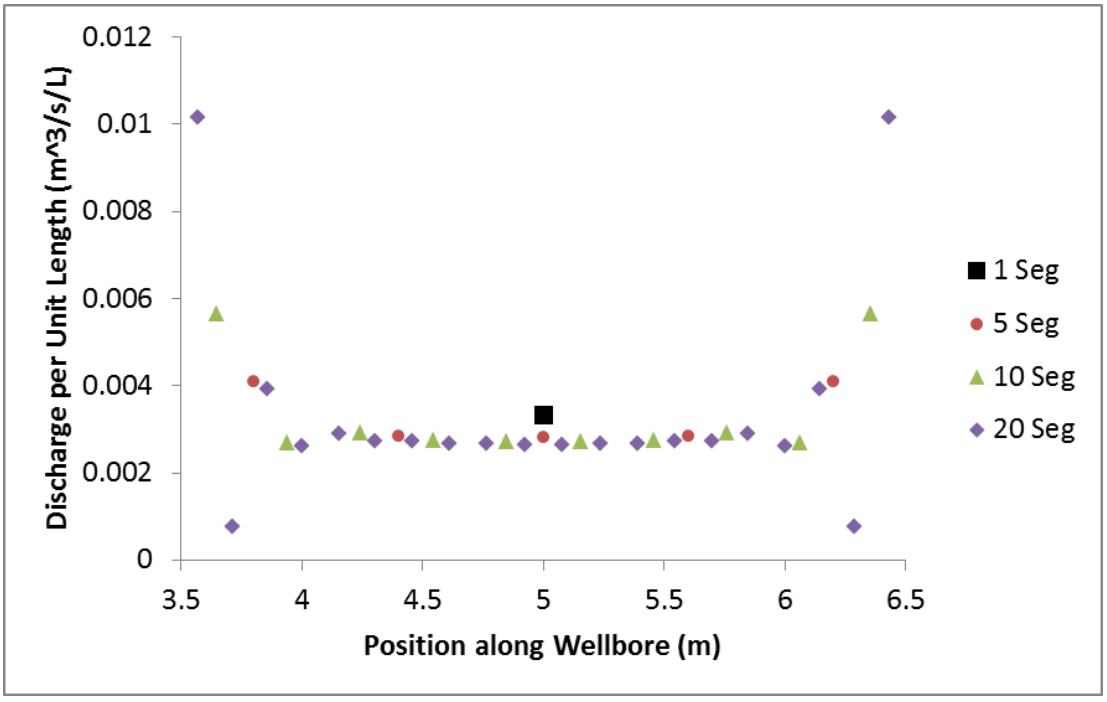

Figure 47. Discharge per unit length using model input data from Table 9.

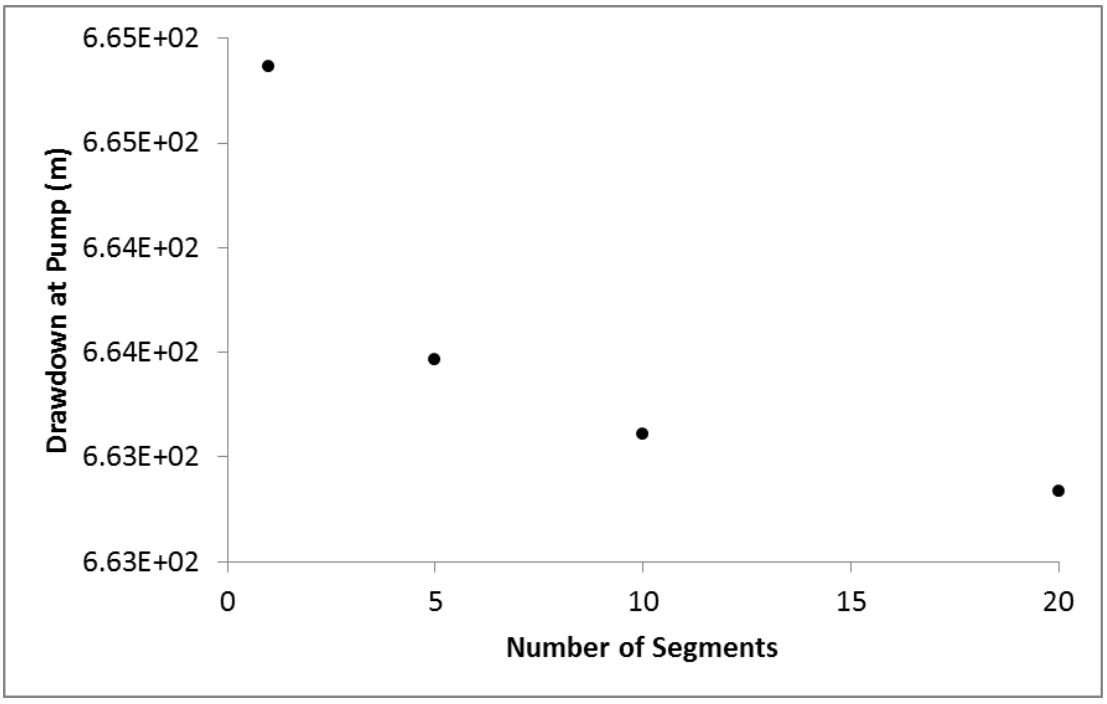

Figure 48. Drawdown for a given number of segments using model input data from Table 9.

In the fourth model run, we allow the *x* & *y* boundaries to go to infinity, but use no flux boundaries for the *z* axis (Table 10, Figure 49 & Figure 50). The error of the uniform flux assumption increases to 3.4 percent. Because other workers have found that the penetration ratios impact uniform flux / head assumptions, it is logical to investigate the case when the penetration ratio is zero. We next investigate the case when all boundaries are infinitely far away (Table 11, Figure 51 & Figure 52). In this case, the error increases to 7.1 percent.

Table 10. Third model input for investigation of uniform flux assumptions.

Model Parameters					
a	Infinity	m	K_x	1E-6	m/s
b	Infinity	m	K_y	1E-6	m/s
c	50	m	K_z	1E-6	m/s
x_1	0	m	S_s	1E-5	1/m
x_2	100	m	Skin	0	
y_1	0	m	Density	997	Kg/m^3
y_2	0	m	Viscosity	8.9E-4	
z_1	10	m	Gravity	9.8	m/s^2
z_2	10	m	Well Diameter	0.3	m
Bound at $x = 0$	N/A		Abs. Pipe Roughness	0.15E-3	m
Bound at $x = a$	N/A		Friction	Off	
Bound at $y = 0$	N/A		Critical Reynolds	2000	
Bound at $y = b$	N/A		Acceleration	Off	
Bound at $z = 0$	No-flux		Integral Abs Error	1E-4	
Bound at $z = c$	No-flux		Integral Rel. Error	1E-6	
One Time Step	50 years		Discharge Limit	1E-4	m^3/s

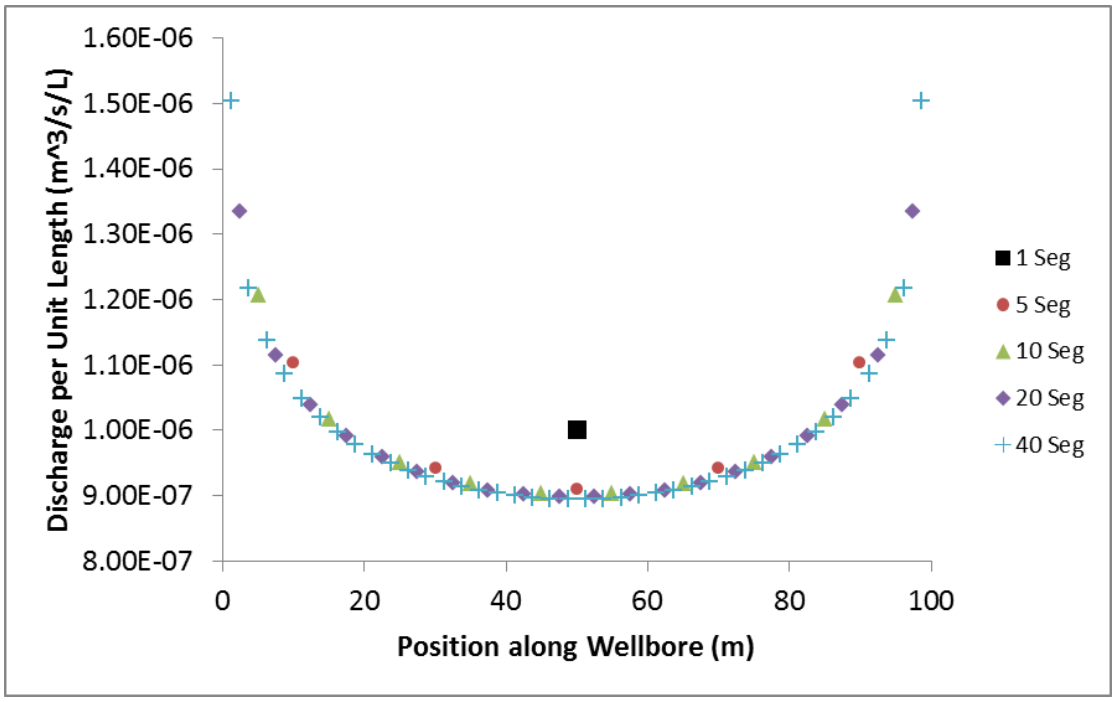

Figure 49. Discharge per unit length using model input data from Table 10.

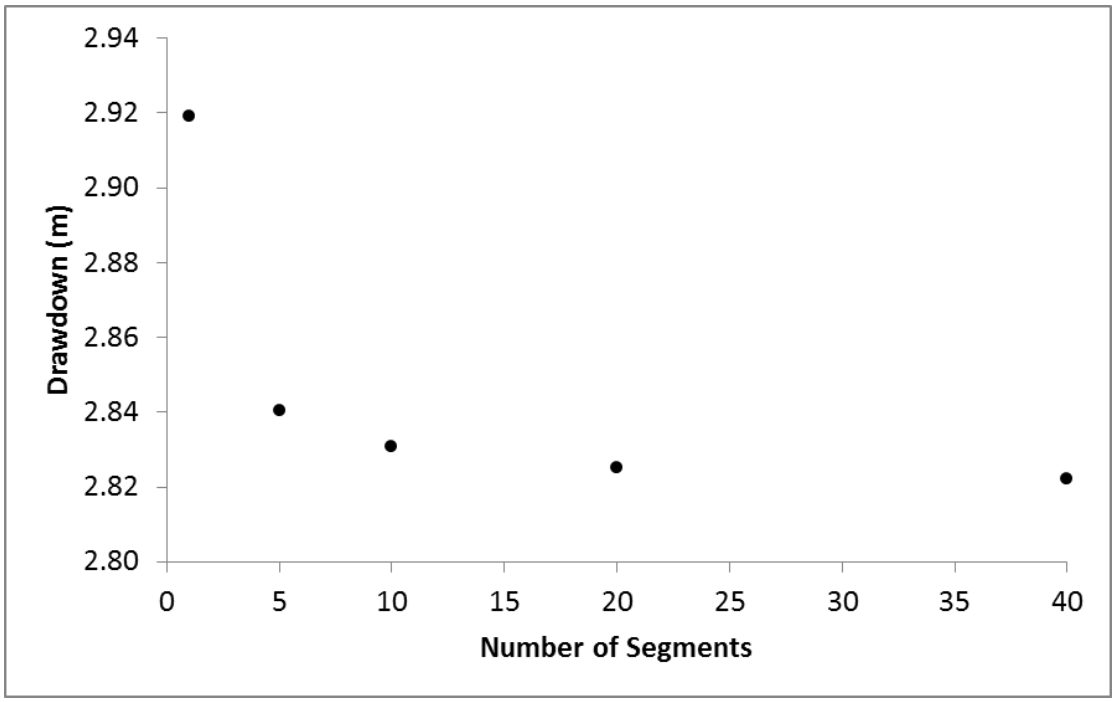

Figure 50. Drawdown for a given number of segments using model input data from Table 10.

Table 11. Fourth model input for investigation of uniform flux assumptions.

Model Parameters					
a	Infinity	m	K_x	1E-3	m/s
b	Infinity	m	K_y	1E-3	m/s
c	Infinity	m	K_z	1E-3	m/s
x_1	0	m	S_s	1E-5	1/m
x_2	10	m	Skin	0	
y_1	0	m	Density	997	Kg/m^3
y_2	0	m	Viscosity	8.9E-4	
z_1	0	m	Gravity	9.8	m/s^2
z_2	0	m	Well Diameter	0.1	m
Bound at $x = 0$	N/A		Abs. Pipe Roughness	0.15E-3	m
Bound at $x = a$	N/A		Friction	Off	
Bound at $y = 0$	N/A		Critical Reynolds	2000	
Bound at $y = b$	N/A		Acceleration	Off	
Bound at $z = 0$	N/A		Integral Abs Error	1E-4	
Bound at $z = c$	N/A		Integral Rel. Error	1E-6	
One Time Step	50 years		Drawdown Limit	1	m

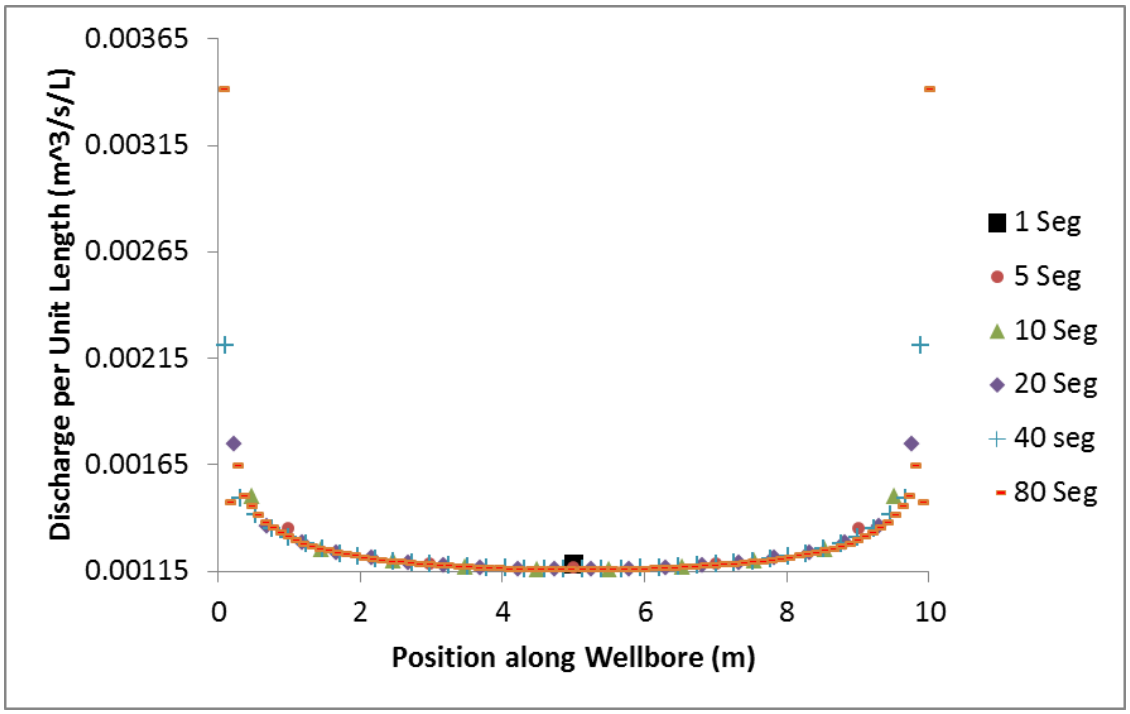

Figure 51. Discharge per unit length using model input data from Table 11.

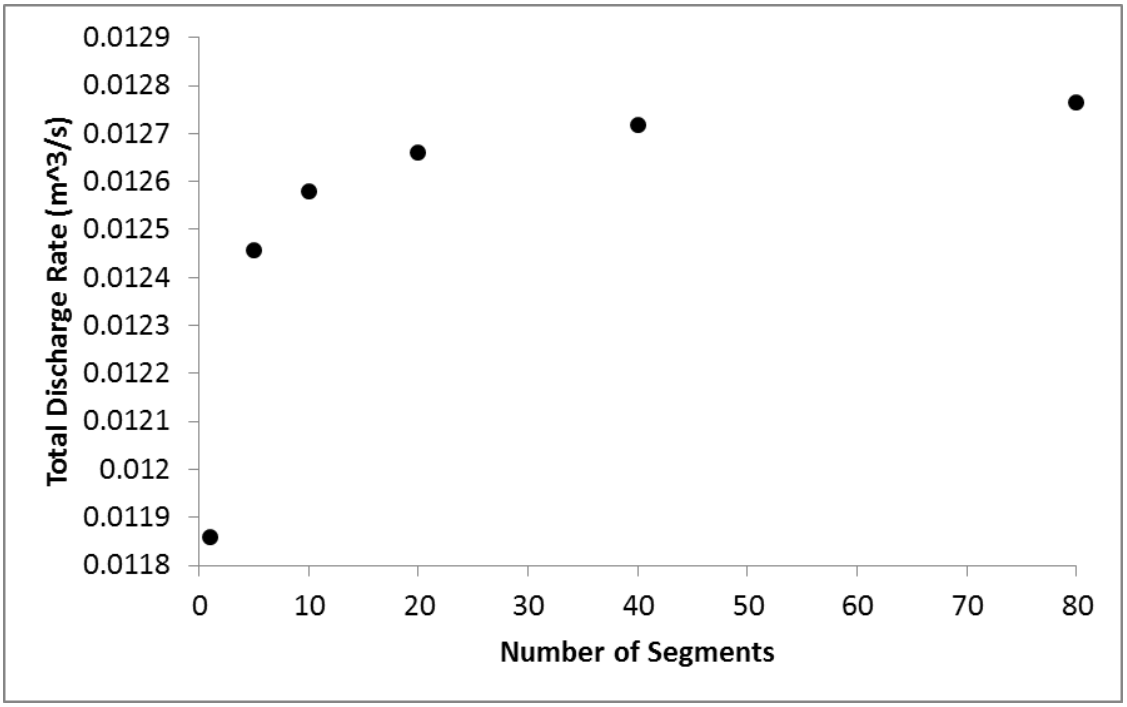

Figure 52. Total discharge for a given number of segments using model input data from Table 11.

In an attempt to understand the impact of penetration ratios (wellbore length divided by aquifer thickness) and wellbore radius ratios (wellbore length divided by wellbore radius) on uniform flux / head assumptions, we ran our model 15 times and plotted the results (Figure 53 & Figure 54). Each model was run until the convergence of three significant figures at the pumping segment. We attempted to model random input within the constraints of possible real scenarios. For instance, we used wellbore radii between 0.1m and 1m, hydraulic conductivity between 1E-2m/s and 1E-7m/s, and random combinations of boundary conditions and wellbore orientations. Interestingly, the model almost always converged to three significant figures upon being modeled with 40 segments; we found similar results when turning intra-wellbore head loss on.

The model output comparing uniform flux / head assumptions is scattered showing a possible trend toward increased error at lower ratios. Because the uniform flux / head assumptions are equivalent when the well is fully penetrating, logically these assumptions should diverge as the penetration ratio decreases from one. However, it is difficult to make broad generalizations. Results show that generally the discrepancy between uniform flux / head assumptions will likely be less than ten percent.

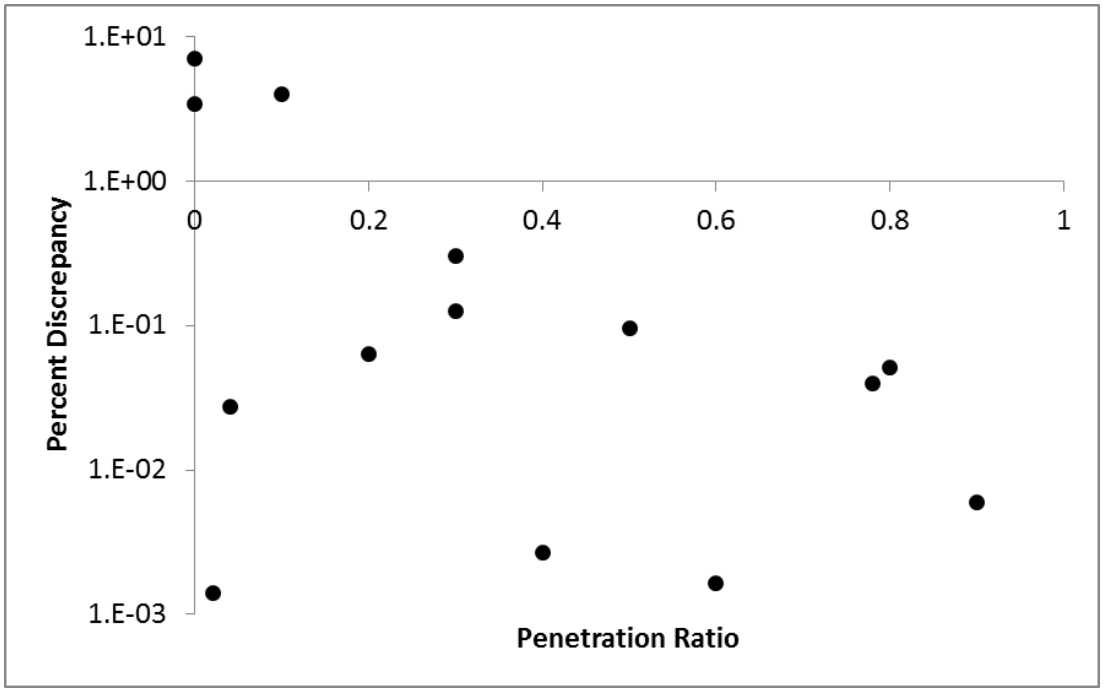

Figure 53. Penetration ratio impact on discrepancy between uniform flux and uniform head assumptions.

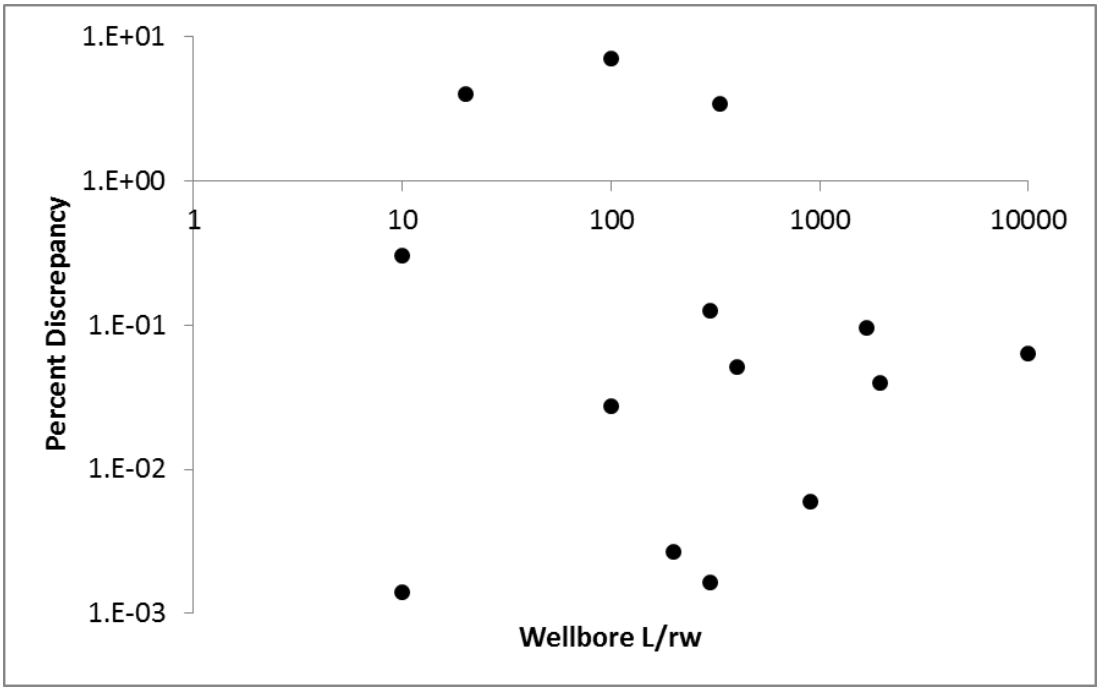

Figure 54. Wellbore length to radius ratio impact on discrepancy between uniform flux and uniform head assumptions.

Intra-Wellbore Head Loss

Our model was run 360 times to investigate how kinetic and frictional head loss impacted the results. There were three hypothetical aquifers modeled. Two aquifers had high hydraulic conductivity, while another had low hydraulic conductivity. Two wells had skin, and another did not. One aquifer could achieve steady state via a constant head boundary, while the others could not.

Each aquifer was modeled using two wellbore sizes, 0.3m and 0.1m in diameter. Two aquifers were modeled for three different pumping rates of: 0.1 m^3/s, 0.01 m^3/s, 0.001 m^3/s. One aquifer was modeled with three pumping rates of: 1 m^3/s, 0.1 m^3/s, 0.01 m^3/s. Each aquifer also was modeled for five different wellbore lengths: 10m, 50m, 100m, 300m, 600m. Each aquifer was modeled using the infinite conductivity wellbore, the friction head loss only wellbore, the kinetic head loss only wellbore, and the kinetic & friction head loss wellbore.

All model input and output from the 360 simulations is in the *Supplemental Material* document accompanying this thesis. For tables describing the three aquifers, please consult *Supplemental Material, Part A.* Following each model input table in *Part A* is model output. Data plotted in *Part A* is for the pumping segment's drawdown.

Model output characterizes two levels of importance for head loss terms, in the relative sense and the absolute sense. The relative impact of head loss is defined as the drawdown accounting for friction and/or kinetic effects at the pumping segment divided by the infinite conductivity drawdown. This measure is a percentage, where a value of zero indicates that no impact occurred and positive value indicates that drawdown

increased compared to the infinite conductivity wellbore. The absolute head loss is the actual head loss experienced by the wellbore in meters. This is defined as the drawdown accounting for friction and/or kinetic effects at the pumping segment minus the infinite conductivity wellbore drawdown.

The most intriguing result of the simulations was an understanding of the importance of kinetic head loss. From our model results we found that kinetic head loss is for the most part constant regardless of the wellbore length. We also found that kinetic head loss is greater than friction head loss for short length wells. As the length of the wellbore goes to zero, frictional head losses also go to zero; however, kinetic head loss remains constant (Figure 55). This feature is an important new finding.

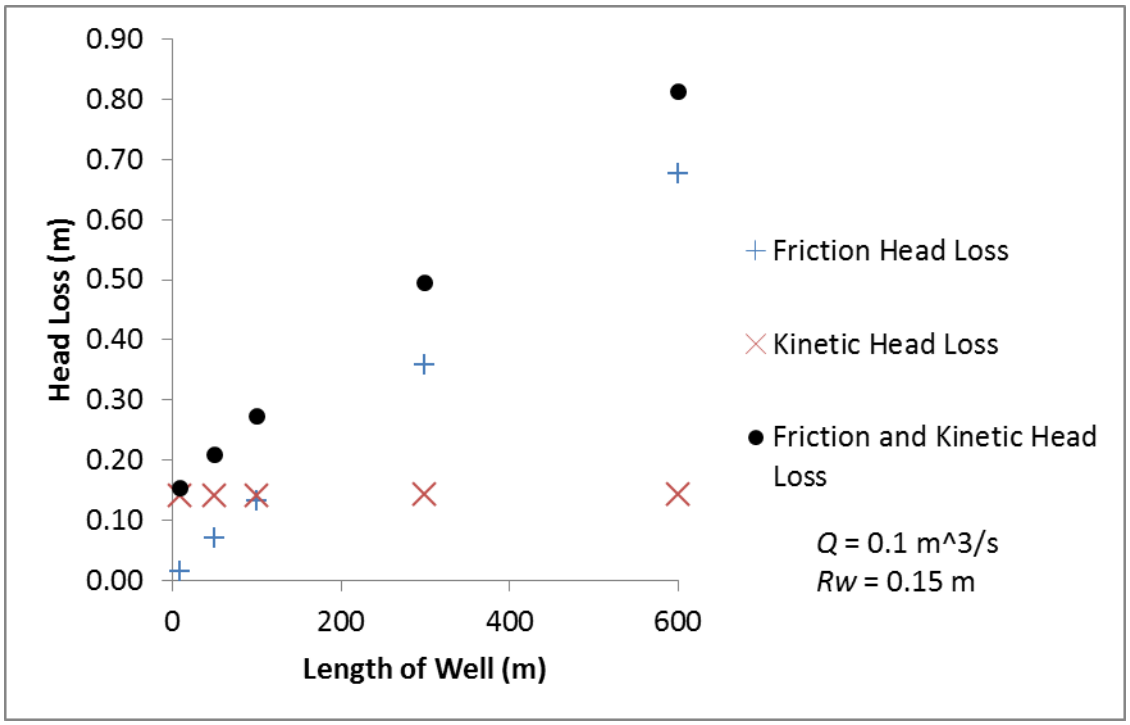

Figure 55. Absolute head losses and importance of kinetic effects.

We also investigated how kinetic and frictional head loss affected the distributions of drawdown and flux along the wellbore. From the two cases plotted, it becomes apparent that the effects of intra-wellbore head loss are quite variable (Figure 56 - Figure 59). In the first plots, intra-wellbore head loss is relatively low and does not affect the flux distribution (Figure 56 & Figure 57). However in the second plots, intra-wellbore head loss is very significant and greatly affects the flux distribution (Figure 58 & Figure 59). These two scenarios capture our main finding from model output. For typical pumping rates and/or typical hydraulic conductivity, intra-wellbore head loss is insignificant. However, if pumping rates and/or hydraulic conductivities are extremely high, the intra-wellbore head loss is very important.

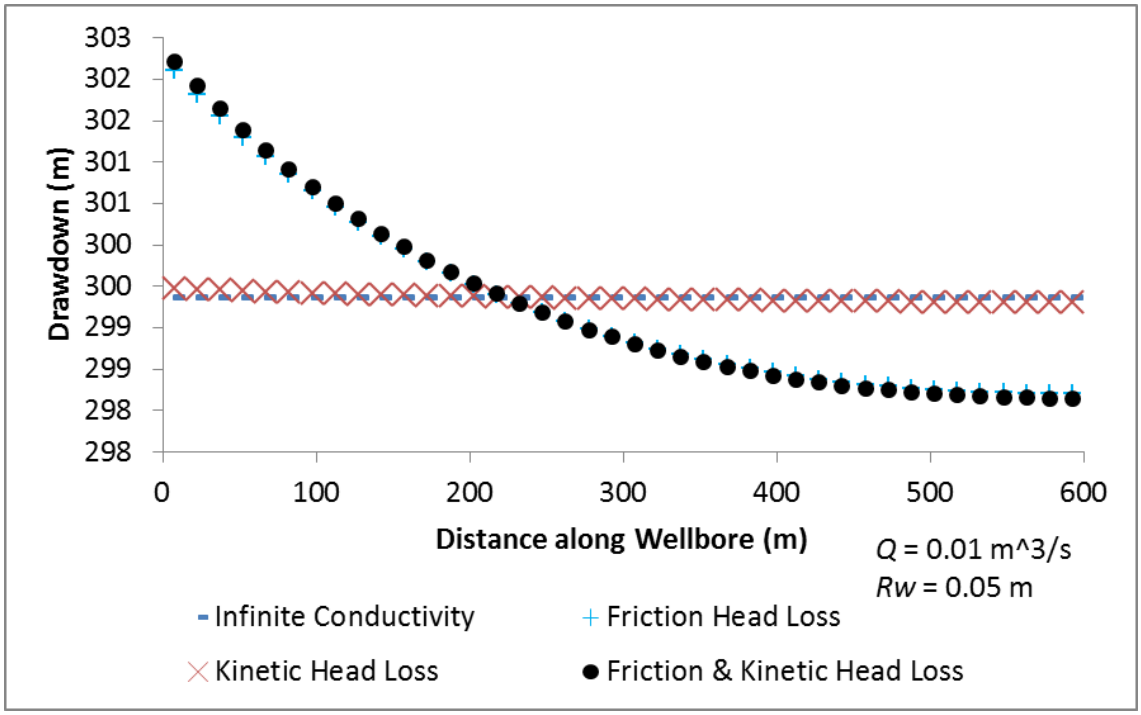

Figure 56. Head loss impact on drawdown distribution in a low hydraulic conductivity aquifer.

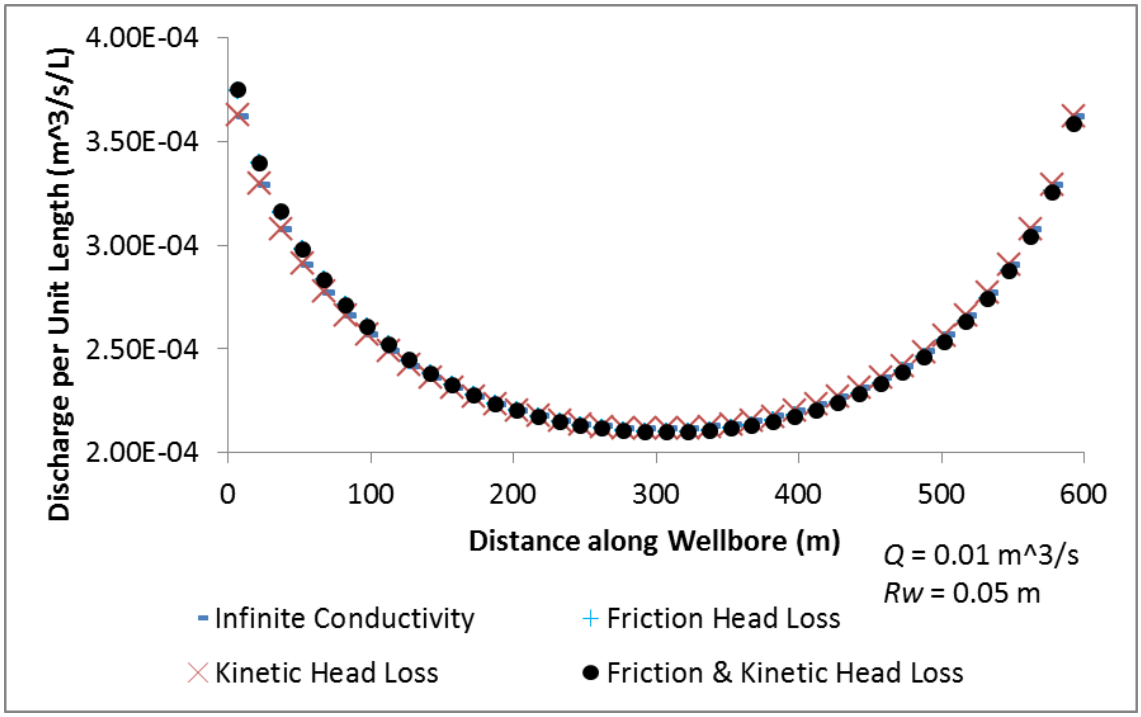

Figure 57. Head loss impact on flux distribution in a low conductivity aquifer.

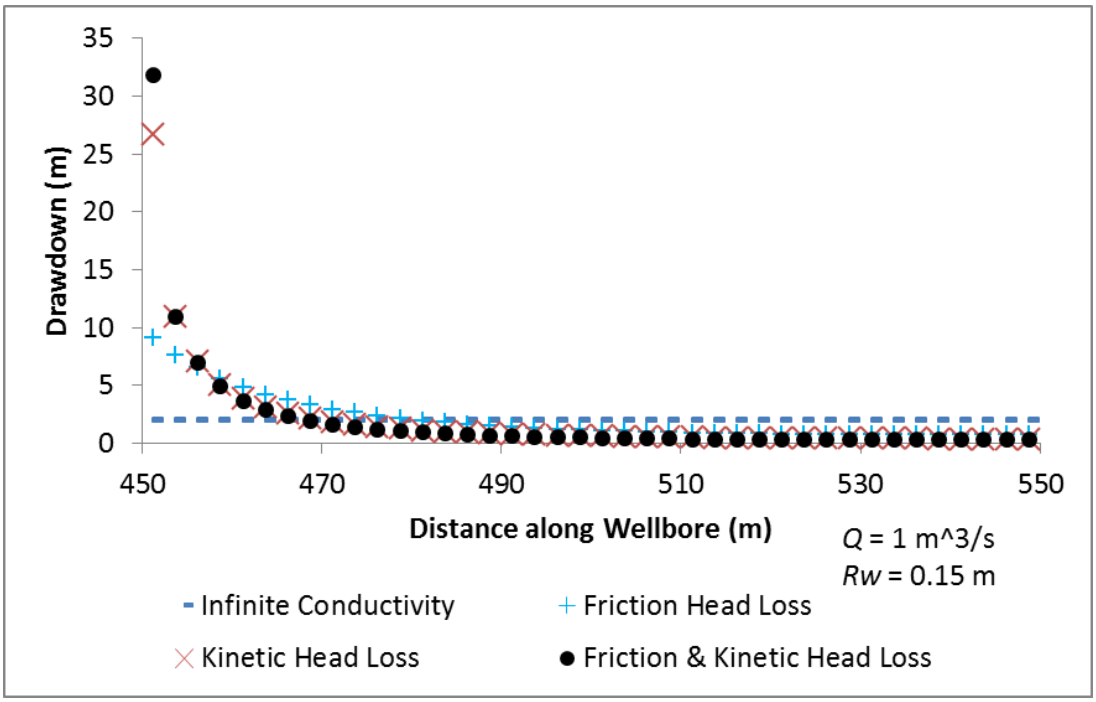

Figure 58. Head loss impact on drawdown distribution in a high hydraulic conductivity aquifer.

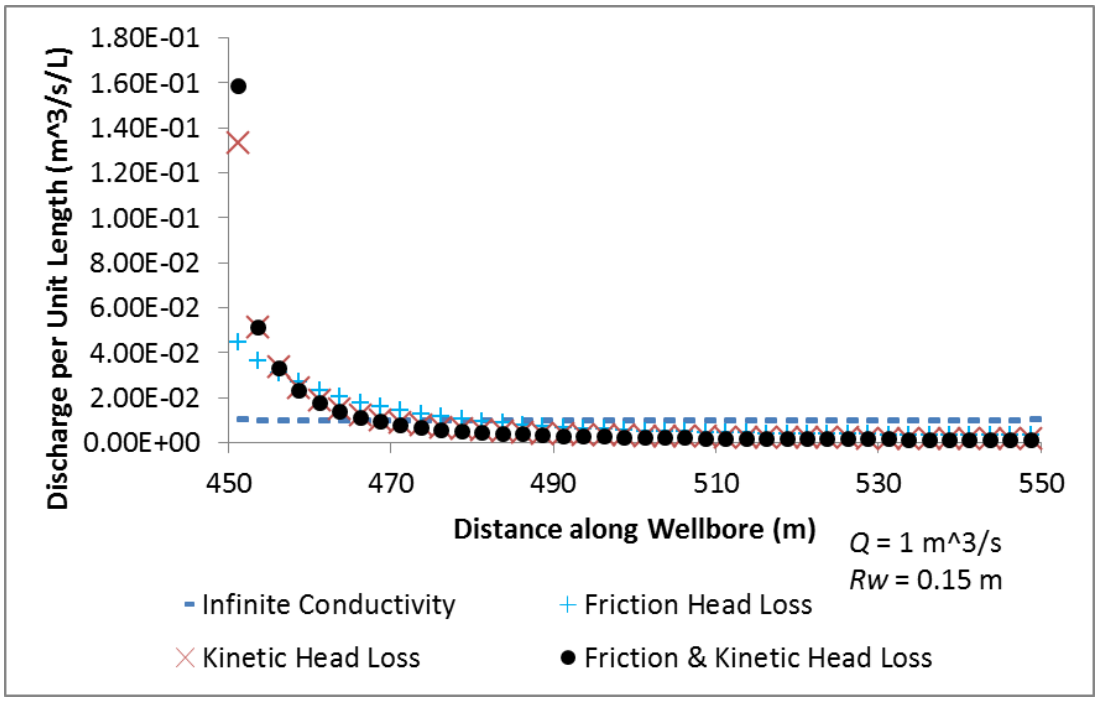

Figure 59. Head loss impact on flux distribution in a high conductivity aquifer.

Overall results show that intra-wellbore head loss is relatively insignificant for most cases (Figure 60). However, that is not to say it is insignificant for all cases (Figure 61). It all depends upon the relative drawdown impact of the aquifer. If the drawdown from the aquifer is less than a few meters, the intra-wellbore head loss can become important if they exceed or approach the aquifer losses. Conversely, if the aquifer losses are greater than several times the intra-wellbore losses, then intra-wellbore head losses are insignificant. Our model output shows that given typical wellbore lengths (0-600m), hydraulic conductivities (1E-3 to 1E-7 m/s), well diameters (0.1m to 0.3m), and pumping rates (less than $0.5 m^3/s$), intra-wellbore head losses are usually insignificant.

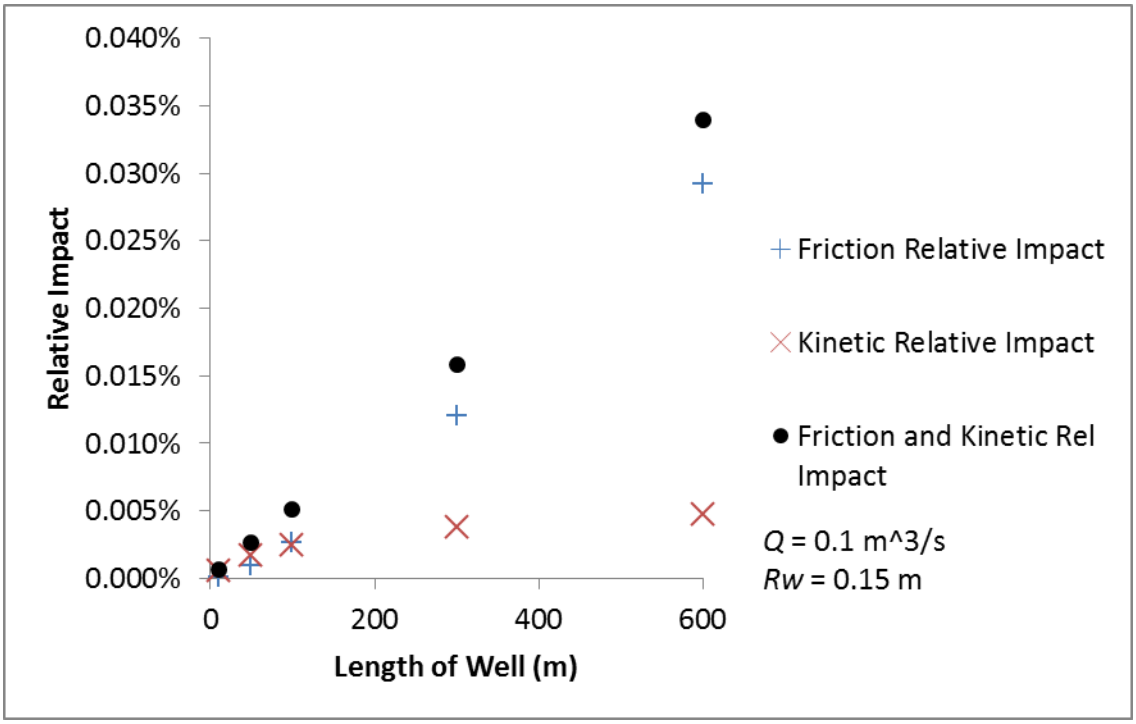

Figure 60. Relative head loss in a low hydraulic conductivity aquifer.

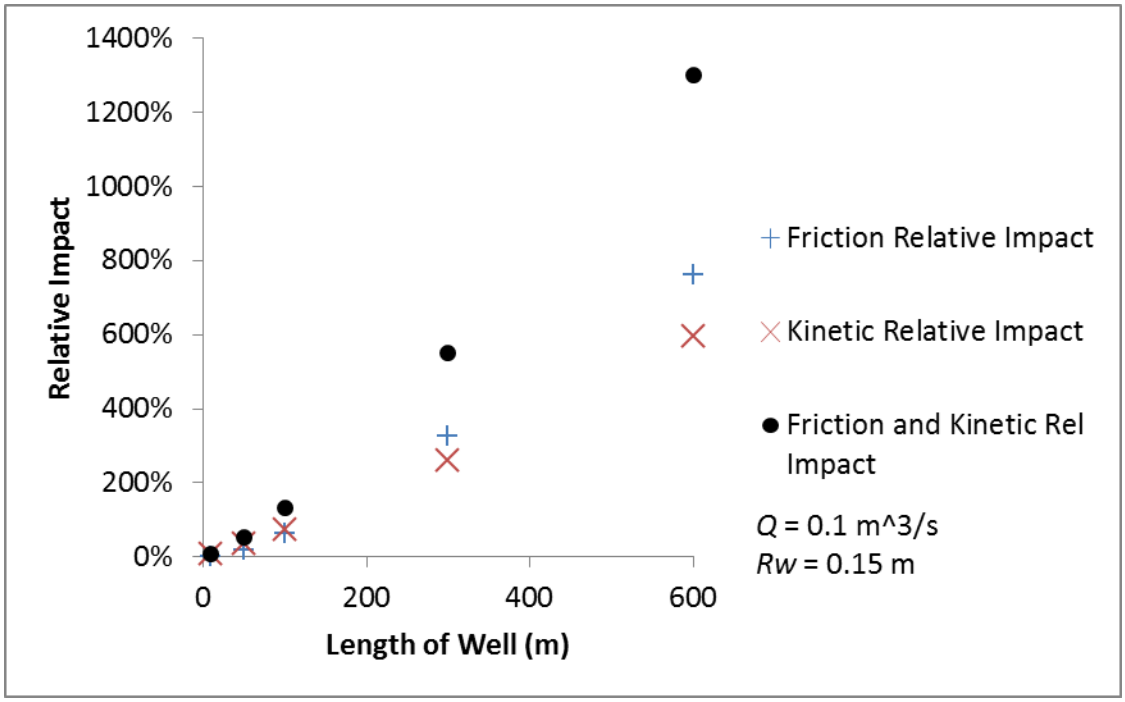

Figure 61. Relative head loss in a high hydraulic conductivity aquifer.

CONCLUSIONS

Intra-wellbore kinetic head loss is more significant than intra-wellbore friction head loss for short wellbores (vertical or horizontal). Our model results show that kinetic head loss was more important than friction head loss if the wellbore was less than 10m long. In some cases the kinetic head loss was greater than frictional head loss in wellbores up to 50m long. The identification that kinetic effects are more important than friction effects is an important new finding for groundwater wells. However, several factors influence kinetic head loss importance relative to frictional head loss importance (such as pipe roughness) and therefore our results must be taken with caution.

Generally, intra-wellbore head loss is not very important relative to aquifer head loss. However, the effects of intra-wellbore head loss may become significant in extreme

cases. Similar to Joshi (1991), a good method to assess the possible need to model intra-wellbore head loss is to assume the total pumping rate enters in the middle of the wellbore and calculate pipe head loss. If this pipe drawdown is significantly less than aquifer drawdown, then a uniform flux / infinite conductivity model will be sufficient. Otherwise use of our model or MODFLOW-CFP is likely required.

It is interesting to consider the empirical work of Jacob (1947) and Rorabaugh (1953) which suggests friction effects caused intra-wellbore head loss to vary by the square of discharge (Ramey, 1982). This finding is logical upon inspection of the Darcy-Weisbach friction head loss equation. However, intra-wellbore head loss will also vary by the square of discharge upon inspection of the kinetic head loss equation derived in this chapter. It is logical to conclude that the similar drawdown-discharge relationship between friction and kinetic effects may have resulted in the misidentification of kinetic head loss as friction head loss.

Using our model to investigate the uniform head / flux assumptions, we found that the approximation of uniform head with uniform flux may at most yield an error of ten percent. This result agrees with other literature findings (Zhan et al., 2001; Zhan and Zlotnik, 2002). However, we did not find the ratio relationships between uniform flux and uniform head as described in Ruud and Kabala (1997) or Park and Zhan (2002). Our comparisons showed much scatter that was difficult to interpret. We only found that when the well is fully penetrating, uniform flux and uniform head are equal; otherwise there will be a discrepancy between the calculations. Upon noticing the significantly

different flux distributions between uniform flux and uniform head models, it is recommended that more effort should be made to develop uniform head derivations.

CHAPTER III

DERIVATION OF A UNIFORM FLUX WELL

DERIVATION OF A POINT SINK / SOURCE

The mathematical relationship between a well's pumping rate and aquifer drawdown begins with the derivation of a point source / sink. This point source / sink has a pumping rate $Q(t)$ [L^3T^{-1}] that is positive for extraction (sink) and negative for injection (source). The point source / sink may be located anywhere inside a box. The dimensions [L] of the box are a, b, c for the x-axis, y-axis and z-axis respectively. The point source / sink is located at x_0, y_0, z_0 [L]. The point source / sink affects drawdown at some point x, y, z [L]. The point x, y, z is termed the sample point in this thesis (Figure 62).

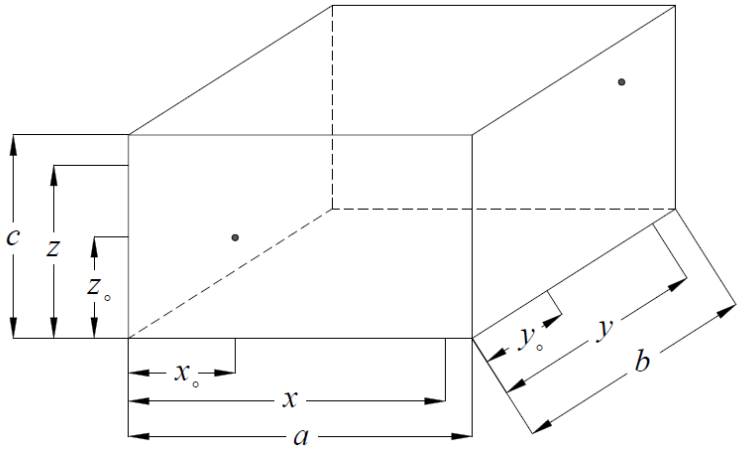

Figure 62. Aquifer conceptual model with source / sink and sample point.

Derivation of our model begins with the differential equation governing confined groundwater flow and a point sink represented by Dirac delta functions. The partial differential equation governing groundwater flow is

$$S_s \frac{\partial h}{\partial t} = K_x \frac{\partial^2 h}{\partial x^2} + K_y \frac{\partial^2 h}{\partial y^2} + K_z \frac{\partial^2 h}{\partial z^2} - Q(t)\delta(x - x_0)\delta(y - y_0)\delta(z - z_0), \qquad (8)$$

where S_s is specific storage [L^{-1}], h is head [L], t is time [T], K_x, K_y, K_z are hydraulic conductivities [LT^{-1}], $Q(t)$ [L^3T^{-1}] is the pumping rate (positive for extraction) as a function of time, and δ is the Dirac delta function (Roscoe Moss Company, 1990). We then change head to drawdown, ($d = h_0 - h_1$). The partial differential equation governing confined groundwater flow is then rewritten using drawdown as

$$S_s \frac{\partial d}{\partial t} = K_x \frac{\partial^2 d}{\partial x^2} + K_y \frac{\partial^2 d}{\partial y^2} + K_z \frac{\partial^2 d}{\partial z^2} + Q(t)\delta(x - x_0)\delta(y - y_0)\delta(z - z_0). \qquad (9)$$

We then compute the time Laplace transform to remove time dependence. The initial condition for all cases is zero drawdown at time zero. The Laplace transform of the groundwater flow equation is

$$p\bar{d} = \left(\frac{K_x}{S_s}\right)\frac{\partial^2 \bar{d}}{\partial x^2} + \left(\frac{K_y}{S_s}\right)\frac{\partial^2 \bar{d}}{\partial y^2} + \left(\frac{K_z}{S_s}\right)\frac{\partial^2 \bar{d}}{\partial z^2} + \left(\frac{\bar{Q}}{S_s}\right)\delta(x - x_0)\delta(y - y_0)\delta(z - z_0), \qquad (10)$$

where the over bar means the variable is in the Laplace domain, and p is the Laplace transform variable. There are two possible boundary conditions for each of the six sides of the box shaped reservoir. The boundary of any one side of the box may be constant head – Neumann or no flux – Dirichlet. We will first solve the boundary value problem (BVP) in the Laplace domain, and then take the inverse Laplace transform to yield

solutions in the real time domain. A few example cases are presented below to explain the methodology.

No Flux Boundaries on Each Side

In this case, we set the spatial partial derivatives of drawdown to zero at all of the boundaries. Stating that there is no flux across any of the boundaries

$$\frac{\partial \bar{d}}{\partial x}|_{x=0} = \frac{\partial \bar{d}}{\partial x}|_{x=a} = \frac{\partial \bar{d}}{\partial y}|_{y=0} = \frac{\partial \bar{d}}{\partial y}|_{y=b} = \frac{\partial \bar{d}}{\partial z}|_{z=0} = \frac{\partial \bar{d}}{\partial z}|_{z=c} = 0, \tag{11}$$

our solution takes the form with undetermined coefficient A (Park and Zhan, 2002; Zhan et al., 2001):

$$\bar{d} = \sum_{n=0}^{\infty}\sum_{m=0}^{\infty}\sum_{l=0}^{\infty} A_{n,m,l} \cos[n\pi x/a]\cos[m\pi y/b]\cos[l\pi z/c], \tag{12}$$

where n, m, l are non-negative integers. Substituting our proposed solution into the Laplace transformed equation from above and computing derivatives where necessary we find

$$\begin{aligned} & p\sum_{n=0}^{\infty}\sum_{m=0}^{\infty}\sum_{l=0}^{\infty} A_{n,m,l} \cos[n\pi x/a]\cos[m\pi y/b]\cos[l\pi z/c] \\ & = \sum_{n=0}^{\infty}\sum_{m=0}^{\infty}\sum_{l=0}^{\infty} A_{n,m,l} \cos[n\pi x/a]\cos[m\pi y/b]\cos[l\pi z/c] \\ & \quad \left(-\left(\frac{K_x}{S_s}\right)\left(\frac{n\pi}{a}\right)^2 - \left(\frac{K_y}{S_s}\right)\left(\frac{m\pi}{b}\right)^2 - \left(\frac{K_z}{S_s}\right)\left(\frac{l\pi}{c}\right)^2\right) \cdot \\ & \quad + \left(\frac{\bar{Q}}{S_s}\right)\delta(x-x_0)\delta(y-y_0)\delta(z-z_0) \end{aligned} \tag{13}$$

Now we must determine coefficients for each iteration of the series. To determine the first coefficient of A when $n = m = l = 0$, we substitute and take three integrals

$$p\int_0^a\int_0^b\int_0^c A_{0,0,0}\cos[0\pi\,x/a]\cos[0\pi\,y/b]\cos[0\pi\,z/c]\;dz\;dy\;dx =$$
$$\int_0^a\int_0^b\int_0^c A_{0,0,0}\cos[0\pi\,x/a]\cos[0\pi\,y/b]\cos[0\pi\,z/c]$$
$$\left(-\left(\frac{K_x}{S_s}\right)\left(\frac{0\pi}{a}\right)^2-\left(\frac{K_y}{S_s}\right)\left(\frac{0\pi}{b}\right)^2-\left(\frac{K_z}{S_s}\right)\left(\frac{0\pi}{c}\right)^2\right) \quad , \qquad (14)$$
$$+\left(\frac{\overline{Q}}{S_s}\right)\delta(x-x_0)\delta(y-y_0)\delta(z-z_0)\;dz\;dy\;dx$$

which yields

$$A_{0,0,0}=\frac{1}{abcS_s}\frac{\overline{Q}}{p}. \qquad (15)$$

Now we determine the coefficients of A when n is non-zero and $m = l = 0$. To generate an orthogonal set, we multiply the Laplace groundwater flow equation by $\cos[n'\pi\,x/a]$, where n' is a non-zero integer. The new equation requiring three integrations is

$$p\int_0^a\int_0^b\int_0^c \cos[n'\pi\,x/a]A_{n',0,0}\cos[n\pi\,x/a]\cos[0\pi\,y/b]\cos[0\pi\,z/c]\;dz\;dy\;dx =$$
$$\int_0^a\int_0^b\int_0^c \cos[n'\pi\,x/a]\left(A_{n',0,0}\cos[n\pi\,x/a]\cos[0\pi\,y/b]\cos[0\pi\,z/c]\right.$$
$$\left(-\left(\frac{K_x}{S_s}\right)\left(\frac{n'\pi}{a}\right)^2-\left(\frac{K_y}{S_s}\right)\left(\frac{0\pi}{b}\right)^2-\left(\frac{K_z}{S_s}\right)\left(\frac{0\pi}{c}\right)^2\right) \quad , \qquad (16)$$
$$\left.+\left(\frac{\overline{Q}}{S_s}\right)\delta(x-x_0)\delta(y-y_0)\delta(z-z_0)\right)\;dz\;dy\;dx$$

which yields

$$p\frac{A_{n',0,0}}{2}abc = -\left(\frac{K_x}{S_s}\right)\left(\frac{n'\pi}{a}\right)^2\frac{A_{n',0,0}}{2}abc + \left(\frac{\overline{Q}}{S_s}\right)\cos\left[n'\pi\, x_0/a\right]$$

$$A_{n',0,0} = \frac{2\overline{Q}\cos\left[n'\pi\, x_0/a\right]}{abcS_s\left(p + \left(\frac{K_x}{S_s}\right)\left(\frac{n'\pi}{a}\right)^2\right)}, \text{ or} \qquad . \qquad (17)$$

$$A_{n,0,0} = \frac{2\overline{Q}\cos\left[n\pi\, x_0/a\right]}{abcS_s\left(p + \left(\frac{K_x}{S_s}\right)\left(\frac{n\pi}{a}\right)^2\right)},\ n \neq 0$$

Similarly, with respect to the other principal directions we find

$$A_{0,m,0} = \frac{2\overline{Q}\cos\left[m\pi\, y_0/b\right]}{abcS_s\left(p + \frac{K_y}{S_s}\left(\frac{m\pi}{b}\right)^2\right)},\ m \neq 0$$

$$A_{0,0,l} = \frac{2\overline{Q}\cos\left[l\pi\, z_0/c\right]}{abcS_s\left(p + \frac{K_z}{S_s}\left(\frac{l\pi}{c}\right)^2\right)},\ l \neq 0 \qquad . \qquad (18)$$

Next we determine the coefficients of *A* when *n* and *m* are non-zero and *l* = 0. To generate an orthogonal set, we multiply the Laplace groundwater flow equation by $\cos\left[n'\pi\, x/a\right]\cos\left[m'\pi\, y/b\right]$, where *n*' and *m*' are non-zero integers. Upon substitution, the new equation requiring three integrations is

$$p\int_0^a\int_0^b\int_0^c \cos[n'\pi x/a]\cos[m'\pi y/b]A_{n',0,0}\cos[n\pi x/a]\cos[0\pi y/b]$$
$$\cos[0\pi z/c]dz\ dy\ dx = \int_0^a\int_0^b\int_0^c \cos[n'\pi x/a]\cos[m'\pi y/b]$$
$$\left(A_{n',0,0}\cos[n\pi x/a]\cos[0\pi y/b]\cos[0\pi z/c]\right. \quad , \qquad (19)$$
$$\left(-\left(\frac{K_x}{S_s}\right)\left(\frac{n'\pi}{a}\right)^2-\left(\frac{K_y}{S_s}\right)\left(\frac{m'\pi}{b}\right)^2-\left(\frac{K_z}{S_s}\right)\left(\frac{0\pi}{c}\right)^2\right)$$
$$\left.+\left(\frac{\overline{Q}}{S_s}\right)\delta(x-x_0)\delta(y-y_0)\delta(z-z_0)\right)\ dz\ dy\ dx$$

which yields

$$p\frac{A_{n',m',0}}{4}abc = \left(-\left(\frac{K_x}{S_s}\right)\left(\frac{n'\pi}{a}\right)^2-\left(\frac{K_y}{S_s}\right)\left(\frac{m'\pi}{b}\right)^2\right)\frac{A_{n',m',0}}{4}abc$$
$$+\left(\frac{\overline{Q}}{S_s}\right)\cos[n'\pi x_0/a]\cos[m'\pi y/b] \quad . \qquad (20)$$

Following the same procedure as above for each of the principal directions, the solution is

$$A_{n,m,0} = \frac{4\overline{Q}\cos[n\pi x_0/a]\cos[m\pi y_0/b]}{abcS_s\left(p+\frac{K_x}{S_s}\left(\frac{n\pi}{a}\right)^2+\frac{K_y}{S_s}\left(\frac{m\pi}{b}\right)^2\right)},\ m\neq 0 \text{ and } n\neq 0$$
$$A_{n,0,l} = \frac{4\overline{Q}\cos[n\pi x_0/a]\cos[L\pi z_0/c]}{abcS_s\left(p+\frac{K_x}{S_s}\left(\frac{n\pi}{a}\right)^2+\frac{K_z}{S_s}\left(\frac{l\pi}{c}\right)^2\right)},\ l\neq 0 \text{ and } n\neq 0 \quad . \qquad (21)$$
$$A_{0,m,l} = \frac{4\overline{Q}\cos[m\pi y_0/b]\cos[L\pi z_0/c]}{abcS_s\left(p+\frac{K_y}{S_s}\left(\frac{m\pi}{b}\right)^2+\frac{K_z}{S_s}\left(\frac{l\pi}{c}\right)^2\right)},\ l\neq 0 \text{ and } m\neq 0$$

Now to determine the coefficients of *A* when *n*, *m*, and *l* are non-zero. To generate an orthogonal set, we multiply the Laplace groundwater flow equation by $\cos[n'\pi x/a]\cos[m'\pi y/b]\cos[l'\pi z/c]$ where *n*', *m*', and *l*' are non-zero integers. Using similar procedures as above, the solution is

$$A_{n,m,l} = \frac{8\overline{Q}\cos[n\pi x_0/a]\cos[m\pi y_0/b]\cos[l\pi z_0/c]}{abcS_s\left(p + \frac{K_x}{S_s}\left(\frac{n\pi}{a}\right)^2 + \frac{K_y}{S_s}\left(\frac{m\pi}{b}\right)^2 + \frac{K_z}{S_s}\left(\frac{l\pi}{c}\right)^2\right)}. \tag{22}$$

Now that the coefficients of *A* have been determined, the solution in the Laplace domain is

$$\begin{aligned}\overline{d} = \frac{\overline{Q}}{abcS_s}\Bigg\{ & \frac{1}{p} + 2\sum_{n=1}^{\infty}\frac{\cos[n\pi x/a]\cos[n\pi x_0/a]}{p + \frac{K_x}{S_s}\left(\frac{n\pi}{a}\right)^2} \\ & + 2\sum_{m=1}^{\infty}\frac{\cos[m\pi y/b]\cos[m\pi y_0/b]}{p + \frac{K_y}{S_s}\left(\frac{m\pi}{b}\right)^2} + 2\sum_{l=1}^{\infty}\frac{\cos[L\pi z/c]\cos[l\pi z_0/c]}{p + \frac{K_z}{S_s}\left(\frac{l\pi}{c}\right)^2} \\ & + 4\sum_{n=1}^{\infty}\sum_{m=1}^{\infty}\frac{\cos[n\pi x/a]\cos[n\pi x_0/a]\cos[m\pi y/b]\cos[m\pi y_0/b]}{p + \frac{K_x}{S_s}\left(\frac{n\pi}{a}\right)^2 + \frac{K_y}{S_s}\left(\frac{m\pi}{b}\right)^2} \\ & + 4\sum_{n=1}^{\infty}\sum_{l=1}^{\infty}\frac{\cos[n\pi x/a]\cos[n\pi x_0/a]\cos[l\pi z/c]\cos[l\pi z_0/c]}{p + \frac{K_x}{S_s}\left(\frac{n\pi}{a}\right)^2 + \frac{K_z}{S_s}\left(\frac{l\pi}{c}\right)^2} \\ & + 4\sum_{m=1}^{\infty}\sum_{l=1}^{\infty}\frac{\cos[m\pi y/b]\cos[m\pi y_0/b]\cos[l\pi z/c]\cos[l\pi z_0/c]}{p + \frac{K_y}{S_s}\left(\frac{m\pi}{b}\right)^2 + \frac{K_z}{S_s}\left(\frac{l\pi}{c}\right)^2}\end{aligned}$$

$$8\sum_{n=1}^{\infty}\sum_{m=1}^{\infty}\sum_{l=1}^{\infty}\cos\left[n\pi\, x/a\right]\cos\left[n\pi\, x_0/a\right]\cos\left[m\pi\, y/b\right]\cos\left[m\pi\, y_0/b\right]$$

$$\left.\frac{\cos\left[l\pi\, z/c\right]\cos\left[l\pi\, z_0/c\right]}{p+\frac{K_x}{S_s}\left(\frac{n\pi}{a}\right)^2+\frac{K_y}{S_s}\left(\frac{m\pi}{b}\right)^2+\frac{K_z}{S_s}\left(\frac{l\pi}{c}\right)^2}\right\} \quad . \tag{23}$$

Conducting an inverse Laplace transform, the equation becomes:

$$d=\frac{1}{abcS_s}\int_0^t Q(t-\tau)\left\{1+2\sum_{n=1}^{\infty}\cos\left[n\pi\, x/a\right]\cos\left[n\pi\, x_0/a\right]\exp\left[-\tau\frac{K_x}{S_s}\left(\frac{n\pi}{a}\right)^2\right]\right.$$

$$+2\sum_{m=1}^{\infty}\cos\left[m\pi\, y/b\right]\cos\left[m\pi\, y_0/b\right]\exp\left[-\tau\frac{K_y}{S_s}\left(\frac{m\pi}{b}\right)^2\right]$$

$$+2\sum_{l=1}^{\infty}\cos\left[l\pi\, z/c\right]\cos\left[l\pi\, z_0/c\right]\exp\left[-\tau\frac{K_z}{S_s}\left(\frac{l\pi}{c}\right)^2\right]$$

$$+4\sum_{n=1}^{\infty}\sum_{m=1}^{\infty}\cos\left[n\pi\, x/a\right]\cos\left[n\pi\, x_0/a\right]\cos\left[m\pi\, y/b\right]\cos\left[m\pi\, y_0/b\right]$$

$$\exp\left[-\tau\left(\frac{K_x}{S_s}\left(\frac{n\pi}{a}\right)^2+\frac{K_y}{S_s}\left(\frac{m\pi}{b}\right)^2\right)\right]$$

$$+4\sum_{n=1}^{\infty}\sum_{l=1}^{\infty}\cos\left[n\pi\, x/a\right]\cos\left[n\pi\, x_0/a\right]\cos\left[l\pi\, z/c\right]\cos\left[l\pi\, z_0/c\right]$$

$$\exp\left[-\tau\left(\frac{K_x}{S_s}\left(\frac{n\pi}{a}\right)^2+\frac{K_z}{S_s}\left(\frac{l\pi}{c}\right)^2\right)\right]$$

$$+4\sum_{m=1}^{\infty}\sum_{l=1}^{\infty}\cos\left[m\pi\, y/b\right]\cos\left[m\pi\, y_0/b\right]\cos\left[l\pi\, z/c\right]\cos\left[l\pi\, z_0/c\right]$$

$$\left.\exp\left[-\tau\left(\frac{K_y}{S_s}\left(\frac{m\pi}{b}\right)^2+\frac{K_z}{S_s}\left(\frac{l\pi}{c}\right)^2\right)\right]\right.$$

$$+8\sum_{n=1}^{\infty}\sum_{m=1}^{\infty}\sum_{l=1}^{\infty}\cos[n\pi x/a]\cos[n\pi x_0/a]\cos[m\pi y/b]\cos[m\pi y_0/b]$$
$$\cos[l\pi z/c]\cos[l\pi z_0/c] \qquad . \qquad (24)$$
$$\exp\left[-\tau\left(\frac{K_x}{S_s}\left(\frac{n\pi}{a}\right)^2+\frac{K_y}{S_s}\left(\frac{m\pi}{b}\right)^2+\frac{K_z}{S_s}\left(\frac{l\pi}{c}\right)^2\right)\right]\Bigg\}$$

Simplifying the equation, we find

$$d=\frac{1}{abcS_s}\int_0^t Q(t-\tau)\left(1+2\sum_{n=1}^{\infty}\cos[n\pi x/a]\cos[n\pi x_0/a]\exp\left[-\tau\frac{K_x}{S_s}\left(\frac{n\pi}{a}\right)^2\right]\right)$$
$$\left(1+2\sum_{m=1}^{\infty}\cos[m\pi y/b]\cos[m\pi y_0/b]\exp\left[-\tau\frac{K_y}{S_s}\left(\frac{m\pi}{b}\right)^2\right]\right) \qquad . \qquad (25)$$
$$\left(1+2\sum_{l=1}^{\infty}\cos[l\pi z/c]\cos[l\pi z_0/c]\exp\left[-\tau\frac{K_z}{S_s}\left(\frac{l\pi}{c}\right)^2\right]\right)$$

As will be seen in following sections, it is important to have the series in a form reflecting the symmetric infinite nature of the function. So using symmetry the equation becomes

$$d=\frac{1}{abcS_s}\int_0^t Q(t-\tau)\sum_{n=-\infty}^{\infty}\cos[n\pi x/a]\cos[n\pi x_0/a]\exp\left[-\tau\frac{K_x}{S_s}\left(\frac{n\pi}{a}\right)^2\right]$$
$$\sum_{m=-\infty}^{\infty}\cos[m\pi y/b]\cos[m\pi y_0/b]\exp\left[-\tau\frac{K_y}{S_s}\left(\frac{m\pi}{b}\right)^2\right] \qquad . \qquad (26)$$
$$\sum_{l=-\infty}^{\infty}\cos[l\pi z/c]\cos[l\pi z_0/c]\exp\left[-\tau\frac{K_z}{S_s}\left(\frac{l\pi}{c}\right)^2\right]$$

It is important to note that the solution of the three dimensional problem (26) is simply the multiplication of each one dimensional solution.

Of interest to future workers, one may write the above summation equations in the form of three Jacobi theta functions (Weisstein, 2014), evaluated in Mathematica® as the EllipticTheta() function. While the theta function removes the need of the series, it has limited indefinite integration from our analysis and is not well implemented numerically. We therefore do not use it. However, perhaps others will be able to effectively use the Jacobi theta function.

Other Boundary Conditions

The solution procedure for each of the other boundary conditions is exactly the same as the no flux case, with one caveat. The first step of the solution procedure defining the proposed solution based on the boundary values is different. Previously we solved the both sides no flux BVP

$$\frac{\partial \bar{d}}{\partial x}|_{x=0} = \frac{\partial \bar{d}}{\partial x}|_{x=a} = 0 \text{ with the proposed soltuion } \cos\left[n\pi\, x/a\right]. \tag{27}$$

Now to solve the one side constant head, one side no flux BVP

$$\frac{\partial \bar{d}}{\partial x}|_{x=0} = \bar{d}\left(x=a\right) = 0 \text{ we use the proposed solution } \cos\left[\left(n+½\right)\pi\, x/a\right]. \tag{28}$$

To solve the both sides constant head BVP

$$\bar{d}\left(x=0\right) = \bar{d}\left(x=a\right) = 0 \text{ we use the proposed solution } \sin\left[n\pi\, x/a\right]. \tag{29}$$

SERIES CONVERGENCE

Accepting the derivations for a point sink / source from the previous section, we complete the following steps for every boundary condition to achieve rapidly convergent solutions at all times. First we derive the Poisson Re-summation equation as outlined in

Strikwerda (2004) for each of the boundary conditions. We then install a switch between the Poisson Re-Summation solutions and the unaltered form of the solutions for each principal direction. Next we determine the number of iterations required for the series to converge. Finally, we prove that the infinite series at early times converges with only three iterations.

Poisson Re-Summation

Use of the Poisson Re-Summation Formula is one of the most important new aspects of our work. While Poisson Re-Summation has been used in petroleum pressure transient solutions by Odeh and Babu (1990), the phrase Poisson Re-Summation was not used in their work, or the method explained. Rather, Odeh and Babu (1990) cited Carslaw and Jaeger (1959) and proceeded to find approximations by tracking the pressure pulse. While approximations are useful, they usually require restrictive conditions to be placed on wellbore location and require careful tracking of the pressure pulse throughout the reservoir.

Another approach to the infinite series is to complete the time integral by letting time go to infinity thereby dropping the exponential terms. With the exponential terms dropped, only infinite summation of cosine / sine is required (Babu and Odeh, 1989a). Closed forms of these summations have been derived for the first and second summation terms (Babu and Odeh, 1989a). However, the third summation term must be approximated by an integral method with variable accuracy especially at low penetration ratios (Babu and Odeh, 1989a). If one avoids the integral approximation and attempts to numerically evaluate, the series is still very slowly convergent (Babu and Odeh, 1989a).

The solution to these issues is the Poisson Re-Summation Formula (Strikwerda, 2004). The Poisson Re-Summation Formula has the interesting property of inverse convergence speed when compared to the unaltered series. Series that are slowly convergent, upon application of the Poisson Re-Summation Formula, are rapidly convergent and vice versa. The Poisson Re-Summation Formula is defined from Strikwerda (2004) as

$$\sum_{n=-\infty}^{\infty} \exp\left[-inj\varepsilon\right] \mathrm{u}\left[nj\right] j = \sqrt{2\pi} \sum_{w=-\infty}^{\infty} \mathrm{U}\left[\varepsilon + 2\pi w j^{-1}\right], \tag{30}$$

where the function U is the Fourier Transform of the function u with respect to the summation variable *n* transformed to the frequency variable *w*.

Before finding equivalent series, we first reiterate that the three dimensional solutions derived in the previous section are simply the product of three one dimensional solutions. With this concept in mind, the three dimensional solution when all sides are no-flux was found to be

$$\begin{aligned} d = \frac{1}{abcS_s} \int_0^t Q(t-\tau) \sum_{n=-\infty}^{\infty} \cos\left[n\pi x/a\right] \cos\left[n\pi x_0/a\right] \exp\left[-\tau \frac{K_x}{S_s}\left(\frac{n\pi}{a}\right)^2\right] \\ \sum_{m=-\infty}^{\infty} \cos\left[m\pi y/b\right] \cos\left[m\pi y_0/b\right] \exp\left[-\tau \frac{K_y}{S_s}\left(\frac{m\pi}{b}\right)^2\right] \\ \sum_{l=-\infty}^{\infty} \cos\left[l\pi z/c\right] \cos\left[l\pi z_0/c\right] \exp\left[-\tau \frac{K_z}{S_s}\left(\frac{l\pi}{c}\right)^2\right] \end{aligned}, \tag{31}$$

where the one dimensional solution in the *x* direction for a no-flux boundary at $x = 0$ and $x = a$ is

$$\frac{1}{a}\sum_{n=-\infty}^{\infty}\cos\left[n\pi x/a\right]\cos\left[n\pi x_0/a\right]\exp\left[-\tau\frac{K_x}{S_s}\left(\frac{n\pi}{a}\right)^2\right]. \tag{32}$$

By dividing each problem into its one dimensional solutions, the combination of several different boundary conditions for each principal direction of the box is easily achieved. This concept is also important when we install the switch between summation methods because each direction has a different switch time. When finding equivalent series, we do so for each of these one dimensional solutions.

To show how we found equivalent series using the Poisson Re-Summation formula, we demonstrate the method on the one dimensional solution for a no flux boundary at $x = 0$ and $x = a$. To transform the infinite series of (32) into the form of (30), we convert the cosine terms into exponentials

$$\begin{aligned}
&\frac{1}{a}\sum_{n=-\infty}^{\infty}\cos\left[\frac{n\pi x}{a}\right]\cos\left[\frac{n\pi x_0}{a}\right]\exp\left[-\tau\frac{n^2\pi^2K_x}{a^2S_s}\right]\\
&=\frac{1}{4a}\sum_{n=-\infty}^{\infty}\exp\left[\frac{i\pi n}{a}\left(-x-x_0\right)\right]\exp\left[-\tau\frac{n^2\pi^2K_x}{a^2S_s}\right]\\
&\quad+\exp\left[\frac{i\pi n}{a}\left(x-x_0\right)\right]\exp\left[-\tau\frac{n^2\pi^2K_x}{a^2S_s}\right]\\
&\quad+\exp\left[\frac{i\pi n}{a}\left(-x+x_0\right)\right]\exp\left[-\tau\frac{n^2\pi^2K_x}{a^2S_s}\right]\\
&\quad+\exp\left[\frac{i\pi n}{a}\left(x+x_0\right)\right]\exp\left[-\tau\frac{n^2\pi^2K_x}{a^2S_s}\right]\quad.
\end{aligned} \tag{33}$$

Next we compute the Fourier Transform of the non-imaginary exponential function in (33) by transforming n to the frequency variable w

$$\int_{-\infty}^{\infty} \exp\left[-\frac{n^2\pi^2 K_x \tau}{a^2 S_s}\right] \exp\left[-2\pi i w n\right] dn = \frac{\exp\left[-\frac{a^2 S_s w^2}{4\pi^2 K_x \tau}\right]}{\pi\sqrt{\frac{2K_x\tau}{a^2 S_s}}} \quad . \tag{34}$$

Now we use (30) by setting $j = 1$, defining ε to each of the four complex exponential terms, and the Fourier Transform of u to U as defined in (34). The Poisson Re-Summed series is

$$\frac{1}{4}\sqrt{\frac{S_s}{\pi K_x \tau}} \sum_{n=-\infty}^{\infty} \left\{ \exp\left[-\frac{a^2 S_s \left(\pi\left(x + x_0\right)/a + 2\pi n\right)^2}{4\pi^2 K_x \tau}\right] + \exp\left[-\frac{a^2 S_s \left(\pi\left(-x + x_0\right)/a + 2\pi n\right)^2}{4\pi^2 K_x \tau}\right] + \exp\left[-\frac{a^2 S_s \left(\pi\left(x - x_0\right)/a + 2\pi n\right)^2}{4\pi^2 K_x \tau}\right] + \exp\left[-\frac{a^2 S_s \left(\pi\left(-x - x_0\right)/a + 2\pi n\right)^2}{4\pi^2 K_x \tau}\right] \right\}. \tag{35}$$

Upon considering the negative and positive iterations, (35) may be simplified to

$$\frac{1}{2}\sqrt{\frac{S_s}{\pi K_x \tau}} \sum_{n=-\infty}^{\infty} \left\{ \exp\left[-\frac{S_s \left(x + x_0 + 2an\right)^2}{4\tau K_x}\right] + \exp\left[-\frac{S_s \left(-x + x_0 + 2an\right)^2}{4\tau K_x}\right] \right\}. \tag{36}$$

As can be seen by comparison of the unaltered summation equation and the Poisson Re-Summation equation, the Poisson Re-Summation technique is well suited for rapid convergence at early times. This is in contrast to the unaltered series which is rapidly convergent at late times.

Catalog of Solutions Rapidly Convergent at All Times

Solutions presented below are the result of derivations similar to the first section of this chapter followed by the Poisson Re-Summation method from the previous

section. In an effort to present solutions in a concise manner, remember that every three dimensional solution can be subdivided into its three one dimensional components. Thus, the three dimensional solutions take the form

$$d = \int_{t_1}^{t_2} \frac{Q(t-\tau)}{S_s} F_x F_y F_z \, \mathrm{d}\tau \,, \tag{37}$$

where F_x, F_y, F_z are the one dimensional solutions for the x, y, and z directions respectively.

To find the three dimensional solution for a particular time and boundary condition, plug in the appropriate directional components into the following equations and multiply each direction together. Boundary conditions below are written for the x component. For the same BVP solution in another direction, simply replace each directional component element wise. For example, if one wants a solution for the z component replace F_x with F_z, x with z, x_0 with z_0, K_x with K_z, n with l, and a with c.

In the following catalog of solutions, the early time (Poisson Re-Summed) equation is presented first and is set equal to the late time (unaltered) equation displayed second. As derived in the previous section, the solution when there is a no-flux boundary at $x = 0$ and $x = a$ is

$$\begin{aligned} F_x &= \frac{1}{2}\sqrt{\frac{S_s}{\pi K_x \tau}} \sum_{n=-\infty}^{\infty} \left\{ \exp\left[-\frac{S_s\left(x + x_0 + 2an\right)^2}{4\tau K_x} \right] + \exp\left[-\frac{S_s\left(-x + x_0 + 2an\right)^2}{4\tau K_x} \right] \right\} \\ &= \frac{1}{a}\left(1 + 2\sum_{n=1}^{\infty} \cos\left[\frac{n\pi x}{a} \right] \cos\left[\frac{n\pi x_0}{a} \right] \exp\left[-\tau \frac{n^2 \pi^2 K_x}{a^2 S_s} \right] \right) \end{aligned} . \tag{38}$$

If there is a no flux boundary at $x = 0$ and a constant head boundary at $x = a$, then the solution is

$$F_x = \frac{1}{2}\sqrt{\frac{S_s}{\pi K_x \tau}} \sum_{n=-\infty}^{\infty} \left\{ \exp\left[-\frac{S_s\left(x + x_0 + 2an\right)^2}{4\tau K_x} \right] \exp\left[-i\frac{\left(\pi\left(x + x_0\right)/a + 2\pi n\right)}{2} + i\frac{\pi\left(x + x_0\right)}{2a} \right] + \exp\left[-\frac{S_s\left(-x + x_0 + 2an\right)^2}{4\tau K_x} \right] \exp\left[-i\frac{\left(\pi\left(-x + x_0\right)/a + 2\pi n\right)}{2} + i\frac{\pi\left(-x + x_0\right)}{2a} \right] \right\}$$
$$= \frac{2}{a} \sum_{n=0}^{\infty} \cos\left[\frac{\left(n + 1/2\right)\pi x}{a} \right] \cos\left[\frac{\left(n + 1/2\right)\pi x_0}{a} \right] \exp\left[-\tau \frac{\left(n + 1/2\right)^2 \pi^2 K_x}{a^2 S_s} \right] \quad (39)$$

If there is a constant head boundary at $x = 0$ and $x = a$, then the solution is:

$$F_x = \frac{1}{2}\sqrt{\frac{S_s}{\pi K_x \tau}} \sum_{n=-\infty}^{\infty} \left\{ \exp\left[-\frac{S_s\left(-x + x_0 + 2an\right)^2}{4\tau K_x} \right] - \exp\left[-\frac{S_s\left(x + x_0 + 2an\right)^2}{4\tau K_x} \right] \right\}$$
$$= \frac{2}{a} \sum_{n=1}^{\infty} \sin\left[\frac{n\pi x}{a} \right] \sin\left[\frac{n\pi x_0}{a} \right] \exp\left[-\tau \frac{n^2 \pi^2 K_x}{a^2 S_s} \right] \quad (40)$$

Another common boundary condition used in aquifer modeling is the infinite extent condition. In this case we assume that there is a no flux boundary at $x = 0$ and the other reservoir bound at a is infinitely far away. To find a solution when the boundary a is infinitely far away, and there is a no flux boundary at $x = 0$, we take the

$$\lim_{a\to\infty} \frac{1}{2}\sqrt{\frac{S_s}{\pi K_x \tau}} \sum_{n=-\infty}^{\infty} \left\{ \exp\left[-\frac{S_s\left(x + x_0 + 2an\right)^2}{4\tau K_x} \right] + \exp\left[-\frac{S_s\left(-x + x_0 + 2an\right)^2}{4\tau K_x} \right] \right\}, \quad (41)$$

which yields

$$F_x = \frac{1}{2}\sqrt{\frac{S_s}{\pi K_x \tau}} \left(\exp\left[-\frac{S_s\left(x + x_0\right)^2}{4\tau K_x} \right] + \exp\left[-\frac{S_s\left(-x + x_0\right)^2}{4\tau K_x} \right] \right). \quad (42)$$

It is interesting to note that the solution (42) is in fact the solution for a no-flux boundary using image wells and the assumption of infinite aquifer extents. Similarly, the solution for a constant head boundary at $x = 0$ in an infinite extent aquifer is

$$\lim_{a\to\infty} \frac{1}{2}\sqrt{\frac{S_s}{\pi K_x \tau}} \sum_{n=-\infty}^{\infty} \left\{ \exp\left[-\frac{S_s\left(-x + x_0 + 2an\right)^2}{4\tau K_x} \right] - \exp\left[-\frac{S_s\left(x + x_0 + 2an\right)^2}{4\tau K_x} \right] \right\}, \qquad (43)$$

which yields

$$F_x = \frac{1}{2}\sqrt{\frac{S_s}{\pi K_x \tau}} \sum_{n=-\infty}^{\infty} \left(\exp\left[-\frac{S_s\left(-x + x_0\right)^2}{4\tau K_x} \right] - \exp\left[-\frac{S_s\left(x + x_0\right)^2}{4\tau K_x} \right] \right). \qquad (44)$$

Assuming no boundary conditions, all one needs to do is delete the superimposed image well and the solution takes the form

$$F_x = \frac{1}{2}\sqrt{\frac{S_s}{\pi K_x \tau}} \exp\left[-\frac{S_s\left(-x + x_0\right)^2}{4\tau K_x} \right]. \qquad (45)$$

As an example of combining the one dimensional solutions, let's say one wants a point sink solution for an early time constant head boundary at $x = 0$ and $x = a$; an early time constant head boundary at $y = 0$ and a no-flux boundary at $y = b$; and a late time no-flux boundary at $z = 0$ and $z = c$. The solution for such a boundary condition scenario is

$$d = \int_{t_1}^{t_2} \frac{Q(t-\tau)}{S_s}$$
$$\left(\frac{1}{2}\sqrt{\frac{S_s}{\pi K_x \tau}} \sum_{n=-\infty}^{\infty} \left\{ \exp\left[-\frac{S_s\left(-x + x_0 + 2an\right)^2}{4\tau K_x} \right] - \exp\left[-\frac{S_s\left(x + x_0 + 2an\right)^2}{4\tau K_x} \right] \right\} \right)$$
$$\left(\frac{1}{2}\sqrt{\frac{S_s}{\pi K_y \tau}} \sum_{m=-\infty}^{\infty} \left\{ \exp\left[-\frac{S_s\left(b - \left(y + y_0\right) + 2bm\right)^2}{4\tau K_y} \right] \right.\right.$$
$$\exp\left[-i\frac{\left(\pi\left(b - \left(y + y_0\right)\right)/b + 2\pi m\right)}{2} + i\frac{\pi\left(b - \left(y + y_0\right)\right)}{2b} \right]$$
$$+ \exp\left[-\frac{S_s\left(b - \left(-y + y_0\right) + 2bm\right)^2}{4\tau K_y} \right]$$
$$\left.\left. \exp\left[-i\frac{\left(\pi\left(b - \left(-y + y_0\right)\right)/b + 2\pi m\right)}{2} + i\frac{\pi\left(b - \left(-y + y_0\right)\right)}{2b} \right] \right\} \right)$$
$$\frac{1}{c}\left(1 + 2\sum_{l=1}^{\infty} \cos\left[\frac{l\pi z}{c}\right] \cos\left[\frac{l\pi z_0}{c}\right] \exp\left[-\tau \frac{l^2 \pi^2 K_z}{c^2 S_s} \right] \right) \mathrm{d}\tau \quad . \tag{46}$$

Summation Method Switch

As mentioned in the previous section, there is a point at which the number of iterations required for convergence between the two methods (unaltered series and Poisson Re-Summed series) is the same. It is at this point that we install a switch between the methods so as to have rapid convergence at all times. To find the switch point (time), we equate the two methods disregarding the spatial components

$$\exp\left[-\frac{S_s\left(2an\right)^2}{4\tau K_x} \right] = \exp\left[-\tau \frac{n^2 \pi^2 K_x}{a^2 S_s} \right]. \tag{47}$$

We then solve for the time when these two functions are equal and find $\tau = \frac{S_s a^2}{\pi K_x}$.

The switch time is graphically seen in Figure 63. It is clear that as time moves away from the Poisson Re-Summation switch point, the number of iterations required for convergence increases exponentially or decreases linearly depending upon which series is used. Thus, finding this switch point and using the appropriate series can dramatically increase computational speed.

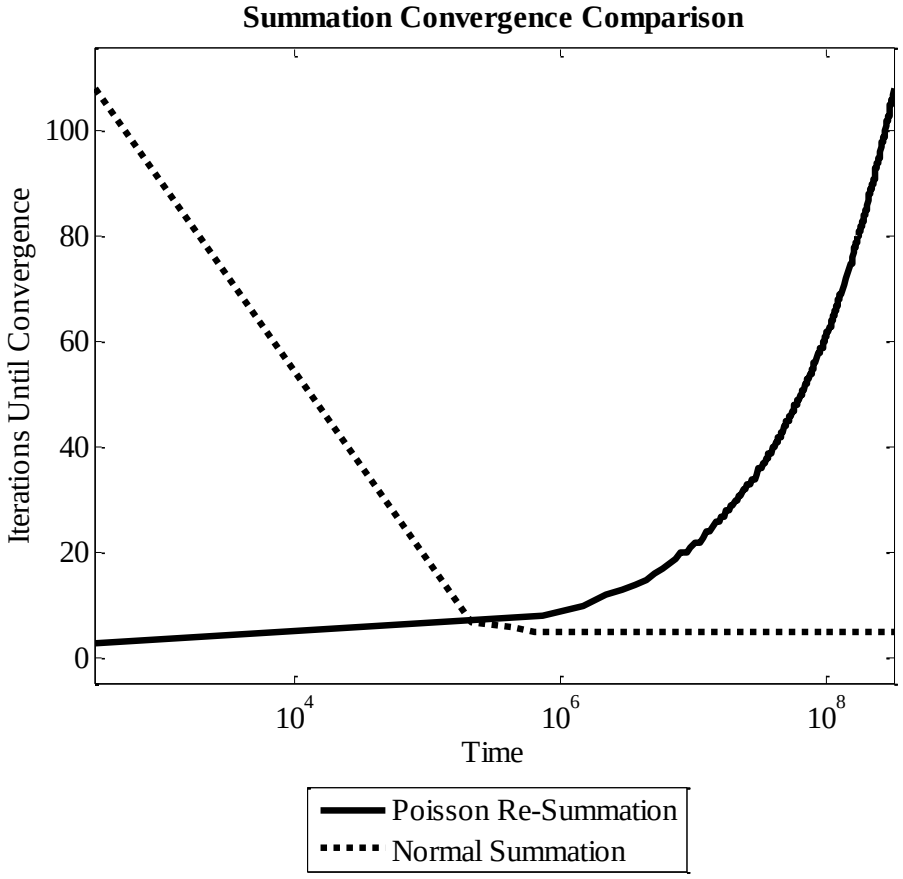

Figure 63. Comparison of series iterations until convergence between the Poisson Re-Summed series and the unaltered series.

With the switch time between equivalent series defined, it is important to note the four cases when Poisson Re-Summation is necessary: all series require Poisson Re-Summation (early time), two series require Poisson Re-Summation, one series requires Poisson Re-Summation, no series require Poisson Re-Summation (late time).

Iterations Required for Convergence

It is useful to determine the number of iterations necessary to achieve convergence and the error involved. First, substitute the time at which the series switch occurs. Substituting the unaltered series,

$$\exp\left[-\tau\frac{n^2\pi^2K_x}{a^2S_s}\right] \text{ with } \tau=\frac{S_s a^2}{\pi K_x}, \text{ yields } \exp\left[-\frac{S_s a^2}{\pi K_x}\frac{n^2\pi^2K_x}{a^2S_s}\right]=\exp\left[-n^2\pi\right]. \tag{48}$$

This equation is the time at which the greatest number of iterations is necessary to achieve convergence.

From numerical investigation, convergence to double data type precision occurs at the fifth iteration. It is important to note that the unaltered (late time) series is symmetric about the vertical axis. Therefore the late time equation is simplified by multiplying the positive side of the summation (from one to infinity) by two. However, the Poisson Re-Summed series is a non-symmetric function upon consideration of the spatial components. The Poisson Re-Summed series is shifted along the iteration axis in the negative or positive direction, at most by one unit. So to conservatively calculate the maximum possible error, the convergence is assumed to be at the fourth iteration.

To compute the error, we take the integral of an upper bounding function after the fourth iteration, from 4.5 to infinity, and multiply by two. This upper bounding function is the series exponential term shifted by ½ of an iteration. To approximate the greatest error of only summing the first four terms, the integration approximation of the upper error bound is

$$2\int_{4.5}^{\infty}\exp\left[-\left(n-0.5\right)^2\pi\right]=1.16\text{ E-23}. \tag{49}$$

Adding this error to the first five iterations of the series, we find

$$\sum_{n=-\infty}^{\infty}\exp\left[-n^2\pi\right]\approx \sum_{n=-5}^{5}\exp\left[-n^2\pi\right]+2\int_{4.5}^{\infty}\exp\left[-\pi\left(n-0.5\right)^2\right]=1.09+1.16\text{E-23}\approx 1.09 \tag{50}$$

which proves that the series can be accurately approximated with only five iteration terms.

Results of the summation from negative five to positive five are theoretically accurate to fifteen significant figures. A conceptual representation of the summation / integration methodology is depicted below (Figure 64). Note that the function plotted is not exactly the one of interest as the coefficient *W* has widened the exponential function for easier viewing. The function plotted was chosen to facilitate a better visual representation of the upper error bound approximation via the integral method.

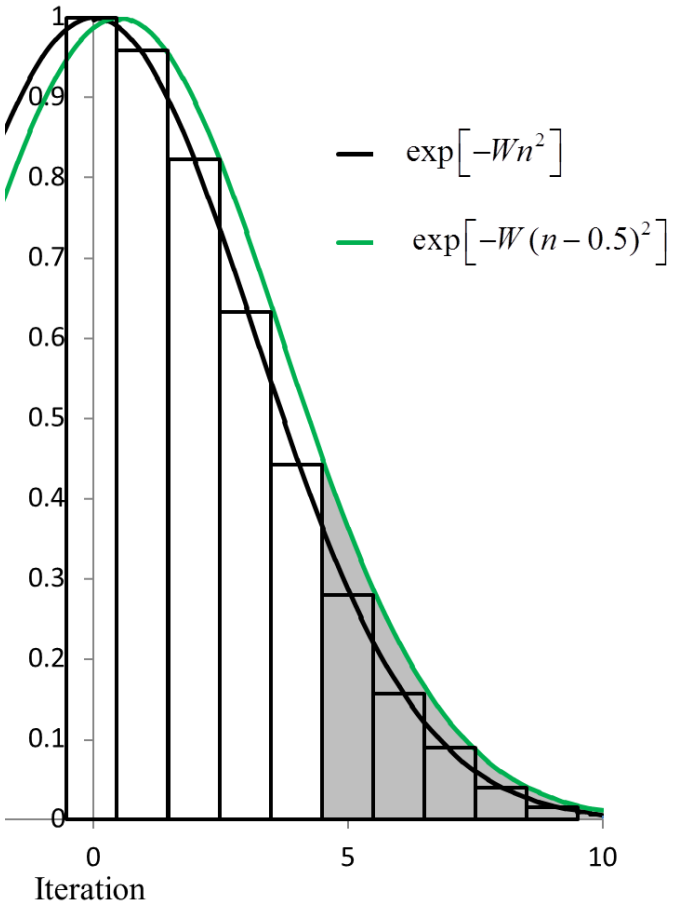

Figure 64. Graphical depiction of integration approximation for the upper error bound.

Early Time Three Term Convergence

While eleven iterations for each directional series summation term may seem computationally fast, it is important to note that upon analytical integration we must loop through each of the three principal directions which results in 11^3 = 1,331 iterations. While numeric integration is rapidly computed at late times, numeric integration at early times proves slow due to the rapidly changing nature of the function. Therefore, analytical integration is preferred for early times. To avoid issues of a slowly computed

analytical integration at early times, we attempt to find a solution that only requires three terms to sum each series instead of eleven.

Upon numerical investigation, it was determined that if the time was less than $1/100^{th}$ of the Poisson Re-Summation switch time, then convergence occurred with only three terms, $3^3 = 27$ iterations. Notice that in the less simplified Poisson Re-Summed equations,

$$\exp\left[-\frac{a^2 S_s\left(\left(\pm x \pm x_0\right)/a + 2n\right)^2}{4K_x\tau}\right], \tag{51}$$

the greatest value that the exponential function can return occurs when the argument inside that function is as close to zero as possible. In this case, we want to minimize $\left(\pm x + x_0\right)/a + 2n$ which means $\left(x + x_0\right)/a + 2n = 0$ so that $n = \left(-x + x_0\right)/2a$.

Upon inspection of this equation, it is apparent that the shift of the exponential function can be at most be plus or minus one along the iteration axis. To investigate the maximum error of only summing the first three terms (-1,0,1), assume that the exponential function is centered on an integer value. Note that the function plotted is not exactly the one of interest as the coefficient *W* has widened the exponential function for easier viewing. The function plotted was chosen to facilitate a better visual representation of the upper error bound approximation (Figure 65).

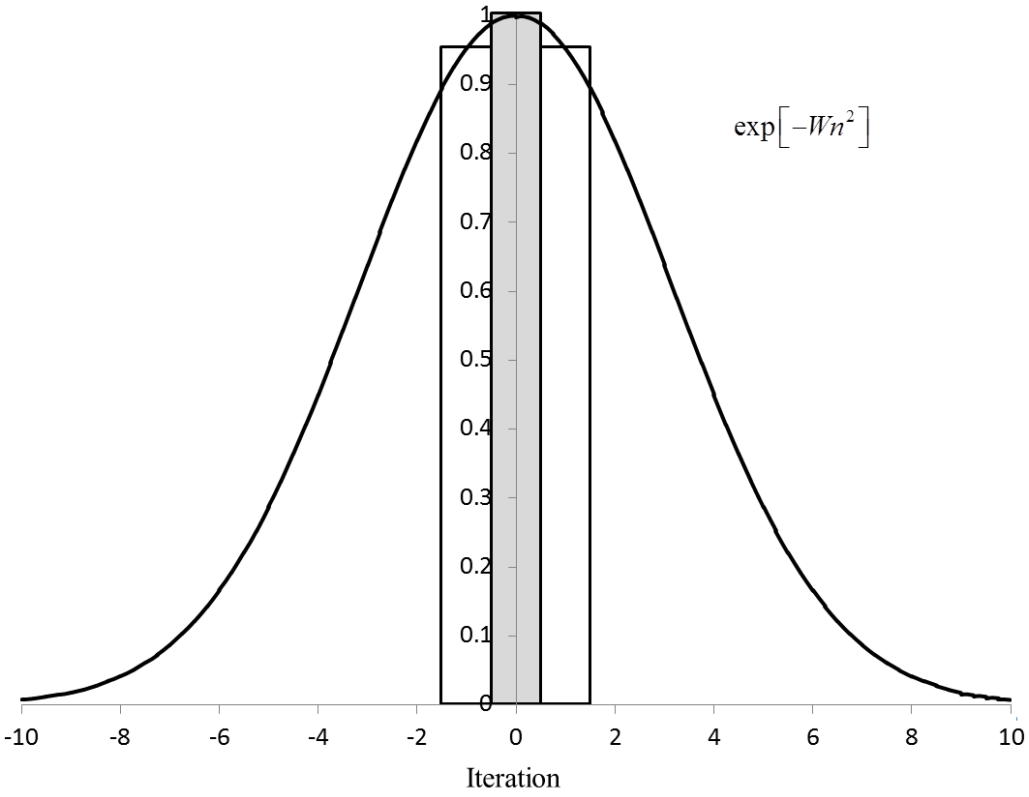

Figure 65. Representation of function only requiring three series iterations.

Centering the exponential function on zero, we find

$$\exp\left[-\frac{100\pi\left(0+2a\times 0\right)^2}{4a^2}\right]+\exp\left[-\frac{100\pi\left(0+2a\times 0\right)^2}{4a^2}\right], \tag{52}$$

which yields $2\exp[0]=2$. Now investigating the next closest series term (either -1 or 1), in this case 1, we find

$$\exp\left[-\frac{100\pi\left(0+2a\right)^2}{4a^2}\right]+\exp\left[-\frac{100\pi\left(0+2a\right)^2}{4a^2}\right], \tag{53}$$

which yields $2\exp[-100\pi] = 7.30\text{E}-137$. Thus, the second and subsequent iterations of the function can be ignored because $2 + 7.30\text{E}-137 \approx 2$. Therefore, three series terms (-1,0,1) are adequate to sum the series at 1/100th the Poisson Re-Summation switch time and earlier.

ANALYTICAL INTEGRATION

At this point in the derivation we have a time derivative, rapidly convergent point source / sink. To convert this point source / sink into a well, we must integrate the solutions through time, along the wellbore length and along the wellbore circumference. Two differing approaches may be considered. One may either numerically integrate the solutions or one may attempt to find analytical time and space integrations. In an effort to find the most numerically stable, rapidly computed solution we attempted analytical integration and then compared to numerical integration. While several analytical time and space integrations were found, the numerical implementation of these analytical integrations was significantly slower; on the order of 100-1,000 times slower.

Reasons for slower analytical integrations are three fold. First, as the analytical functions are non-separateable they require looping through each iteration, 11^3 iterations. In contrast, the exponential functions are separatable and therefore only require 3×11 iterations; $11^3 - 3\times11$ = 1,298 less iterations. Second, the analytical functions are typically very messy and thus require several computer functions() to describe the mathematical equation concisely. Calling several functions() slows computation. Third, many of the analytical integrations require special functions() that are slow to compute.

Several of these special functions() are not found in MATLAB and therefore require outside source code.

Although not used in our work, the analytical integrations found below were necessary in attempting to find the most rapid numerical implementation for the model. Additionally, the analytical integrals were a good check against the accuracy of the numerical integrations. Future workers may find the analytical integrations useful pending the improvement of the computer evaluation of these functions. In our work, the numeric integrations calculated by MATLAB were consistently better than the requested absolute / relative accuracy input into the numeric integration function when compared to the analytical integrations.

Before integrating, it is important to define the integrals needed. As the solution is currently a time derivative, the integration with respect to time is necessary. Spatially, we need to integrate the point source / sink (x_0, y_0, z_0) along the center line of the wellbore. Because we are interested in how the wellbore responds to pumping, we then integrate the sample point (x, y, z) around the radius of the wellbore.

It is important to note that the integrations used to represent the wellbore could be more rigorous than those presented here. The most rigorous integration would perhaps integrate the source / sink along the surface area of the cylinder (wellbore) and the sample point along the surface of the cylinder (wellbore). Or perhaps the integration could be for the entire volume of the wellbore. However, these integrations are not possible with the current implementation of the equations because if at any point $x = x_0$ and $y = y_0$ and $z = z_0$, then the solution goes to infinity; a singularity exists. So to avoid

this singularity, we integrate the source along the wellbore centerline and the sample point along the wellbore circumference at the center of this wellbore centerline (Figure 66).

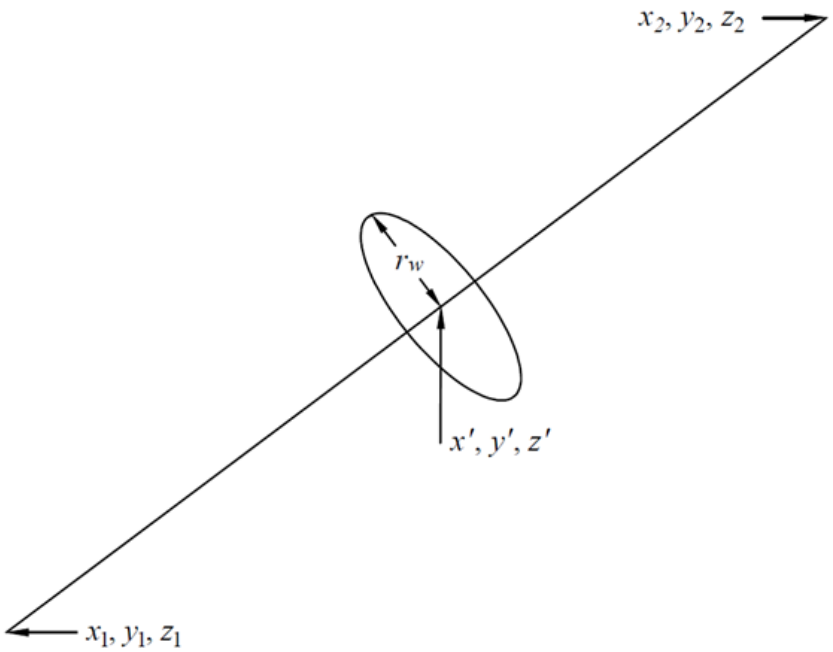

Figure 66. Integration of the point sink and sample point along the centerline of the wellbore and the circumference of the wellbore.

The spatial integrations of the point source / sink are necessary to find an average response between the wellbore and sample point. As such, the integral along the wellbore must be divided by the length of the wellbore to get an averaged aquifer response. Likewise, the integral around the radius of the wellbore must be divided by 2π to get an averaged aquifer response.

For the spatial integration, the function was parameterized to compute the aquifer response for a circular wellbore from any point x_1, y_1, z_1 to x_2, y_2, z_2. The parameterization relies on finding the unit vector f between the starting and ending point of the wellbore and two additional, mutually perpendicular unit vectors U and V.

To begin, we find the unit vector between the start and end of the wellbore as $f_1 = (x_2 - x_1)/L$, $f_2 = (y_2 - y_1)/L$, $f_3 = (z_2 - z_1)/L$ where L is the length [L] of the wellbore found from $L = \sqrt{(x_2 - x_1)^2 + (y_2 - y_1)^2 + (z_2 - z_1)^2}$. Next, we parameterize the point source / sink using the unit vector. The parameterization will be integrated with respect to w from zero to the length of the wellbore. The parameterization of the point source / sink is

$$\begin{aligned} x_0 &= f_1 w + x_1 \\ y_0 &= f_2 w + y_1 \\ z_0 &= f_3 w + z_1 \end{aligned} . \tag{54}$$

Next we determine two unit vectors mutually perpendicular to f, referring to them as V and U. The sample point is then parameterized to trace a radius around the wellbore at some point (x',y',z') as

$$\begin{aligned} x &= x' + r_w \left(U_1 \cos[\theta] + V_1 \sin[\theta]\right) \\ y &= y' + r_w \left(U_2 \cos[\theta] + V_2 \sin[\theta]\right) \\ z &= z' + r_w \left(U_3 \cos[\theta] + V_3 \sin[\theta]\right) \end{aligned} , \tag{55}$$

where r_w is the radius [L] of the wellbore.

Previous workers use various simplifications of the wellbore to account for anisotropic reservoirs, typically by changing the shape of the wellbore. However, as our

study is most concerned with wellbore hydraulics and because of the complex geometries involved, we avoid such simplifications. We therefore integrate with respect to theta around the circumference of the wellbore from zero to 2π using the parameterization (55).

Analytical integration around the circumference of the wellbore is only possible in the special case when no series require Poisson Re-Summation. In this case, integration yields a Bessel function. Parameterization notation of integrations below will reflect the integration being undertaken. For example, because we do not show our attempts to integrate along the circumference of the wellbore, to save space our notation of the point source / sink remains noted as x. We do not show that $x = x' + r_w (U_1 \cos[\theta] + V_1 \sin[\theta])$.

However, to keep track of what integrations have been completed and what integrations are remaining we will leave the remaining integrals unevaluated in our notation. These remaining integrals must be evaluated numerically. Also note that the convolution is not explicitly displayed in the following analytical integration work. Rather, it is simply noted as $Q = Q(t-\tau)$. If Q does not change over time (steady state), then then the convolution integral only involves one term and is therefore a simple multiplication. If a transient solution is desired and the pumping rate changes with time, then a numerical evaluation of the convolution integral is necessary and is outlined in Chapter IV.

We show the analytical integrations found for only one of the boundary conditions, all sides as no-flux boundaries. Integrations for combinations of the other

boundary conditions closely follow the work below and are therefore unnecessary to show. Every attempt to find analytical integrations was made in this analysis. We even attempted to integrate before implementing the Poisson Re-Summation and therefore tried to find difficult Fourier Transforms, however with no success.

All Poisson Re-Sum

There are two possible routes for analytical integration when all series have been Poisson Re-Summed. One may integrate solely with respect to time and stop. Alternatively, one may integrate with respect to space and then with respect to time. We investigate the time only integration first.

Only Time Integration

Early time analytical integration with respect to time followed by a spatial numeric double integral is the only analytical integration used by our model. No analytical spatial integration has been found after the time integration. Note that the +/- notation has reduced the repetitive addition of every combination of the +/- terms, reducing a total of eight terms to one term. Beginning integration when all the series are Poisson Re-Summed, we find

$$d = \frac{Q}{2\pi L}\int_0^{2\pi}\int_0^{L}\int_0^{t}\frac{1}{8}\sqrt{\frac{S_s}{\pi^3 K_x K_y K_z \tau^3}}\sum_{n=-\infty}^{\infty}\sum_{m=-\infty}^{\infty}\sum_{l=-\infty}^{\infty} \exp\left[-\frac{S_s}{4\tau}\left(\frac{\left(\pm x + x_0 + 2an\right)^2}{K_x}+\frac{\left(\pm y + y_0 + 2bm\right)^2}{K_y}+\frac{\left(\pm z + z_0 + 2cl\right)^2}{K_z}\right)\right] d\tau\, dw\, d\theta \tag{56}$$

and remove two constants

$$C_1 = \frac{1}{8}\sqrt{\frac{S_s}{\pi^3 K_x K_y K_z}}$$
$$C_2 = \frac{S_s}{4}\left(\frac{\left(\pm x + x_0 + 2an\right)^2}{K_x} + \frac{\left(\pm y + y_0 + 2bm\right)^2}{K_y} + \frac{\left(\pm z + z_0 + 2cl\right)^2}{K_z}\right) \tag{57}$$

which yields a new equation to integrate

$$d = \frac{Q}{2\pi L}\int_0^{2\pi}\int_0^{L}\sum_{n=-\infty}^{\infty}\sum_{m=-\infty}^{\infty}\sum_{l=-\infty}^{\infty} C_1 \int_0^{t}\frac{1}{\sqrt{\tau^3}}\exp\left[-\frac{C_2}{\tau}\right] d\tau\, dw\, d\theta\,. \tag{58}$$

We then perform u-substitution, taking $u = \frac{1}{\tau}$, $\tau = \frac{1}{u}$ and $d\tau = -\frac{1}{u^2}du$,

and substitute

$$d = \frac{Q}{2\pi L}\int_0^{2\pi}\int_0^{L}\sum_{n=-\infty}^{\infty}\sum_{m=-\infty}^{\infty}\sum_{l=-\infty}^{\infty} C_1 \int_{\infty}^{u} u^{3/2}\exp\left[-uC_2\right]\left(-u^{-2}du\right) dw\, d\theta \tag{59}$$

then simplify

$$d = \frac{Q}{2\pi L}\int_0^{2\pi}\int_0^{L}\sum_{n=-\infty}^{\infty}\sum_{m=-\infty}^{\infty}\sum_{l=-\infty}^{\infty} C_1 \int_{u}^{\infty} u^{-1/2}\exp\left[-uC_2\right] du\, dw\, d\theta\,. \tag{60}$$

To integrate this equation, we use 3.381.3 from Gradshteyn and Ryzhik (2007) and find

$$d = \frac{Q}{2\pi L}\int_0^{2\pi}\int_0^{L}\sum_{n=-\infty}^{\infty}\sum_{m=-\infty}^{\infty}\sum_{l=-\infty}^{\infty} C_1 C_2^{-1/2}\Gamma\left[1/2, uC_2\right] dw\, d\theta\,. \tag{61}$$

where $\Gamma[\ ]$ is the incomplete gamma function. We then use 8.359.3 from Gradshteyn

and Ryzhik (2007) to remove the incomplete gamma function and find

$$d = \frac{Q}{2\pi L}\int_0^{2\pi}\int_0^{L}\sum_{n=-\infty}^{\infty}\sum_{m=-\infty}^{\infty}\sum_{l=-\infty}^{\infty} C_1 C_2^{-1/2}\left(\sqrt{\pi} - \sqrt{\pi}\ \mathrm{erf}\left[\sqrt{uC_2}\right]\right) dw\, d\theta\,. \tag{62}$$

We then simplify using 8.250.4 from Gradshteyn and Ryzhik (2007) and find

$$d = \frac{Q}{2\pi L}\int_0^{2\pi}\int_0^{L}\sum_{n=-\infty}^{\infty}\sum_{m=-\infty}^{\infty}\sum_{l=-\infty}^{\infty} C_1 C_2^{-1/2}\sqrt{\pi}\ \mathrm{erfc}\left[\sqrt{uC_2}\right] dw\, d\theta\,. \tag{63}$$

We then replace the constants which yields a final equation needing two spatial integrations,

$$d = \frac{Q}{2\pi L}\frac{1}{8}\sqrt{\frac{S_s}{\pi^2 K_x K_y K_z}}\sum_{n=-\infty}^{\infty}\sum_{m=-\infty}^{\infty}\sum_{l=-\infty}^{\infty}\int_0^{2\pi}\int_0^{L} \frac{\mathrm{erfc}\left[\sqrt{\frac{S_s}{4t}\left(\frac{\left(\pm x + x_0 + 2an\right)^2}{K_x} + \frac{\left(\pm y + y_0 + 2bm\right)^2}{K_y} + \frac{\left(\pm z + z_0 + 2cl\right)^2}{K_z}\right)}\right]}{\sqrt{\frac{S_s}{4}\left(\frac{\left(\pm x + x_0 + 2an\right)^2}{K_x} + \frac{\left(\pm y + y_0 + 2bm\right)^2}{K_y} + \frac{\left(\pm z + z_0 + 2cl\right)^2}{K_z}\right)}}\, dw\, d\theta \quad . \tag{64}$$

Space and Time Integration

While the early time spatial integration may be useful, when it is followed by time integration a numerically unstable incomplete gamma function is generated. Unfortunately this function routinely evaluates outside of the double data type and therefore is not useful. Remember the that because we are computing the spatial integration we have introduce our parameterization as defined in (54) using the unit vectors *f*. We begin with the all series Poisson Re-Summed,

$$d = \frac{Q}{2\pi L}\int_0^{2\pi}\sum_{n=-\infty}^{\infty}\sum_{m=-\infty}^{\infty}\sum_{l=-\infty}^{\infty}\frac{abc}{8}\sqrt{\frac{S_s^3}{\pi^3 K_x K_y K_z}}\int_{t_1}^{t_2}\frac{1}{\sqrt{\tau^3}}\int_0^{L} \exp\left[-\frac{S_s}{4\tau}\left(\frac{\left(\pm x + f_1 w + x_1 + 2an\right)^2}{K_x} + \frac{\left(\pm y + f_2 w + y_1 + 2bm\right)^2}{K_y} + \frac{\left(\pm z + f_3 w + z_1 + 2cl\right)^2}{K_z}\right)\right] dw\, d\tau\, d\theta \quad . \tag{65}$$

We first take out constants

$$C_1 = \frac{abc}{8}\sqrt{\frac{S_s^3}{\pi^3 K_x K_y K_z}}$$

$$C_2 = \frac{4\left(a^2n^2 + an\left(\pm x + x_1\right)\right)}{K_x} + \frac{4\left(b^2m^2 + bm\left(\pm y + y_1\right)\right)}{K_y} + \frac{4\left(c^2l^2 + cl\left(\pm z + z_1\right)\right)}{K_z}$$
$$+ \frac{x^2 + 2xx_1 + x_1^2}{K_x} + \frac{y^2 + 2yy_1 + y_1^2}{K_y} + \frac{z^2 + 2zz_1 + z_1^2}{K_z} \quad , \qquad (66)$$

$$C_3 = f_1\frac{4an + 2\left(\pm x + x_1\right)}{K_x} + f_2\frac{4bm + 2\left(\pm y + y_1\right)}{K_z} + f_3\frac{4cl + 2\left(\pm z + z_1\right)}{K_z}$$

$$C_4 = \frac{f_1^2}{K_x} + \frac{f_2^2}{K_y} + \frac{f_3^2}{K_z}$$

which yields a new equation

$$d = \frac{Q}{2\pi L}\int_0^{2\pi}\sum_{n=-\infty}^{\infty}\sum_{m=-\infty}^{\infty}\sum_{l=-\infty}^{\infty} C_1\int_{t_1}^{t_2}\frac{1}{\sqrt{\tau^3}}\int_0^{L}\exp\left[-\frac{S_s}{4\tau}\left(C_2 + wC_3 + w^2C_4\right)\right] dw\, d\tau\, d\theta\,. \qquad (67)$$

To integrate this equation we use 2.33.1 from Gradshteyn and Ryzhik (2007) which yields

$$d = \frac{Q}{2\pi L}\int_0^{2\pi}\sum_{n=-\infty}^{\infty}\sum_{m=-\infty}^{\infty}\sum_{l=-\infty}^{\infty} C_1\sqrt{\frac{\pi}{C_4 S_s}}\int_{t_1}^{t_2}\frac{1}{\tau}\exp\left[\frac{S_s\left(C_3^2 - 4C_2C_4\right)}{16C_4\tau}\right]$$
$$\left(\operatorname{erf}\left[\frac{\left(C_3 + 2C_4L\right)}{4}\sqrt{\frac{S_s}{C_4\tau}}\right] - \operatorname{erf}\left[\frac{C_3}{4}\sqrt{\frac{S_s}{C_4\tau}}\right]\right) d\tau\, d\theta \qquad (68)$$

We then take out additional constants

$$C_5 = \frac{S_s\left(C_3^2 - 4C_2C_4\right)}{16C_4}$$
$$C_6 = \frac{\left(C_3 + 2C_4L\right)}{4}\sqrt{\frac{S_s}{C_4}}, \tag{69}$$
$$C_7 = \frac{C_3}{4}\sqrt{\frac{S_s}{C_4}}$$

and find a new equation

$$d = \frac{Q}{2\pi L}\int_0^{2\pi}\sum_{n=-\infty}^{\infty}\sum_{m=-\infty}^{\infty}\sum_{l=-\infty}^{\infty} C_1\sqrt{\frac{\pi}{C_4S_s}}\int_{t_1}^{t_2}\frac{1}{\tau}\exp\left[\frac{C_5}{\tau}\right]\left(\operatorname{erf}\left[\frac{C_6}{\sqrt{t}}\right] - \operatorname{erf}\left[\frac{C_7}{\sqrt{t}}\right]\right) d\tau\, d\theta. \tag{70}$$

We then perform u-substitution, setting $u = \frac{1}{\sqrt{\tau}} \quad t = \frac{1}{u^2} \quad dt = -\frac{2}{u^3}du$ which yields

$$d = \frac{Q}{2\pi L}\int_0^{2\pi}\sum_{n=-\infty}^{\infty}\sum_{m=-\infty}^{\infty}\sum_{l=-\infty}^{\infty} C_1\sqrt{\frac{\pi}{C_4S_s}}\int_{\sqrt{t_2}}^{\sqrt{t_1}}\frac{\exp\left[C_5u^2\right]\left(\operatorname{erf}\left[C_6u\right] - \operatorname{erf}\left[C_7u\right]\right)}{u} du\, d\theta. \tag{71}$$

To solve this equation, we use 06.25.21.0026.01 from Functions.Wolfram (2014). The final equation only requiring one spatial integration along the circumference of the wellbore is

$$d=\frac{Q}{2\pi L}\int_{0}^{2\pi}\sum_{n=-\infty}^{\infty}\sum_{m=-\infty}^{\infty}\sum_{l=-\infty}^{\infty}C_1\sqrt{\frac{\pi}{C_4S_s}}\frac{\sqrt{t_2}}{\sqrt{-\pi C_5t_2}}\sum_{k=0}^{\infty}$$
$$\left\{C_6\left(\frac{C_5^{-k}C_6^{2k}\Gamma\left(k+1/2,\frac{-C_5}{\sqrt{t_2}}\right)}{(2k+1)k!}-\frac{C_6\sqrt{t_1}}{\sqrt{-\pi C_5t_1}}\sum_{k=0}^{\infty}\frac{C_5^{-k}C_6^{2k}\Gamma\left(k+1/2,\frac{-C_5}{\sqrt{t_1}}\right)}{(2k+1)k!}\right)\right. \quad . \qquad (72)$$
$$\left.-C_7\left(\frac{C_5^{-k}C_7^{2k}\Gamma\left(k+1/2,\frac{-C_5}{\sqrt{t_2}}\right)}{(2k+1)k!}-\frac{C_7\sqrt{t_1}}{\sqrt{-\pi C_5t_1}}\sum_{k=0}^{\infty}\frac{C_5^{-k}C_7^{2k}\Gamma\left(k+1/2,\frac{-C_5}{\sqrt{t_1}}\right)}{(2k+1)k!}\right)\right\}d\theta$$

Two Series Require Poisson Re-Summation

We are unable to find an analytical integration with respect to time, so we start with the spatial integration. While the analytical results are useful to check accuracy against MATLAB's numeric integration, the analytical integrations require erf() & erfc() functions with complex arguments. MATLAB erf() & erfc() do not accept complex arguments. We therefore had to use Faddeeva code by Johnson (2014). While the code was accurate and reasonably fast, MATALB numeric integration still proved faster.

To begin, the *x*-axis series is in an unaltered form and the *y* and *z* axes series are Poisson Re-Summed

$$d = \frac{Q}{2\pi L}\frac{1}{4\pi a\sqrt{K_y K_z}}\int_0^{2\pi}\int_{t_1}^{t_2}\int_0^{L}\frac{1}{\tau}\sum_{n=-\infty}^{\infty}\sum_{m=-\infty}^{\infty}\sum_{l=-\infty}^{\infty}$$
$$\exp\left[-\tau\frac{n^2\pi^2 K_x}{a^2 S_s}\right]\cos\left[\frac{n\pi x}{a}\right]\cos\left[\frac{n\pi x_0}{a}\right]$$
$$\exp\left[-\frac{S_s}{4\tau}\left(\frac{\left(\pm y + y_0 + 2bm\right)^2}{K_y}+\frac{\left(\pm z + z_0 + 2cl\right)^2}{K_z}\right)\right]dw\,d\tau\,d\theta\,. \qquad (73)$$

We then parameterize the equation, which yields

$$d = \frac{Q}{2\pi L}\frac{1}{4\pi a\sqrt{K_y K_z}}\int_0^{2\pi}\int_{t_1}^{t_2}\int_0^{L}\frac{1}{\tau}\sum_{n=-\infty}^{\infty}\sum_{m=-\infty}^{\infty}\sum_{l=-\infty}^{\infty}$$
$$\cos\left[\frac{n\pi x}{a}\right]\cos\left[\frac{n\pi\left(f_1 w + x_1\right)}{a}\right]\exp\left[-\tau\frac{n^2\pi^2 K_x}{a^2 S_s}\right] \qquad . \qquad (74)$$
$$\exp\left[-\frac{S_s}{4\tau}\left(\frac{\left(\pm y + f_2 w + y_1 + 2bm\right)^2}{K_y}+\frac{\left(\pm z + f_3 w + z_1 + 2cl\right)^2}{K_z}\right)\right]dw\,d\tau\,d\theta$$

Next, we remove several constants

$$C_1 = -\frac{S_s}{4\tau}\left(\frac{4\left(b^2m^2 + bm\left(\pm y + y_1\right)\right)}{K_y}+\frac{4\left(c^2l^2 + cl\left(\pm z + z_1\right)\right)}{K_z}\right.$$
$$\left.+\frac{y^2 + 2yy_1 + y_1^2}{K_y}+\frac{z^2 + 2zz_1 + z_1^2}{K_z}\right)$$
$$C_2 = -\frac{S_s}{4\tau}\left(f_2\frac{4bm + 2\left(\pm y + y_1\right)}{K_y}+f_3\frac{4cl + 2\left(\pm z + z_1\right)}{K_z}\right) \quad , \qquad (75)$$
$$C_3 = -\frac{S_s}{4\tau}\left(\frac{f_2^2}{K_y}+\frac{f_3^2}{K_z}\right)$$
$$C_4 = n\pi f_1/a$$
$$C_5 = n\pi x_1/a$$

which yields

$$d = \frac{Q}{2\pi L}\frac{1}{4\pi a\sqrt{K_y K_z}}\int_0^{2\pi}\int_{t_1}^{t_2}\frac{1}{\tau}\sum_{n=-\infty}^{\infty}\sum_{m=-\infty}^{\infty}\sum_{l=-\infty}^{\infty}2\exp\left[-\tau\frac{n^2\pi^2 K_x}{a^2 S_s}\right]\cos\left[\frac{n\pi x}{a}\right]$$

$$\int_0^{L}\exp\left[w^2 C_3 + wC_2 + C_1\right]\cos\left[wC_4 + C_5\right]dw\, d\tau\, d\theta \quad . \tag{76}$$

To solve this integration, we use 01.07.21.0216.01 from Functions.Wolfram (2014) and find a final equation that still requires a spatial and temporal integration

$$d = \frac{Q}{2\pi L}\frac{\sqrt{\pi}}{4\pi a\sqrt{K_y K_z}}\int_0^{2\pi}\int_{t_1}^{t_2}\frac{1}{\tau}\sum_{n=-\infty}^{\infty}\sum_{m=-\infty}^{\infty}\sum_{l=-\infty}^{\infty}\exp\left[-\tau\frac{n^2\pi^2 K_x}{a^2 S_s}\right]\cos\left[\frac{n\pi x}{a}\right]$$

$$\frac{1}{4\sqrt{C_3}}\exp\left[-\frac{C_2^2 + 2iC_4C_2 - C_4^2 - 4C_3C_1 + 4iC_3C_5}{4C_3}\right]$$

$$\left(\exp\left[2iC_5\right]\left(\operatorname{erfi}\left[\frac{C_2 + iC_4 + 2C_3L}{2\sqrt{C_3}}\right] - \operatorname{erfi}\left[\frac{C_2 + iC_4}{2\sqrt{C_3}}\right]\right) + \right.$$

$$\left.\exp\left[\frac{iC_2C_4}{C_3}\right]\left(\operatorname{erfi}\left[\frac{C_2 - iC_4 + 2C_3L}{2\sqrt{C_3}}\right] - \operatorname{erfi}\left[\frac{C_2 - iC_4}{2\sqrt{C_3}}\right]\right)\right) d\tau\, d\theta. \tag{77}$$

<u>One Series Requires Poisson Re-Summation</u>

We now move onto the case when two series are unaltered (*x* & *y* axes), and one series has been Poisson Re-Summed (*z* axis). Integration with respect to time was not found, so we move on to the spatial components. The integrations here follow the same pattern of the *Two Series Require Poisson Re-Summation* section. To begin, we write down the equation requiring integration

$$d = \frac{Q}{2\pi L}\frac{\sqrt{S_s}}{2abS_s\sqrt{K_z\pi}}\int_0^{2\pi}\int_{t_1}^{t_2}\frac{1}{\sqrt{\tau}}\int_0^{L}\sum_{n=-\infty}^{\infty}\sum_{m=-\infty}^{\infty}\sum_{l=-\infty}^{\infty}\cos\left[\frac{n\pi x}{a}\right]$$
$$\cos\left[\frac{n\pi x_0}{a}\right]\exp\left[-\tau\frac{n^2\pi^2K_x}{a^2S_s}\right]\cos\left[\frac{m\pi y}{b}\right]\cos\left[\frac{m\pi y_0}{b}\right]$$
$$\exp\left[-\tau\frac{m^2\pi^2K_y}{b^2S_s}\right]\exp\left[-\frac{S_s}{4\tau}\left(\frac{\left(\pm z+z_0+2cl\right)^2}{K_z}\right)\right]dw\,d\tau\,d\theta. \tag{78}$$

Next, we parameterize this equation to integrate with respect to *w* and find

$$d = \frac{Q}{2\pi L}\frac{\sqrt{S_s}}{2abS_s\sqrt{K_z\pi}}\int_0^{2\pi}\int_{t_1}^{t_2}\frac{1}{\sqrt{\tau}}\int_0^{L}\sum_{n=-\infty}^{\infty}\sum_{m=-\infty}^{\infty}\sum_{l=-\infty}^{\infty}$$
$$\cos\left[\frac{n\pi x}{a}\right]\cos\left[\frac{n\pi\left(f_1w+x_1\right)}{a}\right]\exp\left[-\tau\frac{n^2\pi^2K_x}{a^2S_s}\right]$$
$$\cos\left[\frac{m\pi y}{b}\right]\cos\left[\frac{m\pi\left(f_2w+y_1\right)}{b}\right]\exp\left[-\tau\frac{m^2\pi^2K_y}{b^2S_s}\right]$$
$$\exp\left[-\frac{S_s}{4\tau}\left(\frac{\left(\pm z+\left(f_3w+z_1\right)+2cl\right)^2}{K_z}\right)\right]dw\,d\tau\,d\theta. \tag{79}$$

Simplifying the equation and rewriting cosine terms, we find

$$d = \frac{Q}{2\pi L}\frac{\sqrt{S_s}}{2abS_s\sqrt{K_z\pi}}\int_0^{2\pi}\int_{t_1}^{t_2}\frac{1}{\sqrt{\tau}}\frac{1}{2}\int_0^{L}\sum_{n=-\infty}^{\infty}\sum_{m=-\infty}^{\infty}\sum_{l=-\infty}^{\infty}$$
$$\cos\left[\frac{n\pi x}{a}\right]\cos\left[\frac{m\pi y}{b}\right]\exp\left[-\tau\frac{n^2\pi^2K_x}{a^2S_s}-\tau\frac{m^2\pi^2K_y}{b^2S_s}\right]$$
$$\left(\cos\left[w\pi\left(\frac{f_1n}{a}-\frac{f_2m}{b}\right)+\frac{\pi x_1n}{a}-\frac{\pi y_1m}{b}\right]+\cos\left[w\pi\left(\frac{f_1n}{a}+\frac{f_2m}{b}\right)+\frac{\pi x_1n}{a}+\frac{\pi y_1m}{b}\right]\right)$$
$$\exp\left[-\frac{S_s}{4\tau}\left(\frac{\left(\pm z+\left(f_3w+z_1\right)+2cl\right)^2}{K_z}\right)\right]dw\,d\tau\,d\theta. \tag{80}$$

We then remove constants

$$C_1 = -\frac{S_s}{4\tau}\left(\frac{4\left(c^2l^2 + cl\left(\pm z + z_1\right)\right)}{K_z} + \frac{z^2 + 2zz_1 + z_1^2}{K_z}\right)$$

$$C_2 = -\frac{S_s}{4\tau}\left(f_3\frac{4cl + 2\left(\pm z + z_1\right)}{K_z}\right)$$

$$C_3 = -\frac{S_s}{4\tau}\left(\frac{f_3^2}{K_z}\right) \quad , \tag{81}$$

$$C_4 = n\pi f_1/a \pm m\pi f_2/b$$

$$C_5 = n\pi x_1/a \pm m\pi y_1/b$$

which yields

$$d = \frac{Q}{2\pi L}\frac{\sqrt{S_s}}{4abS_s\sqrt{K_z\pi}}\int_0^{2\pi}\int_{t_1}^{t_2}\frac{1}{\sqrt{\tau}}\sum_{n=-\infty}^{\infty}\sum_{m=-\infty}^{\infty}\sum_{l=-\infty}^{\infty}$$
$$\cos\left[\frac{n\pi x}{a}\right]\cos\left[\frac{m\pi y}{b}\right]\exp\left[-\tau\frac{n^2\pi^2K_x}{a^2S_s} - \tau\frac{m^2\pi^2K_y}{b^2S_s}\right]$$
$$\int_0^L \exp\left[w^2C_3 + wC_2 + C_1\right]\cos\left[wC_4 + C_5\right]\, dw\, d\tau\, d\theta \quad . \tag{82}$$

To integrate this equation, we use 01.07.21.0216.01 from Functions.Wolfram (2014), and find the final form of the equation still requiring spatial and temporal integration

$$d = \frac{Q}{2\pi L}\frac{\sqrt{S_s}}{4abS_s\sqrt{K_z\pi}}\int_0^{2\pi}\int_{t_1}^{t_2}\frac{1}{\sqrt{\tau}}\sum_{n=-\infty}^{\infty}\sum_{m=-\infty}^{\infty}\sum_{l=-\infty}^{\infty}\exp\left[-\tau\frac{n^2\pi^2K_x}{a^2S_s} - \tau\frac{m^2\pi^2K_y}{b^2S_s}\right]$$
$$\cos\left[\frac{n\pi x}{a}\right]\cos\left[\frac{m\pi y}{b}\right]\frac{1}{4\sqrt{C_3}}\exp\left[-\frac{C_2^2 + 2iC_4C_2 - C_4^2 - 4C_3C_1 + 4iC_3C_5}{4C_3}\right]$$
$$\left(\exp\left[2iC_5\right]\left(\operatorname{erfi}\left[\frac{C_2 + iC_4 + 2C_3L}{2\sqrt{C_3}}\right] - \operatorname{erfi}\left[\frac{C_2 + iC_4}{2\sqrt{C_3}}\right]\right) + \right.$$
$$\left.\exp\left[\frac{iC_2C_4}{C_3}\right]\left(\operatorname{erfi}\left[\frac{C_2 - iC_4 + 2C_3L}{2\sqrt{C_3}}\right] - \operatorname{erfi}\left[\frac{C_2 - iC_4}{2\sqrt{C_3}}\right]\right)\right) d\tau\, d\theta. \tag{83}$$

No Series Require Poisson Re-Summation

Although analytical integration can be found for each of the three integrals at late time (time, wellbore length, wellbore circumference), at this point the function is very smooth and very quickly numerically integrated. Also, there are singularities in the solution upon inspection of the denominator in the double and triple series. There are special cases when the denominator goes to zero even though the solution does not go to infinity.

To begin, we write the drawdown equation with all unaltered series

$$d = \frac{Q}{2\pi L}\frac{1}{abcS_s}\int_{t_1}^{t_2}\int_{0}^{L}\left(1+2\sum_{n=1}^{\infty}\cos\left[\frac{n\pi x}{a}\right]\cos\left[\frac{n\pi x_0}{a}\right]\exp\left[-\tau\frac{n^2\pi^2K_x}{a^2S_s}\right]\right)$$
$$\left(1+2\sum_{m=1}^{\infty}\cos\left[\frac{m\pi y}{b}\right]\cos\left[\frac{m\pi y_0}{b}\right]\exp\left[-\tau\frac{m^2\pi^2K_y}{b^2S_s}\right]\right)$$
$$\left(1+2\sum_{l=1}^{\infty}\cos\left[\frac{l\pi z}{c}\right]\cos\left[\frac{l\pi z_0}{c}\right]\exp\left[-\tau\frac{l^2\pi^2K_z}{c^2S_s}\right]\right)dw\,\mathrm{d}\tau. \qquad (84)$$

We then expand and integrate each series with respect to τ and w and find:

$$d = \frac{Q}{2\pi L}\int_0^{2\pi}\frac{1}{abcS_s}$$

$$\left\{ L\left(t_2 - t_1\right) + \left[\frac{2S_s a^3}{f_1\pi^3 K_x}\right]\sum_{n=1}^{\infty}\frac{\cos\left[\frac{n\pi x}{a}\right]\left(\sin\left[\frac{n\pi\left(f_1 L + x_1\right)}{a}\right] - \sin\left[\frac{n\pi x_1}{a}\right]\right)}{n^3}\left(\exp\left[-t_1\frac{n^2\pi^2 K_x}{a^2 S_s}\right] - \exp\left[-t_2\frac{n^2\pi^2 K_x}{a^2 S_s}\right]\right)\right.$$

$$+\left[\frac{2S_s b^3}{f_2\pi^3 K_y}\right]\sum_{m=1}^{\infty}\frac{\cos\left[\frac{m\pi y}{b}\right]\left(\sin\left[\frac{m\pi\left(f_2 L + y_1\right)}{b}\right] - \sin\left[\frac{m\pi y_1}{b}\right]\right)}{m^3}\left(\exp\left[-t_1\frac{m^2\pi^2 K_y}{b^2 S_s}\right] - \exp\left[-t_2\frac{m^2\pi^2 K_y}{b^2 S_s}\right]\right)$$

$$\left.+\left[\frac{2S_s c^3}{f_3\pi^3 K_z}\right]\sum_{l=1}^{\infty}\frac{\cos\left[\frac{l\pi z}{c}\right]\left(\sin\left[\frac{l\pi\left(f_3 L + z_1\right)}{c}\right] - \sin\left[\frac{l\pi z_1}{c}\right]\right)}{l^3}\left(\exp\left[-t_1\frac{l^2\pi^2 K_z}{c^2 S_s}\right] - \exp\left[-t_2\frac{l^2\pi^2 K_z}{c^2 S_s}\right]\right)\right.$$

$$+\left[\frac{2S_s ab}{\pi^3}\right]\sum_{n=1}^{\infty}\sum_{m=1}^{\infty}\frac{\cos\left[\frac{n\pi x}{a}\right]\cos\left[\frac{m\pi y}{b}\right]}{\frac{n^2K_x}{a^2}+\frac{m^2K_y}{b^2}}$$

$$\left(\frac{\sin\left[\frac{\pi am\left(Lf_2+y_1\right)-\pi bn\left(Lf_1+x_1\right)}{ab}\right]-\sin\left[\frac{\pi amy_1-\pi bnx_1}{ab}\right]}{af_2m-bf_1n}+\frac{\sin\left[\frac{\pi am\left(Lf_2+y_1\right)+\pi bn\left(Lf_1+x_1\right)}{ab}\right]-\sin\left[\frac{\pi amy_1+\pi bnx_1}{ab}\right]}{af_2m+bf_1n}\right)$$

$$\left(\exp\left[-t_1\frac{\pi^2}{S_s}\left(\frac{n^2K_x}{a^2}+\frac{m^2K_y}{b^2}\right)\right]-\exp\left[-t_2\frac{\pi^2}{S_s}\left(\frac{n^2K_x}{a^2}+\frac{m^2K_y}{b^2}\right)\right]\right)$$

$$+\left[\frac{2S_s bc}{\pi^3}\right]\sum_{l=1}^{\infty}\sum_{m=1}^{\infty}\frac{\cos\left[\frac{l\pi z}{c}\right]\cos\left[\frac{m\pi y}{b}\right]}{\frac{l^2K_z}{c^2}+\frac{m^2K_y}{b^2}}$$

$$\left(\frac{\sin\left[\frac{\pi cm\left(Lf_2+y_1\right)-\pi bl\left(Lf_3+z_1\right)}{cb}\right]-\sin\left[\frac{\pi cmy_1-\pi blz_1}{cb}\right]}{cf_2m-bf_3l}+\frac{\sin\left[\frac{\pi cm\left(Lf_2+y_1\right)+\pi bl\left(Lf_3+z_1\right)}{cb}\right]-\sin\left[\frac{\pi cmy_1+\pi blz_1}{cb}\right]}{cf_2m+bf_3l}\right)$$

$$\left(\exp\left[-t_1\frac{\pi^2}{S_s}\left(\frac{l^2K_z}{c^2}+\frac{m^2K_y}{b^2}\right)\right]-\exp\left[-t_2\frac{\pi^2}{S_s}\left(\frac{l^2K_z}{c^2}+\frac{m^2K_y}{b^2}\right)\right]\right)$$

$$+\left[\frac{2S_s ac}{\pi^3}\right]\sum_{n=1}^{\infty}\sum_{l=1}^{\infty}\frac{\cos\left[\frac{n\pi x}{a}\right]\cos\left[\frac{l\pi z}{c}\right]}{\frac{n^2K_x}{a^2}+\frac{l^2K_z}{c^2}}$$

$$\left(\frac{\sin\left[\frac{\pi al\left(Lf_3+z_1\right)-\pi cn\left(Lf_1+x_1\right)}{ac}\right]-\sin\left[\frac{\pi alz_1-\pi cnx_1}{ac}\right]}{af_3l-cf_1n}+\frac{\sin\left[\frac{\pi al\left(Lf_3+z_1\right)+\pi cn\left(Lf_1+x_1\right)}{ac}\right]-\sin\left[\frac{\pi alz_1+\pi cnx_1}{ac}\right]}{af_3l+cf_1n}\right)$$

$$\left(\exp\left[-t_1\frac{\pi^2}{S_s}\left(\frac{n^2K_x}{a^2}+\frac{l^2K_z}{c^2}\right)\right]-\exp\left[-t_2\frac{\pi^2}{S_s}\left(\frac{n^2K_x}{a^2}+\frac{l^2K_z}{c^2}\right)\right]\right)$$

$$+\left[\frac{2S_s abc}{\pi^3}\right]\sum_{l=1}^{\infty}\sum_{m=1}^{\infty}\sum_{n=1}^{\infty}\frac{\cos\left[\frac{l\pi z}{c}\right]\cos\left[\frac{m\pi y}{b}\right]\cos\left[\frac{n\pi x}{a}\right]}{\frac{l^2K_z}{c^2}+\frac{m^2K_y}{b^2}+\frac{n^2K_x}{a^2}}$$

$$\left(\frac{-\sin\left[\frac{\pi acm\left(f_2L+y_1\right)-\pi abl\left(f_3L+z_1\right)+\pi bcn\left(f_1L+x_1\right)}{abc}\right]+\sin\left[\frac{\pi acmy_1-\pi ablz_1+\pi bcnx_1}{abc}\right]}{abf_3l-acf_2m-bcf_1n}+\right.$$

$$\frac{\sin\left[\frac{\pi abl\left(f_3L+z_1\right)-\pi acm\left(f_2L+y_1\right)+\pi bcn\left(f_1L+x_1\right)}{abc}\right]-\sin\left[\frac{\pi ablz_1-\pi acmy_1+\pi bcnx_1}{abc}\right]}{abf_3l-acf_2m+bcf_1n}+$$

$$\frac{\sin\left[\frac{\pi abl\left(f_3L+z_1\right)+\pi acm\left(f_2L+y_1\right)-\pi bcn\left(f_1L+x_1\right)}{abc}\right]-\sin\left[\frac{\pi ablz_1+\pi acmy_1-\pi bcnx_1}{abc}\right]}{abf_3l+acf_2m-bcf_1n}+$$

$$\left.\frac{\sin\left[\frac{\pi abl\left(f_3L+z_1\right)+\pi acm\left(f_2L+y_1\right)+\pi bcn\left(f_1L+x_1\right)}{abc}\right]-\sin\left[\frac{\pi ablz_1+\pi acmy_1+\pi bcnx_1}{abc}\right]}{abf_3l+acf_2m+bcf_1n}\right)$$

$$\left.\left(\exp\left[-t_1\frac{\pi^2}{S_s}\left(\frac{l^2K_z}{c^2}+\frac{m^2K_y}{b^2}+\frac{n^2K_x}{a^2}\right)\right]-\exp\left[-t_2\frac{\pi^2}{S_s}\left(\frac{l^2K_z}{c^2}+\frac{m^2K_y}{b^2}+\frac{n^2K_x}{a^2}\right)\right]\right)\right\}d\theta. \qquad (85)$$

ANALYTICAL INTEGRATIONS USED IN MODEL

Upon numerical implementation it became apparent that the greatest computational speed occurs when the very early time is integrated analytically, and later times are integrated numerically. As can be seen by the three boundary condition cases for early time, the forms are very similar; the only differences are the constants. Upon inspection of the examples below a simple pattern can be recognized. Four examples are listed below. Within each example, the temporal analytical integration has been completed and the two remaining spatial integrations must be completed numerically. Note that the +/- terms are explicitly written out.

The early time analytical integration solution when all sides of the box are no-flux $\left(\frac{\partial \bar{d}}{\partial x}|_{x=0} = \frac{\partial \bar{d}}{\partial x}|_{x=a} = \frac{\partial \bar{d}}{\partial y}|_{y=0} = \frac{\partial \bar{d}}{\partial y}|_{y=b} = \frac{\partial \bar{d}}{\partial z}|_{z=0} = \frac{\partial \bar{d}}{\partial z}|_{z=c} = 0 \right)$ is

$$d = \frac{Q}{2\pi L}\frac{1}{8}\sqrt{\frac{S_s}{\pi^2 K_x K_y K_z}}\int_0^L\int_0^{2\pi}\sum_{n=-\infty}^{\infty}\sum_{m=-\infty}^{\infty}\sum_{l=-\infty}^{\infty}$$

$$\left\{ \frac{\operatorname{erfc}\left[\sqrt{\frac{S_s}{4t}\left(\frac{(x+x_0+2an)^2}{K_x}+\frac{(y+y_0+2bm)^2}{K_y}+\frac{(z+z_0+2cl)^2}{K_z}\right)}\right]}{\sqrt{\frac{S_s}{4}\left(\frac{(x+x_0+2an)^2}{K_x}+\frac{(y+y_0+2bm)^2}{K_y}+\frac{(z+z_0+2cl)^2}{K_z}\right)}} \right.$$

$$\left. + \frac{\operatorname{erfc}\left[\sqrt{\frac{S_s}{4t}\left(\frac{(-x+x_0+2an)^2}{K_x}+\frac{(y+y_0+2bm)^2}{K_y}+\frac{(z+z_0+2cl)^2}{K_z}\right)}\right]}{\sqrt{\frac{S_s}{4}\left(\frac{(-x+x_0+2an)^2}{K_x}+\frac{(y+y_0+2bm)^2}{K_y}+\frac{(z+z_0+2cl)^2}{K_z}\right)}} \right.$$

$$
+\frac{\operatorname{erfc}\left[\sqrt{\frac{S_s}{4t}\left(\frac{\left(x+x_0+2an\right)^2}{K_x}+\frac{\left(-y+y_0+2bm\right)^2}{K_y}+\frac{\left(z+z_0+2cl\right)^2}{K_z}\right)}\right]}{\sqrt{\frac{S_s}{4}\left(\frac{\left(x+x_0+2an\right)^2}{K_x}+\frac{\left(-y+y_0+2bm\right)^2}{K_y}+\frac{\left(z+z_0+2cl\right)^2}{K_z}\right)}}
$$

$$
+\frac{\operatorname{erfc}\left[\sqrt{\frac{S_s}{4t}\left(\frac{\left(x+x_0+2an\right)^2}{K_x}+\frac{\left(y+y_0+2bm\right)^2}{K_y}+\frac{\left(-z+z_0+2cl\right)^2}{K_z}\right)}\right]}{\sqrt{\frac{S_s}{4}\left(\frac{\left(x+x_0+2an\right)^2}{K_x}+\frac{\left(y+y_0+2bm\right)^2}{K_y}+\frac{\left(-z+z_0+2cl\right)^2}{K_z}\right)}}
$$

$$
+\frac{\operatorname{erfc}\left[\sqrt{\frac{S_s}{4t}\left(\frac{\left(-x+x_0+2an\right)^2}{K_x}+\frac{\left(-y+y_0+2bm\right)^2}{K_y}+\frac{\left(z+z_0+2cl\right)^2}{K_z}\right)}\right]}{\sqrt{\frac{S_s}{4}\left(\frac{\left(-x+x_0+2an\right)^2}{K_x}+\frac{\left(-y+y_0+2bm\right)^2}{K_y}+\frac{\left(z+z_0+2cl\right)^2}{K_z}\right)}}
$$

$$
+\frac{\operatorname{erfc}\left[\sqrt{\frac{S_s}{4t}\left(\frac{\left(-x+x_0+2an\right)^2}{K_x}+\frac{\left(y+y_0+2bm\right)^2}{K_y}+\frac{\left(-z+z_0+2cl\right)^2}{K_z}\right)}\right]}{\sqrt{\frac{S_s}{4}\left(\frac{\left(-x+x_0+2an\right)^2}{K_x}+\frac{\left(y+y_0+2bm\right)^2}{K_y}+\frac{\left(-z+z_0+2cl\right)^2}{K_z}\right)}}
$$

$$
+\frac{\operatorname{erfc}\left[\sqrt{\frac{S_s}{4t}\left(\frac{\left(-x+x_0+2an\right)^2}{K_x}+\frac{\left(-y+y_0+2bm\right)^2}{K_y}+\frac{\left(-z+z_0+2cl\right)^2}{K_z}\right)}\right]}{\sqrt{\frac{S_s}{4}\left(\frac{\left(-x+x_0+2an\right)^2}{K_x}+\frac{\left(-y+y_0+2bm\right)^2}{K_y}+\frac{\left(-z+z_0+2cl\right)^2}{K_z}\right)}}
\Bigg\} d\theta\, dw \quad . \tag{86}
$$

The early time analytical integration solution when all sides of the box are constant head $\left(\overline{d}\left(x=0\right)=\overline{d}\left(x=a\right)=\overline{d}\left(y=0\right)=\overline{d}\left(y=b\right)=\overline{d}\left(z=0\right)=\overline{d}\left(z=c\right)=0\right)$ is

$$d = \frac{Q}{2\pi L}\frac{1}{8}\sqrt{\frac{S_s}{\pi^2 K_x K_y K_z}}\int_0^L\int_0^{2\pi}\sum_{n=-\infty}^{\infty}\sum_{m=-\infty}^{\infty}\sum_{l=-\infty}^{\infty}$$

$$\left\{ -\frac{\operatorname{erfc}\left[\sqrt{\frac{S_s}{4t}\left(\frac{(x+x_0+2an)^2}{K_x}+\frac{(y+y_0+2bm)^2}{K_y}+\frac{(z+z_0+2cl)^2}{K_z}\right)}\right]}{\sqrt{\frac{S_s}{4}\left(\frac{(x+x_0+2an)^2}{K_x}+\frac{(y+y_0+2bm)^2}{K_y}+\frac{(z+z_0+2cl)^2}{K_z}\right)}}\right.$$

$$+\frac{\operatorname{erfc}\left[\sqrt{\frac{S_s}{4t}\left(\frac{(-x+x_0+2an)^2}{K_x}+\frac{(y+y_0+2bm)^2}{K_y}+\frac{(z+z_0+2cl)^2}{K_z}\right)}\right]}{\sqrt{\frac{S_s}{4}\left(\frac{(-x+x_0+2an)^2}{K_x}+\frac{(y+y_0+2bm)^2}{K_y}+\frac{(z+z_0+2cl)^2}{K_z}\right)}}$$

$$+\frac{\operatorname{erfc}\left[\sqrt{\frac{S_s}{4t}\left(\frac{(x+x_0+2an)^2}{K_x}+\frac{(-y+y_0+2bm)^2}{K_y}+\frac{(z+z_0+2cl)^2}{K_z}\right)}\right]}{\sqrt{\frac{S_s}{4}\left(\frac{(x+x_0+2an)^2}{K_x}+\frac{(-y+y_0+2bm)^2}{K_y}+\frac{(z+z_0+2cl)^2}{K_z}\right)}}$$

$$+\frac{\operatorname{erfc}\left[\sqrt{\frac{S_s}{4t}\left(\frac{(x+x_0+2an)^2}{K_x}+\frac{(y+y_0+2bm)^2}{K_y}+\frac{(-z+z_0+2cl)^2}{K_z}\right)}\right]}{\sqrt{\frac{S_s}{4}\left(\frac{(x+x_0+2an)^2}{K_x}+\frac{(y+y_0+2bm)^2}{K_y}+\frac{(-z+z_0+2cl)^2}{K_z}\right)}}$$

$$\left.-\frac{\operatorname{erfc}\left[\sqrt{\frac{S_s}{4t}\left(\frac{(-x+x_0+2an)^2}{K_x}+\frac{(-y+y_0+2bm)^2}{K_y}+\frac{(z+z_0+2cl)^2}{K_z}\right)}\right]}{\sqrt{\frac{S_s}{4}\left(\frac{(-x+x_0+2an)^2}{K_x}+\frac{(-y+y_0+2bm)^2}{K_y}+\frac{(z+z_0+2cl)^2}{K_z}\right)}}\right\}$$

$$-\frac{\operatorname{erfc}\left[\sqrt{\frac{S_s}{4t}\left(\frac{\left(-x+x_0+2an\right)^2}{K_x}+\frac{\left(y+y_0+2bm\right)^2}{K_y}+\frac{\left(-z+z_0+2cl\right)^2}{K_z}\right)}\right]}{\sqrt{\frac{S_s}{4}\left(\frac{\left(-x+x_0+2an\right)^2}{K_x}+\frac{\left(y+y_0+2bm\right)^2}{K_y}+\frac{\left(-z+z_0+2cl\right)^2}{K_z}\right)}}$$

$$+\frac{\operatorname{erfc}\left[\sqrt{\frac{S_s}{4t}\left(\frac{\left(-x+x_0+2an\right)^2}{K_x}+\frac{\left(-y+y_0+2bm\right)^2}{K_y}+\frac{\left(-z+z_0+2cl\right)^2}{K_z}\right)}\right]}{\sqrt{\frac{S_s}{4}\left(\frac{\left(-x+x_0+2an\right)^2}{K_x}+\frac{\left(-y+y_0+2bm\right)^2}{K_y}+\frac{\left(-z+z_0+2cl\right)^2}{K_z}\right)}}\Bigg\}\, d\theta\, dw \tag{87}$$

The early time analytic integration when two sides of the box are constant head and four of the sides are no flux $\left(\bar{d}\left(x=0\right)=\bar{d}\left(x=a\right)=\frac{\partial\bar{d}}{\partial y}|_{y=0}=\frac{\partial\bar{d}}{\partial y}|_{y=b}=\frac{\partial\bar{d}}{\partial z}|_{z=0}=\frac{\partial\bar{d}}{\partial z}|_{z=c}=0\right)$ is

$$d=\frac{Q}{2\pi L}\frac{1}{8}\sqrt{\frac{S_s}{\pi^2K_xK_yK_z}}\int_0^L\int_0^{2\pi}\sum_{n=-\infty}^{\infty}\sum_{m=-\infty}^{\infty}\sum_{l=-\infty}^{\infty}$$

$$\Bigg\{-\frac{\operatorname{erfc}\left[\sqrt{\frac{S_s}{4t}\left(\frac{\left(x+x_0+2an\right)^2}{K_x}+\frac{\left(y+y_0+2bm\right)^2}{K_y}+\frac{\left(z+z_0+2cl\right)^2}{K_z}\right)}\right]}{\sqrt{\frac{S_s}{4}\left(\frac{\left(x+x_0+2an\right)^2}{K_x}+\frac{\left(y+y_0+2bm\right)^2}{K_y}+\frac{\left(z+z_0+2cl\right)^2}{K_z}\right)}}$$

$$+\frac{\operatorname{erfc}\left[\sqrt{\frac{S_s}{4t}\left(\frac{\left(-x+x_0+2an\right)^2}{K_x}+\frac{\left(y+y_0+2bm\right)^2}{K_y}+\frac{\left(z+z_0+2cl\right)^2}{K_z}\right)}\right]}{\sqrt{\frac{S_s}{4}\left(\frac{\left(-x+x_0+2an\right)^2}{K_x}+\frac{\left(y+y_0+2bm\right)^2}{K_y}+\frac{\left(z+z_0+2cl\right)^2}{K_z}\right)}}$$

$$
-\frac{\operatorname{erfc}\left[\sqrt{\frac{S_s}{4t}\left(\frac{\left(x+x_0+2an\right)^2}{K_x}+\frac{\left(-y+y_0+2bm\right)^2}{K_y}+\frac{\left(z+z_0+2cl\right)^2}{K_z}\right)}\right]}{\sqrt{\frac{S_s}{4}\left(\frac{\left(x+x_0+2an\right)^2}{K_x}+\frac{\left(-y+y_0+2bm\right)^2}{K_y}+\frac{\left(z+z_0+2cl\right)^2}{K_z}\right)}}
$$

$$
-\frac{\operatorname{erfc}\left[\sqrt{\frac{S_s}{4t}\left(\frac{\left(x+x_0+2an\right)^2}{K_x}+\frac{\left(y+y_0+2bm\right)^2}{K_y}+\frac{\left(-z+z_0+2cl\right)^2}{K_z}\right)}\right]}{\sqrt{\frac{S_s}{4}\left(\frac{\left(x+x_0+2an\right)^2}{K_x}+\frac{\left(y+y_0+2bm\right)^2}{K_y}+\frac{\left(-z+z_0+2cl\right)^2}{K_z}\right)}}
$$

$$
+\frac{\operatorname{erfc}\left[\sqrt{\frac{S_s}{4t}\left(\frac{\left(-x+x_0+2an\right)^2}{K_x}+\frac{\left(-y+y_0+2bm\right)^2}{K_y}+\frac{\left(z+z_0+2cl\right)^2}{K_z}\right)}\right]}{\sqrt{\frac{S_s}{4}\left(\frac{\left(-x+x_0+2an\right)^2}{K_x}+\frac{\left(-y+y_0+2bm\right)^2}{K_y}+\frac{\left(z+z_0+2cl\right)^2}{K_z}\right)}}
$$

$$
+\frac{\operatorname{erfc}\left[\sqrt{\frac{S_s}{4t}\left(\frac{\left(-x+x_0+2an\right)^2}{K_x}+\frac{\left(y+y_0+2bm\right)^2}{K_y}+\frac{\left(-z+z_0+2cl\right)^2}{K_z}\right)}\right]}{\sqrt{\frac{S_s}{4}\left(\frac{\left(-x+x_0+2an\right)^2}{K_x}+\frac{\left(y+y_0+2bm\right)^2}{K_y}+\frac{\left(-z+z_0+2cl\right)^2}{K_z}\right)}}
$$

$$
+\left.\frac{\operatorname{erfc}\left[\sqrt{\frac{S_s}{4t}\left(\frac{\left(-x+x_0+2an\right)^2}{K_x}+\frac{\left(-y+y_0+2bm\right)^2}{K_y}+\frac{\left(-z+z_0+2cl\right)^2}{K_z}\right)}\right]}{\sqrt{\frac{S_s}{4}\left(\frac{\left(-x+x_0+2an\right)^2}{K_x}+\frac{\left(-y+y_0+2bm\right)^2}{K_y}+\frac{\left(-z+z_0+2cl\right)^2}{K_z}\right)}}\right\} d\theta\, dw \quad . \tag{88}
$$

The early time integration when one side of the box is constant head and the remainder of the sides are no flux $\left(\frac{\partial \bar{d}}{\partial x}|_{x=0}=\bar{d}\left(x=a\right)=\frac{\partial \bar{d}}{\partial y}|_{y=0}=\frac{\partial \bar{d}}{\partial y}|_{y=b}=\frac{\partial \bar{d}}{\partial z}|_{z=0}=\frac{\partial \bar{d}}{\partial z}|_{z=c}=0\right)$ is

$$d = \frac{Q}{2\pi L}\frac{1}{8}\sqrt{\frac{S_s}{\pi^2 K_x K_y K_z}}\int_0^L\int_0^{2\pi}\sum_{n=-\infty}^{\infty}\sum_{m=-\infty}^{\infty}\sum_{l=-\infty}^{\infty}$$

$$\left\{\frac{\operatorname{erfc}\left[\sqrt{\frac{S_s}{4t}\left(\frac{\left(x+x_0+2an\right)^2}{K_x}+\frac{\left(y+y_0+2bm\right)^2}{K_y}+\frac{\left(z+z_0+2cl\right)^2}{K_z}\right)}\right]}{\sqrt{\frac{S_s}{4}\left(\frac{\left(x+x_0+2an\right)^2}{K_x}+\frac{\left(y+y_0+2bm\right)^2}{K_y}+\frac{\left(z+z_0+2cl\right)^2}{K_z}\right)}}\exp\left[-i\frac{\left(\pi\left(x+x_0\right)/a+2\pi n\right)}{2}+i\frac{\pi\left(x+x_0\right)}{2a}\right]\right.$$

$$+\frac{\operatorname{erfc}\left[\sqrt{\frac{S_s}{4t}\left(\frac{\left(-x+x_0+2an\right)^2}{K_x}+\frac{\left(y+y_0+2bm\right)^2}{K_y}+\frac{\left(z+z_0+2cl\right)^2}{K_z}\right)}\right]}{\sqrt{\frac{S_s}{4}\left(\frac{\left(-x+x_0+2an\right)^2}{K_x}+\frac{\left(y+y_0+2bm\right)^2}{K_y}+\frac{\left(z+z_0+2cl\right)^2}{K_z}\right)}}\exp\left[-i\frac{\left(\pi\left(-x+x_0\right)/a+2\pi n\right)}{2}+i\frac{\pi\left(-x+x_0\right)}{2a}\right]$$

$$\left.+\frac{\operatorname{erfc}\left[\sqrt{\frac{S_s}{4t}\left(\frac{\left(x+x_0+2an\right)^2}{K_x}+\frac{\left(-y+y_0+2bm\right)^2}{K_y}+\frac{\left(z+z_0+2cl\right)^2}{K_z}\right)}\right]}{\sqrt{\frac{S_s}{4}\left(\frac{\left(x+x_0+2an\right)^2}{K_x}+\frac{\left(-y+y_0+2bm\right)^2}{K_y}+\frac{\left(z+z_0+2cl\right)^2}{K_z}\right)}}\exp\left[-i\frac{\left(\pi\left(x+x_0\right)/a+2\pi n\right)}{2}+i\frac{\pi\left(x+x_0\right)}{2a}\right]\right.$$

$$+\frac{\operatorname{erfc}\left[\sqrt{\frac{S_s}{4t}\left(\frac{\left(x+x_0+2an\right)^2}{K_x}+\frac{\left(y+y_0+2bm\right)^2}{K_y}+\frac{\left(-z+z_0+2cl\right)^2}{K_z}\right)}\right]}{\sqrt{\frac{S_s}{4}\left(\frac{\left(x+x_0+2an\right)^2}{K_x}+\frac{\left(y+y_0+2bm\right)^2}{K_y}+\frac{\left(-z+z_0+2cl\right)^2}{K_z}\right)}}\exp\left[-i\frac{\left(\pi\left(x+x_0\right)/a+2\pi n\right)}{2}+i\frac{\pi\left(x+x_0\right)}{2a}\right]$$

$$+\frac{\operatorname{erfc}\left[\sqrt{\frac{S_s}{4t}\left(\frac{\left(-x+x_0+2an\right)^2}{K_x}+\frac{\left(-y+y_0+2bm\right)^2}{K_y}+\frac{\left(z+z_0+2cl\right)^2}{K_z}\right)}\right]}{\sqrt{\frac{S_s}{4}\left(\frac{\left(-x+x_0+2an\right)^2}{K_x}+\frac{\left(-y+y_0+2bm\right)^2}{K_y}+\frac{\left(z+z_0+2cl\right)^2}{K_z}\right)}}\exp\left[-i\frac{\left(\pi\left(-x+x_0\right)/a+2\pi n\right)}{2}+i\frac{\pi\left(-x+x_0\right)}{2a}\right]$$

$$+\frac{\operatorname{erfc}\left[\sqrt{\frac{S_s}{4t}\left(\frac{\left(-x+x_0+2an\right)^2}{K_x}+\frac{\left(y+y_0+2bm\right)^2}{K_y}+\frac{\left(-z+z_0+2cl\right)^2}{K_z}\right)}\right]}{\sqrt{\frac{S_s}{4}\left(\frac{\left(-x+x_0+2an\right)^2}{K_x}+\frac{\left(y+y_0+2bm\right)^2}{K_y}+\frac{\left(-z+z_0+2cl\right)^2}{K_z}\right)}}\exp\left[-i\frac{\left(\pi\left(-x+x_0\right)/a+2\pi n\right)}{2}+i\frac{\pi\left(-x+x_0\right)}{2a}\right]$$

$$+\frac{\operatorname{erfc}\left[\sqrt{\frac{S_s}{4t}\left(\frac{\left(-x+x_0+2an\right)^2}{K_x}+\frac{\left(-y+y_0+2bm\right)^2}{K_y}+\frac{\left(-z+z_0+2cl\right)^2}{K_z}\right)}\right]}{\sqrt{\frac{S_s}{4}\left(\frac{\left(-x+x_0+2an\right)^2}{K_x}+\frac{\left(-y+y_0+2bm\right)^2}{K_y}+\frac{\left(-z+z_0+2cl\right)^2}{K_z}\right)}}\exp\left[-i\frac{\left(\pi\left(-x+x_0\right)/a+2\pi n\right)}{2}+i\frac{\pi\left(-x+x_0\right)}{2a}\right]\Bigg\}. \quad (89)$$

CHAPTER IV

DEVELOPMENT OF A NON-UNIFORM FLUX WELL

STEADY STATE NUMERICAL SOLUTION

The steady state solution occurs when additional time yields no change in drawdown. In a rigorous sense, the steady state is possible only when a source of recharge exists within a finite distance from a pumping well. The pseudo-steady state solution occurs in closed systems (all sides no-flux boundary conditions) or in a system whose boundaries are infinitely far from the pumping well. It is defined over a domain when additional time yields a linear drawdown response. Under steady-state condition, both the drawdown and the flux are independent of time; whereas under pseudo-steady, the flux is independent of time but the drawdown can still change uniformly with time over the domain of interest. The terms steady state and pseudo-steady state are used interchangeably throughout this thesis unless specifically noted.

To solve the spatial discretization problem, first the effect of one segment on another is stored in a matrix. This relationship has been previously defined in Chapter III. Using the same nomenclature as Penmatcha and Aziz (1999), the term $F_{M,N}$ denotes how well segment *N* effects well segment *M*. For example, $F_{1,1}$ is how segment one affects itself and $F_{1,2}$ is how segment two affects segment one. In our implementation, how the line sink / source *N* affects the circumference of the well around a point along the center of segment *M*. To further clarify, the well is divided into several segments (Figure 67). In this case, one well has been divided into four segments.

1	2	3	4

Figure 67. Wellbore subdivided into four segments.

Then arguments (position of the wellbore, sample point, etc.) are passed to a function which generates *F* in the equation below. The function *F* is the aquifer response to pumping derived in Chapter III. We have setup the equation to solve for *d*, the drawdown distribution, which is calculated upon multiplication of *F* with the pumping rate distribution, $FQ = d$. The results from calculation of the aquifer function *F* are stored in a matrix (Figure 68).

$$\begin{matrix} F_{1,1} & F_{1,2} & F_{1,3} & F_{1,4} \\ F_{2,1} & F_{2,2} & F_{2,3} & F_{2,4} \\ F_{3,1} & F_{3,2} & F_{3,3} & F_{3,4} \\ F_{4,1} & F_{4,2} & F_{4,3} & F_{4,4} \end{matrix}$$

Figure 68. Storage of results from the aquifer response function *F*.

Putting the matrix of aquifer calculation results into a drawdown solution framework given a pumping rate distribution, we find

$$\begin{pmatrix} F_{1,1} & F_{1,2} & F_{1,3} & F_{1,4} \\ F_{2,1} & F_{2,2} & F_{2,3} & F_{2,4} \\ F_{3,1} & F_{3,2} & F_{3,3} & F_{3,4} \\ F_{4,1} & F_{4,2} & F_{4,3} & F_{4,4} \end{pmatrix} \begin{pmatrix} Q_1 \\ Q_2 \\ Q_3 \\ Q_4 \end{pmatrix} = \begin{pmatrix} d_1 \\ d_2 \\ d_3 \\ d_4 \end{pmatrix}, \tag{90}$$

where Q_1, Q_2, etc. is the pumping rate at a specific segment and d_1, d_2, etc. is the drawdown at a specific segment.

To solve the matrix equations, one has to first determine the pumping rate distribution Q_1, Q_2, Q_3, etc. To begin, we define the head loss (drawdown difference) between each segment. This drawdown difference may be either zero (infinite conductivity), depend on friction (frictional head loss) and/or depend on acceleration (kinetic head loss). The aquifer drawdown difference may be found by subtracting aquifer responses. So, subtracting aquifer responses we find

$$\begin{aligned}&\begin{pmatrix} F_{1,1} & F_{1,2} & F_{1,3} & F_{1,4} \\ F_{2,1} & F_{2,2} & F_{2,3} & F_{2,4} \\ F_{3,1} & F_{3,2} & F_{3,3} & F_{3,4} \end{pmatrix} - \begin{pmatrix} F_{2,1} & F_{2,2} & F_{2,3} & F_{2,4} \\ F_{3,1} & F_{3,2} & F_{3,3} & F_{3,4} \\ F_{4,1} & F_{4,2} & F_{4,3} & F_{4,4} \end{pmatrix} \\ &= \begin{pmatrix} F_{1,1}-F_{2,1} & F_{1,2}-F_{2,2} & F_{1,3}-F_{2,3} & F_{1,4}-F_{2,4} \\ F_{2,1}-F_{3,1} & F_{2,2}-F_{3,2} & F_{2,3}-F_{3,3} & F_{2,4}-F_{3,4} \\ F_{3,1}-F_{4,1} & F_{3,2}-F_{4,2} & F_{3,3}-F_{4,3} & F_{3,4}-F_{4,4} \end{pmatrix}\end{aligned}, \tag{91}$$

which upon putting back into a drawdown solution equation, we find

$$\begin{pmatrix} F_{1,1}-F_{2,1} & F_{1,2}-F_{2,2} & F_{1,3}-F_{2,3} & F_{1,4}-F_{2,4} \\ F_{2,1}-F_{3,1} & F_{2,2}-F_{3,2} & F_{2,3}-F_{3,3} & F_{2,4}-F_{3,4} \\ F_{3,1}-F_{4,1} & F_{3,2}-F_{4,2} & F_{3,3}-F_{4,3} & F_{3,4}-F_{4,4} \end{pmatrix} \begin{pmatrix} Q_1 \\ Q_2 \\ Q_3 \\ Q_4 \end{pmatrix} = \begin{pmatrix} d_1-d_2 \\ d_2-d_3 \\ d_3-d_4 \end{pmatrix}, \tag{92}$$

where $d_1 - d_2$ is the drawdown difference between segment one and segment two.

We are now lacking one equation to close the system. The last equation that closes the system may be either a total pumping rate equation or the drawdown at a specific segment (location of the pump) equation. Assuming a total pumping rate constraint, the solution is

$$\begin{pmatrix} F_{1,1}-F_{2,1} & F_{1,2}-F_{2,2} & F_{1,3}-F_{2,3} & F_{1,4}-F_{2,4} \\ F_{2,1}-F_{3,1} & F_{2,2}-F_{3,2} & F_{2,3}-F_{3,3} & F_{2,4}-F_{3,4} \\ F_{3,1}-F_{4,1} & F_{3,2}-F_{4,2} & F_{3,3}-F_{4,3} & F_{3,4}-F_{4,4} \\ 1 & 1 & 1 & 1 \end{pmatrix} \begin{pmatrix} Q_1 \\ Q_2 \\ Q_3 \\ Q_4 \end{pmatrix} = \begin{pmatrix} d_1-d_2 \\ d_2-d_3 \\ d_3-d_4 \\ Q_{Total} \end{pmatrix}. \tag{93}$$

Assuming a specific drawdown at single segment, segment one in this case, the solution is

$$\begin{pmatrix} F_{1,1}-F_{2,1} & F_{1,2}-F_{2,2} & F_{1,3}-F_{2,3} & F_{1,4}-F_{2,4} \\ F_{2,1}-F_{3,1} & F_{2,2}-F_{3,2} & F_{2,3}-F_{3,3} & F_{2,4}-F_{3,4} \\ F_{3,1}-F_{4,1} & F_{3,2}-F_{4,2} & F_{3,3}-F_{4,3} & F_{3,4}-F_{4,4} \\ F_{1,1} & F_{1,2} & F_{1,3} & F_{1,4} \end{pmatrix} \begin{pmatrix} Q_1 \\ Q_2 \\ Q_3 \\ Q_4 \end{pmatrix} = \begin{pmatrix} d_1-d_2 \\ d_2-d_3 \\ d_3-d_4 \\ d_1 \end{pmatrix}. \tag{94}$$

To solve this matrix equation, one may use a variety of methods ranging from iterative to linear algebraic procedures. We choose MATLAB's fsolve() function which finds the root of a system of nonlinear equations. For an initial condition, we assume uniform flux. The MATLAB fsolve() function finds a solution by guessing for x such that $Ax-b=0$. Therefore, if a total pumping rate constraint is in effect, the fsolve() input is

$$\begin{pmatrix} F_{1,1}-F_{2,1} & F_{1,2}-F_{2,2} & F_{1,3}-F_{2,3} & F_{1,4}-F_{2,4} \\ F_{2,1}-F_{3,1} & F_{2,2}-F_{3,2} & F_{2,3}-F_{3,3} & F_{2,4}-F_{3,4} \\ F_{3,1}-F_{4,1} & F_{3,2}-F_{4,2} & F_{3,3}-F_{4,3} & F_{3,4}-F_{4,4} \\ 1 & 1 & 1 & 1 \end{pmatrix} \begin{pmatrix} Q_1 \\ Q_2 \\ Q_3 \\ Q_4 \end{pmatrix} - \begin{pmatrix} d_1-d_2 \\ d_2-d_3 \\ d_3-d_4 \\ Q_{Total} \end{pmatrix} = \begin{pmatrix} 0 \\ 0 \\ 0 \\ 0 \end{pmatrix}. \tag{95}$$

If the constraint is a specific drawdown at single segment, segment one in this case, the fsolve() input is

$$\begin{pmatrix} F_{1,1}-F_{2,1} & F_{1,2}-F_{2,2} & F_{1,3}-F_{2,3} & F_{1,4}-F_{2,4} \\ F_{2,1}-F_{3,1} & F_{2,2}-F_{3,2} & F_{2,3}-F_{3,3} & F_{2,4}-F_{3,4} \\ F_{3,1}-F_{4,1} & F_{3,2}-F_{4,2} & F_{3,3}-F_{4,3} & F_{3,4}-F_{4,4} \\ F_{1,1} & F_{1,2} & F_{1,3} & F_{1,4} \end{pmatrix} \begin{pmatrix} Q_1 \\ Q_2 \\ Q_3 \\ Q_4 \end{pmatrix} - \begin{pmatrix} d_1-d_2 \\ d_2-d_3 \\ d_3-d_4 \\ d_1 \end{pmatrix} = \begin{pmatrix} 0 \\ 0 \\ 0 \\ 0 \end{pmatrix}. \quad (96)$$

The solution for a well with friction and acceleration head loss has been determined (using a given number of segments). Now we must solve the spatial discretization problem. In other words, determine how many segments are necessary to accurately characterize the well. To accomplish this, a higher level iterative method is employed. We begin by using a given number of segments, call the above functions and then add additional segments at the next iteration.

Assuming the total pumping rate is known and drawdown is unknown, after each iteration of the procedure we save the drawdown at the pumping segment. Once drawdown at the pumping segment has stabilized from one upper level iteration to the next, convergence has been achieved. The distribution of flux along a wellbore accounting for friction and acceleration has been calculated using enough segments to accurately characterize the problem. A similar method is used if the total pumping rate is unknown, but the drawdown at the pumping segment is specified. Once the flow distribution is solved, determining the drawdown distribution is straightforward using (90).

TRANSIENT NUMERICAL SOLUTION

The transient numerical solution assumes that the number of segments needed to accurately characterize the well has already been determined from the steady / pseudo-

steady state calculations in the previous section. As the spatial discretization problem has been solved, we now focus on the time discretization problem.

As the convolution of Q with F is required, our solution must use a discrete convolution approach. This is accomplished using superposition. The well is turned on at a certain initial pumping rate and then imaginary wells are used after that time to define changes in pumping rate. Assuming a uniform time step, the solution for drawdown at time step three is

$$\begin{pmatrix} d_1[3] \\ d_2[3] \\ d_3[3] \\ d_4[3] \end{pmatrix} = \begin{pmatrix} F_{1,1}[1] & F_{1,2}[1] & F_{1,3}[1] & F_{1,4}[1] \\ F_{2,1}[1] & F_{2,2}[1] & F_{2,3}[1] & F_{2,4}[1] \\ F_{3,1}[1] & F_{3,2}[1] & F_{3,3}[1] & F_{3,4}[1] \\ F_{4,1}[1] & F_{4,2}[1] & F_{4,3}[1] & F_{4,4}[1] \end{pmatrix} \begin{pmatrix} Q_1[3-2] \\ Q_2[3-2] \\ Q_3[3-2] \\ Q_4[3-2] \end{pmatrix} + \begin{pmatrix} F_{1,1}[2] & F_{1,2}[2] & F_{1,3}[2] & F_{1,4}[2] \\ F_{2,1}[2] & F_{2,2}[2] & F_{2,3}[2] & F_{2,4}[2] \\ F_{3,1}[2] & F_{3,2}[2] & F_{3,3}[2] & F_{3,4}[2] \\ F_{4,1}[2] & F_{4,2}[2] & F_{4,3}[2] & F_{4,4}[2] \end{pmatrix} \begin{pmatrix} Q_1[2-1] \\ Q_2[2-1] \\ Q_3[2-1] \\ Q_4[2-1] \end{pmatrix} + \begin{pmatrix} F_{1,1}[3] & F_{1,2}[3] & F_{1,3}[3] & F_{1,4}[3] \\ F_{2,1}[3] & F_{2,2}[3] & F_{2,3}[3] & F_{2,4}[3] \\ F_{3,1}[3] & F_{3,2}[3] & F_{3,3}[3] & F_{3,4}[3] \\ F_{4,1}[3] & F_{4,2}[3] & F_{4,3}[3] & F_{4,4}[3] \end{pmatrix} \begin{pmatrix} Q_1[1] \\ Q_2[1] \\ Q_3[1] \\ Q_4[1] \end{pmatrix}, \tag{97}$$

where the number in the bracketed $F[\ ]$ terms represent the aquifer response time integral from zero to the bracketed time step. The bracketed $Q[\ ]$ terms represent the pumping rate where $Q_1[1]$ is the pumping rate at segment one, time step one; where $Q_1[2-1]$ is the pumping rate at time two minus time one at segment one. The bracketed $d[3]$ is the drawdown at time step three.

To calculate the drawdown distribution for four segments at time step three, we first determine the drawdown for each segment at time step three from the previous times. To find the impact from previous time steps on the drawdown distribution at time step three, we use the equation

$$\begin{pmatrix} F_{1,1}[2] & F_{1,2}[2] & F_{1,3}[2] & F_{1,4}[2] \\ F_{2,1}[2] & F_{2,2}[2] & F_{2,3}[2] & F_{2,4}[2] \\ F_{3,1}[2] & F_{3,2}[2] & F_{3,3}[2] & F_{3,4}[2] \\ F_{4,1}[2] & F_{4,2}[2] & F_{4,3}[2] & F_{4,4}[2] \end{pmatrix} \begin{pmatrix} Q_1[2-1] \\ Q_2[2-1] \\ Q_3[2-1] \\ Q_4[2-1] \end{pmatrix} + \begin{pmatrix} F_{1,1}[3] & F_{1,2}[3] & F_{1,3}[3] & F_{1,4}[3] \\ F_{2,1}[3] & F_{2,2}[3] & F_{2,3}[3] & F_{2,4}[3] \\ F_{3,1}[3] & F_{3,2}[3] & F_{3,3}[3] & F_{3,4}[3] \\ F_{4,1}[3] & F_{4,2}[3] & F_{4,3}[3] & F_{4,4}[3] \end{pmatrix} \begin{pmatrix} Q_1[1] \\ Q_2[1] \\ Q_3[1] \\ Q_4[1] \end{pmatrix} = \begin{pmatrix} d_1^{previous}[3] \\ d_2^{previous}[3] \\ d_3^{previous}[3] \\ d_4^{previous}[3] \end{pmatrix}, \quad (98)$$

where $d_1^{previous}[3]$ is the impact of previous time steps on the drawdown at time step three. We then rearrange (97) to solve for the new distributions at time three. Assuming the pumping rate constraint is implemented, the solution is

$$\begin{pmatrix} F_{1,1}[1]-F_{2,1}[1] & F_{1,2}[1]-F_{2,2}[1] & F_{1,3}[1]-F_{2,3}[1] & F_{1,4}[1]-F_{2,4}[1] \\ F_{2,1}[1]-F_{3,1}[1] & F_{2,2}[1]-F_{3,2}[1] & F_{2,3}[1]-F_{3,3}[1] & F_{2,4}[1]-F_{3,4}[1] \\ F_{3,1}[1]-F_{4,1}[1] & F_{3,2}[1]-F_{4,2}[1] & F_{3,3}[1]-F_{4,3}[1] & F_{3,4}[1]-F_{4,4}[1] \\ 1 & 1 & 1 & 1 \end{pmatrix} \begin{pmatrix} Q_1[3-2] \\ Q_2[3-2] \\ Q_3[3-2] \\ Q_4[3-2] \end{pmatrix} + \begin{pmatrix} d_1^{previous}[3]-d_2^{previous}[3] \\ d_2^{previous}[3]-d_3^{previous}[3] \\ d_3^{previous}[3]-d_4^{previous}[3] \\ 0 \end{pmatrix} = \begin{pmatrix} d_1[3]-d_2[3] \\ d_2[3]-d_3[3] \\ d_3[3]-d_4[3] \\ 0 \end{pmatrix}. \quad (99)$$

Note that Q_{total} is used for the first iteration as a seed for the remaining solutions. Otherwise the sum of Q differences is zero. Assuming the drawdown constraint is implemented on segment one, the solution is

$$\begin{pmatrix} F_{1,1}[1]-F_{2,1}[1] & F_{1,2}[1]-F_{2,2}[1] & F_{1,3}[1]-F_{2,3}[1] & F_{1,4}[1]-F_{2,4}[1] \\ F_{2,1}[1]-F_{3,1}[1] & F_{2,2}[1]-F_{3,2}[1] & F_{2,3}[1]-F_{3,3}[1] & F_{2,4}[1]-F_{3,4}[1] \\ F_{3,1}[1]-F_{4,1}[1] & F_{3,2}[1]-F_{4,2}[1] & F_{3,3}[1]-F_{4,3}[1] & F_{3,4}[1]-F_{4,4}[1] \\ F_{1,1}[1] & F_{1,2}[1] & F_{1,3}[1] & F_{1,4}[1] \end{pmatrix} \begin{pmatrix} Q_1[3-2] \\ Q_2[3-2] \\ Q_3[3-2] \\ Q_4[3-2] \end{pmatrix}, \quad (100)$$
$$+ \begin{pmatrix} d_1^{previous}[3]-d_2^{previous}[3] \\ d_2^{previous}[3]-d_3^{previous}[3] \\ d_3^{previous}[3]-d_4^{previous}[3] \\ Y \end{pmatrix} = \begin{pmatrix} d_1[3]-d_2[3] \\ d_2[3]-d_3[3] \\ d_3[3]-d_4[3] \\ d_1 \end{pmatrix}$$

where

$$Y = \begin{pmatrix} F_{1,1}[2] & F_{1,2}[2] & F_{1,3}[2] & F_{1,4}[2] \end{pmatrix} \begin{pmatrix} Q_1[2-1] \\ Q_2[2-1] \\ Q_3[2-1] \\ Q_4[2-1] \end{pmatrix} . \quad (101)$$
$$+ \begin{pmatrix} F_{1,1}[3] & F_{1,2}[3] & F_{1,3}[3] & F_{1,4}[3] \end{pmatrix} \begin{pmatrix} Q_1[1] \\ Q_2[1] \\ Q_3[1] \\ Q_4[1] \end{pmatrix}$$

As explained in the *Steady / Psuedo-Steady State Numerical Solution* section, to solve this matrix equation, one may use a variety of methods ranging from iterative to linear algebraic procedures. We choose MATLAB's fsolve() function which finds the root of a system of nonlinear equations. For an initial condition, we assume uniform flux.

HEAD LOSS

There are three major components of head loss to consider when modeling the head in a well: aquifer head loss, skin head loss, and intra-wellbore head loss. The drawdown inside a well is the sum of these three effects and has been defined as *d* =

$FQ+BQ+ h_f(Q) + h_a(Q)$, where F is the aquifer effect (derived in Chapter III), B is the skin effect, h_f is the fiction effect, and h_a is the kinetic effect (Konikow et al., 2009; Roscoe Moss Company, 1990) .

Kinetic (Acceleration / Velocity)

The kinetic (acceleration, velocity) component of head loss is commonly assumed insignificant; however, recent work has shown otherwise Penmatcha and Aziz (1999). To begin derivation of the acceleration head loss, we use the momentum equation $p = mv$ where m is mass and p is momentum. We then define the change in momentum over time is a force

$$F_a = \frac{\Delta p}{\Delta t} = (\rho A v_2) v_2 - (\rho A v_1) v_1 = \rho A\left[v_2^2 - v_1^2\right], \tag{102}$$

where F_a is the force of acceleration [MLT^{-2}], A is pipe cross-sectional area [L^2], v_1 is the velocity at the beginning of the pipe [LT^{-1}], and v_2 is the velocity at the end of the pipe [LT^{-1}]. We then note that we can account for accelerational forces within the wellbore by taking $v_1 = q_a/A$ and $v_2 = (q_i + q_a)/A$ where q_a is the *axial* flow in the wellbore and q_i is the flow coming *in* through the wellbore screen [L^3T^{-1}].

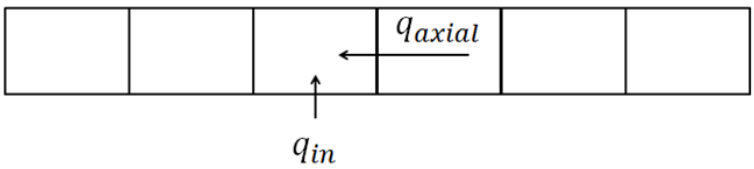

Figure 69. Flow components within a wellbore used to determine kinetic head loss.

We then rewrite the acceleration equation using flow within the wellbore as

$$F_a = \rho A\left[\left(\frac{q_a + q_i}{A}\right)^2 - \left(\frac{q_a}{A}\right)^2\right] = \frac{\rho}{A}\left[q_i^2 + 2q_i q_a\right] . \tag{103}$$

We then convert this accelerational force to pressure as $\frac{F_a}{A} = \frac{\rho}{A^2}\left[q_i^2 + 2q_i q_a\right]$, and then convert pressure to head

$$h_a = \frac{\left[q_i^2 + 2q_a q_i\right]}{A^2 g}, \tag{104}$$

where h_a is the head loss (drawdown) caused by kinetic effects [L].

Friction

Traditionally, head loss terms within wells have been ignored or are only empirically accounted for. Recent work by Ouyang et al. (1998) presents new friction factors to be used accounting for wellbore inflow/outflow; however, the use of these new correlations is not implemented in our model.

The first step in defining the friction effect is to calculate the Reynolds Number,

$$\mathrm{Re} = \frac{v\rho D}{\mu} , \tag{105}$$

where v is average velocity [LT^{-1}], ρ is density [ML^{-3}], D is pipe diameter [L], and μ is viscosity [$MT^{-1}L^{-1}$] (Munson et al., 2012). The head loss (drawdown) due to friction is then calculated using the Darcy-Weisbach head loss equation

$$h_f = f\,\frac{Lv^2}{2Dg}\,\mathrm{sign}\left(\mathrm{Re}\right), \tag{106}$$

where h_f is head loss [L], f is the friction factor [dimensionless], L is the pipe length [L], g is gravity [LT^{-2}] (Munson et al., 2012). Note that we put the sign of the Reynolds number in (106) to ensure that directionality of flow is correctly modeled. It is conceivable that during the iterative procedure to solve for flow distribution that flow could go away from the pumping segment and thus it would be appropriate to calculate the change in head accordingly. Because all other directionality terms are squared or have an absolute value sign, it was necessary to capture this directionality in (106).

The friction factor calculation depends on the Reynolds Number. If the Reynolds Number is less than some user defined critical Reynolds Number the friction factor is

$$f = \frac{64}{|\mathrm{Re}|}. \tag{107}$$

If the Reynolds Number is greater than the same user defined critical Reynolds Number as defined above, the friction factor is

$$\frac{1}{\sqrt{f}} = -2.0\log_{10}\left[\frac{\varepsilon/D}{3.7} + \frac{2.51}{|\mathrm{Re}|\sqrt{f}}\right], \tag{108}$$

where ε is the pipe surface roughness [L] (Munson et al., 2012). The friction factor in equation (108) must be solved numerically via a root finding algorithm; in our model we use MATLAB's fzero() function.

Wellbore Skin Effects

The wellbore skin is defined as a zone of different permeability around the borehole compared to the aquifer. This zone is usually of lower permeability than the aquifer typically caused by the infiltration of drilling mud. However, skin can also be a

zone of enhanced permeability from activities such as fracturing. Skin effects may be calculated using either a finite thickness skin or the infinitesimally thin skin methods.

Finite thickness skin is a more rigorous representation of skin as it accounts for the radial effects of flow. Using the definition of skin from Konikow et al. (2009), skin may be calculated as

$$Skin = \left(\frac{K}{K_s} - 1 \right) \ln \left[\frac{r_s}{r_w} \right], \tag{109}$$

where r_s is the radius of the skin ($r_s = r_w + s_t$) [L], r_w is the radius of the well [L], s_t is the thickness of the skin [L], K is the isotropic aquifer hydraulic conductivity perpendicular to the well [LT^{-1}], and K_s is the skin hydraulic conductivity [LT^{-1}].

Skin was originally derived for vertical wells. Treatment of aquifer anisotropy was achieved by taking the square root of the two horizontal hydraulic conductivities, $K = (K_x K_y)^{-1/2}$. A logical approach to make skin effect calculation accurate for directional wells is to find the isotropic hydraulic conductivity perpendicular to the well. If the well is constrained to one axis, the solution is simple. However, if the well is not constrained to one axis, then it is unclear how to proceed. Future work is needed to solve this issue. For our model, if the well is not constrained to one axis we simply take $K = (K_x K_y K_z)^{-1/3}$. Skin is related back to the coefficient B by Halford and Hanson (2002) as

$$B = \frac{Skin}{2\pi LK}. \tag{110}$$

Park and Zhan (2002) defined the relationship between infinitesimally thin skin and finite thickness skin. This derivation was completed by taking the limit as skin thickness goes to zero

$$Skin = \frac{K}{r_w C_s}, \tag{111}$$

where C_s is wellbore skin conductance defined as K_s / s_t .

Skin is easily added to our model as an addition along the diagonal of our matrix of aquifer solutions. Skin may be added to our model in this way for either steady or transient calculations. The addition of skin to our aquifer solution matrix is

$$\begin{pmatrix} (F_{1,1}+B_1) & F_{1,2} & F_{1,3} & F_{1,4} \\ F_{2,1} & (F_{2,2}+B_2) & F_{2,3} & F_{2,4} \\ F_{3,1} & F_{3,2} & (F_{3,3}+B_3) & F_{3,4} \\ F_{4,1} & F_{4,2} & F_{4,3} & (F_{4,4}+B_4) \end{pmatrix} \begin{pmatrix} Q_1 \\ Q_2 \\ Q_3 \\ Q_4 \end{pmatrix} = \begin{pmatrix} d_1 \\ d_2 \\ d_3 \\ d_4 \end{pmatrix}. \tag{112}$$

Aquifer Loss

Aquifer losses have been derived in Chapter III. However, it is important to note the limitations of our assumptions of Darcy flow in the aquifer. To aid in the interpretation of output from our model, we add critical radius calculations. The critical radius is the radial point from the wellbore at which flow no longer follows Darcy's law. If the critical radius is inside the wellbore radius, then our model assumptions are upheld. If not, then the drawdown distribution is probably different from the one calculated by our model as turbulent aquifer flow is assumed.

It should be noted that turbulent aquifer flow is rare, and even if it does occur it will likely extend only a very short distance into the aquifer from the wellbore. Despite its rare occurrence, in special cases turbulent groundwater flow may be important. Turbulent aquifer flow will likely reduce flux and increase drawdown along segments

where the critical radius has exceeded the wellbore radius. Assuming an aquifer critical Reynolds number of thirty, the critical radius in SI units is calculated as

$$r_c = \frac{(Q/L)\,dia.}{\theta_e} 1.90\text{E}5\,, \tag{113}$$

where r_c is the critical radius in meters [L], *dia.* is the mean grain diameter is meters [L], and θ_e is effective porosity (Roscoe Moss Company, 1990).

MATLAB IMPLEMENTATION

Model input parameters are taken from a main script and then passed to the angleWell() function (Figure 70). This function calculates the Poisson Re-Summation switch times for each of the three principal directions. These times are useful for defining limits of time integration in both steady state and transient settings. As each of these sub-intervals define a relatively smooth function, numeric integration is significantly faster because of such subdivision. The model may determine the upper time limit (model end time) of the last time integration less than or equal to a user defined threshold; or the user may specify an exact time to integrate.

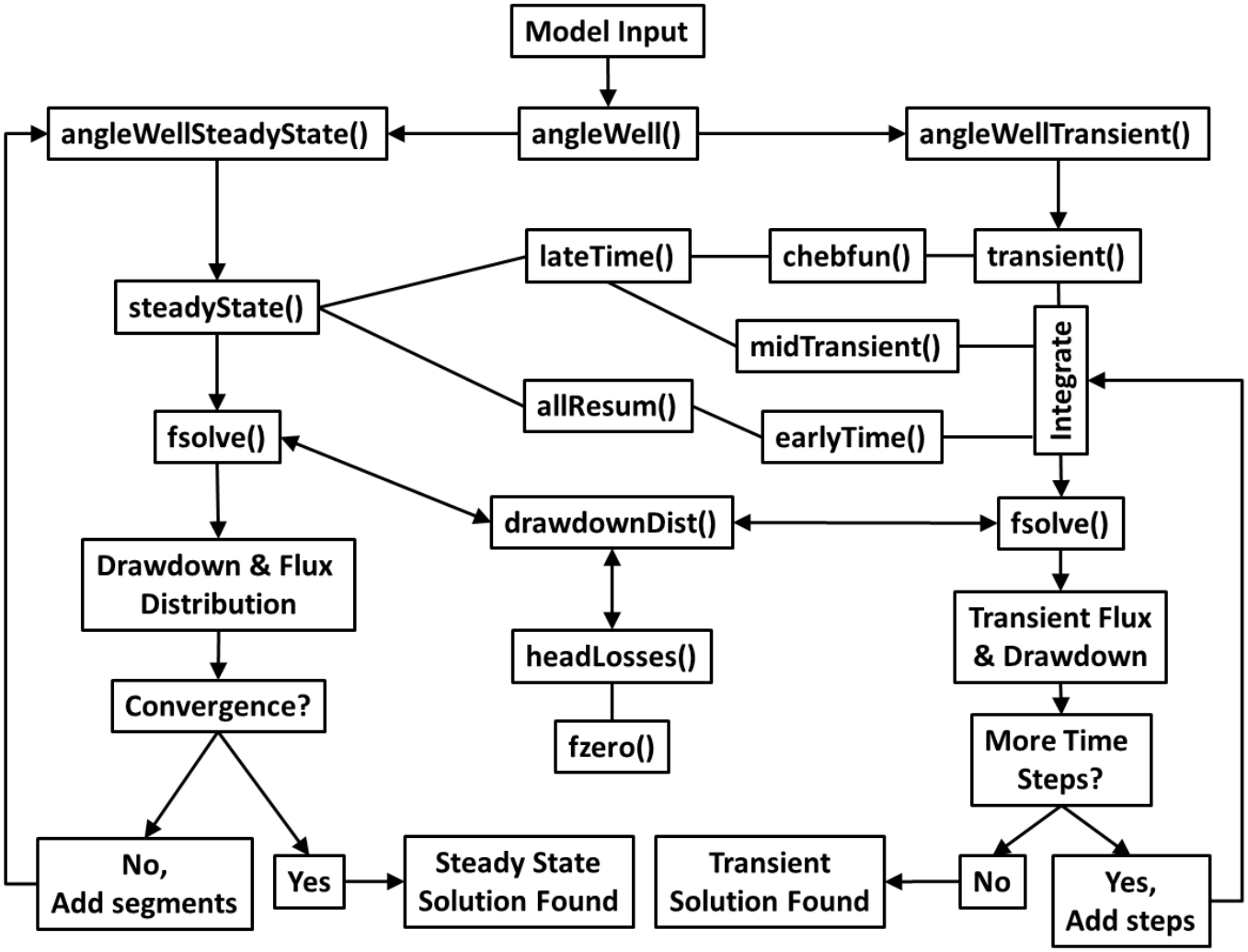

Figure 70. Function map of model MATLAB code.

The time when steady state / pseudo-steady state is reached defines an upper bound for numeric integrations. This calculation is very similar to work already completed in the *Early Time Three Term Convergence* section. To determine the time of steady state, we want only the zero iteration term to be significant. The calculation of steady state time is based on the max Poisson Re-Summation time multiplied by 100, which is the inverse of the *Early Time Three Term Convergence* section. This is the point at which additional time yields a function that is essentially zero for every non-zero iteration. So, taking the late time non-trig components of the aquifer function, we find that substituting

$$\exp\left[-\tau\frac{n^2\pi^2k_x}{a^2S_s}\right] \text{ with } \tau=\frac{100S_sa^2}{\pi k_x} \quad , \tag{114}$$

yields

$$\exp\left[-\frac{100S_sa^2}{\pi k_x}\frac{n^2\pi^2k_x}{a^2S_s}\right]=\exp\left[-100n^2\pi\right]. \tag{115}$$

Because the late time series are from one to infinity, the first term at $n = 1$ shows that non-zero iterations are no longer required as the function evaluates to essentially zero $\exp\left[-100\pi\right]=3.65\text{E}-137$.

Thus, only the series at $n = 0$ impacts the calculation. Recalling the late time solutions, only the no flux condition evaluates to one at $n = 0$; all the other BVP solutions evaluate to zero because of the sine terms. Therefore if all sides of the box are no flux, then the temporal derivative at late time equals one which indicates linear

drawdown. If any constant head condition is implemented, the evaluation becomes essentially zero times one and therefore a true steady state is achieved $3.65\text{E}-137\times 1\approx 0$.

If the box is infinite in all directions, then no steady or psuedo-steady state will be reached. If the box is infinite in all directions except one, then steady/psuedo-steady state will be reached at some time possibly approaching infinity. In these cases, we let the user define an upper bound of the time integration.

Steady State

Once integration limits have been defined from the angleWell() function, if a steady state solution is desired the angleWellSteadyState() function is called. This function calculates segment distribution either linearly or non-linearly. The sample points (center of each well segment) are also calculated. The inputs are then passed to the steadyState() function. In this function, the wellbore source / sink and sample points are parameterized as defined in previous derivation sections. These arguments are then passed to the allResum() function and late() function.

The allResum() function calculates the analytical time integration from zero to the earliest Poisson Re-Sum time divided by 100; which has been previously proven to converge in 3^3 iterations. The allResum() function calculates the spatial numeric integration of the point source / sink along the wellbore, and the spatial integration of the sample point around the radius of the wellbore.

Upon calculation of the very early time integration, numeric integration of the lateTime() function occurs. This second numeric time integration begins where the

allResum() function stopped. The lateTime() function has the time derivate, point source / sink equations for each boundary condition. Arguments passed to lateTime() are screened using if statements, where the result depends upon input boundary conditions.

With the aquifer response calculated for each segment, skin is added. Then the MATLAB fsolve() function is invoked to solve the matrix of solutions. Within each iteration of the fsolve() function, the head losses are calculated between segments using the headLosses() function. Upon convergence of fsolve(), the results are plotted. Segments are then added and angleWellSteadyState() is called again. The cycle repeats until the spatial discretization has been solved, which is defined as convergence at the pumping segment.

Transient

Once time integration subdivisions have been defined from the angleWell() function, if a transient solution is desired the angleWellTransient() function is called. This function calculates segment distribution either linearly or non-linearly. The sample points (center of a well segment) are also calculated. Early time integrations are calculated by the earlyTime() function which calls the allResum() function. To improve computational speed, later transient calculations implement the Chebfun system of functions developed at the University of Oxford (Platte and Trefethen, 2010).

The chebfun() package finds an approximation a passed function based on Chebyshev series and interpolants. The power of chebfun() is that it approximates a function over the domain of interest which thus facilitates easy manipulation. Because we are interested in subdividing the time interval into many time steps and may want to

recalculate with additional time steps, it is significantly faster to find a chebfun() representation once and then integrate it several times.

While it may take one second to find a single integration using MATLAB, chebfun() can define the entire function in ten seconds. With the entire function defined using chebfun(), one can implement integration between any two points in fractions of a second. For example, if 100 time steps were calculated using MATLAB's integral() function it would take about 100 seconds. However, the same calculation would take chebfun() about fifteen seconds. If the user wanted to add time steps, additional computational effort is insignificant because the function is already defined by chebfun(). In contrast, MATLAB numeric integration would have to start with nothing and therefore reintegrate everything. For the readers information, we attempted to use chebfun() for the spatial components as well, however the nature of the spatial components inhibited chebfun() from finding an approximation.

While chebfun() is useful, it is slow at early times when the aquifer response function is not very smooth. It is for these earliest times, typically less than one second, that analytical integration is necessary. These early integrations are performed by either the earlyTime() or midTransient() functions depending on the Poisson Re-Sum switch times; keeping the validity of the 3^3 iterations convergence of allResum(). The user defines when chebfun() representation begins. Upon integration at each time step from zero to the end of the time step, fsolve() is used to solve the system of equations at each time step. As in the steady state model, head losses are calculated at each iteration using headLosses().

Because transient calculation convergence is not easily determined, more emphasis is placed on user interpretation and manipulation. At the end of each transient calculation the user is displayed several plots depicting the transient behavior. The user then has the option to change the number of time steps. For transient calculations, the user determines when the solution has been approximated to their liking.

Intra-Wellbore Head Loss

When calculating the intra-wellbore head losses, we order the calculations so as to calculate the most conservative results; maximum drawdown and minimum pumping rate (Figure 71). This is done by shifting the flow towards the end of the well furthest from the pump, thereby creating the longest possible path for flows. It is important to note that MODFLOW-CFP calculates friction loss by shifting in the other direction. If segments are added until convergence, it should not matter which convention is used; however, it is good modeling practice to use a conservative approach.

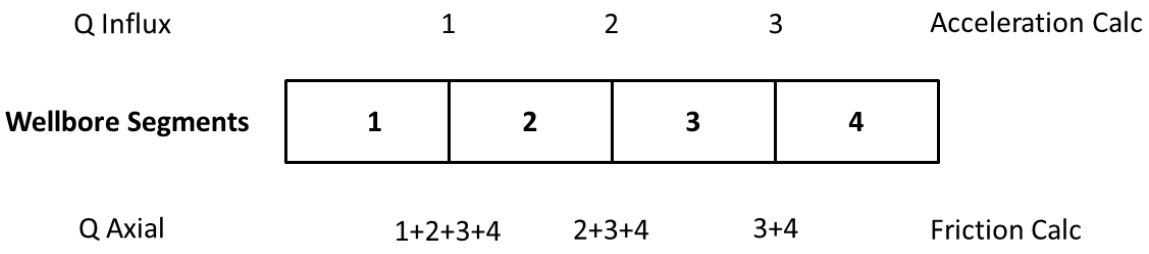

Figure 71. Numerical implementation of head loss between segments.

MATLAB Tips and Tricks

One of the most important aspects of MALTAB is vectorization, especially the vectorization of functions that need to be numerically integrated. In terms of numerical integration, MATLAB has made significant improvements in its algorithms since the quad() functions. The integral(), integral2(), and integral3() functions are very fast and reliable. While previous MATLAB numeric integration techniques relied on nesting integral functions to calculate multiple integrals, the new MATLAB integral2() and integral3() functions have the option to use a 'tiled' method which is significantly faster than the 'iterated' method.

However, sometimes the tiled method does find a solution and the integration terminates with a warning. While the integration may fail using the tiled approach, it almost always will converge with the iterated approach. A simple fix to this problem is to change the warning to an error. With an error defined, it can now be caught in a try catch framework (Figure 72).

```
try
    warning('error', 'MATLAB:integral2:maxFunEvalsPass')
    warning('error', 'MATLAB:integral2:maxFunEvalsFail')
    integral2('tiled')
catch
    warning('on', 'MATLAB:integral2:maxFunEvalsPass')
    warning('on', 'MATLAB:integral2:maxFunEvalsFail')
    integral2('iterated')
end
```

Figure 72. Implementation of the try-catch framework during numeric tiled integration.

One of the easiest ways to improve the speed of MATLAB calculations is to use the parfor loop wherever possible. The parfor loop stands for a parallel for loop. If calculations are independent from loop iteration to loop iteration, then use of parfor will distribute the computational workload across all available central processing units (CPU); up to twelve processors. As most computers have at least two processors, parfor will typically cut computation time in half. Many computers have eight processors (four real processors, each with an imaginary partition). In these cases code execution time could be cut by a factor of eight.

Another tempting method to improve speed is to use the graphics processing unit (GPU). Use of the graphics card to calculate parallel tasks is called GPU computing. MATLAB GPU computing is easy to implement, however it is slow for our model's applications. Because of data type conversions from double to single in addition to the lack of special functions, GPU computing is significantly slower for our model than the normal CPU processors. GPU computing is best for large matrices with simple functions and the single data type.

CHAPTER V

SIMPLE DRILLING MODELS

INTRODUCTION

There has been very limited discussion in the groundwater literature on how to calculate forces when drilling a horizontal well. These calculations are necessary to select the optimal rig size and strength of pipe. Such calculations give insight into the limitations of wellbore construction. While calculation methods for forces were developed in the early days to the petroleum horizontal well revolution, this literature is mostly forgotten / unknown to the groundwater community today.

Optimal slant rig entry angles have not been discussed in either the petroleum or groundwater industries to this author's knowledge. A slant rig entry angle that is nearly horizontal enables the wellbore to reach the horizontal plane at much shallower depths. The calculation of the optimal slant rig entry angle is crucial to understanding the type of slant rig necessary to reach a given shallow target depth. Derivations of the optimal entry angle will likely benefit both groundwater production and shallow petroleum production.

Formulas presented will include the following conventions. Tension will be positive and compression will be negative. This is the engineering convention, but opposite of the geology convention. Vertical will be 90°; horizontal will be zero degrees. This is opposite of the petroleum drilling convention, but the same as geologic dip and utility directional drillers' convention (Figure 73).

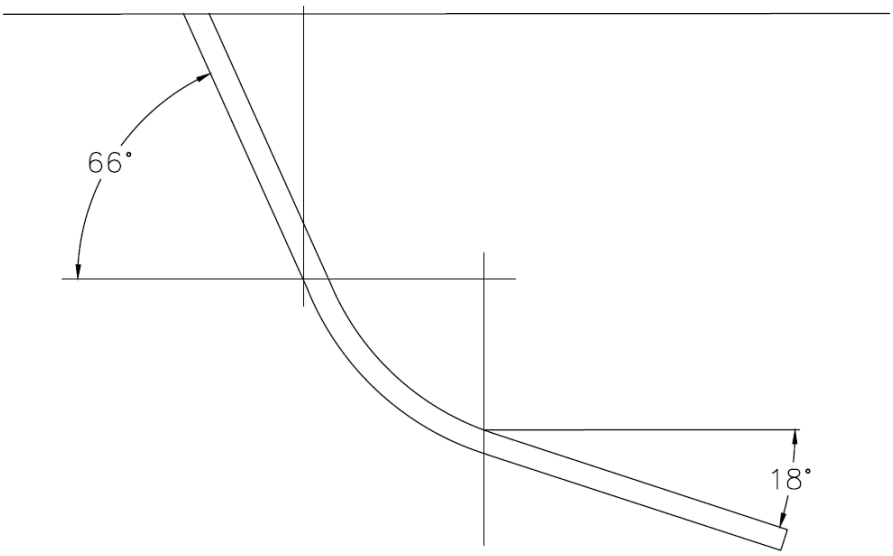

Figure 73. Angle convention.

WELL CONSTRUCTION FORCE MODEL

Models of drilling / casing forces developed here are only intended as a first approximation of the forces that will be experienced. Without additional calculations, this model's accuracy is thought to be 75%. This accuracy suggestion is for radii of curvature following the industry rule of thumb (one hundred feet per inch of diameter of pipe) and casing diameters of less than 16 inches. This theoretical accuracy is not appropriate for rigorous planning of an actual drilling operation. However, these simplified equations (and associated computer program) will allow for investigators to easily screen potential projects and understand the interplay of forces. If these models show a project to benefit from horizontal well technology, then a more thorough investigation may be pursued.

The calculation of drilling forces using analytical models is relatively straight forward. Two papers from twenty years ago outline the procedures shown here and should be referenced for further inquiry (Greenip Jr, 1989; Wu and Juvkam-Wold, 1991). There are three scenarios to consider when completing calculations. The pipe will either be running into the hole (as in drilling), pulling out of the hole (tripping out) or it will be neutral in the hole. Calculations of the lateral and upper sections of the wellbore were outlined in Greenip Jr (1989). Build up section calculations were derived in Wu and Juvkam-Wold (1991).

There are three sections of the wellbore that forces will need to be calculated for. The upper section begins at the earth's surface and extends to the kickoff point. The build (curve) section extends from the kickoff point to the end of build section. And finally, the lateral section extends from the end of build section to the end of the wellbore (Figure 74). Steps to calculate the forces begin with the lateral section and then move up the wellbore to the surface.

Equations presented solve for each section so as to permit a piecewise understanding of forces. If the total forces on any one section are desired, one will need to complete the necessary additions from down hole to up hole. For example, if one wants to know the torque required at the surface to rotate the lateral section, then addition of torque requirements from the lateral section, curve section, and upper section is necessary. If the user wants to know the amount of rig pullback needed to pull out the entire string, then the user must add the force at the kickoff point (which depends upon the lateral section) and the upper section.

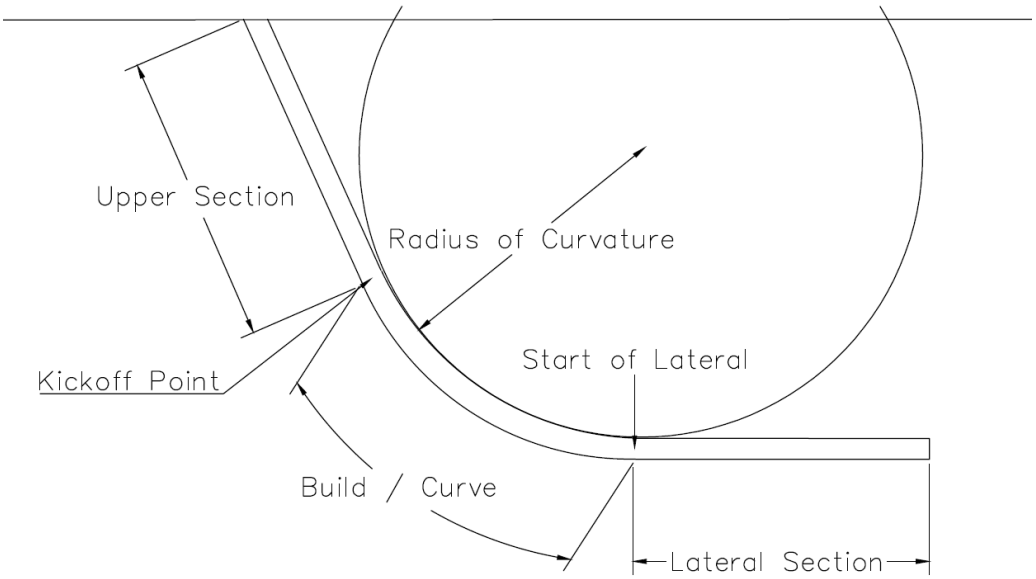

Figure 74. Sections of a directional well.

Lateral Section Forces

We begin with the lateral section. There are two components to consider when calculating axial forces in this section and the other sections: force cause by pipe weight and force cause by drag. Before we begin we need to clarify the difference between nominal pipe weight and effective weight. Nominal weight is the weight calculated at the earth's surface. When a pipe is placed downhole, buoyancy effects must be considered. The relation between nominal weight and effective weight is defined as:

$$W_e = W \times BF \,, \tag{116}$$

where W_e is the effective weight per unit length used for downhole calculation [MT^{-2}], W is the nominal weight [MT^{-2}], and BF is the buoyancy factor. The buoyancy factor depends on the specific weight of the drilling mud compared to the specific weight of the steel pipe. The buoyancy factor is

$$BF = \frac{SW_{pipe} - SW_{mud}}{SW_{pipe}}, \tag{117}$$

where SW_{pipe} is the specific weight of the steel pipe [$ML^{-2}T^{-1}$], and SW_{mud} is the specific weight of the drilling mud [$ML^{-2}T^{-1}$]. As a final note before calculation begins, in field operations drillers refer to angle build rate instead of radius of curvature. The relationship between build angle and radius of curvature is

$$\frac{\Delta\angle}{\Delta C} = \frac{360}{2\pi R}, \tag{118}$$

where $\Delta\angle$ is the build angle [degrees], ΔC is the change in arc length [L], R is the radius of curvature, and $\Delta\angle / \Delta C$ is the build rate.

Beginning calculation, the force required to run-in the lateral section is

$$F_{LI} = L\left(W_e \sin\left[\theta_L\right] - \mu W_e \cos\left[\theta_L\right]\right), \tag{119}$$

where F_{LI} is the force required to run the lateral section in [MLT^{-1}], L is the length of the lateral section [L] μ is the coefficient of friction, and θ_L is the angle of the lateral section (horizontal is zero). The force required to pull the lateral section out is

$$F_{LO} = L\left(W_e \sin\left[\theta_L\right] + \mu W_e \cos\left[\theta_L\right]\right), \tag{120}$$

where F_{LO} is the force required to pull the lateral section out [MLT^{-1}]. The force on the lateral section at a neutral state is

$$F_{LN} = LW_e \sin\left[\theta_L\right], \tag{121}$$

where F_{LN} is the force on the lateral section at a neutral state [MLT^{-1}]. Finally, the torque required to rotate the lateral section is

$$M_L = Lr_w \mu W_e \cos\left[\theta_L\right], \tag{122}$$

where M_L is the torque required to rotate the lateral section [ML^2T^{-1}] , and r_w is the outside radius of the pipe [L].

Buildup Section Forces

The buildup section forces are more complicated to calculate compared to the lateral and upper sections. There are two methods that may be used to model buildup forces, a soft string model or a stiff string model. A soft string model assumes the drill pipe / casing are so flexible that there is no additional normal force in the curve due to pipe bending. A soft string model only accounts for gravity and friction effects. If the string is flexible and the build rate is low (less than 5°/100 feet), the soft string model does not introduce much error into the calculation (Dupriest, 2013). However, if the build rate is high and/or the pipe is stiff (such as large diameter casing), then the true drag will be significantly higher than the soft string model predicts.

Use of a soft string model is usually not a major issue for petroleum drillers because the vertical and horizontal sections of these wells are so long that the buildup friction caused by the stiff string is minor in comparison. However for a shallow horizontal well with a large diameter casing, the error of the soft string model may become significant. Despite the limitations of the soft string model, it is significantly easier to model mathematically and should yield a decent first approximation of expected forces. Excellent work by Wu and Juvkam-Wold (1991) derived and solved the differential equation describing axial load in the build section for the soft string model. For a complete derivation, review their work as only the solution procedure is presented here.

Contact / normal force is a function of the angle along the build section. For pulling the pipe out of the hole or running pipe in, there are three cases of contact force that must be considered. Either the contact force is on the upside of the wellbore over the entire build section, on the downside over the entire section, or there is a transition of normal force within the build section between the downside and upside.

Running-In Forces

We begin with the calculation of force when running pipe into the borehole. First we must determine if a transition occurs in the normal force direction through the buildup section. To do this we calculate the normal force at the start and end of the build section as

$$
\begin{aligned}
N\left(\theta_L\right) &= -W_e \cos\left[\theta_L\right] + \frac{F_{LI}}{R} \\
N\left(\theta_U\right) &= -W_e \cos\left[\theta_U\right] + \frac{1}{R}\Big(\left(F_{LI} + A\sin\left[\theta_L\right] - B\cos\left[\theta_L\right]\right)\exp\left[\mu\left(\theta_U - \theta_L\right)\right] \\
&\qquad -A\sin\left[\theta_U\right] + B\cos\left[\theta_U\right]\Big) \qquad , \quad (123) \\
A &= \frac{2\mu}{1+\mu^2} W_e R \\
B &= -\left(\frac{1-\mu^2}{1+\mu^2} W_e R\right)
\end{aligned}
$$

where N is the normal force [MLT^{-1}], θ_L is the angle of the lateral section, and θ_U is the angle of the upper section. If the normal force at the beginning of the lateral section and the kickoff point are both negative (θ_L & θ_U < 0), then the axial force at the kickoff point to run the pipe in is

$$F_{kopI} = \left(F_{LI} + A\sin\left[\theta_L\right] - B\cos\left[\theta_L\right]\right)\exp\left[\mu\left(\theta_U - \theta_L\right)\right] - A\sin\left[\theta_U\right] + B\cos\left[\theta_U\right],$$

(124)

where F_{kopI} is the force required at the kickoff point to run the pipe in in [MLT^{-1}]. If the normal force at the beginning of the lateral section and the kickoff point are both positive (θ_L & $\theta_U > 0$), then the axial force at the kickoff point to run the pipe in is

$$F_{kopI} = \left(F_{LI} - A\sin\left[\theta_L\right] - B\cos\left[\theta_L\right]\right)\exp\left[-\mu\left(\theta_U - \theta_L\right)\right] + A\sin\left[\theta_U\right] + B\cos\left[\theta_U\right].$$

(125)

If the normal force at the beginning of the lateral section and the kickoff point are of different signs, then there is a transition point that must be located. To do this, use a root finding algorithm and solve for the transition point α_1

$$0 = -W_e\cos\left[\alpha\right] + \frac{1}{R}\left(\left(F_{LI} + A\sin\left[\theta_L\right] - B\cos\left[\theta_L\right]\right)\exp\left[\mu\left(\alpha - \theta_L\right)\right] - A\sin\left[\alpha\right] + B\cos\left[\alpha\right]\right), \quad (126)$$

where α is an angle between θ_L & θ_U and α_1 is the angle solving the above equation. Once α_1 has been found, the axial force at the kickoff point required to run the pipe in is

$$F_{kopI} = \left\{\left(F_{LI} + A\sin\left[\theta_L\right] - B\cos\left[\theta_L\right]\right)\exp\left[\mu\left(\alpha_1 - \theta_L\right)\right] - 2A\sin\left[\alpha_1\right]\right\} \exp\left[-\mu\left(\theta_U - \alpha_1\right)\right] + A\sin\left[\theta_U\right] + B\cos\left[\theta_U\right]. \quad (127)$$

Pulling Out Forces

Next we calculate the force when pulling pipe out of the borehole. First we must determine if a transition occurs in the normal force direction through the buildup section. To do this we calculate the normal force at the start and end of the build section as

$$N(\theta_L) = W_e \cos[\theta_L] - \frac{F_{LO}}{R}$$
$$N(\theta_U) = W_e \cos[\theta_U] - \frac{1}{R}\Big(\big(F_{LO} - A\sin[\theta_L] - B\cos[\theta_L]\big)\exp\big[-\mu(\theta_U - \theta_L)\big] + A\sin[\theta_U] + B\cos[\theta_U]\Big). \quad (128)$$

If the normal force at the beginning of the lateral section and the kickoff point are both positive (θ_L & $\theta_U > 0$), then the axial force required at the kickoff point to pull the pipe out is

$$F_{kopO} = \big(F_{LO} - A\sin[\theta_L] - B\cos[\theta_L]\big)\exp\big[-\mu(\theta_U - \theta_L)\big] + A\sin[\theta_U] + B\cos[\theta_U], \quad (129)$$

where F_{kopO} is the force required at the kickoff point to pull the pipe out [MLT^{-1}]. If the normal force at the beginning of the lateral section and the kickoff point are both negative (θ_L & $\theta_U < 0$), then the axial force required at the kickoff point to pull the pipe out is

$$F_{kopO} = \big(F_{LO} + A\sin[\theta_L] - B\cos[\theta_L]\big)\exp\big[\mu(\theta_U - \theta_L)\big] - A\sin[\theta_U] + B\cos[\theta_U]. \quad (130)$$

If the normal force at the beginning of the lateral section and the kickoff point are of different signs, then there is a transition point that must be located. To do this, use a root finding algorithm and solve for the transition point α_1:

$$0 = W_e \cos[\alpha] - \frac{1}{R}\Big(\big(F_{LO} - A\sin[\theta_L] - B\cos[\theta_L]\big)\exp\big[-\mu(\alpha - \theta_L)\big] + A\sin[\alpha] + B\cos[\alpha]\Big), \quad (131)$$

Once α_1 has been found, the axial force at the kickoff point required to pull the pipe out is

$$F_{kopO} = \left\{\left(F_{LO} - A\sin\left[\theta_L\right] - B\cos\left[\theta_L\right]\right)\exp\left[-\mu\left(\alpha_1 - \theta_L\right)\right] + 2A\sin\left[\alpha_1\right]\right\} \\ \exp\left[\mu\left(\theta_U - \alpha_1\right)\right] - A\sin\left[\theta_U\right] + B\cos\left[\theta_U\right] \quad . \tag{132}$$

Neutral Forces

The axial force when the pipe is in a neutral state is

$$F_{kopN} = F_{LN} - W_e R\left(\cos\left[\theta_U\right] - \cos\left[\theta_L\right]\right), \tag{133}$$

where F_{kopN} is the fore at the kickoff point when the pipe is in a neutral state [MLT^{-1}].

Torque

To calculate the torque required to rotate only the buildup section, first calculate the normal force at each end

$$N\left(\theta_L\right) = W_e\cos\left[\theta_L\right] - F_{LN}/R \\ N\left(\theta_U\right) = 2W_e\cos\left[\theta_U\right] - W_e\cos\left[\theta_L\right] - F_{LN}/R \quad . \tag{134}$$

If the normal force at the beginning of the lateral section and the kickoff point are both positive (θ_L & $\theta_U > 0$), then the torque required to rotate only the buildup section is

$$M_B = R\, r_w \int_{\theta_L}^{\theta_U} \mu\left(2W_e\cos\left[\alpha\right] - W_e\cos\left[\theta_L\right] - F_{LN}/R\right) \mathrm{d}\alpha\,, \tag{135}$$

where M_B is the torque required to rotate only the buildup section [ML^2T^{-1}]. If the normal force at the beginning of the lateral section and the kickoff point are both negative (θ_L & $\theta_U < 0$), then the torque required to rotate only the lateral section is

$$M_B = R\, r_w \int_{\theta_L}^{\theta_U} -\mu\left(2W_e\cos\left[\alpha\right] - W_e\cos\left[\theta_L\right] - F_{LN}/R\right) \mathrm{d}\alpha\,. \tag{136}$$

If the normal force at the beginning of the lateral section and the kickoff point are of different signs, then there is a transition point that must be located at

$$\alpha_1 = \cos^{-1}\left(\frac{W_e \cos\left[\theta_L\right] + F_{LN}/R}{2W_e}\right). \tag{137}$$

Once α_1 has been found, the torque at the kickoff point required to rotate the pipe is

$$M_B = R\, r_w \left(\int_{\theta_L}^{\alpha_1} \mu\left(2W_e \cos\left[\alpha\right] - W_e \cos\left[\theta_L\right] - F_{LN}/R\right) + \int_{\alpha_1}^{\theta_U} -\mu\left(2W_e \cos\left[\alpha\right] - W_e \cos\left[\theta_L\right] - F_{LN}/R\right) \right) \mathrm{d}\alpha \,. \tag{138}$$

Upper Section Forces

Calculation of forces in the upper section is very similar to that of the lower section. The force required to run-in the upper section is

$$F_{UI} = L\left(W_e \sin\left[\theta_U\right] - \mu W_e \cos\left[\theta_U\right]\right), \tag{139}$$

where F_{UI} is the axial force required to run in only the upper section [MLT^{-1}], and θ_U is the angle of the upper section where horizontal is zero. The force required to pull the upper section out is

$$F_{UO} = L\left(W_e \sin\left[\theta_U\right] + \mu W_e \cos\left[\theta_U\right]\right), \tag{140}$$

where F_{UO} is the axial force required to pull out only the upper section pipe. The axial force of only the upper section at a neutral state is

$$F_{UN} = L W_e \sin\left[\theta_U\right], \tag{141}$$

where F_{UN} is the axial force of only the upper section at neutral state [MLT^{-1}]. The torque required to rotate the upper section is

$$M_U = L r_w \mu W_e \cos\left[\theta_U\right], \tag{142}$$

where M_U is the torque required to rotate only the upper section [ML^2T^{-1}].

Bending Force

The pipe bends in the build section, so therefore bending forces must be calculated (Roscoe Moss Company, 1990). There is compression on the inside of the radius of curvature and tension on the outside of the radius of curvature. Therefore the bending force calculation results in a +/- to account for each of these sides.

For the readers benefit, the bending force calculated here would need to be incorporated into the normal force calculation in the buildup section to create a stiff string model. This is because the bending force not only impacts the body of the pipe, but it also increases normal force and hence frictional drag effects.

Bending force impacts only the steel pipe even in our soft string model, and thus needs to be accounted for. The bending fore is

$$\pm S_f = \frac{E r_w}{R}\left(r_w^2 - r_I^2\right)\pi, \tag{143}$$

where S_f is the bending force [MLT^{-1}], E isYoung's Modulus [$ML^{-1}T^{-2}$], and r_I is the inside radius of the pipe [L].

Drill Rig Selection

The forces calculated in the previous sections will mostly determine what size of drilling rig is necessary to complete the desired wellbore. Other forces that will need to be added to the calculation are the weight of the bottom hole assembly, the compression necessary to drill the rock, and some overpull capacity to get stuck pipe out. These

additional calculations are site dependent and will require experienced drilling engineers for exact judgments.

A directional bottom hole assembly that could be used for horizontal water supply wells will be short (90-120 ft) and will weigh about 20,000-25,000 lbs (Dupriest, 2013). Assuming these are soft shallow formations, the weight on bit (WOB) required will be 5,000-10,000 lbs (Dupriest, 2013). As rate of penetration goes up linearly with WOB, normally increased weight would be desired. However, there are also limitations of rig mud handling capacity, so 5,000-10,000 lbs was assumed. It is thought that a 12.25 inch hole with 5,000 lbs WOB using a small rig would have an instantaneous drill rate of 300 feet per hour (Dupriest, 2013).

Normally, weight on bit is generated when the rig slacks off (reduces surface tension) which then increases compression on the drill bit. Alternatively, WOB may be generated by two other means. Either the rig will have a thrust (pull down) capacity or heavy weight drill pipe can be added in the vertical section. If the compression necessary to overcome friction and get WOB is substantial, then the pipe may buckle and therefore additional calculation will be necessary. Our model does not calculate buckling.

Overpull requirements will depend upon site conditions and rig experience. Overpull will increase with depth and complexity of the planned well. Rig pullback capacity [MLT^{-1}] is calculated as:

$$\text{Rig Pullback Capacity} = F_{kopO} + F_{UO} + BHA + OP, \tag{144}$$

where F_{kopO} is the force at the kickoff point when pulling out [MLT^{-1}], F_{UO} is the force of the upper section when pulling out [MLT^{-1}], *BHA* is the force caused by the bottom hole assembly [MLT^{-1}], *OP* is the overpull safety factor for stuck pipe [MLT^{-1}].

Calculation of rig thrust (pull down) capacity is similar to rig pullback capacity. While calculations may indicate the need for a rig with thrust capacity, this issue can be overcome in certain cases with the addition of heavy drill pipe in the vertical section to add additional downward (thrust) force. Clearly an iterative approach to design is necessary to achieve optimal performance. As stated previously, the compression needed to drill through rock is typically applied by reducing tension at the surface. Rig thrust capacity [MLT^{-1}] is calculated as

$$\text{Rig Thrust Capacity} = F_{kopI} + F_{UI} + BHA + Drill\,, \tag{145}$$

where F_{kopI} is the running in force at the kickoff point [MLT^{-1}], F_{UI} is the running in force for the upper section [MLT^{-1}], *BHA* is the effect on force by the bottom hole assembly [MLT^{-1}], *Drill* is the compressive weight on bit necessary to drill the rock [MLT^{-1}].

Rig torque capacity [ML^2T^{-1}] is the simple addition of the torque from each section

$$\text{Rig Torque Capacity} = M_U + M_B + M_L\,. \tag{146}$$

Casing and Drill Pipe Selection

While the equations presented in the previous sections describe several of the forces a casing / drill pipe string must be designed for, there are still several other necessary calculations. These extra calculations include overpull, thermodynamic,

cementing, and buckling effects. Considerations also need to be made for the effects of perforating the casing or the use of wire mesh well screens.

Additional calculations should also include the collapse resistance. There have been many thoughts on how to properly calculate the collapse resistance needed for a given formation. If the target formation is highly unconsolidated, then perhaps a collapse resistance that is double (as a safety factor) the overburden pressure is necessary (El-Sayed et al., 1991). On the other end of the spectrum, if the formation is well consolidated then a production casing may not be necessary as the formation is self-supporting. However, if production casing is required then at a minimum it should be designed for hydrostatic pressure (0.43 psi per foot). A conservative approach is to design casing for the lithostatic pressure at one psi per foot.

In spite of the need for additional, site specific calculations, a rough estimate of casing strength can be made from the equations presented. It is important to remember that these calculations are for casing or drill pipe. Addition of the bottom hole assembly, compressive drilling forces, and required buckling resistance will yield different estimates of pipe strength. Again, these equations are thought to yield an answer with 75% accuracy. Experience and site specific considerations will determine the remainder.

Because the casing will travel through every section of the wellbore, the casing strength must be calculated at each of these points with the maximum and minimum forces determining casing selection. Given the non-linear equations describing axial forces along the buildup section, it is also important to determine the minimum and maximum value within this section (Greenip Jr, 1989). This can be done using a

numerical procedure of stepping through the buildup section from θ_L to θ_U and finding the minimum and maximum. Once the minimum and maximum forces along the buildup section have been calculated, the bending forces must be added and subtracted to make a final casing selection. The required casing compressive strength is calculated as

$$\text{Casing Compressive Strength} = \min\left[F_{UI} + F_{kopI}, MinF_{bI} - S_f \right], \quad (147)$$

where F_{UI} is the force required to run in the upper section [MLT^{-1}], F_{kopI} is the force required to run-in the lateral and build section [MLT^{-1}], $MinF_{bI}$ is the minimum axial force in the buildup section when running in [MLT^{-1}], and S_f is the bending force of the pipe [MLT^{-1}]. The required casing tensile strength [MLT^{-1}] is calculated as

$$\text{Casing Tensile Strength} = \max\left[F_{UO} + F_{kopO}, MaxF_{bO} + S_f \right], \quad (148)$$

where F_{UO} is the fore required to pull out the upper section [MLT^{-1}], F_{kopO} is the force required to pull out the lateral and build section [MLT^{-1}], $MaxF_{bO}$ is the maximum axial force in the buildup section when pulling out [MLT^{-1}], and S_f is the bending force of the pipe [MLT^{-1}].

OPTIMAL SLANT RIG ENTRY ANGLE DERIVATION

Given a target depth of the lateral section, there is an optimal slant rig angle (angle of the upper section) required to minimize the length of the well. Minimizing the length of the well saves money as less drilling and casing is required. This optimal angle does not consider other factors such as friction, weight on bit or pullback issues. The optimal slant rig entry angle is a function of the target depth and the radius of curvature. If the target is deep, then the optimal entry angle is vertical. However, if the target is

shallow – especially if more shallow than the radius of curvature – then optimal slant rig entry angle calculation is necessary. To begin calculation, we define the measured depth of the entire well (149). We then redefine the kickoff point using two chords within the circle (Figure 75). The measured depth (total wellbore length) calculation is

$$MD = MD_U + MD_B + MD_L = \frac{kop}{\sin\left[\theta_U\right]} + R\left(\theta_U - \theta_L\right) + MD_L, \tag{149}$$

where MD_U is the measured length of the upper section, MD_B is the measured length of the buildup section, and MD_L is the measured length of the lower section.

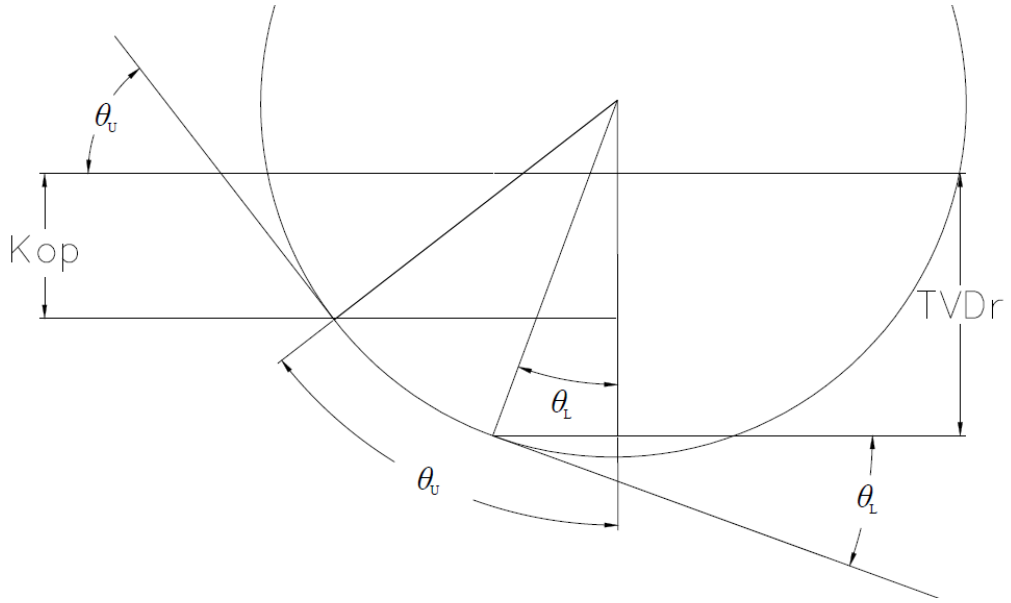

Figure 75. Angles used during optimal slant rig entry angle calculation.

To begin derivation of the optimal slant rig entry angle, we redefine the kickoff point as

$$kop = TVDr - R\left(\cos\left[\theta_L\right] - \cos\left[\theta_U\right]\right). \tag{150}$$

We then plug this new kickoff point relationship into the measured depth equation

$$MD = \frac{TVDr - R\left(\cos\left[\theta_L\right] - \cos\left[\theta_U\right]\right)}{\sin\left[\theta_U\right]} + R\left(\theta_U - \theta_L\right) + MD_L \,. \tag{151}$$

To determine the optimal slant rig entry angle, we want to minimize the measured depth. We therefore need to find the entry angle that will force the derivative to equal zero. So taking the derivative with respect to entry angle, we find

$$\frac{\partial MD}{\partial \theta_U} = \cot\left[\theta_U\right]\csc\left[\theta_U\right]\left(R\cos\left[\theta_L\right] - R\cos\left[\theta_U\right] - TVDr\right), \tag{152}$$

and solve for when the derivative is equal to zero

$$0 = \cot\left[\theta_U\right]\csc\left[\theta_U\right]\left(R\cos\left[\theta_L\right] - R\cos\left[\theta_U\right] - TVDr\right). \tag{153}$$

To solve for theta, we factor out a negative sign then rewrite cosecant and cotangent

$$0 = \frac{\left(TVDr + R\cos\left[\theta_U\right] - R\cos\left[\theta_L\right]\right)\cos\left[\theta_U\right]}{\cos^2\left[\theta_U\right] - 1}. \tag{154}$$

Replacing $\cos\left[\theta_U\right]$ with X and factoring out the denominator, we find

$$0 = X\left(TVDr + RX - R\cos\left[\theta_L\right]\right). \tag{155}$$

We then split this equation into two equations and solve each product separately

$$\begin{aligned} RX - R\cos\left[\theta_L\right] + TVDr = 0 \quad &\text{or} \quad x = 0 \\ X = \cos\left[\theta_L\right] - \frac{TVDr}{R} \quad &\text{or} \quad x = 0 \end{aligned}. \tag{156}$$

Re-substituting X with $\cos\left[\theta_U\right]$ and solving for θ_U, the solution is

$$\theta_U = \cos^{-1}\left[\cos\left[\theta_L\right] - \frac{TVDr}{R}\right] \quad \text{or} \quad \theta_U = \frac{\pi}{2}. \tag{157}$$

RESULTS AND DISCUSSION OF MODEL OUTPUT

Simple drilling models were developed to give insight into expected forces, angles, and lengths for specific input. However, these models are also useful in giving perspective on overall trends. Plots generated were done so to give general insight into the parameters influencing horizontal well construction. Plots were generated using a 100 X 100 linearly spaced grid of data points on both the horizontal and vertical axes. A total of 10,000 data points were used to contour each plot.

To begin, we investigate the simplest equation, the optimal slant rig entry angle. From these two plots it is clear that the optimal entry angle is only important if the radius of curvature is less than the TVDr (Figure 76 & Figure 77). The optimal entry angle is more important at deeper TVDr as the radius of curvature increases.

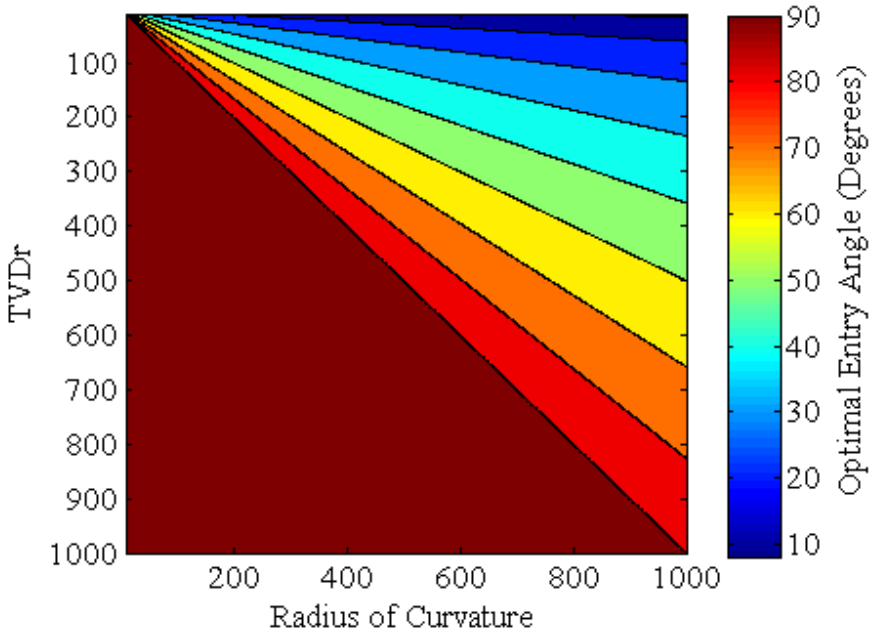

Figure 76. Optimal entry angle, lateral angle at zero degrees.

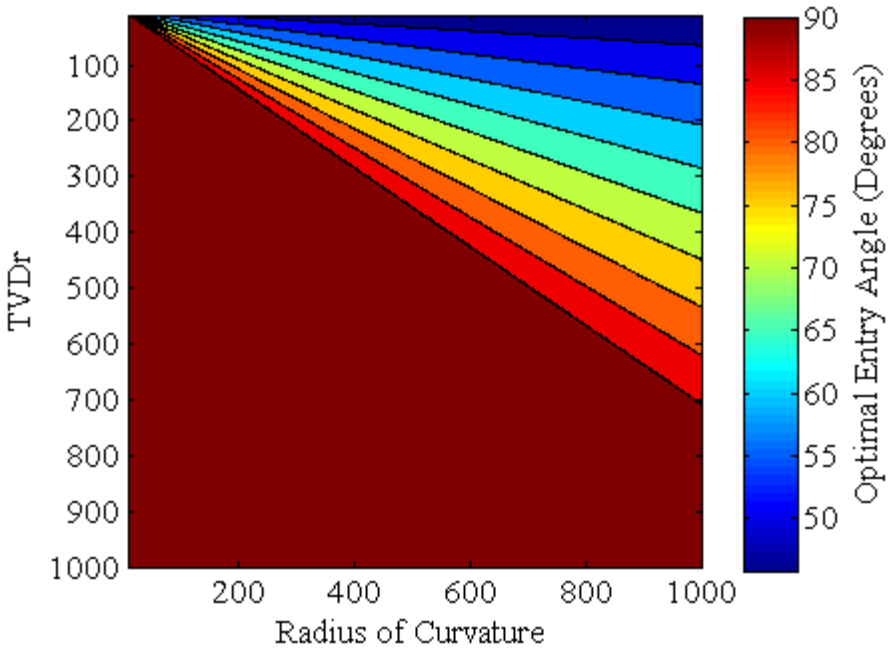

Figure 77. Optimal entry angle, lateral angle at 45°.

Plots of the measured depth as a function of TVDr and lateral length reveal the need for various slant rig types (Figure 78-Figure 80). Plots assume the lateral is horizontal (zero degrees). Groundwater supply aquifers are typically less than 2,000 feet deep. Most wellbores are between eight to eighteen inches, which yields a radius of curvature from 800 feet to 1,800 feet using the industry rule of thumb.

In the optimal situation, rigs for horizontal groundwater wells would be able to use any entry angle (Figure 78). However, because of the limited entry angles for utility rigs (7°-23°) and slant petroleum rigs (45°-90°) a combination of these technologies is necessary (Figure 79 & Figure 80). Utility slant rigs must be relied upon for the majority of the aquifer depth range. Use of utility rigs translates to significantly longer measured lengths than could be achieved with a ‘full range’ slant rig (0°-90°). A vertical rig cannot

hit any depth targets shallower than the radius of curvature, which in most cases is perhaps 800 feet.

All model input and output referenced in the following paragraphs is in the *Supplemental Material* document accompanying this thesis. For tables describing the exact model input, please consult *Supplemental Material, Part B*. The pipe data in each table of *Part B* is from American Petroleum Institute (1982) as cited in Halliburton (1995). Following each table of model input in *Part B* is model output. An example of model input and output is presented below (Table 12, Figure 81-Figure 85).

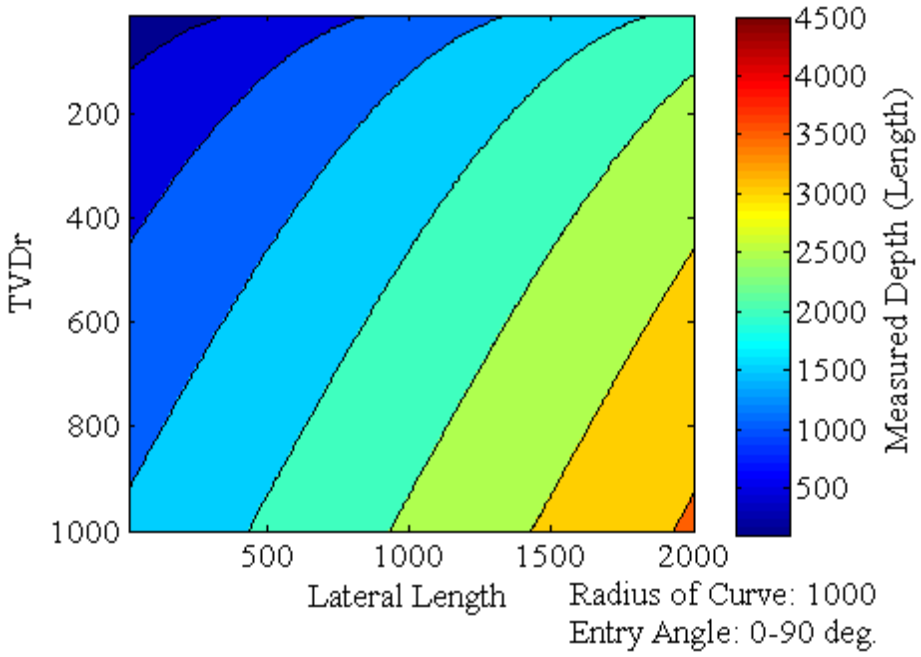

Figure 78. MD vs. TVDr and lateral length, full range of entry angle.

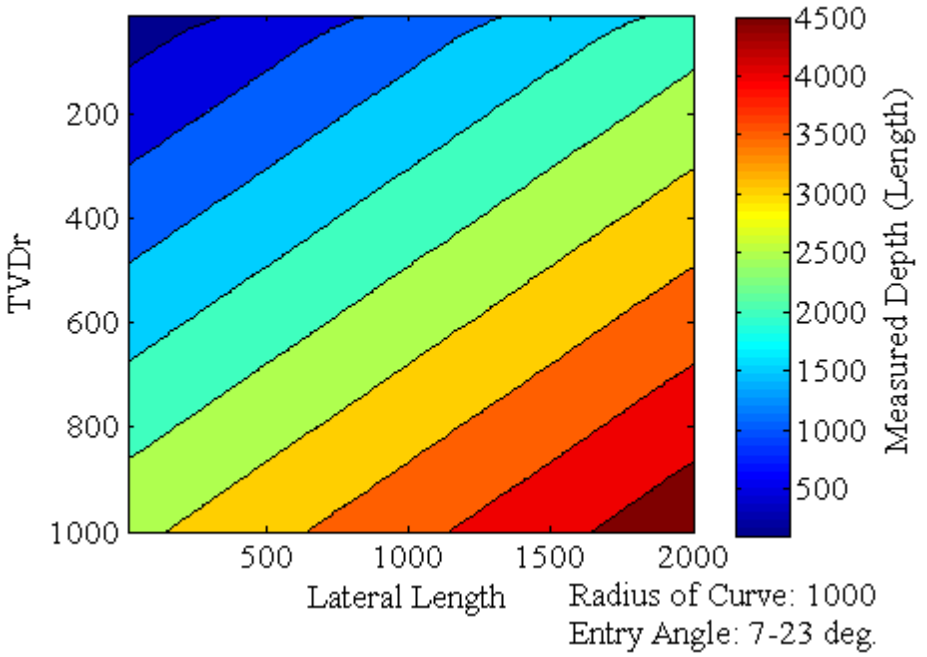

Figure 79. MD vs. TVDr and lateral length, entry angle 7°-23°.

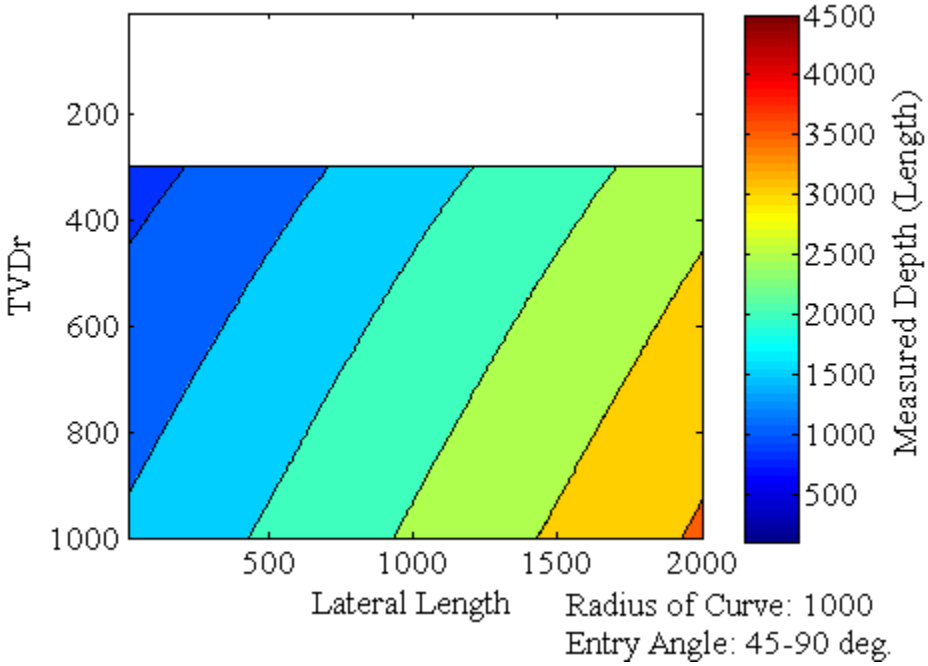

Figure 80. MD vs. TVDr and lateral length, entry angle 45°-90°.

Table 12. Sample input for well construction force model.

Variable	Value
Casing Type	K-55
Outside Diameter	11.75 inches
Inside Diameter	10.88 inches
Wt per ft with cplg	54 lbs
Collapse Resistance	2,070 psi
Body Strength	850,000 lbs
Friction Coefficient	0.4
Buoyancy Factor	0.85
Radius of Curvature	1,200 feet
Entry Min	0
Entry Max	90
Lateral Angle	0
Young's Modulus	29e6 psi

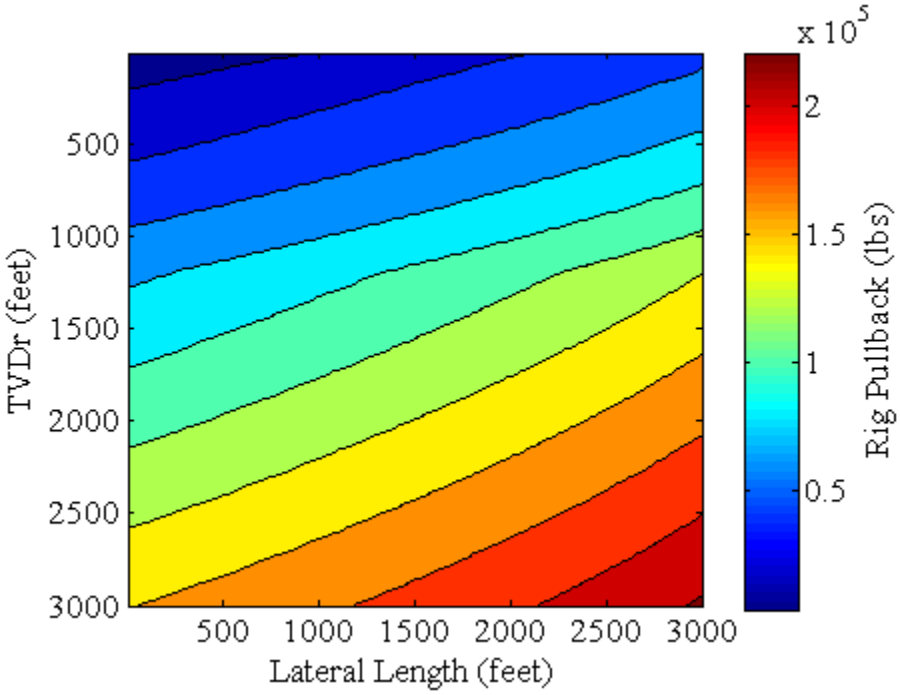

Figure 81. Rig pullback from data in Table 12.

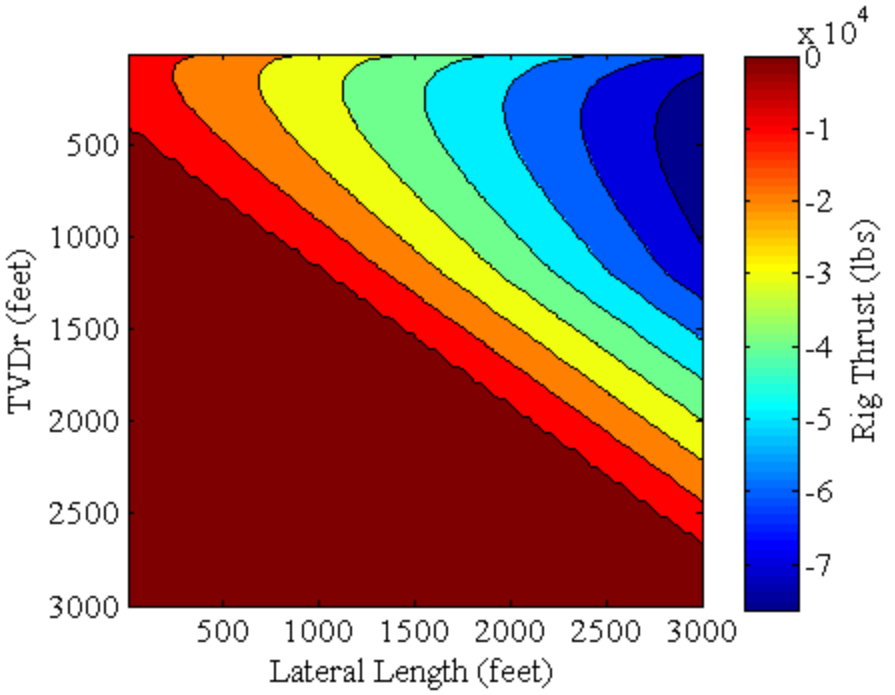

Figure 82. Rig thrust from data in Table 12.

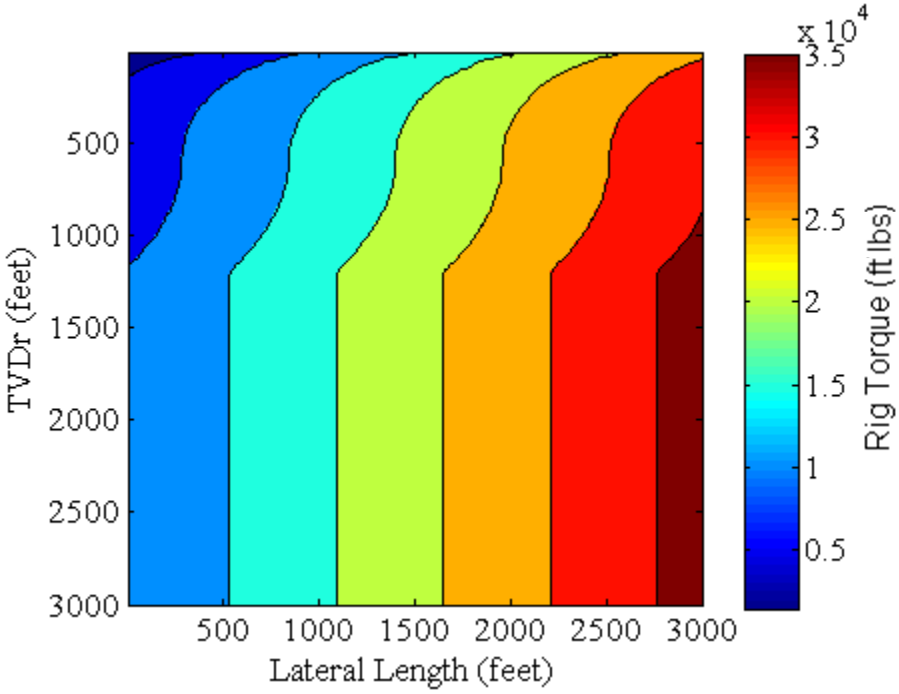

Figure 83. Rig torque from data in Table 12.

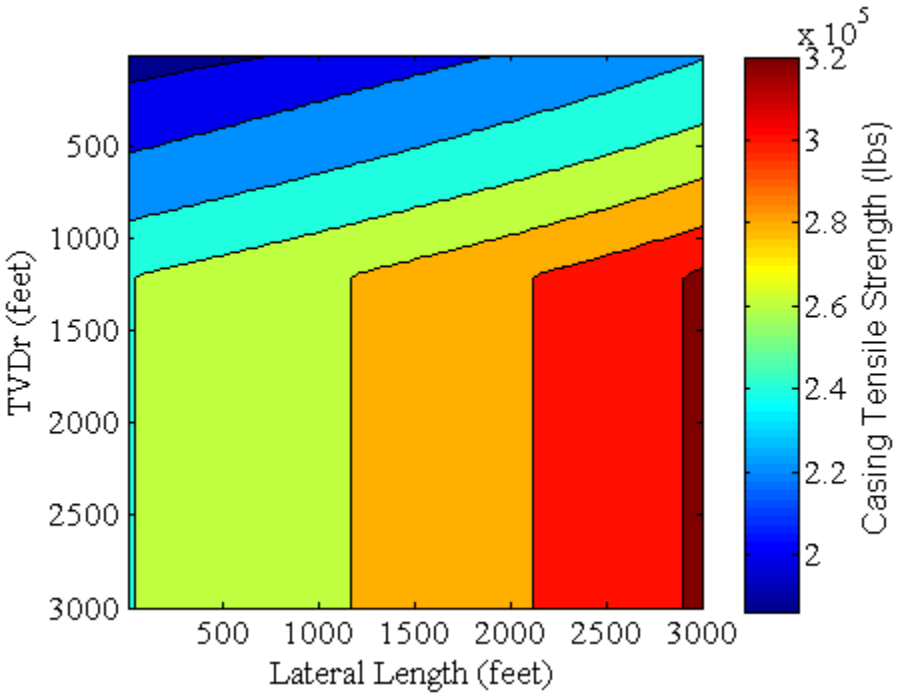

Figure 84. Casing tensile strength from data in Table 12.

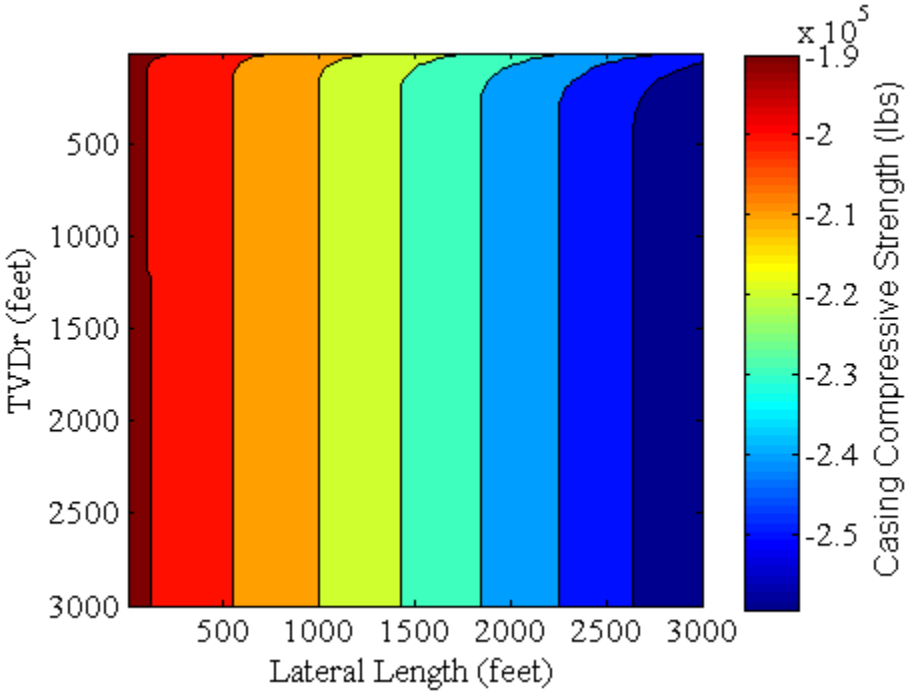

Figure 85. Casing compressive strength from data in Table 12.

We modeled five different pipe scenarios, using a pipe weight from 84 lbs (16 inch diameter) to 20 lbs (six inch diameter). Model input assumes that the entry angle can range from 0°-90°. The radius of curvature was assumed to be the industry rule of thumb. We chose pipe that had a collapse resistance around 1,500 psi. We plotted rig pullback, rig thrust, rig torque, casing tensile, and casing compressive forces over a domain form 0-3,000 feet TVDr and 0-3,000 feet lateral length. Factors not accounted for in these modeling efforts include: rig overpull, rig over-thrust, bottom hole assembly, compressive drilling requirements, cementing, etc. Although these forces were not accounted for, they may generally be thought of as a simple addition to the model output.

The domains of the simulations are such that several different casing designs would be more effective than the one size fits all TVDr / lateral lengths which was assumed. For example, casing design at low TVDr would likely use a lower grade pipe to reduce the magnitude of forces and save money. Furthermore, to avoid having to contract a rig with thrust capacity one could use heavy drill collars. This would reduce the rig thrust requirements, but increase the rig overpull requirements. The variation in target formation could also dictate more or less compressive drilling force and thus change the model output.

In spite of these shortcomings, our modeling efforts give valuable insight into the interplay of forces experienced by the rig and casing / drill pipe. While these model output plots should not be used to contract drilling rigs and/or casing supplies, they do

facilitate an understanding of the order of magnitude and general characteristics of forces. Experienced drilling engineers will need to make site specific decisions.

To begin analysis, we investigated the friction factor first. The friction factor is one of the most subjective parameters to select. Friction factor values have ranged from 0.2 – 0.4 as determined from field experiments (Johancsik, 1984; Sheppard et al., 1987). Our investigation found that rig thrust and casing compressive strength are affected most by the change in friction factor whereas the rig pullback is affected the least.

We found that rig pullback requirements range from 10,000 lbs to 300,000 lbs. Groundwater rigs typically have less than 100,000 lbs of pullback, although some may be closer to 200,000 lbs pullback. Petroleum rigs generally have pullback of greater than 200,000 lbs. This variability in pullback requirement shows the possibility of using groundwater rigs to save money at shallow depths and the need to use petroleum rigs at greater depths. However, one cannot forget the radius of curvature and entry angle limitations at shallow TVDr and therefore the need for slant rigs.

Rig thrust / heavy drill collar requirements become an issue at step out ratios (lateral length divided by TVD) of greater than 1:1 for high friction factors and 2:1 for low friction factors. Rig thrust capacity is especially important at shallow depths because the upper section does not have the length necessary to overcome lateral section friction forces. Rig thrust capacity ranges from 0 lbs to -120,000 lbs.

Rig torque requirements show an interesting pattern on each plot that is clearly influenced by the radius of curvature / optimal slant rig entry angle. It is also clear that

the friction factor has a substantial impact on the torque. Rig torque requirements range from 0 to 80,000 ft-lbs.

Casing tensile requirements are the least variable parameter. Casing tensile requirements vary from 110,000 lbs to 500,000 lbs. This relative lack of variability compared to other parameters occurs because the radius of curvature and diameter of the pipe has a strong control on the bending force. The bending force increases as the radius of curvature decreases and/or as the diameter of the pipe increases. However, as the pipe diameter decreases, so does the radius of curvature (assuming the industry rule of thumb). Therefore these factors cancel each other out to some degree and hence the lack of variability.

Casing compressive requirements follow a similar trend as the casing tensile requirements. Casing compressive requirements vary from -450,000 lbs to -70,000 lbs. The most interesting aspect of casing compressive requirements is the change in plot shape when the friction factor is decreased. While is difficult to explain such a change, it is perhaps because of the non-linear axial forces within the buildup section.

CHAPTER VI

HORIZONTAL WELL COST – BENEFIT ANALYSIS

INTRODUCTION

The cost analysis section of this thesis attempts to quantify the economic context of directional water supply wells compared to vertical water supply wells. Without an economic perspective, groundwater professionals will be unable to quantitatively judge the benefit of new well designs. As has been shown in Chapter I, directional groundwater production wells have been completed with a thought to competitive cost - benefits. Simple cost models for directional and vertical wells are developed in this chapter to understand this component. We then pair these cost models with the drilling forces models in Chapter V to make well cost estimates. Finally, we add a benefit calculation via our aquifer model.

Well Cost Components

The cost of a well may be divided into four major components: drilling & well completion, pumps, connections & structures, and operations & maintenance. While these parameters may be thought of separately, to achieve the most economic well they must be economized and optimized in tandem (Helweg, 1982; Stoner et al., 1979). For example, increasing the casing diameter will increase total drilling & well completion costs, but perhaps will facilitate a larger, more efficient pump.

Such cost optimizations may induce a marginal increase in drilling & well completion cost with a significant decrease in drawdown / increase in pumping.

Determining the optimal design for each well will reduce the cost of produced water per unit volume. However given the inter-relationships of costs and efficiency, this is a complex, iterative process.

Drilling & Well Completion

Drilling & well completion costs are site specific in nature and therefore difficult to accurately describe in broad terms. There are perhaps 40 parameters that influence drilling, and by extension costs as cited by Campbell and Lehr (1973) in Gatlin (1960). The well construction cost estimate is complex, but has been characterized by Devereux (1999) and Willoughby (2005), among others, into six categories:

Base - fixed costs include the construction / deconstruction of the drill pad including surveying, clearing, utilities, and restoration is a significant portion of drilling cost (Petrey and Bennett, 2006). Fixed costs also include the mobilization cost. The movement of equipment to the well site (mobilization) will vary depending upon the value of equipment, distance traveled, insurance, and personnel logistics (Wilson and Losonsky, 1995). The mobilization cost will be greater for highly specialized, expensive equipment that is in high demand at other projects (Wilson et al., 1993). For example, a directional slant rig designed to extract shallow petroleum in Alberta will be significantly more costly to mobilize to Texas than to Montana simply based on location. Upon consultation with a petroleum slant rig service company in Canada, mobilization for such a slant petroleum rig to Texas will be approximately $400,000; the same rig would mobilize intra-state for $25,000 and $5,000-$10,000 for intra-site mobilization.

Time dependent costs include personnel time, rental equipment rates, fuel, and water. Typically petroleum drillers operate on day rates and therefore keep spreadsheet units in time to complete projects. This facilitates easy updates as costs change continuously, but drilling and completion time remains more constant. In contrast, water well drilling is typically based on lump sum turnkey contracts. Water wells inherently have time dependent costs. However, these costs are typically expressed through cost per foot during bidding.

Length dependent costs are based on casing, cement, drill bits, drill fluid, wellbore diameter, filter pack material, formation strength, and disposal of cuttings (Petrey and Bennett, 2006). These are all the material costs associated with the length of the wellbore.

Support costs are office related including engineering/geological work and other support staff. Such costs may be distributed between other categories or may be completely separate. Suitable other categories for these costs include fixed or time dependent costs. For groundwater projects, these costs may be expressed as consulting fees, perhaps on a percentage basis.

Contingency - managing risk is an important cost component. Evaluating the risk as a percentage of occurrence and then multiplying by the cost of contingency (loss of equipment, etc.) has been suggested as a means to achieve an appropriate cost estimate (Devereux, 1999). For example, the risk of losing a down hole motor at a cost of $100,000 is an important risk to plan for and may yield a project uneconomical (Williams, 2008; Wilson and Losonsky, 1995). While overall drilling costs may be linear

during conservative drilling scenarios, they become non-linear as the drilling envelope is extended to its limits due to increases in contingency (Dupriest, 2013). It is suggested that contingency for directional groundwater wells be 20%. However, a competent engineer will need to make final economic decisions.

Contract type between the operator and rig contractor can affect the quality and cost of the hole. The optimal solution is to align the interests of both parties, thereby encouraging optimal completion (Devereux, 1999). The earliest types of contracts in the petroleum industry were based on cost per foot or turnkey (lump sum) payments which promoted low quality holes (Devereux, 1999). The day rate contract is now the most common contract in the petroleum industry. There are mechanisms that maybe used to incentivize day rate contracts to improve performance, such as bonus payments for safety, hole quality, and timeliness.

Pumps

Pump cost is related to the operating parameters desired. Overall pump cost is affected by total head requirements, desired discharge, horsepower, bowl configuration, net pressure suction head, and pump housing diameter (pump size). Each pump cost category must be optimized in an effort to maximize cost efficiency. In addition, pump selection / cost may be affected by the pump orientation (horizontal well vs. vertical well). These costs are too site specific and therefore will not be considered in this study.

Connections and Structures

Connection and structures may be accounted for in drilling costs during the pad construction (i.e. fences, roads); however, many additional costs are possible.

Construction of the well house, road connections, well communications, transmission main connections, and the like can greatly influence the final well cost. These costs will vary depending if several wells are constructed in a centralized manner (lower costs) or decentralized manner (higher costs). These costs are too site specific and therefore will not be considered in this study.

Operations and Maintenance

Costs in this category include: well redevelopment, pump servicing, electricity, and testing / monitoring. While the initial cost of a directional well may be more than a vertical well, yearly operation and maintenance may prove the horizontal design to be cost competitive over time (Allouche et al., 1998). Such costs are especially important when considering pump efficiency and head requirements. Determining the optimal discharge form an efficiency standpoint can generate substantial cost savings (Helweg, 1975). These costs are too site specific and therefore will not be considered in this study.

Well Cost Model Considerations

Given the highly site dependent cost of pumps, connections & structures, and operations & maintenance, an attempt to quantitatively describe these components was avoided. Qualitatively, connection & structure costs may be reduced based on the number of wells saved (not constructed) due to replacement of several vertical wells by one horizontal well, a move to greater centralization. Furthermore, the economies of scale for larger pumps (as needed for high capacity directional wells) points to increased efficiency and therefore decreased operations cost. However, considering the possible maintenance costs and/or pump replacement due to the inclined position of the pump,

this may not be true. As cited for the Castle Pines North directional well (Jehn-Dellaport, 2013), pump savings for directional wells may quickly be erased and must therefore be assessed more closely.

The cost model developed assumes the end user will use representative pump costs and connection & structure costs in their personal assessment. Once connection & structure and pumping costs have been determined, they may be placed in the fixed costs category of the model developed here. It is outside the scope of this study to investigate optimal pump or well head construction. Those interested in such economic optimization should consult Helweg (1975), Stoner et al. (1979), Helweg (1982), Swamee et al. (1999), and Petrey and Bennett (2006).

With these considerations, a cost model was developed to aid in cost analysis. A deterministic representation of cost parameters was used. While a purely stochastic drilling model may seem preferred, doing so would restrict applicability due to the many parameters involved, perhaps 40 parameters as cited by Campbell and Lehr (1973) in Gatlin (1960). The lack of extensive directional water well cost data would also preclude any stochastic methods for such purposes.

However, such a lack of data has not limited stochastic model development for geothermal well costs. Through use of the land based petroleum drilling data, correlations and stochastic models have been developed for geothermal wells (Augustine et al., 2006; Mansure et al., 2005; Milora and Tester, 1977; Tester and Herzog, 1990). Given the number variables required and therefore unknown deterministic inter-dependencies, it becomes difficult to decipher where the cost variance originates. More

importantly, the common occurrence of groundwater and rare occurrence of petroleum at shallow depths precludes a stochastic approach.

In this deterministic study, first cost estimate models were developed for vertical and directional wells. Once models were developed, literature, post bids and personal communication established reasonable model input values. Finally, with the models developed and input parameters determined, cost estimates were made.

WELL COST MODEL

The first step in model development is the separation of time dependent and time independent variables (Figure 86). Time independent costs include measured depth (well length) dependent and measured depth independent costs. Measured depth dependent costs include casing, filter pack material, cement, etc. Measured depth independent costs include mobilization of equipment and other fixed costs. Other fixed costs may include drill pad construction, pumps, consulting / geologic / engineering work.

Time dependent costs are calculated differently between horizontal and vertical wells. Vertical well time dependent costs are a function of measured depth, rate of penetration, completion time and the non-directional spread rate. Directional well time dependent costs are a function of the same parameters in addition to the measured length of directional drilling, and a factor accounting for slower directional rates of penetration.

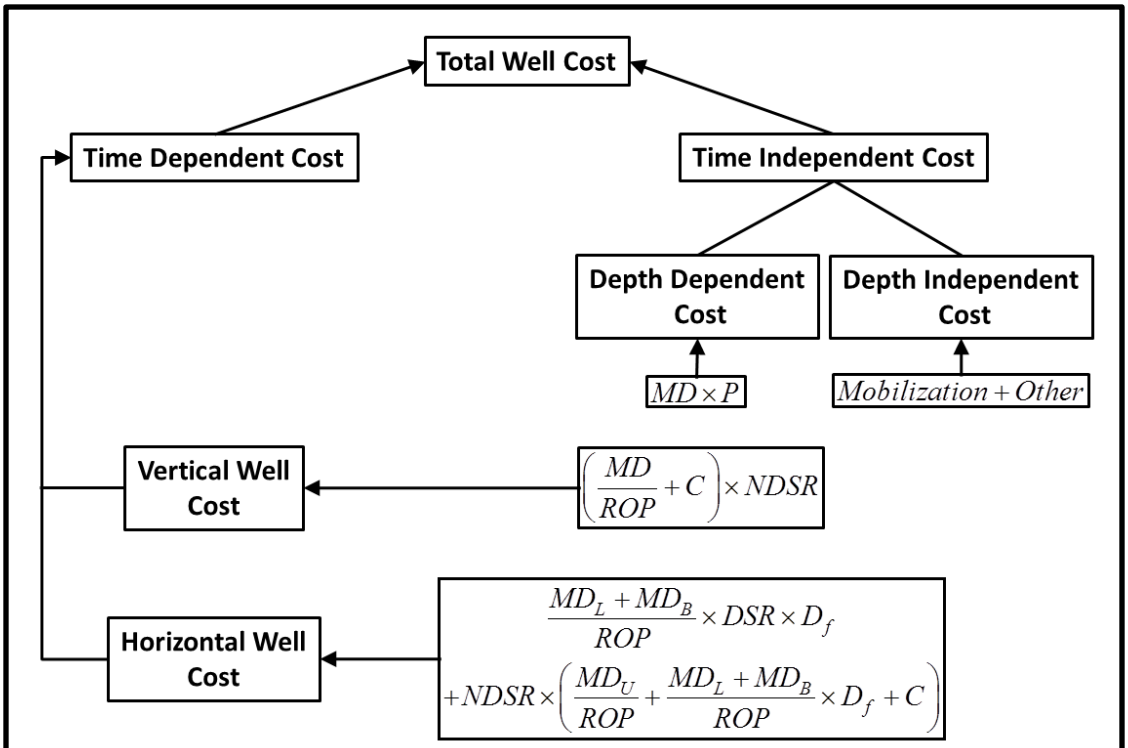

where

P is the cost of material (casing, cutting disposal, etc) per unit length of borehole

MD is the total measured depth (length) of the borehole

MD_L is the measured depth (length) of only the lateral section

MD_B is the measured depth (length) of only the buildup section

MD_U is the measured depth (length) of only the upper section

ROP is the rate of penetration (length per time) of drilling

D_f is the directional slowness factor, unitless variable describing how many times slower the rate of penetration is due to directional drilling

C is the time required to complete the well (install casing, filter pack, etc.)

$NDSR$ is the non-directional spread rate (cost of drilling operations per unit time, not including directional equipment)

DSR is the directional spread rate (cost of only directional drilling equipment per unit time)

Figure 86. Vertical and horizontal well cost flow chart.

WELL COST DATA COLLECTION

In an effort to provide realistic parameters for the developed cost model, assistance from the professional community was enlisted. To obtain parameters for vertical water well daily rig rates, 14 water well drilling companies were contacted. To obtain daily rates for directional services, 11 directional drilling service companies were contacted. To obtain daily rates for petroleum slant rig rates, three companies were contacted. To obtain rates from the utility HDD industry, six companies were contacted. To obtain casing costs, six casing companies were contacted. Finally, a data set of oil country tubular goods and petroleum daily rig rate costs were obtained from professional service companies (Murphy, 2013; Rig Data, 2014).

Results & Discussion

While many companies were contacted, only a few were able to provide the requested information. Furthermore, because of the competitive nature of the industry, the names associated with the costs have been omitted. Given the continuous fluctuation and site specific nature of costs, a qualified professional must conduct a project specific budget at that time.

Drilling Cost

Of interest to note, each directional drilling company contacted was asked how they determined radius of curvature and casing to hole size ratios. While only rigorous calculation would yield an accurate radius of curvature, every company verified the conservative, ratio of 100 feet of turning radius per inch of hole diameter. For example, a 12 inch wellbore requires a 1,200 foot turning radius. Another general ratio verified was

casing diameter to borehole diameter, which is commonly 2:3. As a disclaimer, these are conservative ratios and better performance is routinely achieved.

Utility HDD

Three slant utility drillers from the United States were able to provide cost estimates (Table 13, Figure 87). The closest distance between any two companies is 1,000 miles. Interestingly, no data was obtainable on a day rate basis, only on a per foot basis. Lower costs are associated with continuous completions, shallower TVD, and softer formations. Higher costs are associated with blind completions, deeper TVD, and harder formations such as metamorphic or igneous rock. The range of ROP is 150 feet per day to 500 feet per day with a best guess of 200 feet per day, but possibly much less in hard formations. Costs provided include the directional drilling device, with lower costs reflecting jetting techniques and higher costs reflecting a mud motor.

Slant Petroleum

Only one slant petroleum rig company was able to provide cost estimates (Table 14). However, a wealth of additional information was provided on this rare technology. The only region where these rigs proliferate is in the Canadian shallow heavy oil sands. The three main manufacturers of these rigs are Ensign, Precision, and Ground Force Canada. These rigs are using 1,000 hp triplex mud pumps, fully integrated top-drives, Range III drill pipe, and a hydraulic ram with 20,000 lbs pull down (thrust) capacity. Pullback capacity of 100,000 lbs to 150,000 lbs are common. The max MD is 11,000 feet. These rigs also have automated pipe handling which greatly improves rate of penetration.

Most of these slant petroleum rigs are drilling angle wells rather than horizontal laterals. For one of the rigs operating at 600m TVD with a 1,700m horizontal lateral and nine and five-eighths inch hole; from spud to rig release was taking two to two and a half days. This gives a daily ROP of 3,000 feet per day. These holes have two casing strings with a slotted liner in the production zone. For a similar rig operating at 800m TVD, with the same borehole diameter, from spud to rig release was taking three days. Assuming this was simply a vertical borehole, ROP is estimated at 875 feet per day.

Directional Equipment and Services

Seven directional service companies provided cost information (Table 15). Five of the companies were based out of Texas and two from Canada. The rates from the Canadian companies were within the data range from Texas companies. The costs for services would include down hole calculations to inform the operator of expected pullback, weight on bit, torque, and required mud pump capacity. Day rates include the mud motor and field staff. The reason for zero mobilization cost as a minimum is because some companies wrapped the mobilization into the day rate provided. The main reason for cost variance was attributed to the down hole logging and measurement equipment desired. The largest mud motors commonly available are 17.5 inches.

Information on the rigs using these directional services was also obtained from the directional drillers. Most rigs running at 9,000 feet TVD that are completing horizontal wells have 350,000 lbs of pullback. The instantaneous ROP at these depths is 150-200 feet per hour. It was thought that instantaneous ROPs at 2,000 feet TVD would be 500-700 feet per hour. The mud pumps required to operate the downhole equipment

and clean the hole are positive displacement pumps with rates of 300 to 900 gallons per minute.

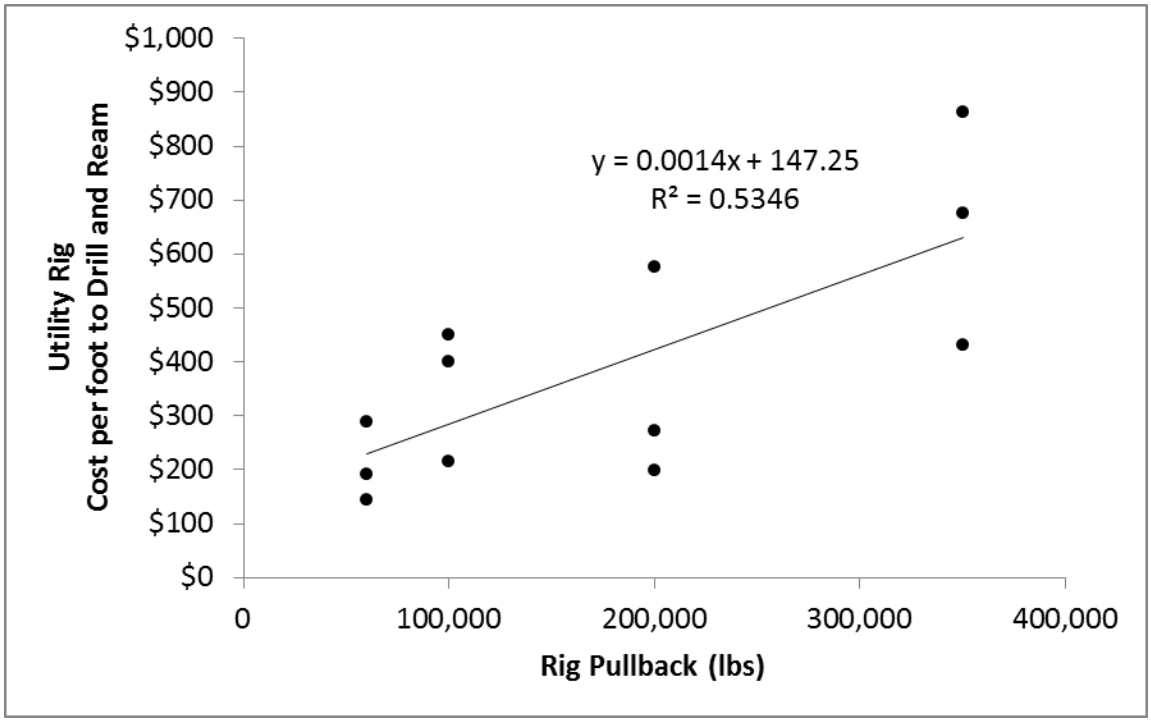

Figure 87. Utility rig cost per foot to drill & ream versus rig pullback.

Table 13. Drilling cost for HDD utility rigs from three companies.

Companies participating	Pullback & Thrust lbs	Torque ft lbs	Mobilization Per Day	Dollars per foot		
				Lowest	Median	Highest
2	350,000	45,000	$50,000	$432	$675	$864
2	200,000	60,000	$50,000	$199	$273	$576
2	100,000	12,000	$50,000	$216	$401	$450
2	60,000	10,000	$50,000	$144	$192	$288

Table 14. Slant petroleum daily rig rates.

Number of companies participating	Max MD	Max Diameter in inches		Mobilization			Rig Rate per Day		
	Feet	Borehole	Casing	To Texas	Intra-State	Intra-Site	Lowest	Median	Highest
1	11,000	17.5	11.7	$400,000	$25,000	$7,500	$20,000	$22,500	$25,000

Table 15. Day rates for down hole directional equipment and services.

Type	Number of Companies Participating	Mobilization per Day	Daily Rate		
			Lowest	Median	Highest
Mud motor and MWD	7	0-$15,000	$7,000	$10,500	$15,000
Gamma Logging	2	-	$1,000	-	$1,200
Resistivity and Gamma Logging	1	-	-	$5,000	-
RSS with MWD	1	$22,000	-	$28,000	-

Vertical Daily Rig Rate

Data obtained for drilling rig costs came from three sources: two water well drillers, petroleum service company data, a groundwater well construction time table, and post bids. Of the 14 drilling companies contacted, only three from Texas gave any information (Table 16). A timetable for nine municipal wells drilled in Texas from 2012 was also obtained (Table 17).

Seventy-one post bids were obtained from Arizona (Glotfelty, 2013), and three from Texas (Figure 88-Figure 93, Table 18). Because the data for the wells began in 1996, an adjustment for inflation using the Construction Cost Index (CCI) was implemented (Engineering News Record, 2013). The CCI is similar to the Consumer Price Index. The Consumer Price Index quantifies buying power for urban consumers determined from housing and food costs, etc. The CCI quantifies buying power for labor, steel, and lumber. While a well cost index would be more appropriate, none exists and hence the CCI was thought to be the best alternative. All costs were adjusted to 2012 using CCI yearly data (Engineering News Record, 2013).

Overall, the post bid data is surprisingly depth independent. It was assumed that drilling and reaming cost per foot would increase with depth. Interestingly, the time table data shows that water wells are drilled an order of magnitude slower (200 feet per day) than petroleum wells (100 feet per hour). It is not immediately clear why there is such a difference, although it has been suggested that water wells must be very straight so as to fit large pumps (Jehn-Dellaport, 2013).

Table 16. Cost for traditional vertical water well rigs.

Sample Size	Pullback in lbs	Hole Diameter and Depth	Mobilization per Day	Daily Rate			Cost per Foot		ROP in Feet per Day
				Lowest	Mid	Highest	Drill Case and Complete	Casing	
1	200,000	36" @ 1,000' 12.75" @ 5,000'	$50,000-$75,000				$200 to $250	$50 to $100	200 - 300
2	100,000	24" @ 600' 12" @ 1,800'	$5,000	$6,450	$6,975	$8,600	$75 to $100	8" @ $18 10" @ $24 12" @ $32 slotted liner @ $20	50 - 300

Table 17. Timetable for nine Texas, municipal, vertical water wells constructed in 2012. Data from Dwyer (2013).

	Min	Median	Max	Units
Total Depth of Pilot Hole	2,030	2,230	2,500	Feet
8” Pilot Hole Drilling	7	16	27	Day
Inferred ROP	92	139	290	Feet per Day
Geophysical Logging	1	1	1	Day
Upper Casing Length	1,210	1,380	1,606	Feet
Upper Casing Reaming	16	30	51	Day
Upper Casing Reaming ROP	28	49	82	Feet per Day
Upper Casing Installation	1.5	2	2	Day
Cementing	0.5	1	4	Day
Production Casing Length	430	490	730	Feet
Production Casing Reaming	4	7	17	Day
Production Casing Reaming ROP	25	82	117	Feet per Day
Production Casing Installation	1	1.5	2	Day
Gravel Pack Installation	0.5	1.5	2.5	Day
Well Development	8	46	156	Day
Constant-Rate Test AND Water Sampling	8	10	36	Day
Video Survey	1	1	1	Day
Total Work Days	**55**	**113**	**249**	Day
Total Days to Create Well	**35**	**58**	**84**	Day
Total Days to Develop and Test	**19**	**59**	**165**	Day
Start Day to End Day	89	142	272	Day
Total non-work Days	9	23	61	Day

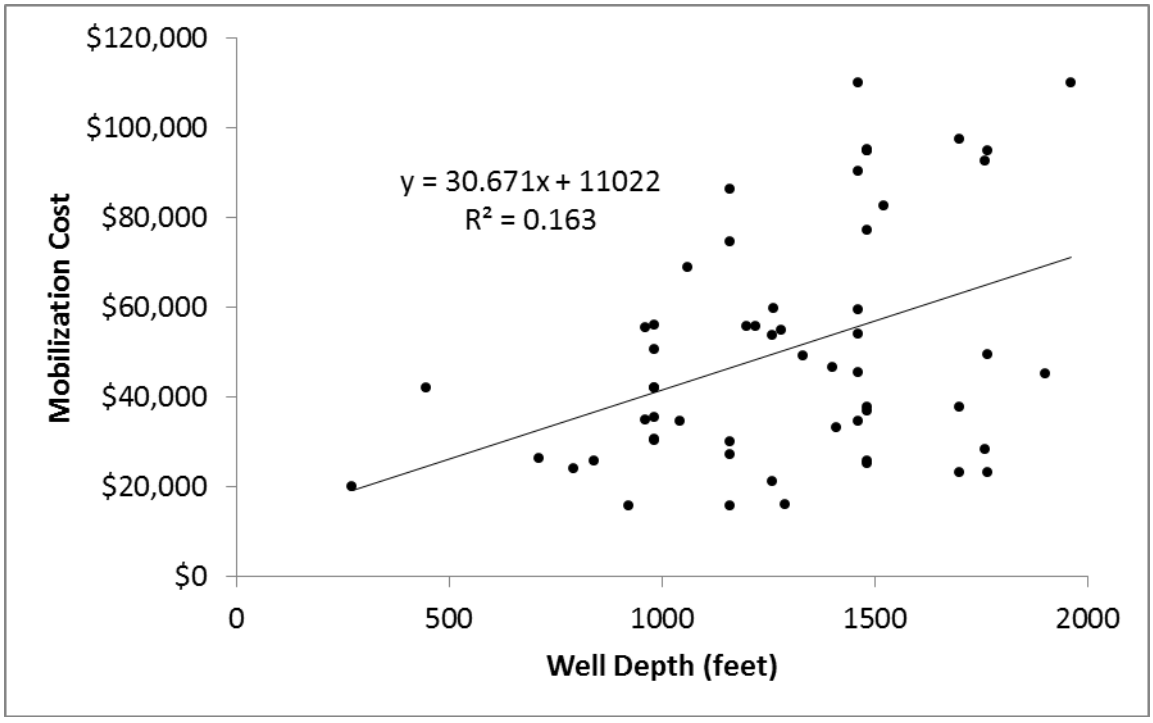

Figure 88. Mobilization/demobilization costs. Data from Glotfelty (2013).

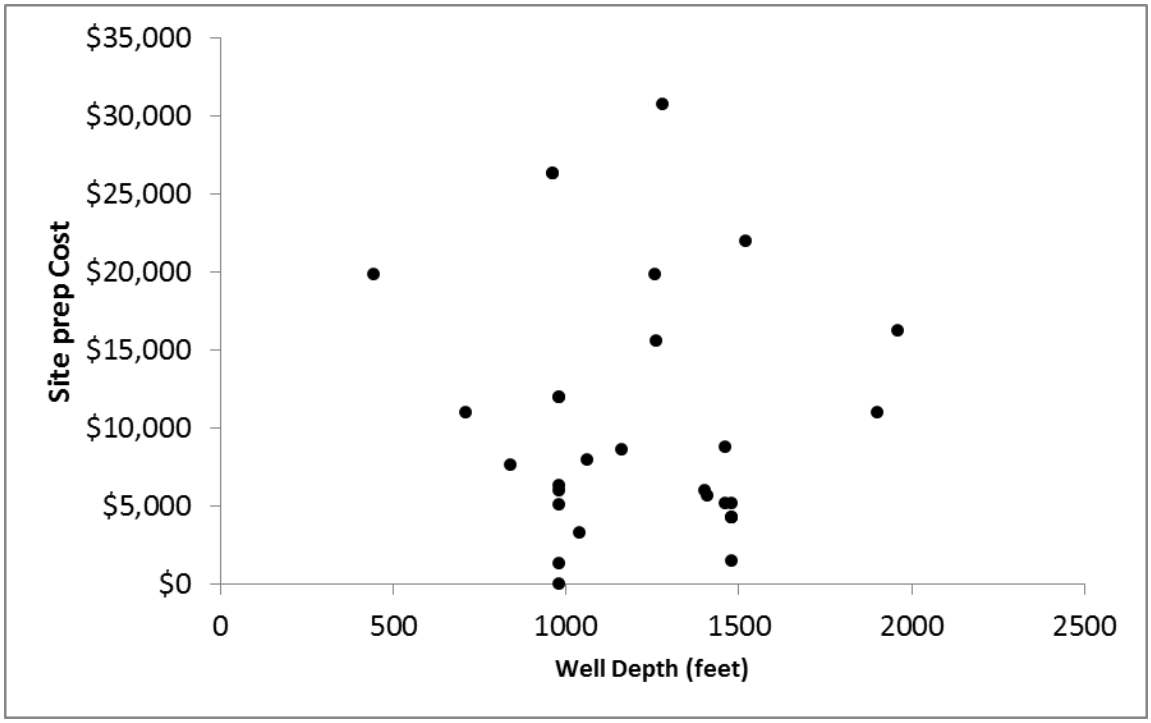

Figure 89. Site preparation costs. Data from Glotfelty (2013).

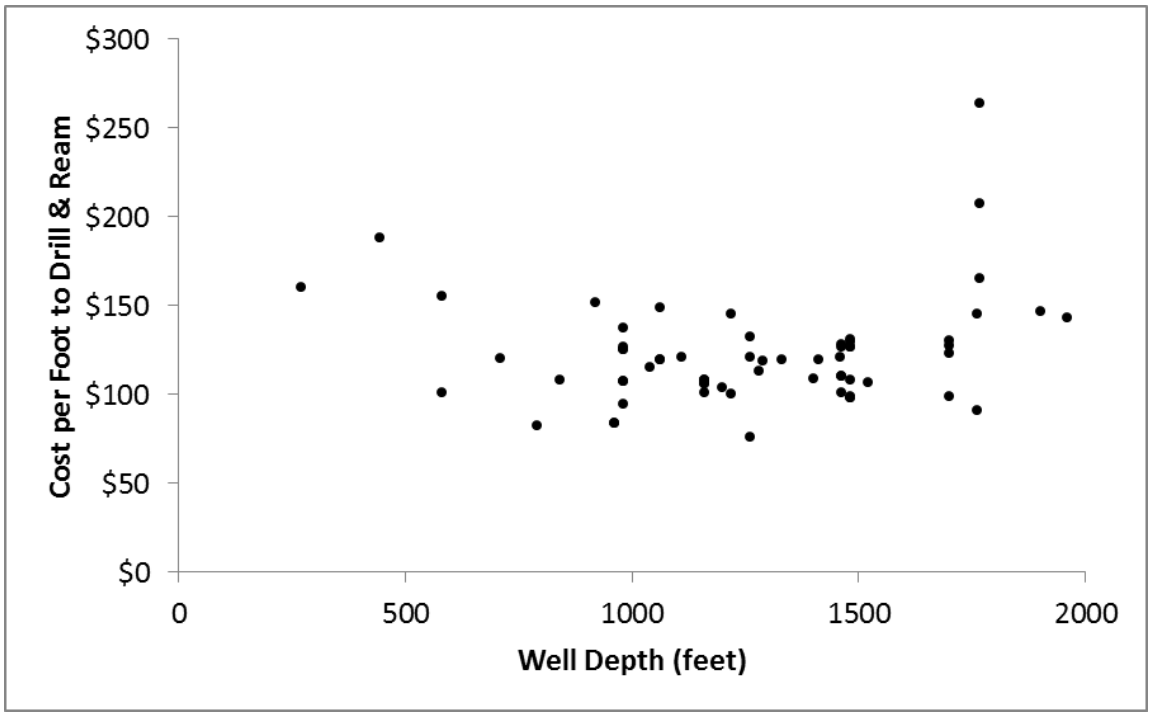

Figure 90. Cost per foot to drill and ream. Data from Glotfelty (2013).

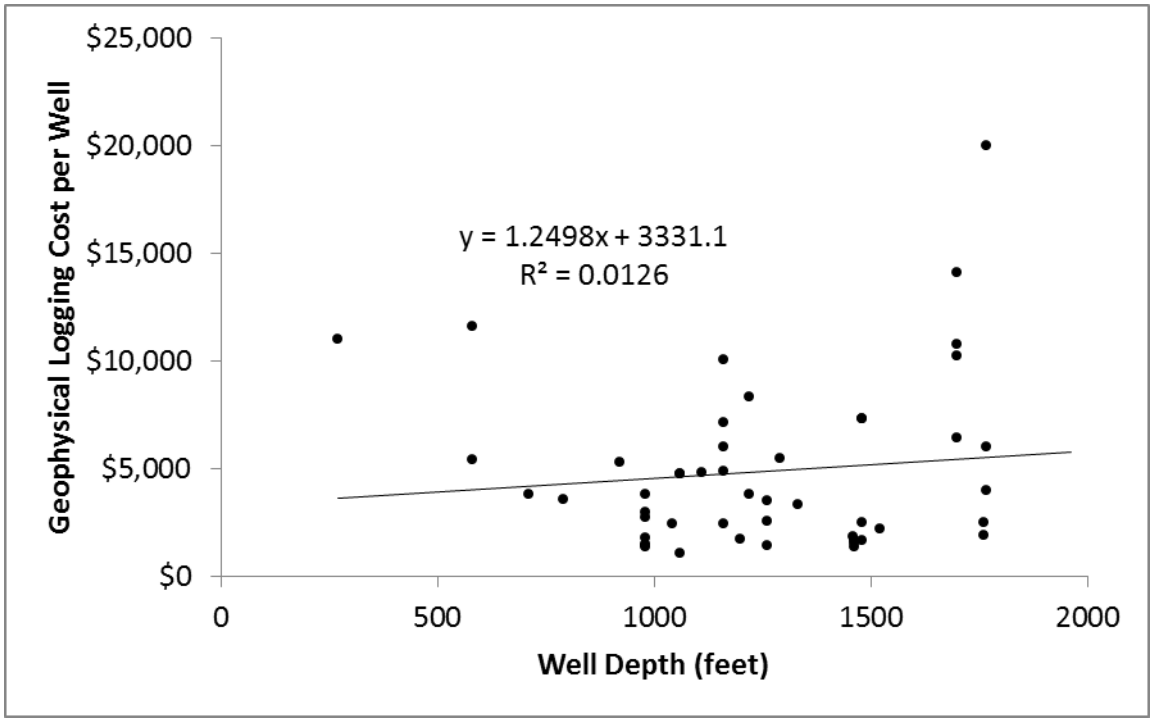

Figure 91. Geophysical logging costs. Data from Glotfelty (2013).

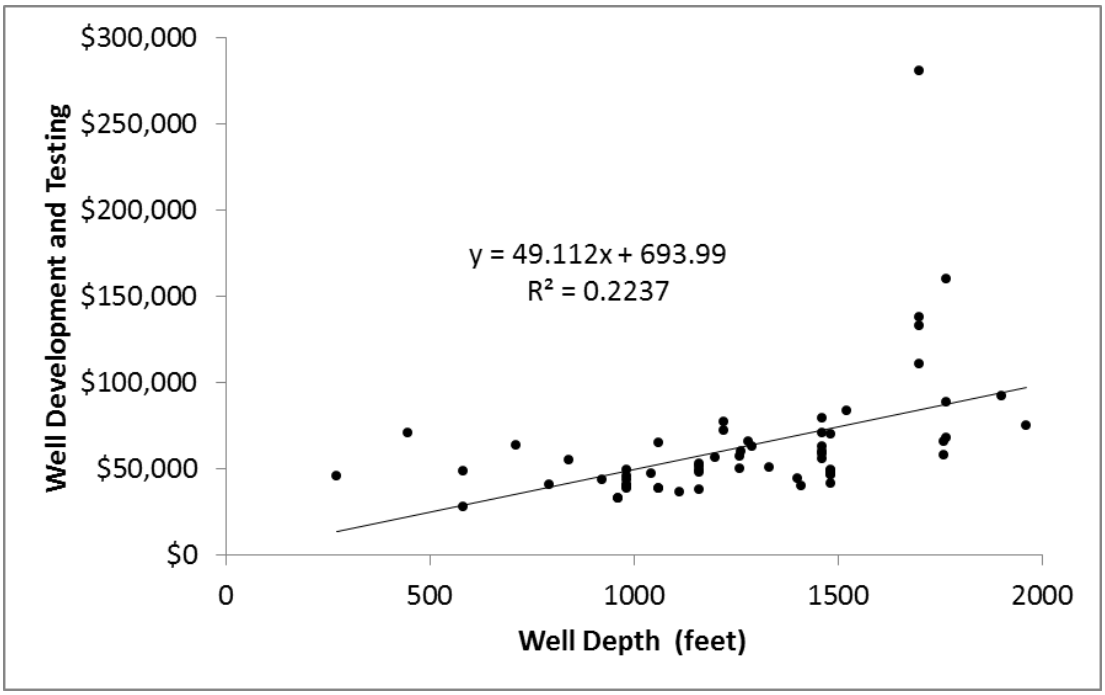

Figure 92. Well development and testing costs. Note: Costs include emplacement and removal of pumps for well tests, a 72-hour pump test, water quality sample, gyroscopic alignment survey, well disinfection, and a well video. Data from Glotfelty (2013).

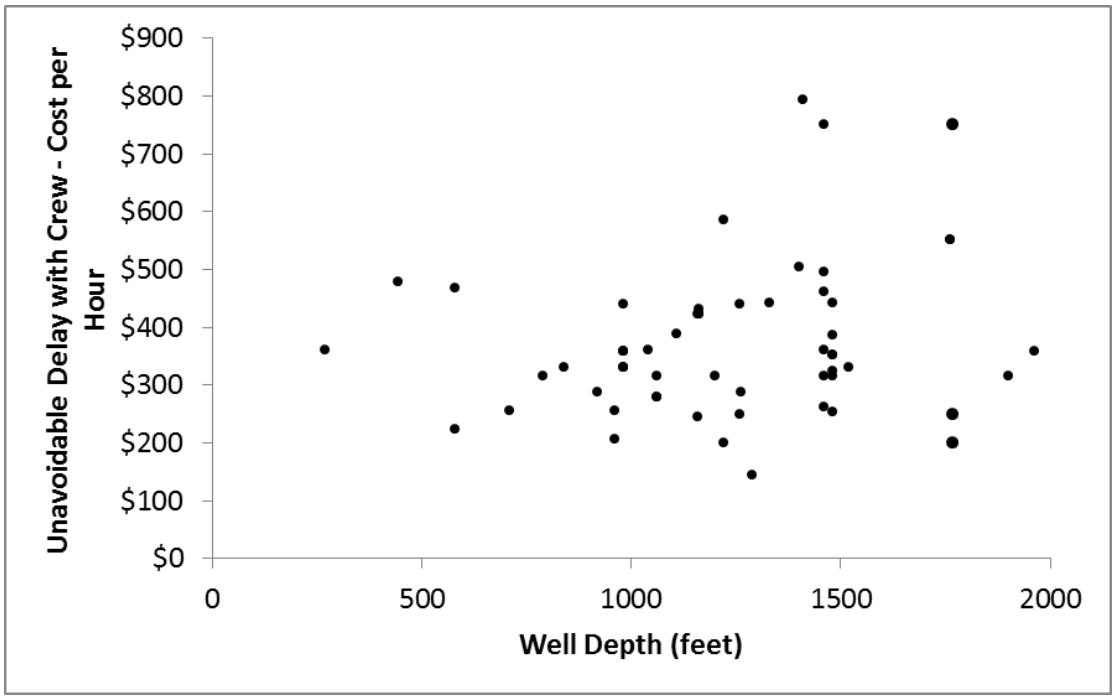

Figure 93. Unavoidable delay with crew, cost per hour. Data from Glotfelty (2013).

Because only two water well drillers were able to provide estimates on daily rig rates and as these rates were only for medium depth wells, an alternative approach was necessary. *Unavoidable Delay with Crew* was a section on most of the post bids received, so simply converting this cost to a day rate was logical (Table 18). We also added the day rate for the rig used to drill the Castle Pines, Colorado directional groundwater well.

Table 18. Hourly to day rig rates calculated from post bids: *Unavoidable Delay with Crew* and Williams (2008)*.

Water Rig Rates	Hourly	Calculated Daily
First Quartile	$302	$7,240
Median	$351	$8,436
Third Quartile	$436	$10,466
Rig for Castle Pines, CO horizontal well*		$20,731

Because rig rate data was still lacking, daily petroleum rig rate data from April 2014 was used with permission from Rig Data (2014). The Rig Data (2014) dataset provides the daily rig rates for five different petroleum rig classes based on horse power and rated depth. Data is then additionally classified by six continental U.S. locations. Because the distribution of cost within each depth bin is unknown, the cost plotted was assumed to be for a rig in the middle of the depth range bin. The rated depth category of 0-7,000 ft was altered to reflect the fact that petroleum rigs drilling at less than 1,000 ft is rare and thus the cost should not be plotted in the middle of the 0-7,000 ft bin but rather the middle of a bin from 1,000 ft to 7,000 ft (2,500 ft). Rig Data was plotted and

linearly regressed with a high correlation coefficient (Figure 94). The linear regression seemed reasonable because as rated depth went to zero, there was still a day rate of $7,000. This perhaps reflects the base cost of labor and equipment that is always necessary, regardless of borehole length.

The three quartiles of water day rig rates were also added to the plot (Figure 94). The rated depth for the water rigs was unknown. However the median depth of the post bids was 1,263 feet. The rated depth is likely greater than this median depth; perhaps around 5,000 feet. Interestingly, the groundwater rig day rate is near the linear regression of the petroleum rigs day rate when using the median groundwater post bid depth.

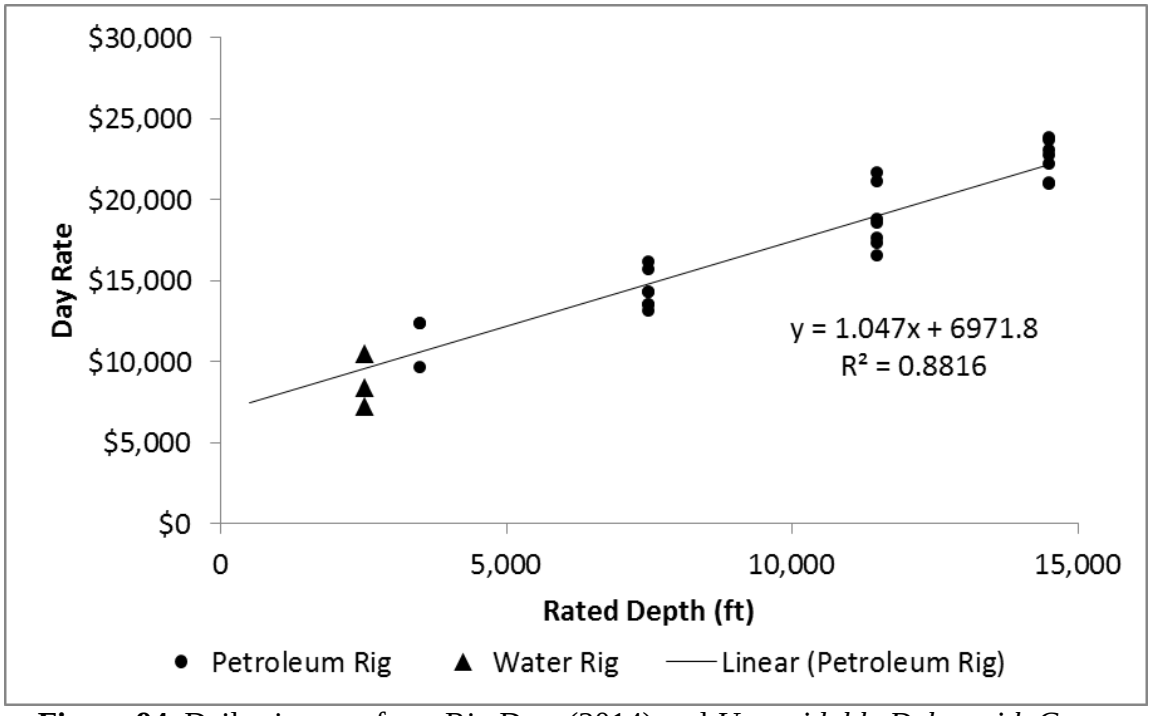

Figure 94. Daily rig rates from Rig Data (2014) and *Unavoidable Delay with Crew*.

Selection of the correct rig depends on pullback capacity and horse power to run draw works & mud pumps. The optimal rig selection will require an iterative approach to well design and the possible addition of extra equipment (mud pumps, generators etc.). However, as a first approximation one may utilize the rated depth day rate. As the rig selection will primarily be based on pullback capacity, it is necessary to convert the rated depth to pullback capacity. The rated depth is the maximum pullback capacity assuming a vertical hole for a given drill pipe weight and bottom hole assembly weight.

Unfortunately there is no standard method to calculate rated depth from pullback capacity. Rigs operating at deeper depths will require heavier drill pipe to withstand increased forces, in this case the manufacturer will calculate rated depth with a heavier drill pipe assumption and greater overpull. To overcome this issue, we searched the internet for as many pullback & rated depth combinations as we could find. With 57 pullback & rated depth data points, we plotted the data and regressed it using a polynomial fit. The R^2 showed a high correlation and the fit seemed reasonable.

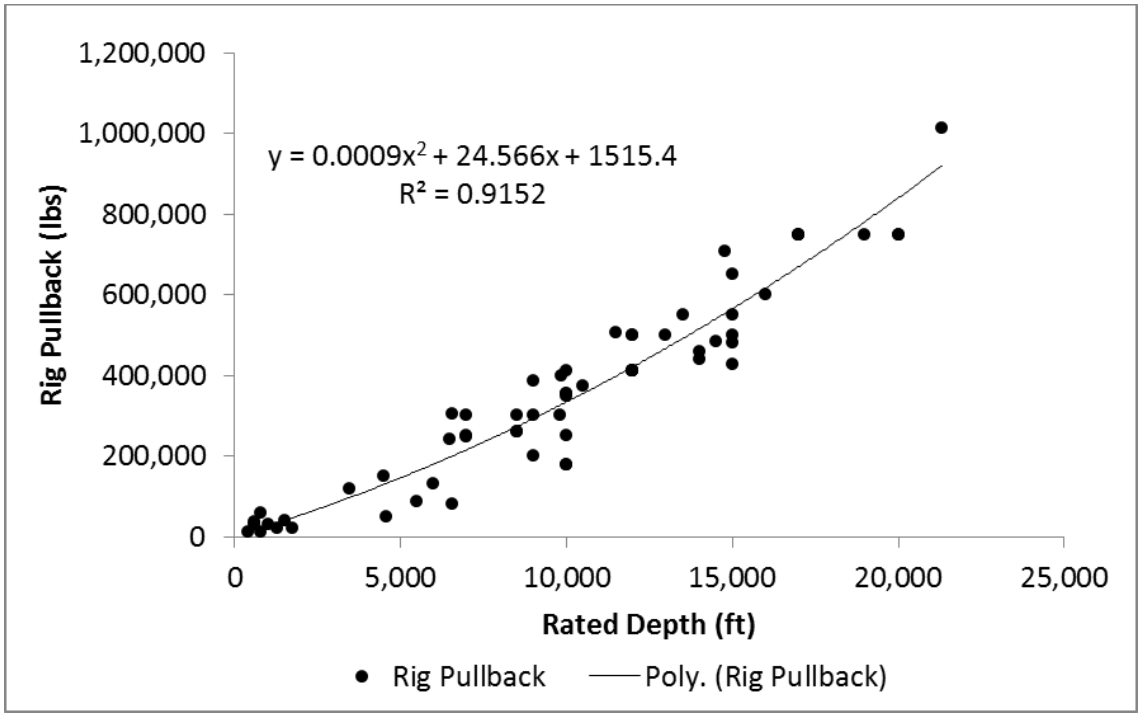

Figure 95. Rated depth to rig pullback relationship.

A new plot of day rate for a given pullback capacity is generated using this regression (Figure 96). While it was not possible to add the water rig day rates from the post bid data (too many assumptions at this point), we did have pullback capacity and day rate from a water well driller (Table 16) which was added to the plot (Figure 96). Note that our regression included the water rig day rates.

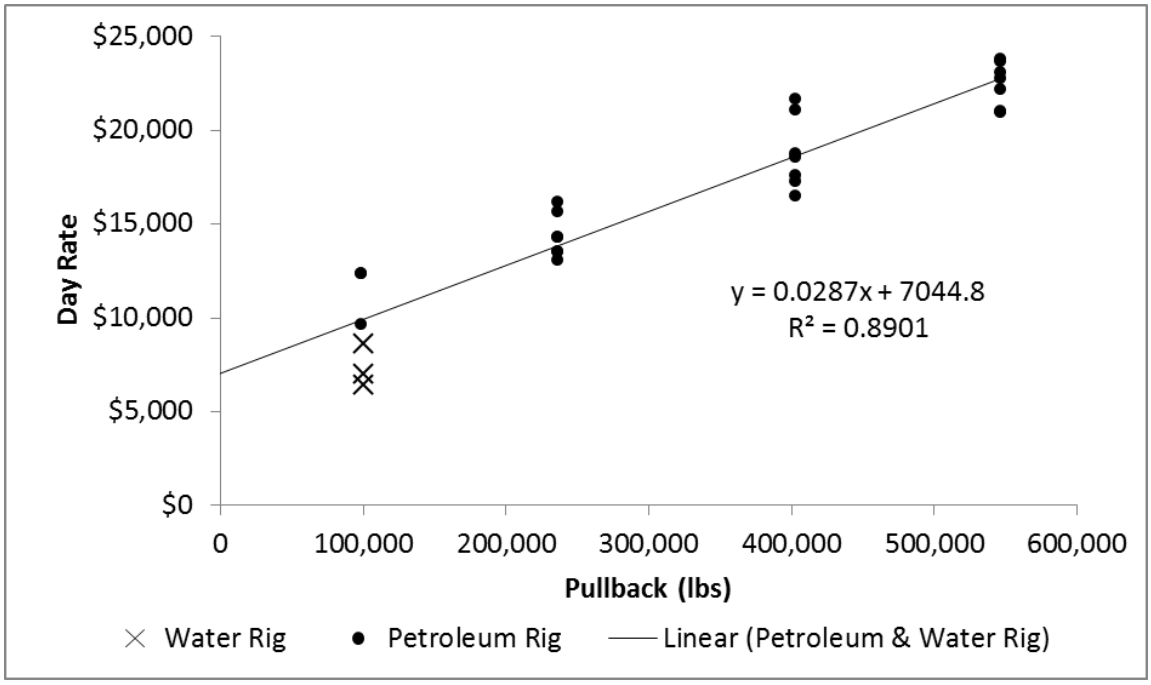

Figure 96. Daily rig rate using a regression of rated depth to pullback capacity. Water rig day rate / pullback from Table 16, remaining data from Rig Data (2014).

Length Dependent Costs

Length dependent cost data collected included casing, cement, and mud disposal. Because casing is the most expensive length dependent cost, most effort was expended on this category. Cement and mud disposal costs together are roughly as important as the casing cost.

Casing Costs

Casing costs were requested from six companies with four companies supplying data. The data in Table 19 was retrieved for pressure tested pipe with the outside diameters listed and thickness around 0.25 inches. The cost per foot quotes were then changed to cost per cubic foot using the specific weight of steel as 490 lbs per cubic foot (Table 19).

Additional data was collected from *The OCTG Situation Report* which tabulates OCTG prices from across the country, Figure 97 (Murphy, 2013). It should be noted that the data used from Murphy (2013) was only for non-premium pipe connections and was an average of seamless and electric welded pipe. With the data collected, we also made a regression of cost per cubic foot versus minimum yield strength (Figure 98). Please note that we only plotted the LCS data from Table 19 in Figure 98 because the cost data of special alloys (HSLA, SS) were not comparable.

Casing costs per cubic foot are relatively independent of diameter (Figure 97). Because the cost of casing is essentially independent of diameter and hence volume, one can easily estimate cost. A reasonably accurate cost estimate for a given pipe can be made by first determining the yield strength of pipe needed. Next determine the cost per unit volume for the required yield strength (Figure 98). Then, determine the volume of steel necessary to build the pipe for a desired diameter and wall thickness. Finally, multiply the volume of steel needed by the cost per volume of the selected pipe grade.

Table 19. Cost of casing per cubic foot.

Outside Diameter in inches	Blank Casing (Cost per cubic Foot)			Full Flow Louvered Screen (Cost per cubic Foot)	
	LCS	HSLA	SS	HSLA	SS
24.00	$232	$983	$2,631	$1,489	$3,138
16.00	$231	$982	$2,651	$1,546	$3,216
12.75	$250	$1,003	$2,679	$1,631	$1,811
8.625	$247	$956	$2,667	$1,733	$3,422
Median	**$240**	**$982**	**$2,659**	**$1,589**	**$3,177**
Companies Participating	3	1	1	1	1

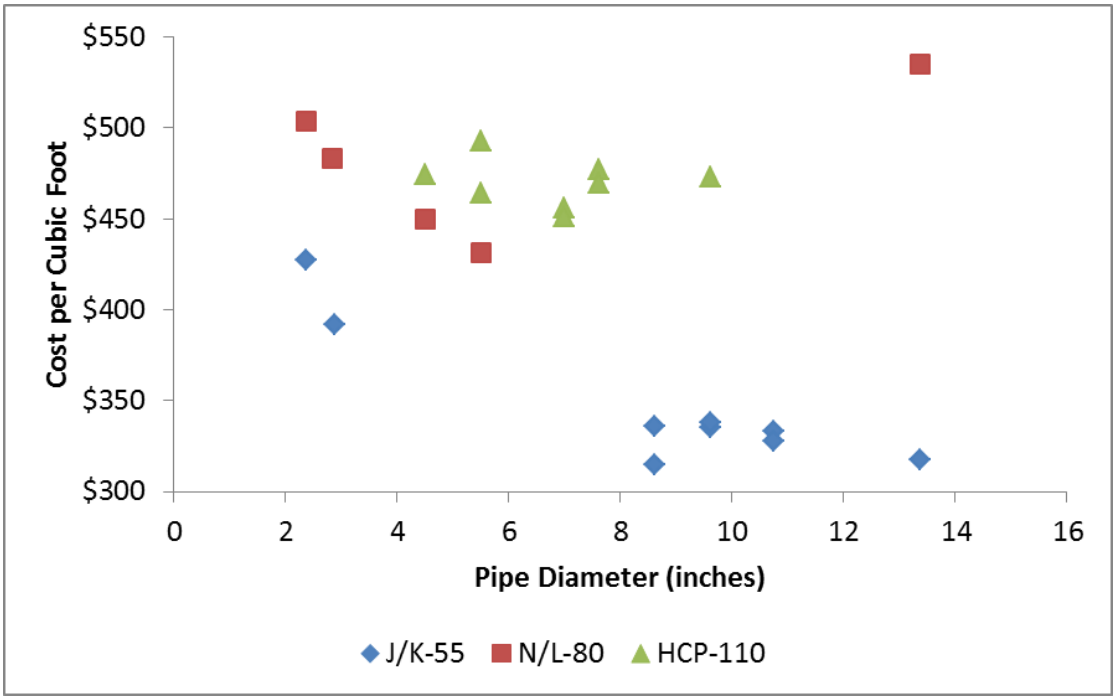

Figure 97. OCTG cost per cubic foot. Data from Murphy (2013).

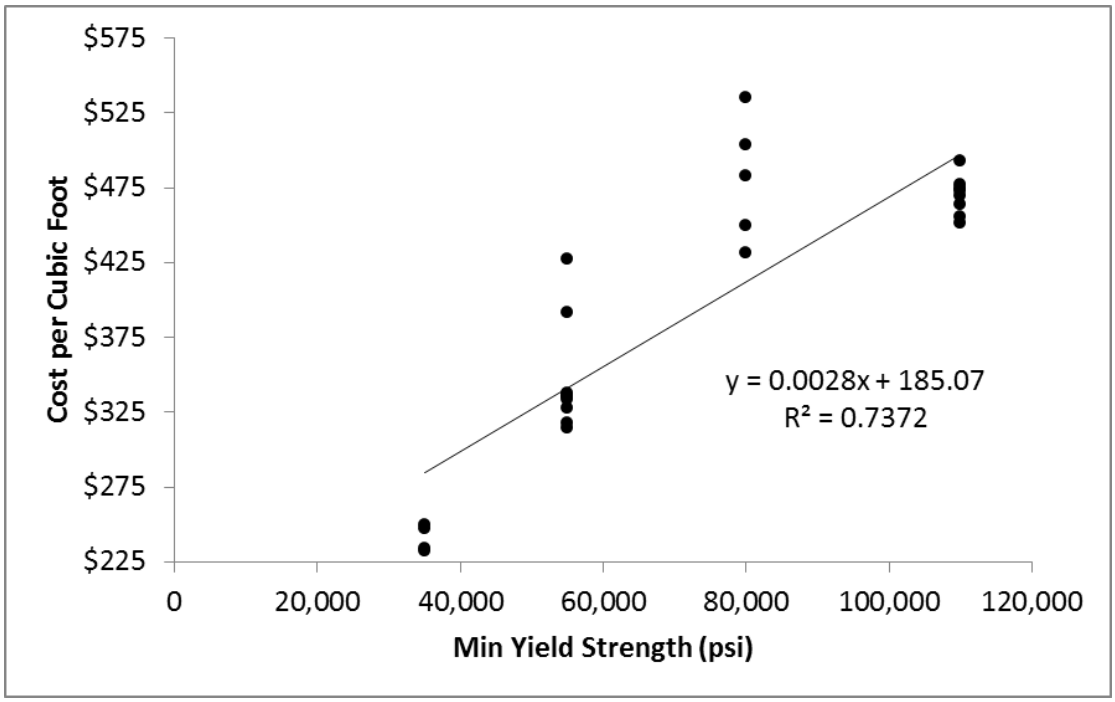

Figure 98. Casing cost per cubic foot versus yield strength. Data from LCS in Table 19 and Murphy (2013).

Other Costs

Other length dependent costs include cement, mud disposal, and filter pack material. Only limited data was available for this component of cost, with a majority of it coming from Petrey and Bennett (2006). It is interesting to note that both the cement costs from the post bids and Petrey and Bennett (2006) are in excellent agreement. Fixed site costs were put in this section so as to add continuity to the data from Petrey and Bennett (2006).

Table 20. Cost data from Petrey and Bennett (2006) adjusted for inflation using CCI.

	Misc. Fixed Costs	Low	High
Site	Site Prep/Restoration	$3,579	$8,948
	Drill Pad Cost	$11,930	$41,755
Mud Disposal	**Hole Diameter**	**Cost per Foot**	**Cost per Cubic Foot**
	12	$9.54	$12.15
	18	$17.90	$10.13
	24	$29.83	$9.49
	36	$59.65	$8.44
Cement	**Casing-Hole Diameter**	**Cost per Foot**	**Cost per Cubic Foot**
	8-12	$5.97	$13.67
	12-17	$10.74	$13.58
	16-22	$17.30	$13.91
	24-29	$19.09	$13.21

Table 21. Cement and filter pack costs from post bid data.

	Cement Cost per Cubic Foot	Filter Pack Cost per Cubic Foot
Min	$6	$7
Median	$14	$22
Max	$25	$37

COST – BENEFIT RESULTS

Cost Model Input

Estimating the cost of a well requires many assumptions. The cost estimate accuracy is thought to be around 50%. Actual well costs may be twice as much or half as much as those modeled here. We attempted to be as conservative as possible when estimating cost. Because we were interested in comparing the cost of vertical wells to horizontal wells, conservative in our methodology meant modeling vertical well cost as

low as reasonably possible and horizontal well cost as high as reasonably possible. By modeling in this way we hoped to bracket the maximum horizontal well to vertical well cost ratio.

Vertical well casing strength requirements were taken from the AWWA Standard A 100-84 in Roscoe Moss Company (1990). This standard gives the minimum recommended casing thicknesses for various casing sizes at a given depth. For the horizontal wells, we ensured that the casing collapse resistance was at least 1.5 times greater than the overburden pressure (1 psi/ft). For casing yield strength, we used a safety factor of 1.5 with the calculations from models developed in Chapter V. The safety factor of 1.5 was chosen based on recommendations from Roscoe Moss Company (1990).

The model cost parameters were determined from the regressed equations found in the data collection section. For the vertical rig rate, the equation used was

$$RigRate_{Vertical} = 0.0287 Rig_{Pull} + 7044, \tag{158}$$

where $RigRate_{Vertical}$ is the rig rate in dollars per day, and Rig_{Pull} is the pullback requirement in lbs. The calculation of Rig_{Pull} was outlined in Chapter V. In this calculation we chose overpull to be 70% of the required pullback. This choice was based upon the rated depth to pullback capacity findings (Figure 96). The rated depth already has an overpull built into it. Our goal was to find this ‘standard’ overpull and then use it in our modeling. To determine ‘standard’ overpull, we made assumptions of drill pipe weight at various rated depths: at 3,500 feet – 14 lbs/ft; at 7,500 feet – 17 lbs/ft; at 11,500 feet – 19.5 lbs/ft; and at 14,500 feet – 24.7 lbs/ft. We then added a bottom hole

assembly at 20,000 lbs. Using these assumptions, we found that if overpull was 70% of the required pullback, then a very close match between the pullback methods was achieved and hence the built in overpull determined (Table 22). Mobilization was assumed to be one day.

Table 22. Rig overpull determination.

Rated Depth (ft)	Regression Pullback (lbs)	Drill Pipe Assumptions Pullback (lbs)	Ratio
3,500	98,521	103,300	1.05
7,500	236,385	236,750	1.00
11,500	403,049	401,225	1.00
14,500	546,947	628,855	1.15

For the utility rig rate, we used the regressed equation determined in the data collection section. The utility rig rate is

$$RigRate_{Utility} = \max\left[\text{abs}\left[Rig_{Thrust}\right], Rig_{Pull}\right] \times 0.0014 + 147.3, \tag{159}$$

where $RigRate_{Utility}$ is the utility rig rate in dollars per foot and Rig_{Thrust} is the rig thrust requirement calculated using methods in Chapter V. Overpull and over-thrust were taken to be 70% of required pullback or thrust depending on which was greater. Mobilization was taken to be $50,000.

Because we only had one data value for the slant petroleum rig rate, we simply set $RigRate_{SlantPetrol}$ = $22,500 per day. Slant petroleum rig mobilization was taken to be one day. While we did calculate required rig torque capacity, we did not attempt to match any rig (vertical, slant, or utility) to required torque capacity. We assumed that the

rig chosen via the pullback calculation would have enough torque to complete the project.

The single greatest variation of model input is the rate of drilling penetration. From Table 17 and discussions with groundwater drillers, the average daily ROP for water wells is 50 feet per day to 300 feet per day. This is slower than petroleum drillers which reported ROP from 800 feet per day to 2,400 feet per day. To account for this spread, we modeled two ROPs, a slow ROP of 50 ft/day and a fast ROP of 1,000 ft/day. We would have liked to complete a similar evaluation for the utility rigs, however we were only able to obtain cost per foot. In addition, the variability on a cost per foot basis for utility rigs was only two to three times.

For downhole directional equipment, we took the day rate to be $11,000 and did not use a mobilization fee. The directional slowness factor was taken to be 1.3; in other words, directional components (buildup & horizontal section) ROP is 1.3 times slower than vertical ROP. In the petroleum industry, this directional slowness factor is usually taken to be 1.05-1.15. We chose a slower factor to be conservative.

We chose a borehole diameter of 17.5 inches. We kept the outside diameter of the casing constant at 13.38 inches, only adding thickness to the inside diameter. We assumed the radius of curvature was 1,338 feet, instead of 1,750 feet as would be suggested by the industry rule of thumb. This less conservative, tighter radius was chosen because radii tighter than the industry rule of thumb are routinely achieved especially at larger borehole diameters. This radius of curvature equals a conservative

build rate of 4.28° per 100 feet. This build rate also does not invalidate our soft string model, as referenced in Chapter V.

For the casing specifications we used tables of common OCTG pipe from American Petroleum Institute (1982) as referenced in Halliburton (1995). Once a specific pipe for a given well was chosen from these tables (based on calculation from Chapter V), we then needed to calculate its cost. The cost per unit volume was determined from the linear regression based on yield strength (Figure 98). The casing cost per unit volume was determined as

$$CasingCost_{UnitVol} = 0.0028 Yield_{psi} + 185.07, \quad (160)$$

where $CasingCost_{UnitVol}$ is the cost of casing in dollars per cubic foot, and $Yield_{psi}$ is the yield strength of the casing in psi. To determine the cost per foot of casing, we simply used the pipe outside & inside diameter to calculate the volume of steel needed per foot of hole.

Cement and filter pack costs were taken to be equal so as to eliminate the need to assume a production interval length. It is logically assumed that wherever cement is needed that a filter pack is not needed and vice versa. The cement & filter pack cost was taken to be \$16 ft^{-3}; the cost per foot simply being the void space between the casing the borehole. Mud disposal cost was taken to be \$10 ft^{-3}. Site prep and geophysical logging costs were taken to be \$5,000 and \$2,000 respectively; these costs are likely on the low side.

Well development and testing cost likely has the greatest variability and therefore error in computation. From the post bid data, well development ranged from \$20,000 to

$250,000. The data did show a weak trend towards higher well development costs at greater depths. The cost of equipment travelling down hole is marginal. The increased cost is likely derived from greater wellbore screened length and therefore a longer interval to develop. Our approach to the estimate this cost parameter is weak at best. We simply took the cost of well development and testing as the regression (Figure 92):

$$WellDev = ScreenLength \times 49.112 + 639.99, \quad (161)$$

where *WellDev* is the cost to develop and test the well in dollars, and *ScreenLength* is the length of the horizontal section if the well is horizontal or it is the depth of the well if it is vertical. If the *WellDev* cost of the vertical well was greater than the *WellDev* cost of the shortest horizontal well for a given TVD, we changed the vertical *WellDev* cost to that of the shortest horizontal well *WellDev* cost.

To generate output comparing similar wells, we kept much of the input data the same from case to case. The input that was held constant may be found in (Table 23). Note that we assume one casing size throughout the length of the well. We did not account for surface / conductor casing, intermediate casing, or production casing / well screen. We simply assumed the 13.38 inch outside diameter pipe was the same throughout the length of the well and perforated (at no additional cost) where necessary.

All model input referenced in this section and output referenced in next section is in *Supplemental Material, Part C* accompanying this thesis. The vertical well for a specific depth is displayed first in *Part C*, followed by the horizontal wells at the same depth from shortest to longest. Once all the cost estimates for horizontal wells have been determined at a given depth, the next table is for a vertical well at the next deeper depth.

Table 23. Model input / output setup with constant parameters.

Parameter	Value	Unit	Parameter	Value	Unit
TVD	Varies	feet	Upper Section Length	Varies	feet
Borehole Diameter	17.5	inch	Buildup Section Length	Varies	feet
Casing Diameter	13.38	inch	Horizontal Section Length	Varies	feet
Radius of Curvature	1,338	feet	Total Well Length	Varies	feet
Horiz. Section Angle	0	deg	Calc. Optimal Rig Angle	Varies	deg
ROP Slow	50	ft/day	Calc. Rig Pullback	Varies	lbs
ROP Fast	1,000	ft/day	Overpull	Varies	lbs
Rig Up & Complete	Varies	days	Selected Rig Pullback	Varies	lbs
Rig Type	Varies		Calc. Rig Thrust	Varies	lbs
Min Rig Entry Angle	Varies	deg	Over-thrust	Varies	lbs
Max Rig Entry Angle	Varies	deg	Selected Rig Thrust	Varies	lbs
Friction Coefficient	0.4		Calc. Rig Torque	Varies	ft-lbs
Buoyancy Factor	0.85		Calc. Collapse Resistance	Varies	psi
Directional Factor	1.3		Calc. Casing Compress	Varies	lbs
			Calc. Casing Tensile	Varies	lbs
AWWA A 100-84 Min Req			Well Cost		
Wall Thickness	Varies	inch	Rig Mobilization	Varies	
Outside diameter	12.75	inch	Rig Rate	Varies	/day
Inside diameter	Varies	inch	Directional Rate	Varies	days
Collapse Resistance	Varies	psi	Directional Days Slow	Varies	days
Body Yield Strength	Varies	lbs	Directional Days Fast	Varies	days
			Days to D&C Slow	Varies	days
Casing Specifications			Days to D&C Fast	Varies	/day
Casing Type	Varies		**Total Rig Cost Slow**	Varies	
Min Yield Strength	Varies	psi	**Total Rig Cost Fast**	Varies	
Outside Diameter	13.38	inch	Casing cost	Varies	/ft
Inside Diameter	Varies	inch	Cement / Filter Pack	$11	/ft
Wt per ft with cplg	Varies	lbs/ft	Mud disposal	$17	/ft
Collapse Resistance	Varies	psi	**Depth Dpnd. Total Cost**	Varies	
Body Yield Strength	Varies	lbs	Site Prep	$5,000	
Young's Modulus	2.9E+07	psi	Geophysical Logging	$2,000	
			Well Develop / Testing	Varies	
Safety Factor			**Fixed Cost**	Varies	
Collapse Resistance	Varies				
Body Strength	Varies		Total Well Cost Slow	Varies	
			Total Well Cost Fast	Varies	
Length Depend. Cost			Contingency	Varies	
Casing Cost	Varies	/ft^3	**Final Well Cost Slow**	Varies	
Cement/Filter Pack Cost	$16	/ft^3	**Final Well Cost Fast**	Varies	
Mud Disposal Cost	$10	/ft^3			

Cost Model Output

We made cost estimates for 60 wells (Table 24-Table 27). The most important finding from our cost estimates was that the relative cost of a horizontal well compared to a vertical well decreased with depth. At greater depths a horizontal well is significantly more economically feasible compared to a vertical well (Table 25 & Table 27). This cost competitive trend may reveal why horizontal wells are more prevalent in the petroleum industry than the groundwater industry.

We also found that the relative cost between a horizontal well and a vertical well is not dramatically impacted by the rate of penetration. It is logical to assume that the penetration rate for a horizontal well will be similar to a vertical well (1.3 times slower for directional sections). It is interesting, upon comparison of Table 25 & Table 27 that the relative cost of the horizontal well compared to the vertical well is roughly the same (within a factor of two) despite a rate of penetration difference of greater than twenty times.

Other workers have found that horizontal wells cost 1.5-3 times as much as vertical wells (Jehn-Dellaport, 2004; Joshi, 2003). Our results show similar findings at deeper TVDs and shorter horizontal sections. It must be reiterated that our model input attempted to find the maximum relative cost ratios between horizontal and vertical wells. Actual relative cost ratios are likely lower than those presented here.

Table 24. Cost model output assuming ROP is 50 ft/day.

ROP = 50 ft/day		Length of Horizontal Section (ft)						Rig for Horizontal
		0	500	1,000	1,500	2,000	3,000	
TVD (ft)	50	$41,964	$262,460	$445,236	$655,567	$889,743	$1,429,605	Utility
	250	$88,864	$457,806	$668,705	$897,803	$1,145,088	$1,695,513	Utility
	500	$179,268	$763,800	$1,014,463	$1,283,325	$1,570,374	$2,200,536	Utility
	1,000	$329,705	$2,733,186	$3,326,791	$3,920,396	$4,514,001	$5,701,210	Slant Petrol
	1,500	$502,193	$2,459,639	$2,986,529	$3,536,314	$4,111,904	$5,360,300	Vertical
	2,000	$704,236	$2,909,282	$3,483,623	$4,082,936	$4,710,447	$6,072,046	Vertical
	3,000	$1,252,260	$4,330,350	$5,056,038	$5,814,803	$6,611,047	$8,346,189	Vertical

Table 25. Cost model output assuming ROP is 50 ft/day, normalized to vertical well cost.

ROP = 50 ft/day		Length of Horizontal Section (ft)						Rig for Horizontal
		0	500	1,000	1,500	2,000	3,000	
TVD (ft)	50	1.0	5.8	9.9	14.5	19.7	31.7	Utility
	250	1.0	5.2	7.5	10.1	12.9	19.1	Utility
	500	1.0	4.3	5.7	7.2	8.8	12.3	Utility
	1,000	1.0	8.3	10.1	11.9	13.7	17.3	Slant Petrol
	1,500	1.0	4.9	5.9	7.0	8.2	10.7	Vertical
	2,000	1.0	4.1	4.9	5.8	6.7	8.6	Vertical
	3,000	1.0	3.5	4.0	4.6	5.3	6.7	Vertical

Table 26. Cost model output assuming ROP is 1,000 ft/day.

ROP = 1,000 ft/day		Length of Horizontal Section (ft)						Rig for Horizontal
		0	500	1,000	1,500	2,000	3,000	
TVD (ft)	50	$41,964	$262,460	$445,236	$655,567	$889,743	$1,429,605	Utility
	250	$57,186	$457,806	$668,705	$897,803	$1,145,088	$1,695,513	Utility
	500	$103,289	$763,800	$1,014,463	$1,283,325	$1,570,374	$2,200,536	Utility
	1,000	$149,448	$481,986	$593,191	$704,396	$775,401	$997,810	Slant Petrol
	1,500	$200,267	$520,498	$637,558	$725,540	$845,862	$1,060,876	Vertical
	2,000	$243,346	$635,939	$740,743	$853,181	$959,925	$1,209,467	Vertical
	3,000	$385,408	$968,578	$1,088,294	$1,224,021	$1,346,481	$1,646,698	Vertical

Table 27. Cost model output assuming ROP is 1,000 ft/day, normalized to vertical well cost.

ROP = 1,000 ft/day		Length of Horizontal Section (ft)						Rig for Horizontal
		0	500	1,000	1,500	2,000	3,000	
TVD (ft)	50	1.0	5.8	9.9	14.5	19.7	31.7	Utility
	250	1.0	8.0	11.7	15.7	20.0	29.6	Utility
	500	1.0	7.4	9.8	12.4	15.2	21.3	Utility
	1,000	1.0	3.2	4.0	4.7	5.2	6.7	Slant Petrol
	1,500	1.0	2.6	3.2	3.6	4.2	5.3	Vertical
	2,000	1.0	2.6	3.0	3.5	3.9	5.0	Vertical
	3,000	1.0	2.5	2.8	3.2	3.5	4.3	Vertical

Aquifer (Benefit) Model Input

As shown in Chapter II, the effects of intra-wellbore head loss can be ignored in most cases. It was also found in Chapter II that uniform flux is a reasonable approximation, no worse than 10% discrepancy compared to uniform drawdown. Given this finding, we conduct aquifer (benefit) modeling assuming that one uniform flux segment is adequate. By using one segment to model the well, we therefore generate solutions that are independent of pumping rate. Because we generate aquifer drawdown solutions that are proportional to pumping rate, we can thus compare relative drawdown responses without inherent assumptions on pumping rates. We ran the aquifer model assuming that the discharge was unity; the model output is then simply the aquifer response, $FQ = d,\ F \times 1 = d,\ F = d$.

We used no flux bounds are at $z = 0$ and $z = c$ for all model runs. For some of the runs we assumed the remaining bounds were infinitely far away. For other runs we assumed there were constant head boundaries at $y = 0$ and $y = b$ and the x bounds were infinitely far away. When no steady state is reached, we take the model end time to be 50 years for some cases and one year for other cases. When modeling the vertical well, we assume it is fully penetrating. When modeling the horizontal well, we assume it is located in the midpoint of the aquifer (c/2). When using the constant head boundary conditions, we take the well to be at (b/2). Specific input assumptions are displayed in the bottom cell of each table.

Aquifer (Benefit) Model Output

Model output is normalized to the fully penetrating vertical well. The results tabulated below represent the number of vertical wells replaced by the horizontal well (vertical well replacement ratio). In the first set of simulations, we assumed that vertical hydraulic conductivity was ten times less than lateral hydraulic conductivity. This is similar to clastic aquifers with inter-bedded clays. We set the simulation end time to 50 years. The first set of model output shows that the replacement ratio is higher for lower permeability aquifers (Table 28 & Table 29). This result shows the increased utility for horizontal wells in lower permeability aquifers.

Table 28. Vertical well replacement ratios for first set of model input, gravel aquifer.

Aquifer Vertical Thickness (ft)	100	1.00	1.22	1.45	1.57	1.65	1.72	1.77
	90	1.00	1.25	1.47	1.59	1.67	1.73	1.78
	80	1.00	1.29	1.49	1.60	1.68	1.74	1.79
	70	1.00	1.32	1.51	1.62	1.70	1.75	1.80
	60	1.00	1.35	1.53	1.64	1.71	1.77	1.81
	50	1.00	1.38	1.55	1.65	1.72	1.78	1.82
	40	1.00	1.42	1.58	1.67	1.73	1.79	1.83
	30	1.00	1.45	1.60	1.68	1.75	1.80	1.84
	20	1.00	1.48	1.61	1.70	1.76	1.81	1.85
	10	1.00	1.51	1.63	1.71	1.77	1.82	1.86
k_x & k_y = 1E-2 ft/s		0	500	1000	1500	2000	2500	3000
$k_z = k_x/10$		**Horizontal Well Length (ft)**						
Gravel		S_s = 1E-5 /ft, r_w = 0.5 ft, end time 50 years, no flux at z = 0 & $z = c$, remaining bounds infinitely far away						

Table 29. Vertical well replacement ratios for first set of model input, silt aquifer.

Aquifer Vertical Thickness (ft)								
	100	1.00	1.42	1.99	2.41	2.76	3.07	3.36
	90	1.00	1.49	2.06	2.48	2.82	3.13	3.42
	80	1.00	1.56	2.13	2.54	2.89	3.20	3.49
	70	1.00	1.64	2.20	2.61	2.95	3.26	3.55
	60	1.00	1.72	2.28	2.68	3.02	3.33	3.61
	50	1.00	1.81	2.36	2.75	3.09	3.39	3.68
	40	1.00	1.91	2.44	2.82	3.16	3.46	3.74
	30	1.00	2.01	2.52	2.89	3.22	3.52	3.88
	20	1.00	2.11	2.59	2.96	3.33	3.62	3.91
	10	1.00	2.20	2.68	3.04	3.36	3.65	3.93
k_x & k_y = 1E-7 ft/s		0	500	1000	1500	2000	2500	3000
$k_z = k_x/10$		**Horizontal Well Length (ft)**						
Silt		S_s = 1E-5 /ft, r_w = 0.5 ft, end time 50 years, no flux at z = 0 & $z = c$, remaining bounds infinitely far away						

In the second set of simulations, we assumed the same input as the first set of simulations but changed the end time from 50 years to one year. This second set of simulations shows the dynamic nature of replacement ratios through time (Table 30 & Table 31). The vertical well replacement ratio is greater at earlier times than at later times. As time goes to infinity, these results show that the three dimensional size of the well (length and circumference) essentially becomes a point sink. It is thought that as time goes to infinity, the replacement ratios go to unity. When deciding between a vertical and a horizontal well, the replacement ratios of the entire lifecycle of the well must be considered.

Table 30. Vertical well replacement ratios for second set of model input, gravel aquifer.

Aquifer Vertical Thickness (ft)								
	100	1.00	1.27	1.55	1.71	1.83	1.92	2.00
	90	1.00	1.30	1.58	1.74	1.85	1.94	2.02
	80	1.00	1.34	1.61	1.76	1.87	1.96	2.03
	70	1.00	1.38	1.64	1.78	1.89	1.98	2.05
	60	1.00	1.43	1.67	1.81	1.91	1.99	2.06
	50	1.00	1.47	1.69	1.83	1.93	2.01	2.08
	40	1.00	1.51	1.72	1.85	1.95	2.03	2.09
	30	1.00	1.56	1.75	1.87	1.96	2.04	2.11
	20	1.00	1.60	1.78	1.89	1.98	2.05	2.12
	10	1.00	1.63	1.80	1.91	2.00	2.07	2.13
k_x & k_y = 1E-2 ft/s		0	500	1000	1500	2000	2500	3000
$k_z = k_x/10$		**Horizontal Well Length (ft)**						
Gravel		S_s = 1E-5 /ft, r_w = 0.5 ft, end time one year, no flux at z = 0 & $z = c$, remaining bounds infinitely far away						

Table 31. Vertical well replacement ratios for second set of model input, silt aquifer.

Aquifer Vertical Thickness (ft)								
	100	1.00	1.59	2.67	3.71	4.76	5.85	6.96
	90	1.00	1.70	2.83	3.91	5.01	6.15	7.31
	80	1.00	1.82	3.00	4.12	5.27	6.47	7.69
	70	1.00	1.96	3.18	4.36	5.56	6.81	8.10
	60	1.00	2.12	3.39	4.61	5.87	7.18	8.54
	50	1.00	2.30	3.62	4.90	6.22	7.60	9.02
	40	1.00	2.51	3.88	5.22	6.62	8.08	9.60
	30	1.00	2.72	4.11	5.49	6.92	8.44	10.71
	20	1.00	2.96	4.38	5.80	7.59	9.23	11.07
	10	1.00	3.20	4.70	6.20	7.78	9.45	11.19
k_x & k_y = 1E-7 ft/s		0	500	1000	1500	2000	2500	3000
$k_z = k_x/10$		**Horizontal Well Length (ft)**						
Silt		S_s = 1E-5 /ft, r_w = 0.5 ft, end time one year, no flux at z = 0 & $z = c$, remaining bounds infinitely far away						

In the third set of simulations, we assumed the same input as the second set of simulations but changed the specific storativity from 1E-5 ft^{-1} to 1E-4 ft^{-1}. This third set of simulations shows the dynamic nature of replacement ratios as a function of specific storativity (Table 32 & Table 33). Similar to the second set of simulations, this third set shows the influence of time on replacement ratios. Because specific storativity was increased, the pressure pulse moves through the aquifer at a slower rate, thus effectively moving the end time earlier.

Table 32. Vertical well replacement ratios for third set of model input, gravel aquifer.

Aquifer Vertical Thickness (ft)								
	100	1.00	1.30	1.64	1.84	1.99	2.11	2.21
	90	1.00	1.34	1.67	1.87	2.02	2.13	2.23
	80	1.00	1.39	1.71	1.90	2.04	2.16	2.26
	70	1.00	1.44	1.74	1.93	2.07	2.18	2.28
	60	1.00	1.49	1.78	1.96	2.09	2.20	2.30
	50	1.00	1.54	1.82	1.99	2.12	2.22	2.32
	40	1.00	1.59	1.85	2.02	2.14	2.25	2.34
	30	1.00	1.64	1.89	2.04	2.16	2.27	2.35
	20	1.00	1.69	1.92	2.07	2.19	2.28	2.37
	10	1.00	1.74	1.95	2.09	2.21	2.31	2.39
k_x & k_y = 1E-2 ft/s $k_z = k_x/10$ **Gravel**		0	500	1000	1500	2000	2500	3000
		Horizontal Well Length (ft)						
		S_s = 1E-4 /ft, r_w = 0.5 ft, end time one year, no flux at z = 0 & $z = c$, remaining bounds infinitely far away						

Table 33. Vertical well replacement ratios for third set of model input, silt aquifer.

Aquifer Vertical Thickness (ft)	100	1.00	1.75	3.39	5.07	6.76	8.45	10.14
	90	1.00	1.91	3.69	5.53	7.37	9.21	11.05
	80	1.00	2.10	4.05	6.06	8.08	10.10	12.11
	70	1.00	2.33	4.47	6.68	8.91	11.14	13.36
	60	1.00	2.60	4.96	7.42	9.90	12.37	14.84
	50	1.00	2.92	5.56	8.31	11.08	13.85	16.62
	40	1.00	3.32	6.28	9.38	12.50	15.62	18.75
	30	1.00	3.81	7.14	10.66	14.21	21.27	25.53
	20	1.00	4.40	8.17	12.18	18.07	22.59	28.17
	10	1.00	5.21	9.97	15.07	20.08	25.10	30.12
k_x & k_y = 1E-7 ft/s		0	500	1000	1500	2000	2500	3000
$k_z = k_x/10$		**Horizontal Well Length (ft)**						
Silt		S_s = 1E-4 /ft, r_w = 0.5 ft, end time one year, no flux at z = 0 & $z = c$, remaining bounds infinitely far away						

In the fourth set of simulations, we assumed the same input as the first set of simulations except that vertical hydraulic conductivity was ten times greater than the lateral hydraulic conductivity. This is similar to fractured carbonate aquifers. Because the horizontal well intersects vertical fractures, the replacement ratios in this fourth model output are higher (Table 34 & Table 35) than the first simulations. The increase in replacement ratios between model output from the first and fourth simulation sets is only minor for the thinnest aquifer, but significant for the thicker aquifers. Vertical fractures improve the utility of horizontal wells for thicker aquifers.

Table 34. Vertical well replacement ratios for fourth set of model input, gravel aquifer.

Aquifer Vertical Thickness (ft)								
	100	1.00	1.50	1.62	1.70	1.77	1.82	1.86
	90	1.00	1.50	1.63	1.71	1.77	1.82	1.86
	80	1.00	1.51	1.63	1.71	1.77	1.82	1.86
	70	1.00	1.51	1.63	1.71	1.77	1.82	1.86
	60	1.00	1.51	1.63	1.71	1.77	1.82	1.86
	50	1.00	1.52	1.64	1.71	1.77	1.82	1.86
	40	1.00	1.52	1.64	1.71	1.77	1.82	1.86
	30	1.00	1.52	1.64	1.71	1.77	1.82	1.86
	20	1.00	1.52	1.64	1.71	1.77	1.82	1.86
	10	1.00	1.53	1.64	1.72	1.77	1.82	1.86
k_x & k_y = 1E-2 ft/s		0	500	1000	1500	2000	2500	3000
$k_z = k_x$*10		**Horizontal Well Length (ft)**						
Fractured Gravel		S_s = 1E-5 /ft, r_w = 0.5 ft, end time 50 years, no flux at z = 0 & $z = c$, remaining bounds infinitely far away						

Table 35. Vertical well replacement ratios for fourth set of model input, silt aquifer.

Aquifer Vertical Thickness (ft)								
	100	1.00	2.16	2.67	3.04	3.36	3.65	3.93
	90	1.00	2.17	2.64	3.04	3.36	3.65	3.93
	80	1.00	2.18	2.65	3.04	3.36	3.65	3.93
	70	1.00	2.20	2.66	3.04	3.36	3.65	3.93
	60	1.00	2.21	2.69	3.05	3.36	3.65	3.93
	50	1.00	2.23	2.69	3.05	3.36	3.65	3.93
	40	1.00	2.24	2.69	3.05	3.36	3.65	3.93
	30	1.00	2.24	2.69	3.05	3.36	3.66	3.93
	20	1.00	2.25	2.70	3.05	3.37	3.66	3.93
	10	1.00	2.25	2.70	3.05	3.37	3.66	3.94
k_x & k_y = 1E-7 ft/s		0	500	1000	1500	2000	2500	3000
$k_z = k_x$*10		**Horizontal Well Length (ft)**						
Fractured Silt		S_s = 1E-5 /ft, r_w = 0.5 ft, end time 50 years, no flux at z = 0 & $z = c$, remaining bounds infinitely far away						

In the fifth set of simulations, we attempted to investigate the possible effects of hydraulic fracturing the well. Our model can only change the vertical hydraulic conductivity for the entire aquifer. We therefore cannot rigorously model a discrete fracture zone along the wellbore as would be the case for a stimulated well. Nevertheless, we assume that changing the vertical hydraulic conductivity of our model will at least approximate a hydraulically fractured well. With this goal, we took vertical hydraulic conductivity as 10,000 times greater than the lateral (shale) hydraulic conductivity. The results show a significant increase in replacement ratios (Table 36) compared to the previous simulation.

Table 36. Vertical well replacement ratios for sixth set of model input, shale aquifer.

Aquifer Vertical Thickness (ft)								
	100	1.00	3.76	5.73	7.87	10.19	12.63	15.12
	90	1.00	3.76	5.73	7.87	10.19	12.63	15.12
	80	1.00	3.76	5.73	7.87	10.19	12.63	15.12
	70	1.00	3.76	5.73	7.87	10.19	12.63	15.12
	60	1.00	3.76	5.73	7.87	10.19	12.63	15.12
	50	1.00	3.76	5.73	7.87	10.19	12.63	15.12
	40	1.00	3.76	5.73	7.87	10.19	12.63	15.12
	30	1.00	3.76	5.73	7.87	10.19	12.63	15.12
	20	1.00	3.76	5.73	7.87	10.19	12.63	15.12
	10	1.00	3.76	5.73	7.87	10.19	12.63	15.12
k_x & k_y = 1E-9 ft/s		0	500	1000	1500	2000	2500	3000
$k_z = k_x$*10,000		**Horizontal Well Length (ft)**						
Hydro-Fractured Shale		S_s = 1E-5 /ft, r_w = 0.5 ft, end time 50 years, no flux at z = 0 & $z = c$, remaining bounds infinitely far away						

In the sixth set of simulations, we investigated the effects of hydraulic fracturing the well in less permeable shale with a greater vertical anisotropy. Results from this case show a significant replacement ratio increase with length of horizontal well (Table 37). The two hydraulic fracture simulation sets show significant improvements in replacement ratios. However, our methodology for modeling such a discrete fracture network is quite rudimentary. It is unclear how accurate it is to use vertical hydraulic conductivity to represent a finite zone of fractures and what the vertical hydraulic conductivity value should be. All that is known for certain is that vertical fractures can significantly increase vertical well replacement ratios. By extension, hydraulic fracturing dramatically increases the utility of horizontal wells.

Table 37. Vertical well replacement ratios for seventh set of model input, shale aquifer.

Aquifer Vertical Thickness (ft)								
	100	1.00	17.09	34.20	51.33	68.50	85.71	102.9
	90	1.00	17.09	34.20	51.33	68.49	85.71	102.9
	80	1.00	17.09	34.20	51.33	68.49	85.70	102.9
	70	1.00	17.09	34.20	51.33	68.49	85.70	102.9
	60	1.00	17.09	34.20	51.33	68.49	85.70	102.9
	50	1.00	17.09	34.20	51.33	68.49	85.70	102.9
	40	1.00	17.09	34.20	51.33	68.49	85.70	102.9
	30	1.00	17.09	34.20	51.33	68.49	85.69	102.9
	20	1.00	17.09	34.20	51.32	68.49	85.69	102.9
	10	1.00	17.09	34.20	51.32	68.48	85.68	102.9
k_x & k_y = 1E-11 ft/s		0	500	1000	1500	2000	2500	3000
$k_z = k_x$*1,000,000		**Horizontal Well Length (ft)**						
Hydro-Fractured Shale		S_s = 1E-5 /ft, r_w = 0.5 ft, end time 50 years, no flux at z = 0 & $z = c$, remaining bounds infinitely far away						

In the eighth set of simulations, we attempted to investigate the effects of nearby constant head boundaries (rivers). In this set of model simulations, we simulated a constant head boundary at $y = 0$ and $y = b$, with the horizontal well paralleling these boundaries at $y = b/2$. The x boundaries were taken to be infinitely far away. Model output shows that the replacement ratios are high when implementing constant head boundaries (Table 38 & Table 39). This output shows why Ranney wells and other types of horizontal wells are advantageous in aquifers with nearby constant head boundaries.

These model results also resemble the results from the second set of simulations, which had a model end time of one year. Because the constant head boundary establishes a steady state condition, the well's pressure pulse no longer goes infinitely far away but is arrested at that boundary. This finite boundary condition means that the well size no longer trends to a point sink as time goes to infinity. Therefore, higher replacement ratios are expected in aquifers that have constant head boundaries nearby; with closer boundaries generating higher replacement ratios.

Table 38. Vertical well replacement ratios for eighth set of model input, sand aquifer.

Aquifer Vertical Thickness (ft)								
	100	1.00	1.62	2.82	4.01	5.21	6.45	7.70
	90	1.00	1.74	3.01	4.25	5.52	6.82	8.14
	80	1.00	1.88	3.21	4.52	5.86	7.23	8.63
	70	1.00	2.04	3.43	4.81	6.23	7.69	9.17
	60	1.00	2.21	3.68	5.13	6.64	8.18	9.76
	50	1.00	2.42	3.95	5.49	7.08	8.72	10.40
	40	1.00	2.65	4.26	5.88	7.56	9.31	11.09
	30	1.00	2.91	4.59	6.29	8.08	9.93	11.83
	20	1.00	3.19	4.94	6.73	8.62	10.58	12.59
	10	1.00	3.49	5.28	7.15	9.32	11.43	13.59
k_x & k_y = 1E-3 ft/s		0	500	1000	1500	2000	2500	3000
$k_z = k_x/10$		**Horizontal Well Length (ft)**						
Coarse Sand		S_s = 1E-5 /ft, r_w = 0.5 ft, end time steady state, no flux at z = 0 & $z = c$, constant head at y = 0 and $y = b$, other bounds infinitely far away						

Table 39. Vertical well replacement ratios for eighth set of model input, silt aquifer.

Aquifer Vertical Thickness (ft)								
	100	1.00	1.62	2.82	4.00	5.19	6.42	7.65
	90	1.00	1.74	3.00	4.24	5.50	6.79	8.09
	80	1.00	1.88	3.20	4.50	5.83	7.19	8.57
	70	1.00	2.03	3.42	4.79	6.20	7.64	9.10
	60	1.00	2.21	3.67	5.11	6.60	8.13	9.68
	50	1.00	2.41	3.94	5.47	7.04	8.66	10.31
	40	1.00	2.64	4.24	5.85	7.52	9.24	10.99
	30	1.00	2.90	4.57	6.26	8.03	9.85	12.73
	20	1.00	3.19	4.92	6.69	8.98	10.99	13.27
	10	1.00	3.48	5.35	7.26	9.25	11.32	13.44
kx & ky = 1E-7 ft/s		0	500	1000	1500	2000	2500	3000
kz = kx/10		**Horizontal Well Length (ft)**						
Silt		S_s = 1E-5 /ft, r_w = 0.5 ft, end time steady state, no flux at z = 0 & $z = c$, constant head at y = 0 and $y = b$, other bounds infinitely far away						

CONCLUSIONS

From our analysis, it is clear that the cost and benefit of horizontal wells is very site specific. It is possible that in some cases a horizontal well will cost twice as much as a vertical well and produce fifteen times as much water. Conversely, a horizontal well can cost thirty times more than a vertical well and only produce twice as much water.

The relative cost of a horizontal well compared to a vertical well decreases with increasing depth. The benefit of a horizontal well compared to a vertical well depends on several parameters. Horizontal wells are more effective when: located near a constant head boundary, the aquifer has vertical fractures, the aquifer has lower permeability, the aquifer has higher specific storativity, and the time since the start of pumping is minimal.

Given all the parameters influencing horizontal well cost and benefit, only project specific calculation will determine the most effective well type (vertical or horizontal). From our analysis it is clear that horizontal wells have the potential to be very useful in certain operational and hydrogeologic conditions. It is outside the scope of this thesis to rigorously calculate the overall percentage of groundwater projects that may benefit from horizontal drilling. However, we can speculate on the possible impact of horizontal drilling for groundwater projects by inspecting the use of horizontal drilling in the petroleum industry.

If petroleum wells are assumed similar to groundwater wells, then one may predict the overall utility of horizontal wells for groundwater projects. There are several important caveats to this assumption. First, petroleum wells are usually deeper than

groundwater wells, therefore decreasing the relative cost of horizontal wells for petroleum projects. Second, many groundwater wells are located near surface waterbodies, therefore increasing the utility of horizontal wells for groundwater projects. Third, permeability is typically lower in petroleum reservoirs due to compaction, therefore increasing the utility of horizontal wells for petroleum projects. Fifth, specific storativity is typically less in petroleum reservoirs than aquifers due to compaction, therefore increasing the utility of horizontal wells for groundwater projects.

Finally, the most important difference between petroleum and groundwater wells is the extensive use of hydraulic fracturing in the petroleum industry. Hydraulic fracturing inceases the benefits of horizontal petroluem wells because the fractures propogate vertically (in most cases). No comprehensive history has been found documenting the increase of hydraulic fracturing in the past twenty years. It is thought that the two governmental actions regarding hydraulic fracturing mark the beginning of its extensive use. First was the United States Environmental Protection Agency finding that ther was little to no risk of hydraulic fracturing fluid contaminating groundwater drinking supplies (U.S. EPA, 2004). Second was the 2005 Energy Policy Act that omitted fracturing fluid from the Safe Drinking Water Act (U.S. Congress, 2005).

From our aquifer simulations, vertical fractures are one of the most important factor improving the cost effectiveness of horizontal wells. This is perhaps why the use of horizontal wells in the petroluem industry has increased so rapidly since 2005 (Figure 99). Despite the widespread use of hydraulic fracturing for petroleum wells, such well stimulation will likely not be used in groundwater wells for some time. Therefore, we

assume that the proportion of groundwater projects potentially benefiting from horizontal wells is equal to the percentage of horizontal wells in the petroleum indsutry prior to the widespread implementation of hydraulic fracturing. Using this assumpition, we estimate that horizontal / directional drilling may benefit perhaps 10% - 20% of groundwater projects (Figure 99).

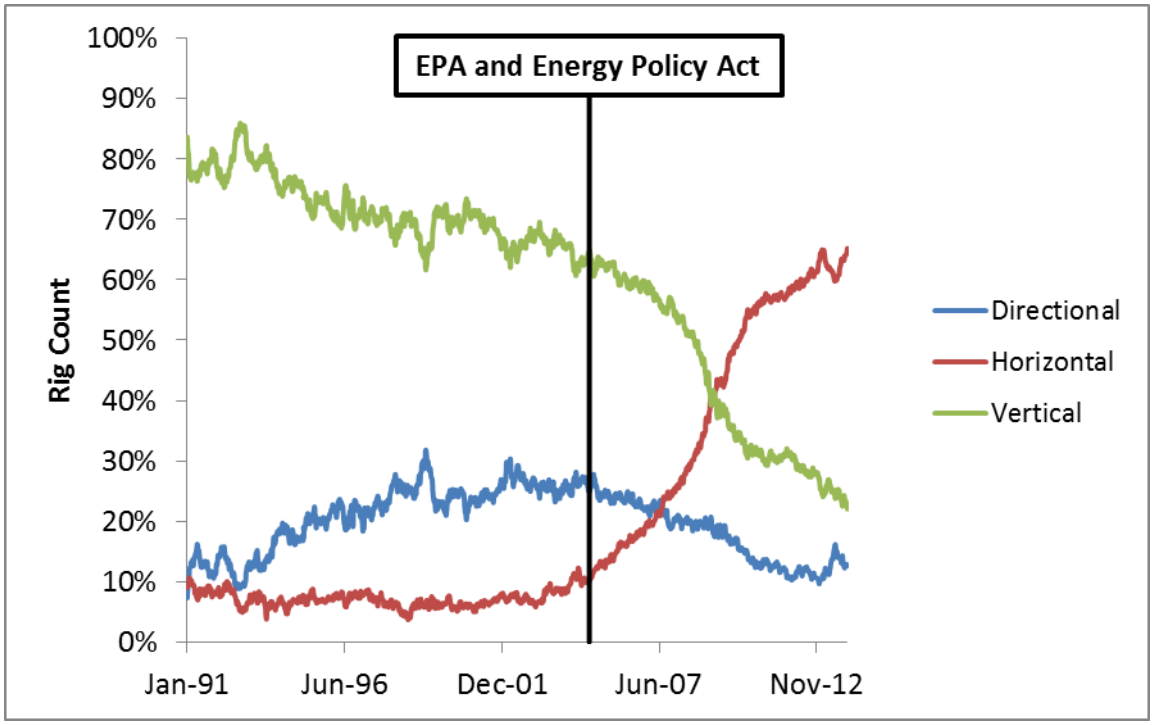

Figure 99. North American petroleum rig count percentages from 1991 to 2013 categorized by drilling type. Data from Baker Hughes (2014).

CHAPTER VII

CONCLUSIONS

LITERATURE REVIEW

From the literature review we find that chemically bound ASR systems have higher recovery efficiencies in aquifers that minimize the mixing of native and injected waters (Merritt, 1986). Aquifers minimizing buoyancy segregation of injected freshwater and native salt water must be thin and/or have a low permeability (Kumar and Kimbler, 1970). However, wells in these aquifers have excessive pressure buildup when injecting and excessive pressure drawdown when extracting.

From the literature review we also find that horizontal wells can benefit traditional groundwater production and physically bound ASR systems. Groundwater wells do not target thin, low permeability aquifers. However, if this is the only aquifer available then excessive pressure buildup and drawdown will occur. Horizontal wells mitigate these pressure buildup and drawdown issues because they have greater contact with the aquifer than vertical wells.

Longer horizontal wells have increased discharge for a given drawdown (specific capacity). The longer the horizontal well, the more effective it will be. From the literature review we find that there are two issues limiting the length and therefore utility of a horizontal well. First, it is possible that well construction will limit the length that the wellbore can be constructed. Second, it is possible that intra-wellbore friction and kinetic head loss will limit the effective length of the wellbore. Stated another way,

intra-wellbore head loss may become so great that additional well length only marginally increases production.

From the literature review, we find that there are several directional groundwater well research needs. First, discussion of intra-wellbore head loss calculation methodologies has been minimal in the groundwater literature. Second, there has been limited discussion in the groundwater literature on how to calculate drilling forces of directional wells. Third, there has been no discussion regarding optimal slant rig entry angles which could minimize the length of the borehole and therefore reduce cost. Fourth, there has been essentially no work completed investigating the cost-benefits of horizontal groundwater wells.

RESEARCH COMPLETED

To address the research needs found through literature review, several models were developed in this thesis. An aquifer model for a directional well accounting for intra-wellbore friction and kinetic head loss was developed. An optimal rig entry angle equation was derived. A drilling force model was developed. A cost-benefit analysis was completed.

When developing the aquifer model, new analytical derivations for several boundary conditions were made. These new derivations are significant in that the infinite series solutions are always rapidly convergent. These new equations are more elegant than previous equations as they do not require approximation or tracking of the pressure pulse. These derivations have also been successfully linked to other boundary conditions and a lack thereof through the evaluation of limits.

Using these new aquifer derivations, we incorporated intra-wellbore kinetic and friction head loss along the producing section of the well. Our work was based on petroleum reservoir engineering literature (Ouyang et al., 1998; Penmatcha and Aziz, 1999). No study in the groundwater literature has cited this petroleum reservoir modeling methodology. Our work is significant for two reasons. First, we introduce this petroleum methodology into the groundwater literature. Second, we more fully explain the model's numerical implementation than previous authors.

Upon development of the intra-wellbore head loss model, we used it to investigate intra-wellbore head loss effects along the producing section of the well. For most cases, the well length at which intra-wellbore head loss becomes significant exceeds current drilling capabilities. Drilling is the current limiting factor to increased horizontal well effectiveness (specific capacity). We found intra-wellbore head loss along the production section of the well to be relatively insignificant for all but extreme cases. Scenarios in which the aquifer drawdown is low and the pumping rate is high may yield significant intra-wellbore head loss. However, given typical parameters of aquifers and wells, these cases will be less common.

We also found that kinetic head loss is greater than friction head loss for shorter producing lengths. These shorter producing lengths are perhaps less than 10 m - 100 m in length depending on aquifer and well parameters. Most groundwater wells are within this range. Therefore, it is likely that most groundwater well's screened lengths are dominated by kinetic effects. This is a major shift from previous work which has assumed friction was the most important head loss component. As the length of a well

goes to zero, logically so does frictional head loss. On the contrary, kinetic head loss remains essentially constant as it is only dependent upon a change in fluid velocity along the producing section. Because kinetic head loss is length independent, it will become more significant than frictional head loss at some point as wellbore length goes to zero.

We also used our intra-wellbore head loss model to investigate uniform flux and uniform drawdown (infinite conductivity) assumptions. To do this, we turned friction and kinetic effects off, thus modeling the wellbore with a constant drawdown. We found that the uniform flux assumption does not have a significant impact on overall well performance (well drawdown or pumping rate) when compared to the uniform head assumption. The overall well performance discrepancy between these two methods is at most 10%. However, we did find that the uniform head assumption generates a significantly non-uniform flux along the wellbore. This finding shows the need for a uniform head (rather than uniform flux) wellbore when modeling contaminant transport processes or chemically bound ASR. This is because the well tips have much greater flux than the center of the well. However, if one is only interested in overall well pumping and drawdown relationships, then the two assumptions may be used interchangeably with minimal error (<10%).

With the intra-wellbore head loss model developed and impact characterized, we then investigated well construction aspects. We developed a drilling model based on petroleum engineering literature (Greenip Jr, 1989; Wu and Juvkam-Wold, 1991). This model calculates the rig pullback, thrust, and torque requirements. This model also calculates the casing collapse, tensile, and compressive strength requirements. While

these models are relatively simple and based on previous petroleum engineering work, such work has not been cited or completed in the groundwater literature.

Using a soft string drilling model, we investigated the distribution of rig and casing strengths necessary to construct horizontal wells at various depths and horizontal lengths. We found that horizontal groundwater wells may use a variety of rig types including slant utility, slant petroleum, vertical groundwater, and vertical petroleum rigs. We also found that at shallow depths the rig will need a thrust capacity to overcome friction effects.

Next we derived an equation for the optimal slant rig entry angle. Such an equation has not been discussed in any literature to our knowledge. This equation is significant for shallow horizontal wells using slant rigs. The equation determines the surface entry angle that minimizes the length of the borehole, thus reducing horizontal well cost.

Using the optimal rig entry angle equation, we found that a significant proportion of groundwater wells will need to be drilled using utility slant rigs. Because slant utility rigs have a limited surface entry angle (7°-23°), many shallow horizontal boreholes will be much longer than necessary. For a more cost effective wellbore, new rig designs are necessary to facilitate a wider range of entry angles (0°-90°).

We also developed a deterministic vertical well and horizontal well cost model. This model is based on a time and materials methodology for determining cost. With the cost model developed, we gathered a significant amount of well cost data. We then made assumptions and regressions of this cost data to estimate costs of rigs, casing, cement,

etc. Cost data assumptions & regressions were then incorporated into the well construction cost and force models described above. We then used these models and cost data to make estimates of well cost for various depths and horizontal reaches.

Our well cost estimates show that the relative cost of a horizontal well compared to a vertical well decreases with depth. This occurs because high cost slant rigs are necessary at shallow depths. In addition, these slant rigs have limited surface entry angles and therefore cannot always implement the optimal rig entry angle derived in this thesis. This causes the borehole to be much longer than necessary. However, for wells targeting deeper aquifers the economics of horizontal wells become more favorable. This is perhaps why horizontal wells are used more extensively in the petroleum industry. Overall, we found that horizontal wells cost 2.5 – 31.7 times as much as vertical wells.

After calculating the cost of horizontal wells, we also calculated the benefit of horizontal wells. We found that several parameters influence the number of vertical wells replaced by a single horizontal well (vertical well replacement ratio). All of these parameters relate to the expansion of the pressure pulse through the aquifer. Parameters slowing the lateral expansion of the pressure pulse benefit horizontal wells. These parameters include time, permeability, specific storativity, and proximity of constant head boundaries. Our simulation results show that a horizontal well can replace 1.2 – 30.1 vertical wells without hydraulic fracturing. The most important finding from these modeling efforts is that a lifecycle approach to vertical well replacement ratios is necessary. The vertical well replacement ratio will decrease through time until a steady state is reached.

FUTURE WORK

There are several research needs not addressed in this thesis. First, future work will need to improve drilling mud to avoid excessive skin and borehole stability issues. Directional groundwater wells drilled to date have had significant issues that all relate to drilling mud. This work will likely involve the use of bridging solids.

Second, there is a current issue when calculating wellbore skin drawdown effects for directional wells in anisotropic aquifers. Skin effect calculation requires an isotropic aquifer hydraulic conductivity. If the wellbore is along one dimension, the treatment of anisotropy is simple. For example, if the well is along the *z* axis, then isotropic aquifer hydraulic conductivity is $(K_x K_y)^{-1/2}$. However, if the well is not perpendicular to two axes then the correct calculation methodology is unknown.

Third, we were unable to find rapidly convergent series at early times for a leaky aquifer boundary condition. This Cauchy boundary condition eluded our use of Poisson Re-Summation in an attempt to find an early time rapidly convergent solution. The leaky aquifer boundary solution would be a valuable addition to our work as it would complete every boundary condition possible: no boundary, Neumann
Dirichlet, Cauchy.

Fourth, future research will need to improve finite difference / element models for chemically bound ASR systems. These new finite difference / element models must account for intra-wellbore head loss, solute transport, and density effects simultaneously. Despite the need for more advanced finite difference / element models, our research shows that intra-wellbore head loss is insignificant for most cases. If one assumes intra-

wellbore head loss is insignificant, then one may use existing models for chemically bound ASR such as MODFLOW-MNW2 paired with solute transport and density effects.

REFERENCES

Aadnøy, B.S., Andersen, K., 2001. Design of oil wells using analytical friction models. Journal of Petroleum Science and Engineering, 32(1): 53-71.

Aadnøy, B.S., Chenevert, M., 1987. Stability of highly inclined boreholes. SPE Drilling Engineering, 2(4): 364-374.

Aarrestad, T., 1994. Torque and drag-two factors in extended-reach drilling. Journal of Petroleum Technology, 46(9): 800-803.

Abrams, A., 1977. Mud design to minimize rock impairment due to particle invasion. Journal of Petroleum Technology, 29(5): 586-592.

Allen, F., Tooms, P., Conran, G., Lesso, B., Slijke, P.V.d., 1997. Extended-reach drilling: breaking the 10-km Barrier. Oilfield Review, 9(4): 32-47.

Allouche, E.N., Ariaratnam, S.T., Biggar, K.W., 1998. Environmental remediation using horizontal directional drilling: applications and modeling. Practice Periodical of Hazardous, Toxic, and Radioactive Waste Management, 2(3): 93-99.

Allouche, E.N., Ariaratnam, S.T., Lueke, J.S., 2000. Horizontal directional drilling: profile of an emerging industry. Journal of Construction Engineering and Management, 126(1): 68-76.

Andreassen, E., Blikra, H., Hjelle, A., Kvamme, S., Haugen, J., 1998. Rotary steerable system improves reservoir drilling efficiency and wellbore placement in the Statfjord Field. IADC/SPE Drilling Conference, Dallas, Texas, pp. 313-326.

Anglea, M., 1998. Aquifer storage and recovery preliminary investigation and feasibility analysis step 1. San Antonio Water System and Bexar Metropolitan Water District, CH2MHILL, San Antonio, Texas, 241 pp. Accessed November 7, 2013. http://www.twdb.texas.gov/innovativewater/asr/docs.asp

Anglea, M., 1999. Aquifer storage and recovery feasibility investigation, step 2. City of Laredo, Texas, CH2MHILL, San Antonio, Texas. 422 pp. Accessed November 7, 2013. http://www.twdb.texas.gov/innovativewater/asr/docs.asp

American Petroleum Institute, 1982. Bulletin 5C2, Bulletin for Performance Properties of Casing, Tubing, and Drillpipe. Dallas, Texas. 32 pp.

Arfib, B., de Marsily, G., 2004. Modeling the salinity of an inland coastal brackish karstic spring with a conduit-matrix model. Water Resources Research, 40(11): W11506 1-10.

Augustine, C., Tester, J.W., Anderson, B., Petty, S., Livesay, B., 2006. A comparison of geothermal with oil and gas well drilling costs. Thirty-First Workshop on Geothermal Reservoir Engineering, Stanford, California.

Babu, D., Odeh, A., 1989a. Productivity of a horizontal well appendices A and B. SPE Annual Technical Conference and Exhibition, Houston, Texas, 34 pp.

Babu, D., Odeh, A.S., 1989b. Productivity of a horizontal well. SPE Reservoir Engineering, 4(4): 417-421.

Baker Hughes, 2014. North American rig count. Accessed October 10, 2014. http://phx.corporate-ir.net/phoenix.zhtml?c=79687&p=irol-reportsother

Bardsley, D., 2001. Horizontal wells: what are the 'records'?. Water Well Journal, 55(8): 14.

Beljin, M.S., Losonsky, G., 1992. HWELL: A horizontal well model. IGWMC, Dallas, Texas, pp. 45-54.

Borisov, J.P., 1964. Oil production using horizontal and multiple deviation wells. Nedra, Moscow, 1954. Translated into English by J. Strauss, edited by S.D. Joshi, Phillips Petroleum Company, the R&D library translation, Bartlesville, Oklahoma.

Bouwer, H., 2002. Artificial recharge of groundwater: hydrogeology and engineering. Hydrogeology Journal, 10(1): 121-142.

Brown, C., 2005. Planning decision framework for brackish water aquifer, storage and recovery (ASR) projects. Ph.D. Dissertation, University of Florida, Gainesville, Florida, 415 pp.

Campbell, M.D., Lehr, J.H., 1973. Water well technology; field principles of exploration drilling and development of ground water and other selected minerals. McGraw-Hill Book Company, Montreal, Canada, 681 pp.

Carslaw, H.S., Jaeger, J.C., 1959. Conduction of Heat in Solids, second edition. Oxford University Press, New York City, 517 pp.

Cech, T.V., 2009. Principles of water resources: history, development, management, and policy. John Wiley and Sons Inc, Danvers, Massachusetts, 576 pp.

Cederstrom, D.J., 1947. Artificial recharge of a brackish water well. Virginia Chamber of Commerce, Richmond, Virginia, 14(12): 31 71-73.

Cederstrom, D.J., 1957. Geology and ground-water resources of the York-James Peninsula, Virginia, Geological Survey Water-Supply Paper 1361. U.S. Geological Survey, Washington D.C., 254 pp.

Chen, C., Wan, J., Zhan, H., 2003. Theoretical and experimental studies of coupled seepage-pipe flow to a horizontal well. Journal of Hydrology, 281(1): 159-171.

Cole, K., Zlotnik, V., 1994. Modification of Dagan's numerical method for slug and packer test interpretation. Computational Methods in Water Resources X, 1: 719-726.

Cooley, R.L., Cunningham, A.B., 1979. Consideration of total energy loss in theory of flow to wells. Journal of Hydrology, 43(12): 161-184.

Crawford, D., Johnson, P., 1967. An investigation of the effect on the mechanism of hydraulic formation fracturing in water injection of a sandface filter cake deposited from waters carrying high colloidal and solid suspensions of organic and/or inorganic origin. Department of Petroleum Engineering, Texas Technological College, Lubbock, Texas, 22 pp.

Cressey, G.B., 1958. Qanats, karez, and foggaras. Geographical Review, 48(1): 27-44.

Dean, E.G., 2001. Special report: practical drilling technology: PLCS, hydraulics improve slant rig shallow-drilling operations. Oil & Gas Journal, 99(9): 86.

Debrine, B.E., 1970. Electrolytic model study for collector wells under river beds. Water Resources Research, 6(3): 971-978.

Delleur, J.W., Simon, A.L., 1959. Model study of horizontal collector wells. Hydraulic Laboratory, Civil Engineering, Purdue University, Lafayette, Indiana, 12 pp.

Denham, M., Lombard, K., 1995. A synopsis of environmental horizontal wells at the Savannah River site. Westinghouse Savannah River Company, Aiken, South Carolina, 18 pp.

Devereux, S., 1999. Drilling technology: in nontechnical language. PennWell Books, Tulsa, Oklahoma, 336 pp.

Dick, M., Heinz, T., Svoboda, C., Aston, M., 2000. Optimizing the selection of bridging particles for reservoir drilling fluids. SPE International Symposium on Formation Damage Control, Lafayette, Louisiana, 8 pp.

Dikken, B., 1990. Pressure drop in horizontal wells and its effect on production performance. Journal of Petroleum Technology, 42(11): 1426-1433.

Dillon, P., Pavelic, P., Page, D., Beringen, H., Ward, J., 2009. Managed aquifer recharge. National Water Commission, Commonwealth of Australia, Canberra, Australia, 77 pp.

Doesburg, J., 2005. Operating and maintaining horizontal wells. Water Well Journal, 59(12): 40-42.

Downton, G., Hendricks, A., Klausen, T., Pafitis, D., 2000. New directions in rotary steerable drilling. Oilfield Review, 12(1): 18-29.

Driscoll, F.G., 1986. Groundwater and wells. Johnson Filtration Systems Inc., St. Paul, Minnesota, 1089 pp.

Dupriest, F., 2013. Personal communication. December 2013. College Station, Texas.

Dwyer, J., 2013. Personal communication. September 2013. Austin, Texas

El-Sayed, A.H., Khalaf, F., Ghzaly, S., 1991. Casing design considerations for horizontal wells. Erdöl, Erdgas, Kohle, 109(2): 56-59

Engineering News Record, 2013. Construction cost index. Accessed July 2014. http://enr.construction.com/economics/

English, P.W., 1968. The origin and spread of qanats in the old world. Proceedings of the American Philosophical Society, 112(3): 170-181.

Esmail, O.J., Kimbler, O.K., 1967. Investigation of the technical feasibility of storing fresh water in saline aquifers. Water Resources Research, 3(3): 683-695.

Faure, Y.-H., Baudoin, A., Pierson, P., Ple, O., 2006. A contribution for predicting geotextile clogging during filtration of suspended solids. Geotextiles and Geomembranes, 24(1): 11-20.

Fetter, C.W., Fetter, C., 2001. Applied hydrogeology. Prentice Hall, Upper Saddle River, New Jersey, 621 pp.

Frederick, K., Kelsey, T., Minn, K., Mirecki, J., Parker, T., and five others, 2010. NGWA information brief: aquifer storage and recovery. National Ground Water Association, 6 pp. Accessed January 12, 2013. http://www.ngwa.org/Media-Center/briefs/Documents/info_brief_enhanced_gw_storage.pdf

Functions.Wolfram, 2014. The Wolfram Functions Site. Accessed January 25, 2013 http://functions.wolfram.com/

Garg, S.P., Lal, J., 1971. Rational design of well screens. Journal of the Irrigation and Drainage Division, 97(1): 131-147.

Gatlin, C., 1960. Petroleum engineering, drilling and well completions. Prentice Hall, Englewood Cliffs, New Jersey, 341 pp.

Gavignet, A., Sobey, I., 1989. Model aids cuttings transport prediction. Journal of Petroleum Technology, 41(9): 916-921.

Giger, F., 1983. Réduction du nombre de puits par l'utilisation de forages horizontaux. Oil & Gas Science and Technology, 38(3): 351-360.

Giger, F., Reiss, L., Jourdan, A., 1984. The reservoir engineering aspects of horizontal drilling. SPE Annual Technical Conference and Exhibition, Houston, Texas, 8 pp.

Gleason, S., 1934. Slanted oil wells work new marvels. Popular Science Monthly, 124(5): 40-41.

Glotfelty, M., 2013. Personal communication. December 2013. Scottsdale, Arizona.

Goode, P., 1987. Pressure drawdown and buildup analysis of horizontal wells in anisotropic media. SPE Formation Evaluation, 2(4): 683-697.

Gradshteyn, I.S., Ryzhik, I.M., 2007. Table of integrals, series, and products, seventh edition. Elsevier, Burlington, Massachusetts, 1221 pp.

Greenip Jr, J.F., 1989. How to design casing strings for horizontal wells. Petroleum Engineer International, 61(12): 34-38.

Gringarten, A.C., Ramey, H.J., Jr., Raghavan, R., 1974. Unsteady-state pressure distributions created by a well with a single infinite-conductivity vertical fracture. SPE Journal 14(4): 347-360.

Halford, K.J., Hanson, R.T., 2002. User guide for the drawdown-limited, multi-node well (MNW) package for the U.S. Geological Survey's modular three-dimensional finite-difference ground-water flow model, MODFLOW-96 and MODFLOW-2000. U.S. Geological Survey and the Santa Clara Valley Water District, Sacramento, California, 80 pp.

Halliburton, 1995. Halliburton cementing tables, Redbook ®. ASIN: B000H44KDW, Halliburton, Houston, Texas.

Hantush, M., Papadopulos, I., 1962. Flow of ground water to collector wells. Journal of the Hydraulics Division of the American Society of Civil Engineers, 88(5): 221-244.

Hantush, M.S., 1964. Hydraulics of wells. Academic Press, New York City, 432 pp.

Harbaugh, A., 2005. MODFLOW-2005, the U.S. Geological Survey modular ground-water model—the Ground-Water Flow Process. U.S. Geological Survey, Reston, Virginia, 253 pp.

Hardcastle, B., 1987. Wells ancient and modern—an historical review. Quarterly Journal of Engineering Geology and Hydrogeology, 20(3): 231-238.

Hart, K., Jankowski, L., 1984. The application of slant hole drilling in development of shallow heavy oil deposits. Journal of Canadian Petroleum Technology, 23(1): 51-55.

Hashash, Y., Javier, J., Osborne, E., 2011. Evaluation of horizontal directional drilling (HDD). University of Illinois at Urbana, Champaign and Illinois Center for Transportation Series, Springfield, Illinois, 51 pp.

Helweg, O.J., 1975. Determining optimal well discharge. Journal of the Irrigation and Drainage Division, 101(3): 201-208.

Helweg, O.J., 1982. Economics of improving well and pump efficiency. Ground Water, 20(5): 556-562.

Hubbs, S.A., 2006. Riverbank filtration hydrology. NATO Science Series, Springer, Bratislava, Slovakia, 339 pp.

Hunt, H., 2002. American experience in installing horizontal collector wells. In: Ray, C., Gina Melin, Linsky, R.B. (Eds.), Riverbank filtration: improving source-water quality. Kluwer Academic Publishers, New York City, pp. 29-34.

Hunt, H., 2003. Leo Ranney: industry inventor and innovator. Water Well Journal, 57(10): 60.

Jacob, C., 1947. Drawdown test to determine effective radius of artesian well. Transactions of the American Society of Civil Engineers, 112(1): 1047-1064.

Jehn-Dellaport, T., 2004. Innovative water well completion in the Denver Basin, Colorado. The Mountain Geologist, 41(4): 211-217.

Jehn-Dellaport, T., 2013. Personal communication. September 2013. Denver, Colorado.

Jerez, H., Dias, R., Tilley, J., 2013. Offshore West Africa deep water ERD: drilling optimization case history. 2013 SPE/IADC Drilling Conference and Exhibition, Amsterdam, The Netherlands, 10 pp.

Johancsik, C., Friesen, D., Dawson, R., 1984. Torque and drag in directional wells-prediction and measurement. Journal of Petroleum Technology, 36(6): 987-992.

Johnson, S., 2014. Faddeeva Package in C++. Accessed June 10, 2014. http://ab-initio.mit.edu/wiki/index.php/Faddeeva_Package

Jones, G.W., Pichler, T., 2007. Relationship between pyrite stability and arsenic mobility during aquifer storage and recovery in southwest central Florida. Environmental Science & Technology, 41(3): 723-730.

Joshi, S., 1987. A review of horizontal well and drainhole technology. SPE annual technical conference and exhibition, Dallas, Texas, pp. 330-347.

Joshi, S.D., 1988. Augmentation of well productivity with slant and horizontal wells. Journal of Petroleum Technology, 40(6): 729-739.

Joshi, S.D., 1991. Horizontal well technology. PennWell Books, Tulsa, Oklahoma, 535 pp.

Joshi, S.D., 2003. Cost/benefits of horizontal wells. SPE Western Regional/AAPG Pacific Section Joint Meeting, Long Beach, California, 9 pp.

Kaback, D., 1998. Horizontal wells, subsurface contaminants focus area. Office of Environmental Management, Office of Science and Technology, U.S. Department of Energy, Washington D.C., 28 pp.

Kaback, D., 2002. Technology status report: a catalogue of the horizontal environmental wells in the United States. Ground-Water Remediation Technologies Analysis Center, 70 pp.

Karlsson, H., 1993. Horizontal systems technology for shallow site remediation. Journal of Petroleum Technology, 45(2): 160-165.

Kawecki, M.W., 2000. Transient flow to a horizontal water well. Ground Water, 38(6): 842-850.

K&M Technology Group, 2013. Personal communication. September 2013. Spring, Texas. Accessed October 14, 2013. http://www.kmtechnology.com/

Killeen, P., Bernius, G., Mwenifumbo, C., 1995. Surveying the path of boreholes: a review of orientation methods and experience. Proceedings of the 6th International MGLS Symposium on Borehole Geophysics for Minerals, Geotechnical and Groundwater Applications, Santa Fe, New Mexico, pp. 22-25.

Kimbler, O.K., 1970. Fluid model studies of the storage of freshwater in saline aquifers. Water Resources Research, 6(5): 1522-1527.

King, R.F. Drilling sideways: a review of horizontal well technology and its domestic application. U.S. Department of Energy, Washington, D.C., 30 pp.

Kompani-Zare, M., Zhan, H., Samani, N., 2005. Analytical study of capture zone of a horizontal well in a confined aquifer. Journal of hydrology, 307(1): 48-59.

Konikow, L.F., Hornberger, G.Z., 2006. Use of the Multi-Node Well (MNW) package when simulating solute transport with the MODFLOW ground-water transport process. U.S. Geological Survey, Reston, Virginia, 34 pp.

Konikow, L.F., Hornberger, G.Z., Halford, K.J., Hanson, R.T., 2009. Revised multi-node well (MNW2) package for MODFLOW ground-water flow model. U.S. Geological Survey, Reston, Virginia, 80 pp.

Kumar, A., Kimbler, O.K., 1970. Effect of dispersion, gravitational segregation, and formation stratification on the recovery of freshwater stored in saline aquifers. Water Resources Research, 6(6): 1689-1700.

L Espoir, J., 2003. Core drilling-cable tools-horizontal drilling. Water Well Journal, 57(5): 62-71.

Lacombe, P.J., 1996. Artificial recharge of ground water by well injection for storage and recovery, Cape May County, New Jersey 1958-92. U.S. Geological Survey, West Trenton, New Jersey, 34 pp.

Lambert, R., Grimm, K., Lee, R., 2000. Hydrogeology, hydrologic budget and water chemistry of the Medina Lake Area, Texas. U.S. Geological Survey, Austin, Texas, 190 pp.

Landman, M.J., 1994. Analytic modelling of selectively perforated horizontal wells. Journal of Petroleum Science and Engineering, 10(3): 179-188.

Larsen, T., Pilehvari, A., Azar, J., 1997. Development of a new cuttings-transport model for high-angle wellbores including horizontal wells. SPE Drilling & Completion, 12(2): 129-136.

Leising, L., Newman, K., 1993. Coiled-tubing drilling. SPE Drilling & Completion, 8(4): 227-232.

Lightfoot, D.R., 2000. The origin and diffusion of qanats in Arabia: new evidence from the northern and southern peninsula. Geographical Journal, 166(3): 215-226.

Lowry, C.S., Anderson, M.P., 2006. An assessment of aquifer storage recovery using ground water flow models. Ground Water, 44(5): 661-667.

Maidla, E., Haci, M., 2004. Understanding torque: the key to slide-drilling directional wells. IADC/SPE Drilling Conference, Dallas, Texas, 7 pp.

Malcolm Pirnie Inc, ASR Systems LLC, Jackson, S., McCarthy, Wilson LLP, 2011. An assessment of aquifer storage and recovery in Texas. Texas Water Development Board, Austin, Texas, 206 pp.

Maliva, R.G., Missimer, T.M., 2010. Aquifer storage and recovery and managed aquifer recharge using wells: planning, hydrogeology, design, and operation. Methods in water resources evaluation. Schlumberger, Sugar Land, Texas, 578 pp.

Mansure, A., Bauer, S., Livesay, B., 2005. Geothermal well cost analyses 2005. Geothermal Resources Council Transactions, 29: 515-519.

Mason, C., Judzis, A., 1998. Extended-reach drilling--what is the limit? SPE Annual Technical Conference and Exhibition, New Orleans, Louisiana, pp. 87-98.

Merkulov, V., 1958. Le debit des puits devies et horizontaux. Neft Khoz, 6(1): 51-56.

Merritt, M.L., 1986. Recovering fresh water stored in saline limestone aquifers. Ground Water, 24(4): 516-529.

Mikels, F.C., Klaer, F.H., 1956. Application of ground water hydraulics to the development of water supplies by induced infiltration. Symposium Darcy, International Association Scientific Hydrology, Dijon, France.

Milora, S.L., Tester, J.W., 1977. Geothermal energy as a source of electric power. The Massachusetts Institute of Technology Press, Cambridge, Massachusetts, 196 pp.

Missimer, T.M., Guo, W., Walker, C.W., Maliva, R.G., 2002. Hydraulic and density considerations in the design of aquifer storage and recovery systems. Florida Water Resources Journal, 55(2): 30-36.

Mody, F.K., Hale, A., 1993. Borehole-stability model to couple the mechanics and chemistry of drilling-fluid/shale interactions. Journal of Petroleum Technology, 45(11): 1093-1101.

Moore, C., 2013. Personal communication. July 2013. College Station, Texas.

Moore, T., 1995. Hydro group's Ranney division: on the cutting edge. Water Well Journal, 49(7): 54-56.

Morgan, J.H., 1992. Horizontal drilling applications of petroleum technologies for environmental purposes. Ground Water Monitoring & Remediation, 12(3): 98-102.

Motiee, H., Mcbean, E., Semsar, A., Gharabaghi, B., Ghomashchi, V., 2006. Assessment of the contributions of traditional qanats in sustainable water resources management. Water Resources Development, 22(4): 575-588.

Munson, B.R., Rothmayer, A.P., Okiishi, T.H., Huebsch, W.W., 2012. Fundamentals of fluid mechanics. Wiley and Sons, New York City.

Murdoch, L., 1995. Alternative methods for fluid delivery and recovery. Center for Environmental Research Information, Office of Research and Development, U.S. Environmental Protection Agency, Cincinnati, Ohio, 87 pp.

Murphy, S., 2013. April edition. The OCTG situation report, 28(299): 1-10.

National Research Council, 2008. Prospects for managed underground storage of recoverable water. The National Academic Press, Washington, D.C., 350 pp.

Novy, R., 1995. Pressure drops in horizontal wells: when can they be ignored? SPE Reservoir Engineering, 10(1): 29-35.

Oakley, D., Thacker, M., Singer, K., Koelsch, J., Mabson, B., 1994. The use of horizontal wells in remediating and containing a jet fuel plume-preliminary findings. WEF Specialty Conference Series Proceedings on Innovative Solutions for Contaminated Site Management, Houston, Texas, 342 pp.

Oberdorfer, J.A., Peterson, F.L., 1985. Waste-water injection: geochemical and biogeochemical clogging processes. Ground Water, 23(6): 753-761.

Odeh, A.S., Babu, D., 1990. Transient flow behavior of horizontal wells, pressure drawdown, and buildup analysis. SPE Formation evaluation, 5(1): 7-15.

Ouyang, L.-B., Arbabi, S., Aziz, K., 1998. General wellbore flow model for horizontal, vertical, and slanted well completions. SPE Journal, 3(2): 124-133.

Ouyang, L.-B., Aziz, K., 1998. A simplified approach to couple wellbore flow and reservoir inflow for arbitrary well configurations. SPE Annual Technical Conference and Exhibition, New Orleans, Louisiana.

Park, E., Zhan, H., 2002. Hydraulics of a finite-diameter horizontal well with wellbore storage and skin effect. Advances in Water Resources, 25(4): 389-400.

Park, E., Zhan, H., 2003. Hydraulics of horizontal wells in fractured shallow aquifer systems. Journal of hydrology, 281(1): 147-158.

Parmentier, P.P., Klemovich, R.M., 1996. A new direction in remediation. Civil Engineering—ASCE, 66(4): 55-57.

Penberthy Jr, Bickham, K., Nguyen, H., Paulley, T., 1997. Gravel placement in horizontal wells. SPE Drilling & Completion, 12(2): 85-92.

Penmatcha, V., Aziz, K., 1999. Comprehensive reservoir/wellbore model for horizontal wells. SPE Journal, 4(3): 224-234.

Petrey, P., Bennett, M., 2006. Reducing the high cost of an ASR test well. Florida Water Resources Journal, 58(2): 20-26.

Platte, R.B., Trefethen, L.N., 2010. Chebfun: A new kind of numerical computing. Progress in Industrial Mathematics at ECMI 2008, 19 pp.

Pollock, D., 1994. User's guide for MODPATH/MODPATH-PLOT, version 3: a particle tracking post-processing package for MODFLOW, the U.S. Geological Survey finite-difference ground-water flow model. U.S. Geological Survey, Reston, Virginia.

Price, R.E., Pichler, T., 2006. Abundance and mineralogical association of arsenic in the Suwannee Limestone (Florida): implications for arsenic release during water–rock interaction. Chemical Geology, 228(1–3): 44-56.

Pyne, R.D.G., 1995. Groundwater recharge and wells: a guide to aquifer storage recovery. Lewis Publishers, Boca Raton, Florida, 400 pp.

Pyne, R.D.G., 2005. Aquifer storage recovery: a guide to groundwater recharge through wells. ASR Systems Gainesville, Florida, 608 pp.

Pyne, R.D.G., 2013. Personal communication. September 2013. Gainesville, Florida.

Pyne, R.D.G., Howard, J.B., 2004. Desalination/aquifer storage recovery (DASR): a cost-effective combination for Corpus Christi, Texas. Desalination, 165: 363-367.

Ramey, H.J., 1982. Well-loss function and the skin effect: a review. Geological Society of America Special Papers, 189: 265-272.

Rash, V., 2001. Predicting yield and operating behavior of a horizontal well. AWWA Annual Conference, Washington D.C., 15 pp.

Rash, V., 2013. Personal communication. September 2013. Des Moines, Iowa.

Rebhun, M., 1968. Clogging and contamination processes in recharge wells. Water Resources Research, 4(6): 1207-1217.

Reimann, T. et al., 2013. Representation of water abstraction from a karst conduit with numerical discrete-continuum models. Hydrology and Earth System Sciences Discussions, 10(4): 4463-4487.

Rig Data, 2014. Q2 continues day rate resurgence begun in Q1. Day Rate Report, 26(4): 1-22.

Rinck-Pfeiffer, S., Ragusa, S., Sztajnbok, P., Vandevelde, T., 2000. Interrelationships between biological, chemical, and physical processes as an analog to clogging in aquifer storage and recovery (ASR) wells. Water Research, 34(7): 2110-2118.

Rorabaugh, M.I., 1953. Graphical and theoretical analysis of step-drawdown test of artesian well. Transactions, American Society of Civil Engineers, 79: 1-23.

Roscoe Moss Company, 1990. Handbook of ground water development. John Wiley and Sons, Wiley-Interscience Publication, New York City, 490 pp.

Rushford, J.D., 1993. The evolution of slant drilling in Canada: improvements in drilling performance and rig design. SPE Drilling & Completion, 8(4): 239-245.

Ruud, N., Kabala, Z., 1997. Response of a partially penetrating well in a heterogeneous aquifer: integrated well-face flux vs. uniform well-face flux boundary conditions. Journal of Hydrology, 194(1): 76-94.

SAWS, 2012. Twin Oaks - Aquifer storage & recovery, San Antonio, Texas. Accessed October 12, 2013. www.saws.org/Your_Water/WaterResources/projects/asr.cfm

Sheng, Z., 2005. An aquifer storage and recovery system with reclaimed wastewater to preserve native groundwater resources in El Paso, Texas. Journal of Environmental Management, 75(4): 367-377.

Sheppard, M., Wick, C., Burgess, T., 1987. Designing well paths to reduce drag and torque. SPE Drilling Engineering, 2(4): 344-350.

Shoemaker, W.B., Kuniansky, E.L., Bauer, S., Swain, E.D., 2007. Documentation of a conduit flow process (CFP) for MODFLOW-2005. U.S. Geological Survey, Reston, Virginia, 58 pp.

Short, J.A., 1993. Introduction to directional and horizontal drilling. PennWell Books, Tulsa, Oklahoma, 232 pp.

Spiessl, S.M., Prommer, H., Licha, T., Sauter, M., Zheng, C., 2007. A process-based reactive hybrid transport model for coupled discrete conduit–continuum systems. Journal of Hydrology, 347(1–2): 23-34.

Spiridonoff, S.V., 1964. Design and use of radial collector wells. Journal of the American Water Works Association, 56(6): 689-698.

Stoner, R., Milne, D., Lund, P., 1979. Economic design of wells. Quarterly Journal of Engineering Geology and Hydrogeology, 12(2): 63-78.

Strikwerda, J.C., 2004. Finite difference schemes and partial differential equations. Society for Industrial and Applied Mathematics, Philadelphia, Pennsylvania, 435 pp.

Stuart, S., Demos, P., Eric, G., 2000. Application of a point the bit rotary steerable system in directional drilling prototype well-bore profiles. SPE/AAPG Western Regional Meeting, Long Beach, California, 7 pp.

Subsurface Technologies Inc., 2013. Collector, horizontal, angle & directional wells - case studies. Accessed August 23, 2013. http://www.subsurfacetech.com/aqua-freed-case-studies

Sun, D., Zhan, H., 2006. Flow to a horizontal well in an aquitard–aquifer system. Journal of Hydrology, 321(1): 364-376.

Swamee, P.K., Tyagi, A., Shandilya, V.K., 1999. Optimal configuration of a wellfield. Ground Water, 37(3): 382-386.

Tamburrino, A., 2010. Water technology in ancient Mesopotamia. In: Mays, L.W. (Ed.), Ancient water technologies. Springer Netherlands, pp. 29-51.

Tarshish, M., 1992. Combined mathematical model of flow in an aquifer-horizontal well system. Groundwater, 30(6): 931-935.

Tessari, B., Madell, G., Warren, T., 1999. Drilling with casing promises major benefits. Oil & Gas journal, 97(20): 58-62.

Tester, J.W., Herzog, H.J., 1990. Economic predictions for heat mining: a review and analysis of hot dry rock (HDR) geothermal energy technology. Energy Laboratory, Massachusetts Institute of Technology, Cambridge, Massachusetts.

Thompson, J., 1979. Deep directional drilling. SPE Deep Drilling and Production Symposium, Amarillo, Texas, 8 pp.

Todd, D.K., 1959. Annotated bibliography on artificial recharge of ground water through 1954. U.S. Geological Survey, Washington, D.C., 119 pp.

Tomren, P., Iyoho, A., Azar, J., 1986. Experimental study of cuttings transport in directional wells. SPE Drilling Engineering, 1(1): 43-56.

TWDB, 2012. Water for Texas 2012 state water plan. Texas Water Development Board, Austin, Texas, 299 pp.

U.S. Congress, 2005. Energy policy act of 2005, title III - oil and gas, section 322.

U.S. EPA, 2004. Evaluation of impacts to underground sources of drinking water by hydraulic fracturing of coalbed methane reservoirs. U.S. Environmental Protection Agency, Office of Water, Office of Ground Water and Drinking Water, Drinking Water Protection Division, Prevention Branch, Washington, D.C.

U.S. EPA, 2013. Secondary drinking water regulations: guidance for nuisance chemicals. U.S. Environmental Protection Agency. Accessed December 11, 2013. http://water.epa.gov/drink/contaminants/secondarystandards.cfm#tabletop

Vacher, H.L., Hutchings, W.C., Budd, D.A., 2006. Metaphors and models: the ASR bubble in the Floridian aquifer. Ground Water, 44(2): 144-154.

Vecchioli, J., 1970. A note on bacterial growth around a recharge well at Bay Park, Long Island, New York. Water Resources Research, 6(5): 1415-1419.

Viessman, W., Klapp, J.W., Lewis, G.L., Harbaugh, T.E., 1977. Introduction to hydrology. Harper & Row, New York City.

Ward, J.D., Simmons, C.T., Dillon, P.J., 2007. A theoretical analysis of mixed convection in aquifer storage and recovery: how important are density effects? Journal of Hydrology, 343(3–4): 169-186.

Warren, T., Houtchens, B., Madell, G., 2005. Directional drilling with casing. SPE Drilling & Completion, 20(1): 17-23.

Warren, T.M., 1997. Trends toward rotary steerable directional systems. World Oil, 218(5).

Warren, T.M., 1998. Technology gains momentum. Oil & Gas journal, 96(51): 101-105.

Weisstein, E.W., 2014. Jacobi theta functions. MathWorld - A Wolfram Web Resource. Accessed July 19, 2014. http://mathworld.wolfram.com/JacobiThetaFunctions.html

Wells, C.L., 1955. Directional drilling tool. U.S. Patent 2,712,434.

Williams, D.E., 2008. Research and development for horizontal/angle well technology. Geoscience Support Services, Desalination and Water Purification Research and Development Program Report No. 151, Fountain Valley, California, 71 pp.

Williams, D.E., 2013. Drawdown distribution in the vicinity of nonvertical wells. Ground Water, 51(5): 745-751.

Willoughby, D.A., 2005. Horizontal directional drilling: utility and pipeline applications. McGraw-Hill Professional, New York City, 400 pp.

Wilson, D., Kaback, D., Denhan, M., Watkins, D., 1993. Industry survey for horizontal wells. Westinghouse Savannah River Company, Aiken, South Carolina.

Wilson, D., Losonsky, G., 1995. Horizontal environmental well cost evaluation methods. Energy and Environmental Exposition American Society of Mechanical Engineers, pp. 43-50.

Wu, A., Hareland, G., Fazaelizadeh, M., 2011. Torque & drag analysis using finite element method. Modern Applied Science, 5(6): 13-27.

Wu, J., Juvkam-Wold, H.C., 1991. Drag and torque calculations for horizontal wells simplified for field use. Oil & Gas journal, 89(19): 49-56.

Wulff, H.E., 1968. The qanats of Iran. Scientific American, 218(4): 94-105.

Zhan, H., 1999. Analytical study of capture time to a horizontal well. Journal of Hydrology, 217(1): 46-54.

Zhan, H., Cao, J., 2000. Analytical and semi-analytical solutions of horizontal well capture times under no-flow and constant-head boundaries. Advances in Water Resources, 23(8): 835-848.

Zhan, H., Park, E., 2003. Horizontal well hydraulics in leaky aquifers. Journal of Hydrology, 281(1): 129-146.

Zhan, H., Wang, L.V., Park, E., 2001. On the horizontal-well pumping tests in anisotropic confined aquifers. Journal of Hydrology, 252(1–4): 37-50.

Zhan, H., Zlotnik, V.A., 2002. Groundwater flow to a horizontal or slanted well in an unconfined aquifer. Water Resources Research, 38(7): 1-10.

Zheng, C., Wang, P.P., 1999. MT3DMS: a modular three-dimensional multispecies transport model for simulation of advection, dispersion, and chemical reactions of contaminants in groundwater systems; documentation and user's guide. U.S. Army Corps of Engineers, University of Alabama, Tuscaloosa Alabama, 219 pp.

Zuurbier, K., Stuyfzand, P., Kooiman, J., 2013. The freshmaker: enabling aquifer storage and recovery (ASR) of freshwater using horizontal directional drilled wells (HDDWs) in coastal areas. Eighth International Symposium on Managed Aquifer Recharge (ISMAR8), Beijing, China, 6 pp.